# The Development of Novel Silver Brazing Alloys


Rob Snell

Department of Materials Science and Engineering

University of Sheffield

A thesis submitted for the degree of

*Doctor of Philosophy*

September 2017

This thesis is dedicated to Cinnamon and Alf.

# Acknowledgements

I would like to thank both the EPSRC and Johnson Matthey for the funding of this project.

There are many people from the department that I have to thank. Russell for his continual guidance, advice and effort, especially during the thesis write-up as well as Iain for his valuable insight and advice. Also within the department I am indebted to the technical staff for their tremendous help. In particular Ian, Kyle, Dean, Lisa and Neil.

I have also received invaluable assistance from Johnson Matthey Metal Joining. Jack in particular has been incredible in everything from teaching me how to braze to helping with the most awkward and technical of challenges. Also at JM I would like to thank Neil and Will as supervisors as well as Phil and Alan for their assistance at the start of the project.

Finally I would like to thank my family and friends. Rose for her support, patience and understanding (with the help of Cinnamon and Alf). My parents for their support both during my PhD and the 24 years prior to my PhD. And lastly my PhD support group of Ellie, Greg and Keshia.

# Abstract

This research was primarily focussed on finding novel silver brazing alloys. The first alloy development method used to achieve this goal was a CALPHAD-based approach. This was used to predict melting temperatures and the intermetallic content of alloys. The method was developed and then applied to a commonly used silver brazing alloy, Ag55Cu21Zn22Sn2 by wt.% (Ag155). A number of alloys with potentially superior properties were selected, produced and tested. However, none of the alloys offered improved overall properties and the method was not advanced any further.

An alternative method was developed based on High Entropy Alloys (HEAs). Simple HEA formation rules based on atomic size and enthalpy were used as a predictive tool for HEA formation. This method was then scaled to analyse large numbers of compositions, from many systems.

The large-scale HEA modelling method was applied to silver brazing alloys. Novel brazing alloys were found using a process of filtering and optimisation. One particular alloy, BHEA-1 offered a 5 wt.% reduction in Ag compared to the Ag155 and had properties that were suitable for brazing. The properties though were not as good as Ag155. Further investigations then explored the effects of adjusting the composition..

The large-scale HEA modelling method was also applied to a number of other applications. The approach was used to successfully predict and produce HEAs with different criteria. Several HEAs were created that had a high silver content and two HEAs were developed that had a high number of elements and a single phase.

# Contents

# Chapter 1

# Introduction

Brazing is a metal joining process that uses a molten low-melting metal to join two, unmelted materials together. There are many metals that can be used for brazing with properties and cost tailored to the requirements of different brazed joints. This research will investigate brazing alloys and look to develop novel brazing alloys.

Brazing has similarities with two other metal joining processes, soldering and welding. Brazing and soldering both rely on a molten alloy to form the joint and they do not melt the materials that are being joined (parent materials). The main differences between brazing and soldering are the melting temperature, mechanical performance and the applications of the joints. Soldered joints are formed at a low temperature, are mechanically weak and are primarily used for joining electrical components.

Welded joints are usually stronger than brazed joints, but there are limitations in what materials can be welded. The welding process involves melting and mixing of the parent materials. Brazing does not melt the parent materials and this means that many more materials can be used. It even means that entirely different materials can be joined together using brazing (e.g. a ceramic to a metal) [1].

The alloys used in brazing have a number of properties that are key to the brazing process and the brazed joint performance. New alloys that can improve on these properties, or can reduce the use of precious metals that often feature in their com-

positions, are desirable and may have the potential to be sold commercially.

There are many driving factors for the development of new brazing alloys. The fluctuating prices of pure metals mean that some alloys, particularly alloys with a high precious metal content, are susceptible to price increases. Developing alloys that use less precious metal would mean alloys are lower cost and have a more stable price. Alternatively, finding alloys that can perform better with same precious metal content would have a similar cost reduction effect.

Finding new brazing alloys is a difficult process as there are many properties to consider and often improving one of the key properties will adversely affect another. Modelling of these various properties accelerates the alloy development process and is achieved here by making use of thermodynamic modelling. This is a method that allows many of the key properties to be predicted, so they could then be optimised and used to find potentially improved alloys.

The important properties that need to be considered when finding new alloys can be approximately divided into three groups; those of importance before, during and after brazing. The alloy characteristics during the industrial manufacturing of the brazing alloy need to be considered to ensure that any promising alloy could be successfully commercialised. As most silver-based brazing alloys are used in rod, foil or wire form it means alloys need to be ductile enough to be processed. The properties during brazing are obviously important and ideally brazing alloys will be as low melting and easy flowing as possible. Finally the performance of the joint once brazed needs to be fit for purpose, offering a strong joint that will last in service.

There are countless commercial brazing alloys from a large number of different alloy systems with a wide variety of different elements. These elements and compositions are designed to optimise the properties mentioned previously as well as to meet specific needs for specific applications or materials. These alloy systems are often based on a precious metal, and so cost is of course a big factor in selecting a brazing alloy.

An alternative approach to finding new alloys developed in this work is to adapt some techniques and theories that are used for High Entropy Alloys (HEAs) and to apply them to brazing alloys. Using such modelling techniques it is possible to predict whether unusual compositions will form a solid solution or form intermetallic compounds (IMCs). This approach has the potential to discover radically different compositions and alloys with significantly improved properties.

The overall aims of this research are to investigate and develop new silver brazing alloys. These aims are to be achieved using thermodynamic and phase prediction techniques. The research will also use the developed methods to find new non-brazing alloys with atypical elements and unusual compositions.

# Chapter 2

# Literature Review

## 2.1 Brazing

### 2.1.1 Definition

Brazing is a versatile process that is used to join materials together. The process involves the melting of a brazing alloy (also referred to as brazing filler metal) between two surfaces and then allowing it to solidify and form a joint. Brazing is often compared to two other metal joining processes; soldering and welding.

Soldering is very similar in terms of process of melting an alloy to join surfaces. However, brazing by definition takes place above 450°C and soldering takes place below 450°C; brazed joints also tend to have a greater emphasis on strength and mechanical performance compared to soldered joints.

Welding differs from brazing as the parent materials are melted during the heating process. In a welded joint the two materials that are being joined are melted and mixed together [1]. Parent materials in a brazed joint do not melt and are not in direct contact. Usually the brazing alloy can be seen as a distinct layer between the two parent materials, as shown in Fig. 2.1. The advantages of this are that dissimilar materials can be joined together and a number of materials that cannot be welded can be brazed, such as ceramics and carbides. Examples of some different brazed

joints can be seen in Fig. 2.1 from papers by Nowacki et al. [2] and Ghosh et al. [3].

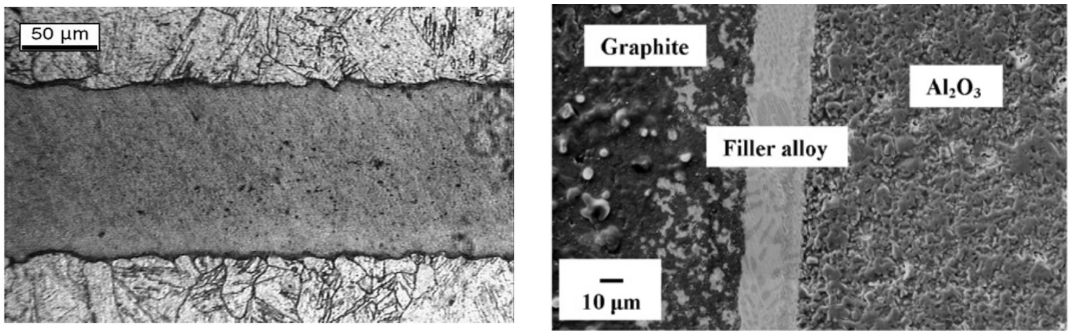


(a) Brazed joint from Nowacki et al. [2]. (b) Brazed joint from Ghosh et al. [3].

Figure 2.1: Micrographs of two different brazed joints with On the left, (a) two 15-5 PH steel pieces with an Au-Ni brazing alloy [2] and (b) graphite joined to $Al_2O_3$ using a Ag-Cu based brazing alloy [3].

All brazing involves the process of heating and melting an alloy, but almost every other facet of the brazing process varies depending on the joint requirements. The heat source, parent materials, brazing alloy, joint configuration and even the atmospheric conditions all vary depending on the application but all result in processes which can be classified as brazing.

### 2.1.2 Origins

Brazing can be traced back to ancient times where precious metals were used to repair cracks in pottery and ceramics. The method was documented formally in the 12th century by Theophilus in his work De Diversis Artibus [4] and was described in more detail by the goldsmith Benvenuto Cellini during the Renaisance [5].

During the industrial revolution advances in scientific understanding and technology revolutionised the field of brazing. Technological advances in heating methods, the availability of purer elements and a greater understanding of alloy systems and compositions all contributed to the advancement of brazing.

The 20th and 21st centuries saw the continued advancement of the brazing methods as well as the development of many of the compositions that are still in use today. Brazing alloys available today range from only a few years old to some dating back many decades Although brazing does use techniques and alloys that are decades old, it is still a commonly used technique in the modern day. There are many joints that could not be joined in any other way despite recent advancements in other metal joining techniques.

### 2.1.3 Brazing Processes

The process of brazing can be broken down into a number of steps. Johnson Matthey Metal Joining [6] and Luca-Milhaupt [7], two brazing companies, outline six stages as follows:-

1. Checking fit and clearance
2. Cleaning of the materials
3. Applying the flux
4. Assembling the brazed joint
5. Brazing
6. Cleaning the joint

The fit and the cleanliness of the materials are important for ensuring joints are consistent and defect free. A proper fit is ensured by good joint design and care when assembling the materials prior to brazing. The cleanliness of a joint is an often overlooked consideration and is quite often the source of problems with brazed joints. Oil, dirt and grease are some of the most common contaminants which can inhibit alloy flow and cause defects such as voids [6, 7].

The flux is a chemical compound that protects the brazed joint from oxidation while being heated. Oxidation of the parent materials and the brazing alloy is undesirable for a number of reasons. Metal oxides stop brazing alloys from flowing correctly, can lead to defects forming in the joint and can affect the properties of the parent materials. The application of the flux does vary significantly with different brazing processes. Flux can be applied as a paste, powder or already attached to filler metal prior to heating as well as other lesser used forms [8]. However, not all brazing processes require flux. Any brazing that takes place in a vacuum or an inert atmosphere work without flux as there is no oxygen to oxidise the materials.

The assembling of the joint is similar to first step. As the specifications of brazed joints are quite precise it is common practise to assemble the joint prior to heating. The brazing of the joint has many different options and variations in terms of heat source. There are a number of conventional heating methods such as furnaces, blow-torches and induction. The brazing method might also have adaptations, such as a vacuum system or some automation. There are some less common examples of heat source as well, such as using electron beams [9], or exothermic mixtures from the joining alloy (such as thermite) [10] and even using explosives [11].

The final stage is almost universal in brazing. The heating process almost always leaves some sort of dirt or residue that should be cleaned away. Even when the brazing is in a vacuum or without flux there is usually some residue left from the brazing. For some brazing processes this is just for the aesthetics of the joint but some flux residues, such as borates, can be corrosive and harmful to the long term performance of the joint [12].

### 2.1.4 Example Joints

There are many variations of joints that are designed to meet the needs of particular requirements or applications. However, most joints can be described as examples or adaptations of a handful well known joint configurations [12, 13]. An example of one

of these joints is a T-joint, which is shown in Fig. 2.2. The two coupons that are joined are 60 × 30 × 2.5 mm in size.

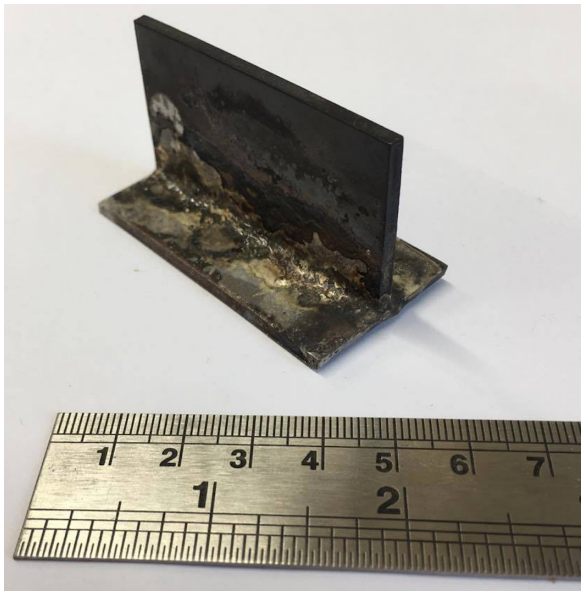


Figure 2.2: An example T-joint of mild steel.

The brazing of the T-joint is done by contacting the brazing rod to the joint and allowing capillary flow to fill the joint void. In this example the joint is 60mm long. This joint is also an example of high strength exhibited by most brazed joints. The example brazed joint in Fig. 2.2 is able to withstand significant impacts and forces. An identical T-joint has been subject to numerous high energy impacts and is shown in Fig. 2.3. The damage and deformation on the 2.5mm steel pieces shows the high forces involved in the testing process. The pieces are still connected though, showing the strength of brazing alloy and brazed joint.

Figure 2.3: The mild steel T-joint from Fig. 2.2 after impact testing.

### 2.1.5 Important properties

There are a number of important properties when considering brazing alloys and the design of new compositions. These properties relate to the processing of the alloy, the brazing of the joint and the performance of the joint once completed. The specific requirements of brazed joints and brazing alloys vary significantly and there is no specification that can be a blueprint for all new alloys. There are however some aims that are useful for most brazing alloys and will form the basis of trying to find new brazing alloy compositions.

#### Alloy processing

The most important property for alloy production is the ductility of the alloy. The majority of brazing alloys that are sold tend to be in foil, wire or rod form [14]. To get the alloys in these forms they need to be processed, typically through rolling or wire drawing. Alloys that are ductile enough to be processed in these ways can be commercialised a lot more easily than alloys that cannot.

There are other production methods available, such as melt spinning, that may have advantages depending on the alloy. Taking melt spinning as an alloy this may be used when a fine ribbon is desired or when alloys are too brittle to be rolled or drawn.

One example of a melt spun alloy is a Ni-Pd-Co-Si-Mo alloy sold by Johnson Matthey [15] and there are other examples [16, 17]. Even so, it still remains an objective to find an alloy that is sufficiently ductile to be produced using rolling and drawing.

### Brazing Process - Melting

For the process of brazing there are two main characteristics to consider, the melting properties and the flow behaviour. Brazing alloys by definition have to have a melting temperature lower than the materials that are being joined. This inevitably means that alloys designed for brazing low melting point materials (e.g. aluminium or brass) have to have a much lower melting than alloys designed for high melting temperature materials (e.g. steel or stainless steel).

Even with vastly different melting temperatures there is almost always a preference for melting temperatures to be as low as possible. A lower melting temperature means the brazing alloy is more versatile and in terms of industry means less expense is spent heating and parent materials are less altered by the heating process. A low melting temperature is one of the main drivers for alloy development and probably the biggest influencing factor in which alloy users would purchase.

Less important than low melting temperature is having a narrow melting range. Large melting ranges can lead to the problem of partial melting, which is called liquation or liquidation [12]. If a brazing alloy has a large melting range there would be a greater chance that part of the alloy might melt and form a joint before the entire alloy has melted. This means that the composition of joint will be unknown and so the properties of the joint are unknown also.

### Brazing Process - Wetting and Flow

Brazed joints rely on wetting and capillary flow to fill joint voids. The capillary action allows brazing filler metals to travel a relatively large distance (some joints can extend over several centimetres), fill complex joint voids and even flow against

gravity. There are many capillary flow formulae that can determine the different flow properties, such as speed, distance and how far it can travel against gravity [18].

One example of these formulae is the average velocity, $v$, of the capillary flow

$$v = \frac{D\gamma cos\theta}{6\eta s} \tag{2.1}$$

where $D$ is the joint gap, $\gamma$ the surface tension (or surface energy density) of brazing alloy, $\theta$ is the wetting angle (see Fig. 2.4), $\eta$ is the viscosity and $s$ is the distance the brazing alloy has travelled already [18]. As can be seen from formula 2.1 the best flowing alloys have a low wetting angle and a low viscosity. The wetting angle of a liquid alloy is controlled by the surface energies of molten alloy and the substrate the alloy is resting upon, as seen in Fig. 2.4.

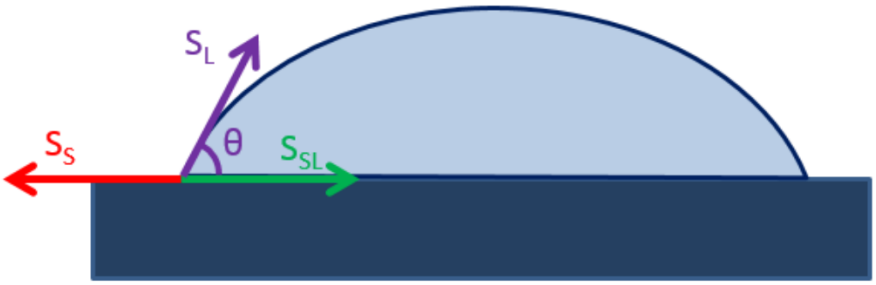


Figure 2.4: The balance of forces at the edge of the liquid alloy. The forces are described in formula 2.2.

The forces at the edge of the alloy, as seen in Fig. 2.4 can be expressed as

$$S_S = S_{SL} + S_L cos\theta \tag{2.2}$$

where $S_S$, $S_{SL}$ and $S_L$ are the surface tensions for the solid, solid-liquid interface and the liquid respectively [19]. Reducing the liquid surface energy value is one of the reasons that small additions of elements, such as tin, are added to brazing alloys [12].

The modelling of surface tension (which is the same as surface energy density) is a large area of research that has both relatively simple and complex models available

[19]. In this project the surface energy modelling will form a relatively minor part of the research and so the theory behind the modelling will be kept brief.

Surface tensions of pure elements can be found easily from a number of sources [20, 21]. The values are given as a linear equation dependent on Temperature, $T$. Formulae for multicomponent alloys are given using Butler's equations [22]. There are many forms with some based on Gibbs energies and others based on the activities of the elements. One form of Butler's equation is

$$\sigma_i = \sigma_i^0 + \frac{RT}{A_i} ln \frac{a_i^*}{a_i} \tag{2.3}$$

where $\sigma_i$ and $\sigma_i^0$ are the surface energies of element i in the alloy and the pure form respectively. $A_i$ is molar surface area of element $i$, $a_i$ is the activity and $a_i^*$ is the activity in the surface, all for element $i$. $R$ is the universal gas constant [22]. The Butler equations also show that the surface energy of each element in the alloy must be equal to each other [22].

**Reactive Wetting**

The wetting and surface energy formulae described previously are for non-reactive situations in which the liquid alloy and the solid substrate do not change composition. However, many brazing examples do involve a change in composition, with the elements moving between the molten brazing alloy and the solid substrate that is being brazed. This can lead to formation of an interfacial layer between the surfaces that is some mixture of the components or a new structure entirely (for example an IMC formed of elements from the liquid and substrate) [19, 23].

The differences between reactive wetting and non-reactive wetting are significant. In terms of modelling it means that many of the coefficients involved in the calculations change, often significantly. Essentially the molten brazing is now wetting on a thin layer of a different substrate than the remainder of the substrate. This layer will have a closer chemistry to the brazing alloy and so will usually aid wetting [24, 25].

Non-reactive wetting occurs instantly and once equilibrium has been reached (as in Fig. 2.4) then the alloy will remain in that state. Reactive wetting, however, involves the diffusion of elements and even the formation of IMCs. This can mean that liquid alloys can reach an initial wetting angle and then a final wetting angle once the reaction at the interface has completed. An example of this is shown in Fig. 2.5.

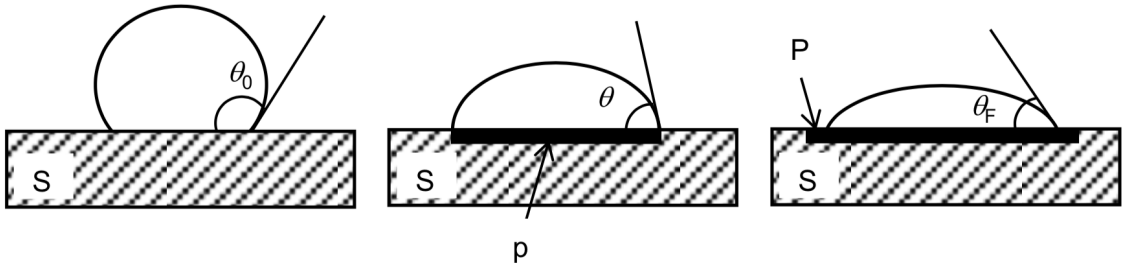


Figure 2.5: The three stages of reactive wetting. The left image shows the initial wetting angle, $\theta_0$, before wetting. The centre image shows the wetting angle, $\theta$ during wetting with only some diffusion into the layer, $p$. The right image shows the final interface layer, $P$, with the final wetting angle $\theta_f$. Image from Eustathopoulos [25].

The time scale for the reaction and formation of the interface layer can vary significantly. Some reactions can occur almost instantly and would occur almost simultaneously with the initial wetting and some reactions may occur over a longer time scale. An example is shown in Fig. 2.6.

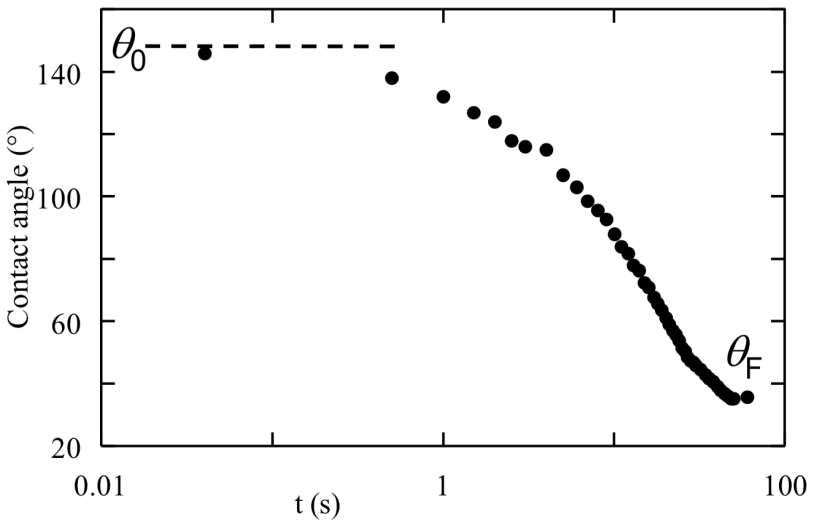


Figure 2.6: The change in wetting angle with time for the substrate in Fig. 2.5. The initial angle $\theta_0$ decreases to the final wetting angle, $\theta_f$. Image from Eustathopoulos [25].

#### Brazed Joint

Brazed joints, unlike soldered joints, have to be strong with joints often exceeding the strength of the parent materials. Comparison of the strength of brazing alloys is difficult as the strength of joints depends on many other factors besides the alloy. Joint type, dimensions, parent materials and the brazing technique all play a role in the strength of a brazed joint [12, 26].

Other properties, such as corrosion resistance, have variable importance. General corrosion resistance is required for all alloys but there are some alloys and applications where there is a special emphasis, for example brazed joints near seawater [27].

### 2.1.6 Brazing Alloy Systems, Compositions and Elements

#### Alloy Systems

There are countless alloy systems that are used for brazing. Using Johnson Matthey Metal Joining as an example of a supplier there are over 40 alloy systems (i.e. com-

binations of principal alloying elements) [14]. These systems are usually tailored for particular materials or techniques. In Table 2.1 there are some examples of the alloy systems and their intended uses.

Table 2.1: Examples of commonly used alloy systems that are used in brazing with their intended purposes and an approximate range of the liquidus temperatures [14, 28].

| **Alloy Systems** | **Intended Use** | **Range of Liquidus (°C)** |
|---|---|---|
| Ag-Cu-Zn-Sn | Versatile, low melting | 600-700 |
| Ag-Cu-Zn-Mn-Ni | Tungsten Carbide (WC) brazing | 700-800 |
| Ag-Cu-P | Brazing copper | 644-825 |
| Au-Cu | Aerospace | 850-1050 |
| Cu-Ni-Mn | High temperature steel brazing | 900-1000 |
| Cu-Zn-Ni-Si | Tungsten Carbide (WC) brazing | 900-920 |

### Compositions

Even within an alloy system there can be a great deal of variation in terms of the composition. Using the Ag-Cu-Zn-Sn system (the ISO 17672 range [14]) as an example, each element varies by a large amount. The major elements, Ag, Cu and Zn vary largely and even the Sn content varies by a small amount. The cost of the alloy depends significantly on the composition, especially the silver content. In Fig. 2.7 there are the compositions for some of the commercially available alloys in the Ag-Cu-Zn-Sn system [14].

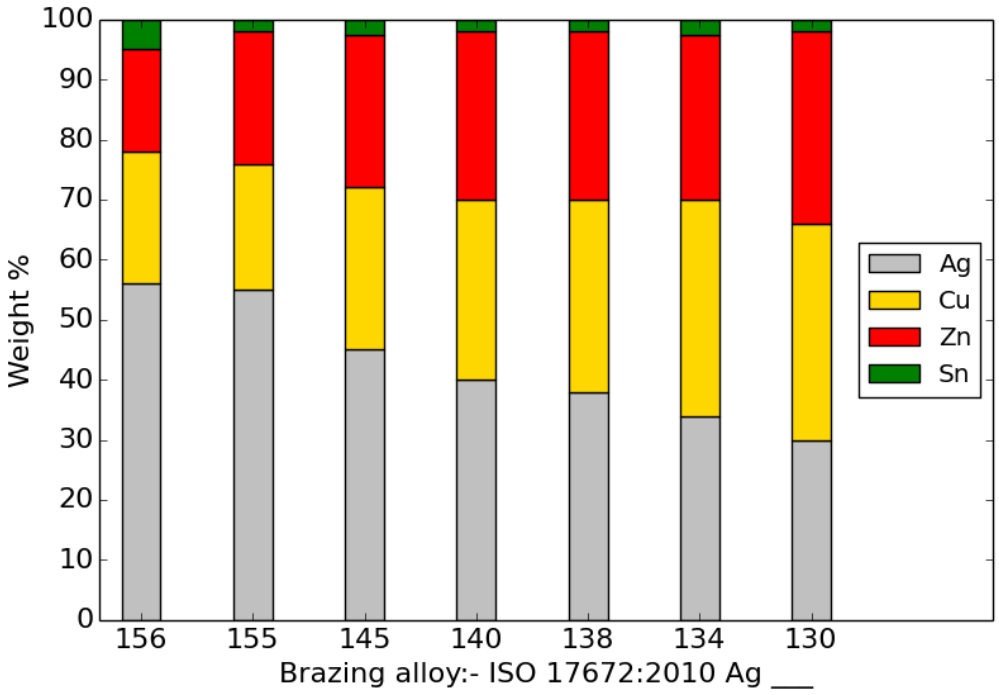


Figure 2.7: Compositions for several of the Ag-Cu-Zn-Sn brazing alloys that are available commercially listed by the alloy ISO designations [14].

As would be expected, the performance and the costs of these alloys vary significant with the changes in composition. The cost of the silver though does tend to dominate, with the other elements and processing costs relatively small in comparison. The brazing properties also vary significantly across the range, with an approximate relationship between cost and performance. More detail about the performance of these alloys can be found in Chapter 3. Similar ranges in composition and variation in properties are found in many of the other alloy systems that are used in brazing [14, 28].

### Elements

Brazing alloys, as with most alloys, achieve properties that are superior than elements in the alloy in isolation. Brazing alloys combine contrasting general properties of different elements. Mechanically excellent elements, such as silver and copper, offer

desirable mechanical properties but are high melting point. By contrast elements like zinc and tin have low melting temperatures but tend to form weak or brittle joints. Alloys will often try to combine these contrasting properties to achieve the best brazing alloys [29].

There are also considerations about how the elements interact. Eutectic compositions are ideal for brazing due to the reduced melting point, generally higher strength and toughness afforded by the microstructure and are frequently exploited within brazing alloys [12]. The solubilities of the elements with each other are also important for how controlling the phases once the elements are mixed. There is also the effect of the elements that are added in small amounts. For example, elements such as tin can be added to help the flow properties and silicon can be used to form a barrier to oxidation [30].

Elements are also selected or avoided for brazing specific materials or in particular techniques. An example of this is Co which is known to bond well to tungsten carbide [12, 31]. A counter example is zinc which cannot be included in vacuum brazing alloys due to its high vapour pressure. There are at least 15 elements [14, 28] commonly included in brazing alloys, a summary of the key elements is shown in Table 2.2. The positives and negatives of the elements also depend on the type of brazing. For example, increased copper may have a negative impact on silver brazing alloys by increasing the melting temperatures. However, the increasing copper content used in palladium brazing alloys would have an opposite, potentially positive, effect by reducing the melting temperature.

Table 2.2: Some of the most commonly used elements in brazing alloys. The strengths and weaknesses are listed with a focus on silver brazing alloys.

| **Element** | **Strengths** | **Weaknesses** |
|---|---|---|
| Ag | Ductile [12, 32], forms a eutectic with copper [33], flows well [34] | Precious metal |
| Cu | Ductile [35], good mechanical properties [35], forms a eutectic with silver [33] | Relatively high melting [36], moderately high cost |
| Zn | Low melting temperature [36] | Can form intermetallics, volatile, high vapour pressure, |
| Sn | Very low melting temperature [36], can improve wetting and flow [37] | Can form intermetallics, low solubility in zinc |
| Mn | Used for WC brazing | High melting temperature [36], can inhibit flow, leaves a residue |
| Ni | Used for WC brazing, aids wetting on steels | High melting temperature [36], can make inhibit flow |
| Co | Good high temperature properties [38], corrosion resistance [39] | High melting temperature [36] |
| In | Low melting temperature [36], improves wetting on steels [40] | Precious metal |
| Cd | Low melting temperature [36], Enhances the flow [41] | Toxic, banned in the UK and Europe [42] |

## 2.2 High Entropy Alloys

### 2.2.1 Definition

High Entropy Alloys (HEAs) are a set of alloys that form a simple structure despite having many components and no dominant element. A commonly used composition limit requires that HEAs have five or more components between 5 at.% and 35 at.% [43, 44, 45]. These composition limits, however, are not strict and there are many examples of alloys that are stated as being a HEA while not abiding by the rules stated above. There are many HEAs that have only four components [45, 46], HEAs that have a component above 35 at.% [46] and HEAs that have a component below 5 at.% [46, 47].

The definition of a simple structure has previously been defined as a single phase solid solution with a no intermetallic compounds (IMC) present [44, 45]. However, there are many HEAs that have two phases present [48, 45] and some reports that allow small amount of IMC to be present [49]. A broader definition can be summarised as proposed by Dahlborg et al. that HEAs are "multicomponent alloys presenting simple diffraction patterns" [50].

The compositional HEA definition naturally imposes an entropy limit on the alloys, as they have to adhere to the composition limits. These limits though are somewhat arbirary and were not designed with the entropy values in mind. The configurational entropy, $\Delta S_{mix}$ can be calculated using a form of Boltzmann's equation

$$\Delta S_{mix} = -R \sum_{i=1}^{n} c_i ln c_i \tag{2.4}$$

where $R$ is the universal gas constant and $c_i$ is the atomic fraction of element $i$ from $n$ number of total elements [51]. An entropy-based definition of HEAs is given based in terms of R. The definition defines low entropy as $\Delta S_{mix}$<0.69R, high entropy as $\Delta S_{mix}$>1.61R and medium in between the two limits [45, 52].

This limit would mean almost all six component alloys to count as high entropy, but would restrict five component alloys to just those near equiatomic and four component HEAs would be impossible. Entropy calculations and HEA limits are discussed further in section 2.3.

### 2.2.2 Origins

Most conventional alloys either have one dominant element with a handful of trace elements, such as many constructional steels, or just a few elements alloyed together, such as brass or bronze. HEAs can be regarded as an evolution from these alloys, moving from the corners and edges of a phase diagram towards the centre. This is the case for some research where HEA research has overlapped with stainless steel research [53]. For the most part though HEA research is considered as its own field with its own history and community.

As a separate subject, the origin of HEAs is usually attributed to Brian Cantor in 1981. Cantor, with his student Alain Vincent, was working on multi-component alloys in 1981 when they noticed that one of the compositions formed a single face centred cubic (FCC) phase [45]. The alloy, FeCrNiMnCo, has later become known as Cantor's alloy and has become the basis of a great deal of HEA research [54, 55, 56].

In the decades that followed Cantor's work there were a number of independent studies looking at multi-component alloys. Hsu [57] and Yeh [49] both contributed significant publications along with other authors investigating multi-component alloy formation or some related property. A significant milestone for the concept of HEAs, was in 2004 with the publication of, "Nanostructured high entropy alloys with multi-principal elements - novel alloy design and concepts", by Yeh et al. [49] and the term HEAs became a much more widely accepted and prominent field of research. T

### 2.2.3 The Elements Involved in HEA Research

In recent years HEA research has rapidly expanded with new elements, greater levels of fundamental understanding and studies into enhanced properties. HEA research is now well established with many books and thousands of specific journals published [45, 52]. There is also a HEA community of scientists with symposia and conferences annually.

The first HEAs were based on transition metal elements, often focused on CoCrFeMnNi. The majority of research on HEAs since then has been based on these elements and other transition metal elements such as Al, Cu and Ti [52]. There has been a smaller, but significant, off-shoot from this set of elements though, with refractory elements such as Zr, Nb, Mo and Ta also featuring prominently in HEAs. The element distribution in reported research has been collected and summarised by Miracle and Senkov [52] and is shown in Fig. 2.8.

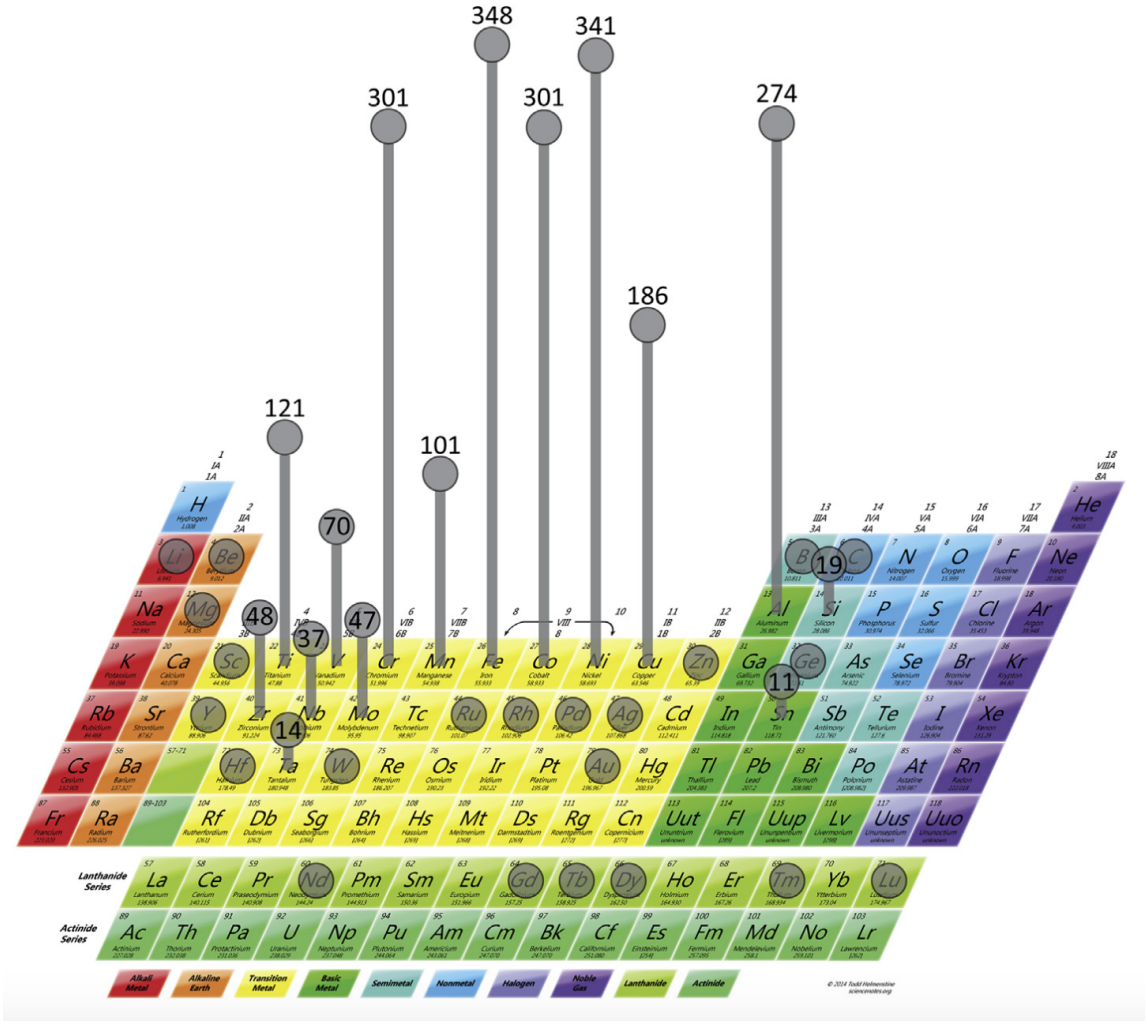


Figure 2.8: A periodic table showing the frequency of HEAs from the review paper by Miracle and Senkov. The frequency are from a total of 408 HEAs included in the review. Research and image from Miracle and Senkov [52]. The original periodic table prior to editing is from Sciencenotes.org at http://sciencenotes.org/printable-periodic-table as referenced by Miracle and Senkov.

As can be seen in Fig. 2.8 there are some but not many HEAs with atypical elements. There are small numbers of HEAs that contain zinc, precious metals and other atypical elements from around the periodic table. These are a very small minority though in comparison to the main group of elements. Among the atypical elements were a handful of HEAs that featured Ag, which is an element of particular interest

in brazing alloys. Among the papers featuring Ag were Hsu et al. [58] and Munitz et al. [59] who had similar papers on a particular HEA. Also, Laktionova et al. [60] and Sohn et al. [61] had reports on other aspects of Ag-based HEAs.

Hsu et al. in 2007 and Munitz et al. in 2012 both worked on a AlCoCrCuNi-based HEA. Both reports investigated the addition of silver to the alloy and the resultant phases. Hsu et al. was looking at the alloying effects additional Ag, Fe and Au while Munitz et al. was looking specifically at Ag and the melt separation that occurs. Both papers found that Ag was incompatible with the HEA mixture. The Ag would mix with the Cu and form a separate phase macroscopically segregated from the other HEA ingredients [59]. Munitz also investigated AlCoCrCuFeNi with the addition of silver and found similar results. By contrast, Hsu trialled the same approach but with Au had found the opposite result, that the gold helped the copper mix and there was no segregation [58].

Laktionova et al. [60] worked on the mechanical properties of $Ag_{0.5}$CoCrCuFeNi at low temperatures. The alloy was tested from 300K down to 4.2K in order to measure the difference in yield strength and plasticity. The changes with temperature were as expected with a significant increase in yield strength from 450 MPa to 750 MPa. The alloy had two FCC phases, with no report of IMC content, and so by most definitions counted as a HEA. The silver content of 9.09 at.% though is not high, so although it is a silver containing HEA the silver is only a minor constituent.

Sohn et al. [61] researched a number of HEAs containing noble metals. The main alloy researched was a PtPdRhIrCuNi that formed a single phase FCC solid solution. The alloy was annealed confirming its status as a HEA as no phase changes were found and was mechanically tested revealing high strength and large ductility. A number of other noble metal HEAs were created with many containing silver. Of the alloys that were single phase one of them contained silver. The four component alloy AuPdAgPt had one phase and can be defined as a HEA even though it only contains four components. There were also some two phase structures among the

alloys researched. AuPdAgPtCu had two FCC phases, with the copper contributing to formation of the second phase [61].

### 2.2.4 Thermodynamics of HEAs

#### Gibbs Energies and Phase Selection

A large amount of the HEA thermodynamics relates to the competition between phases using Gibbs energy equations. The thermodynamics of HEAs refers to the tendency of HEAs to form solid solution rather than IMCs. As stated previously, this does not necessarily mean a single phase alloy with no other phases. Various definitions allow for multi-phase HEAs and small amounts of IMC.

The tendency to form solid solutions rather than IMCs is the main difference between a HEA and a non-HEA composition. In a multi-component alloy there are many interactions as there are many element pairs. It is often expected that some of these interactions will lead to IMC formation, segregation and sub-lattices [45]. These would usually, but not always, then cause embrittlement of the alloy and would prevent the alloy from being used in service.

The formation of a simple structure (HEA) can be thought of by considering classical Gibbs energy rules, with different structures competing to find the lowest energy. Using the Gibbs energy equation

$$\Delta G_{mix} = \Delta H_{mix} - T\Delta S_{mix} \tag{2.5}$$

where $\Delta G_{mix}$ is the Gibbs energy of mixing, $\Delta H_{mix}$ is the enthalpy of mixing and $T$ is the temperature. The competing possible structures are elemental phases, separate compounds, IMCs and a random solid solution (which is the structure associated with a HEA). When these Gibbs energies are calculated for each possible structure the random solid solution will form when it has the lowest Gibbs energy. The full calculations and explanations of the derivations are explained in multiple sources [62].

Of course this is not the complete picture and many other factors have to be considered. This is only the simplest form of the Gibbs energy equations, there are more complex forms that have more terms and extra factors to consider [62]. Another significant factor that has been largely ignored so far is the potential lattice distortion and the strain energy that is stored with this effect [62].

### Lattice Energy, Distortion and Phase Selection

The lattice energy of the HEA structures is used to describe whether HEAs will form, the structure and the various properties that are dependent on the lattice. The lattice in a random solid solution, usually either FCC or BCC, contains different elements randomly distributed on the atom sites. A diagram of this arrangement can be seen in Fig. 2.9.

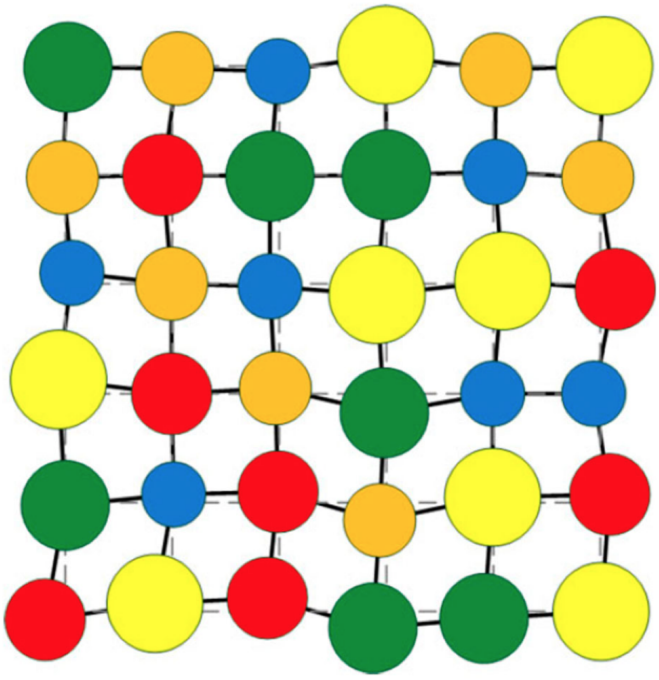

Figure 2.9: A monolayer of atoms representing the strained lattice of a HEA. Different sized and coloured circles represent the different atoms that comprise a HEA. Image from Pickering and Jones [63].

The lattice being made up entirely of differently sized atoms leads to the lattice distortion being so large, often labelled as being 'severe'. This severe lattice distortion has a number of effects on the properties of HEAs. It can impede dislocation motion causing a large amount of solid solution strengthening, which in turn produces an increase in hardness and strength. The enhanced strength properties is a common motivation for HEA research, with numerous examples of research into high hardness or high strength HEAs [64, 65]. The lattice distortion also has effects on the electron based properties. Both the electrical and thermal conductivities are reduced due to the electron and phonon scattering.

The lattice distortion and the stored strain energy also have an important role in the prediction of HEAs. If the size of the atoms differ greatly then the lattice distortion becomes too large and the HEA will not form. This is addressed in more detail later in this chapter.

One effect that has been used as evidence to support the theories around severe lattice distortion is the XRD results. The XRD scans show a lower intensity which is attributed to the distortion of the phases that the XRD is detecting [52]. Despite this evidence and many publication that refer to the effect, there are recent studies that cast doubt on how much can be attributed purely to lattice distortion. Review papers by Miracle and Senkov [52] and Pickering and Jones [63] are two recent examples.

The uncertainty falls into two categories. There are questions about just how much lattice distortion is actually present. There is relatively little experimental evidence that the distortion predicted is present. It could be that the distortion is of a similar magnitude as conventional alloys that have solid solutions present.

There are also some questions about whether the lattice distortion is the only factor affecting the properties that are attributed to lattice distortion, such as enhanced strength and resistivity. There are many other effects that may have a role in affecting these properties and more research is required to fully understand which are the most critical.

### The Four Core Effects of HEAs

The previously mentioned effects, high entropy and strained lattice, are often grouped together with two other effects and referred to as the four core effects of HEAs. The previously discussed high entropy effect and the severe lattice distortion effect are accompanied by the sluggish diffusion effect and the cocktail effect. These effects are widely cited and feature in prominent books and papers on HEAs. However, there is some scepticism of the four core effects with concerns over a lack of evidence and potential contrary evidence [52, 63].

### The Sluggish Diffusion Effect

This effect refers to the potentially slow diffusion of atoms in HEAs. The hypothesis is that as the HEA has a structure made up of different elements it is harder for elements to diffuse through compared to a regular solid solution [45]. Some have attributed this to variations in potential energies between lattice sites [66]. Other though suggest it is related the distorted lattice [67]. The effect is referred to as an explanation for experiment results by multiple reports [68, 69, 70]

A significant problem with assessing the sluggish diffusion effect is the difficulty in directly measuring diffusion coefficients. To the knowledge of the author there is only one paper to date that has measured the values experimentally. Tsai et al. [71] examined CrMnFeCoNi and found that the activation energies were higher in the HEA. The majority of the evidence to support sluggish diffusion comes from secondary measurements of effects that were caused by sluggish diffusion.

Two examples of evidence for sluggish diffusion come from the appearance of nanocrystals. Nanocrystals found in $Al_xCoCrCuFeNi$ [70] and AlCrMoSiTi [72] were both thought to be explained by sluggish diffusion. However, review papers on HEAs [52, 63] have found an overwhelming number of examples that contradict these results. Ultimately there is enough evidence to doubt the presence of the sluggish diffusion effect and so it can be ignored.

#### The Cocktail Effect

This cocktail effect refers to how the properties of HEAs can be superior than any of the constituent elements. It was originally coined by Ranganathan et al. in his paper from 2003 [73].

A major problem with the cocktail effect as a useful concept is that it can refer to almost any alloy. An alloy having properties that are superior that the constituent parts describes most alloys employed and is often the main reason an alloy was created in the first place. Alternatively some sources use the effect to simply describe the effect as unexpected or unusual properties that are associated with HEAs. Regardless of the exact definition, the effect is not implementable for predictions and can be ignored for any HEA calculations or design considerations.

### 2.2.5 Potential Uses of HEAs for Brazing

Some of the enhanced properties associated with HEAs have already been mentioned in this chapter. Due to the wide variety of brazing methods and applications there are many different situations where these enhanced or unusual properties may have a benefit.

Due to the solid solution strengthening there are many reported cases of HEAs having enhanced strength and hardness [64, 65]. Most brazed joints rely on their mechanical properties in one form or another, so an increase in strength would be useful for some brazed joints in particular applications.

Enhanced thermal stability has not been discussed so far in this thesis but has been reported multiple times [74, 75]. There are a number of applications that use brazed joints and operate at an elevated temperature. One example would be a deep sea drill that uses tungsten carbide. The hard but brittle tungsten carbide pieces are brazed to the more ductile steel pieces usually with a silver-based brazing alloy. This drill piece will operate at elevated temperature due to the friction while drilling. If

any novel brazing alloy could be designed to have a higher operating temperature it would mean the drill could operate at a higher temperature and be used to be a provide a superior cutting performance. This does not alter the fact that a relatively low melting point is desirable in these brazing alloys.

There are many other brazing related properties that can potentially be improved by using HEAs. These properties are not achieved using HEA effects rather they are effects associated with elements that can be used in novel compositions. As HEAs offer entirely new regions of composition space to explore it means some elements can be used in greatly different quantities compared to conventional alloys.

Access to radically different compositions has the potential to improve almost any brazing property. Alloys that have lower melting temperatures, better flow properties and lower cost could potentially be achieved by increasing elements that are known to be effective at those respective properties. Such elements include zinc that is low cost and used to lower melting temperatures and tin that has a very low melting temperature. Increasing the quantities of these elements is usually limited as these elements and similar are known to form IMC.

### 2.2.6 Cooling rate, critical temperature, metastability.

The issue of metastability is an important one for HEAs in terms of understanding the thermodynamics and the production of the alloys. The metastability of these alloys can be explained using some theories already discussed, although these theories are not universally accepted and so have some doubts attached. As mentioned the random solid solution of a HEA is in competition with a myriad of lattices and IMCs that could form from the elements in the alloy [45]. The sluggish diffusion has been to help prevent these IMCs forming [76]. It would be expected that annealing these alloys would allow some IMCs to form and it to be no longer a HEA.

The results of annealing support the arguments about metastability. The majority of research into HEAs uses as-cast alloys. When these alloys are compared to the

alloys that have been annealed, there is a clear difference. Many of the HEAs that were reported as being entirely solid solution (SS) were reported after annealing as being a mixture of solid solution and intermetallic (SS+IM). A comparison of results from before and after annealing is shown in Fig. 2.10a. The number of phases present also increased with annealing Fig. 2.10b. The data for HEAs were collected by Miracle and Senkov [52] and shown in the graphs in Fig.2.10.

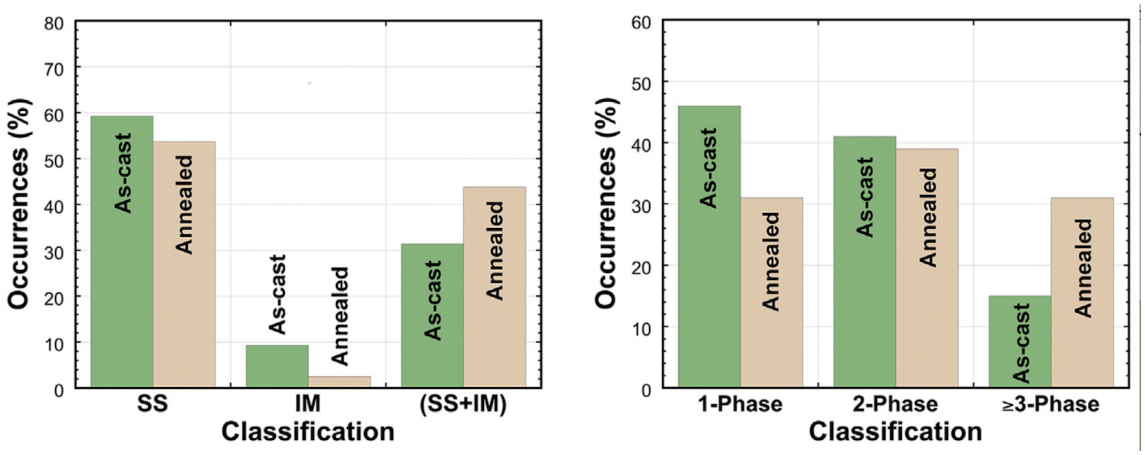


(a) The types of phase present.

(b) The number of phases present.

Figure 2.10: The microstructure results from a review of 239 reports and 46 alloys. The effects of annealing by comparing the as-cast results and the annealed results from the various data sources. Fig. 2.10a shows the types of phases present and Fig. 2.10b shows the number of phases present. Data was collected and the graph produced by Miracle and Senkov [52].

Two properties directly connected to the metastability are the critical temperature and the cooling rate. Both of these terms go toward determining the stability of the HEA metastable state. The critical temperature refers to the temperature at which entropy term is large enough to make the Gibbs energy equal to zero [77]. According to the Gibbs equation (equation 2.5) the temperature independent enthalpy is countered by the negative entropy term that increases with temperature. This has a direct effect on whether HEAs are likely to form or not [77].

The cooling rate is important for controlling IMC formation. A slow cooling rate will allow the IMCs that would normally be suppressed to form [77]. This reason means that the majority of HEA research uses methods with a fairly rapid cooling rate, such as arc melting or melt spinning, for the production of alloys.

### 2.2.7 Processing of HEAs

The vast majority of HEAs are produced using some form of melting and casting technique. Vacuum arc melting is the most commonly used technique but induction melting and melt spinning are also used [52, 63]. There are a few key criteria that these techniques need to meet.

High melting temperatures are required to melting the higher melting elements and to ensure the alloy is properly mixed, an oxygen free atmosphere is necessary for the sake of alloy purity and finally a relatively rapid cooling rate is necessary to prevent IMCs forming [52, 77].

There are other techniques used to produce HEAs that are not based on melting and casting. Two examples are mechanical alloying and deposition. Mechanical alloying is a method that uses a ball mill, or similar device, to mix and grind the alloy elements into a fine powder before being pressed together. This process causes deformation in the solid state with no external heating with the end result being a bulk sample. An examples of this can be found by Mohanty et al. [78].

Deposition techniques, such as sputtering, have been used to create thin-film HEAs. One example is Braeckman and Depla who sputtered NbCoCrCuFeNi thin films [79]. There are many other examples of similar techniques but the alloys made this way still only make a small fraction of the HEAs produced.

## 2.3 Prediction and Modelling of HEAs

The extremely large number of potential HEA systems and compositions present a daunting challenge without the aid of modelling. These predictions are focussed on whether an alloy will form a random solid solution (a HEA) or will form something else, such as an IMC or a segregated alloy. HEA predictions are also used to look at more detailed aspects of phase structure including the type of structure and the number of phases [80].

Although different in a number of significant ways there is some overlap with HEA predictions and Bulk Metallic Glass (BMG) predictions. There are a number of parameters that are used for both HEA formation and BMG formation. The formation regions though for HEAs and BMGs are usually very different, with ideal values at opposite ends of the scale. One example would be the atomic size difference (which is covered in more detail in the next subsection). Multiple papers use the atomic size difference to look at HEA and BMG formation [81, 82]. The HEA formation region though requires a low value, so the atoms can fit together into lattice, but the BMG formation region requires a high value that so that atoms can greatly reduce the amount of free space and can form a glass structure.

There are countless modelling techniques that have been proposed based on different aspects of HEA formation and with varying levels of accuracy and success. Most of these techniques are based on a physical property that is thought to be relevant to the formation of HEAs [45]. However, the limits or thresholds that these rules use tend to be empirical rather than having a calculated origin.

While some modelling techniques are more successful than others none of them are perfect. In all of the modelling techniques there are examples of alloys that do not adhere to the predictions. Even with this degree of uncertainty most modelling methods offer significantly improved chances of finding a HEA than a random sampling of alloys. The modelling techniques are sometimes used independently but some of the rules, usually the simpler ones, are used in conjunction with each other.

### 2.3.1 Predicting HEA Formation with Hume-Rothery Based Rules

#### Atomic Size Difference

The atomic size difference is one of the most widely used parameters in HEA prediction. It is also referred to as the atomic size mismatch, delta or $\delta$ just as the symbol. $\delta$ uses the atomic radii values of the elements to provide a measure of how well these atoms can fit together in a lattice. It is similar to one of the Hume-Rothery rules, specifically the first rule relating to atomic radii [83]. The first Hume-Rothery rule is a measure of the % difference in atomic size between a solute and a solvent, which is given as,

$$\% \text{ difference} = \left( \frac{r_{solute} - r_{solvent}}{r_{solvent}} \right) \times 100\% \leq 15\%. \tag{2.6}$$

where $r$ is the atomic radius of the solute and the solvent. The rule states that for a solid solution to form, assuming the other Hume-Rothery criteria are met, the value has to be equal or less than 15%.

The HEA equivalent of this rule, $\delta$, does not have a solute and solvent as described in equation 2.7 due to the nature of the composition not having a dominant element. The $\delta$ equation is given by,

$$\delta = 100 \sqrt{\sum_{i=1}^{n} c_i \left(1 - \frac{r_i}{\bar{r}}\right)^2} \tag{2.7}$$

where $c_i$ is the atomic concentration of element $i$ for $n$ elements, $r_i$ is the radius for element $i$ and $\bar{r}$ is the average atomic radius. The average radius is given by

$$\bar{r} = \sum_{i=1}^{n} c_i r_i \tag{2.8}$$

using the same terms as used in equation 2.7.

A number of sources refer to limits on $\delta$ for where HEAs will form. Values as low as possible are preferred with various upper limits set out by different sources. Maximum values of 8.5% [81] and 6.5% [84] have both been quoted. The upper limits

are sometimes also dependent on other properties. For example, the HEA region used by Zhang et al. [85], shows that for if the enthalpy of mixing is lower then a larger atomic size difference can be allowed. This plot is shown in Fig. 2.11.

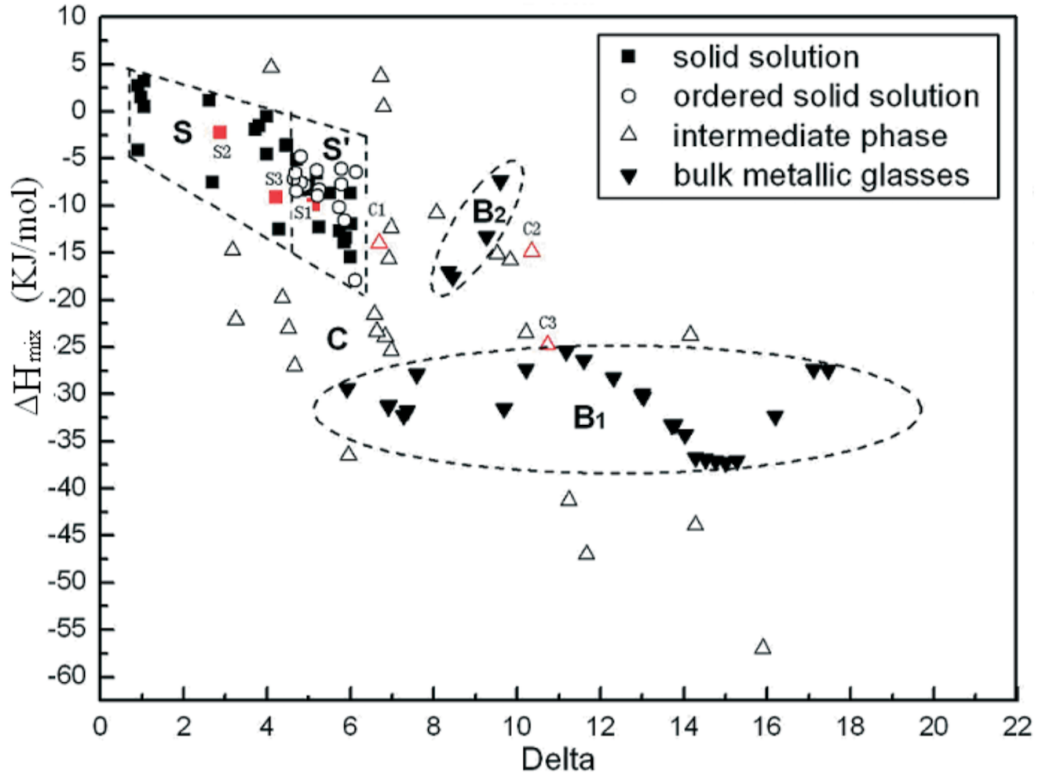


Figure 2.11: Data plotted for various phases with regions for phases shown with dashed lines and the legend provided. This plot is from Zhang et al. [85].

Most publications that use atomic size difference do not quote a lower limit on the $\delta$. The plot in Fig. 2.11 by Zhang et al. does show a HEA region that has a lower $\delta$ limit of 1% rather than 0% that would be expected. However, this can likely be attributed to the source of the plot. As the plot was developed using experimental data points, and the discrepancy between 0% and 1% is likely just due to a lack of data in this region.

The $\delta$ is not usually used on independently. It is usually used with some other modelling parameter, usually a method that is connected to the enthalpy or the Gibbs energies in some way. Examples are shown later in this section of $\delta$ being used with

the enthalpy of mixing and the Yang parameter.

The $\delta$ method used here is not unique and there are other methods that attempt to measure essentially the same property but using different formulae. One example of another is from Wang et al. in 2015 [86]. This paper attempted to predict how much atoms were displaced away from their location in an ideal, unstrained lattice.

This is expressed in its simplest form as,

$$\alpha_1 = \sum_{i}^{n} \frac{c_i |r_i - \bar{r}|}{\bar{r}} \tag{2.9}$$

where $\alpha_1$ is a dimensionless measurement of the displacement and the other terms are the same as the previously stated. The paper found this measure too simple however and often provides an overestimate of the true value. A better way to use this equation was to consider pairs of atoms, and each possible pair of atoms will displace from the ideal lattice.

$$\alpha_2 = \sum_{i}^{n} \sum_{j \geq i}^{n} \frac{c_i c_j |r_i + r_j - 2\bar{r}|}{2\bar{r}} \tag{2.10}$$

with subscript term $j$ referring to element j and with the symbols remaining the same. In the full calculations by Yang et al. there are further formulae that add extra atoms to the calculation. The example goes up to $\alpha_5$ but could go to any number, $\alpha_n$. However, the more atoms that are added this will have the effect of averaging out distortions and reducing the $\alpha_n$ to zero. The paper proposes that $\alpha_2$ be used as the HEA parameter.

There does appear to be some benefits to this method. The main parameter, $\alpha_2$, is used for various calculations and predictions within the publication. However, other use of the parameter is limited, especially in comparison to the $\delta$ parameter.

In terms of using this parameter in future work, the main problem is the lack of publications. Compared to the $\delta$ parameter there are a lot fewer publications and a predictive modelling methods available to use and to refer to.

### Electronegativity

Analysis of the electronegativity relates closely to the fourth Hume Rothery rule [83]. The rule states that for complete solubility the difference in electronegativities between solvent and solute needs to be small [83]. As there is no dominant element to be the solvent structure, an average of the electronegativity is used to compare the different elegtronegativity values. This is expressed in an equation as

$$\chi = \sqrt{\sum_{i=1}^{n} c_i(\chi_i - \bar{\chi})^2} \tag{2.11}$$

where $c_i$ is the atomic concentration of element $i$ for $n$ elements, $\chi_i$ is the eletronegativity of element $i$ and $\bar{\chi}$ is the average electronegativity, which is calculated using,

$$\bar{\chi} = \sum_{i=1}^{n} c_i\chi_i \tag{2.12}$$

where terms are the same as in equation 2.11

However, while a number of papers refer to electronegativity calculations and even have the data listed in the results table, they do not use them for any HEA predictions [81]. Most HEA prediction papers do not use or discuss electronegativity modelling at all.

### Residual strain

Using the residual strain of lattices for HEA calculations has similarities with the atomic size difference measurement used within the Hume-Rothery rules. Both measurements are based on the different sizes of the atoms in HEAs and the effect that has on the subsequent lattice. Also, both show HEA regions are more likely at low values and measurements are often used on plots with enthalpy of mixing measurements. One difference however is the level of complexity. The residual strain measurements have a much more involved derivation and more complex resultant equation.

The equation was developed by Ye et al. where a full derivation can be found [87]. The reason the equation was created was to address problems with calculating

the residual strain of a random solid solution. Existing residual strain equations are equipped to deal with the effect of a solute on a solvent [88]. This is problematic for HEAs as there is no solvent or solute in the usual sense. The equation used for measuring HEAs therefore attempts to solve by looking at all the different atomic interactions of all the species.

The equation for the residual strain, $\epsilon$, is especially complicated with many terms requiring long and detailed explanations. The derivation works with the solid angles between atoms $\omega_{ij}$ to calculate the atomic packing efficiency $\eta$. This can then be used to calculate the incremental changes in atomic packing due to neighbouring atoms and the residual strain that is caused by this.

The residual strain for each atom $\epsilon_j$ can then be calculated. The weighted sum of these residual strains is equal to zero, or

$$\epsilon = \sum_{i=1}^{n} c_i \epsilon_i = 0 \tag{2.13}$$

where $c_j$ is the atomic fraction of element $j$. This is apparent as the total volume of the alloy remains constant. Any lattice distortion, and the residual strain caused by it, in one direction will be countered by a different pair of atoms. So for example, moving an atom closer to one neighbouring atom will mean that the atom is further away from the neighbour in the opposite direction. To measure how much residual strain is in an alloy it is necessary to use the root mean squared (RMS). Once the $\epsilon$ has been squared,

$$\langle \epsilon^2 \rangle = \sum_{j=1}^{n} c_j \epsilon_j^2 \tag{2.14}$$

the RMS residual strain, $\langle \epsilon^2 \rangle^{0.5}$, can then be calculated and can be used for HEA prediction.

Ye et al. who carried out this work and derivation of the equation, used the RMS residual strain with a number of other properties. One measurement that RMS residual strain was plotted against was a dimensionless elastic energy. This elastic energy was demonstrated to be proportional to the RMS residual strain and is shown

on a plot in Fig. 2.12.

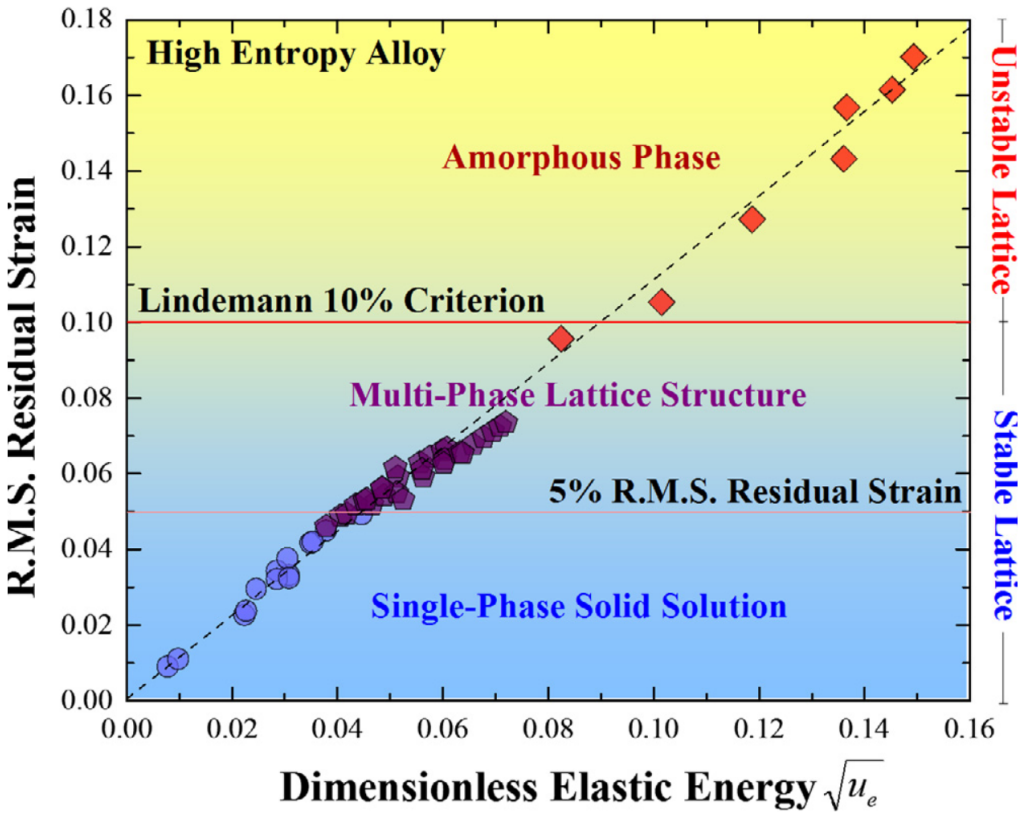


Figure 2.12: The RMS residual strain plotted against the dimensionless elastic energy. The blue shading indicates the stable lattice region and the yellow shading indicates the unstable lattice region. The data, work and graphs all from Ye et al. [87].

The results in Fig. 2.12 shows some limits on HEA formation. The 10% RMS residual strain is reported as the value that is the limit between a stable and unstable structure. The 5% RMS residual strain is proposed as a limit for the formation of single phase structures.

More useful for this study of HEAs though is the plot of RMS residual strain with the enthalpy of mixing, $\Delta H_{mix}$. This plot was also included by Ye et al., for the same data set, and is shown in Fig. 2.13. As residual strain can be related to the atomic size difference it means that this plot is similar in appearance to the plot in Fig. 2.13.

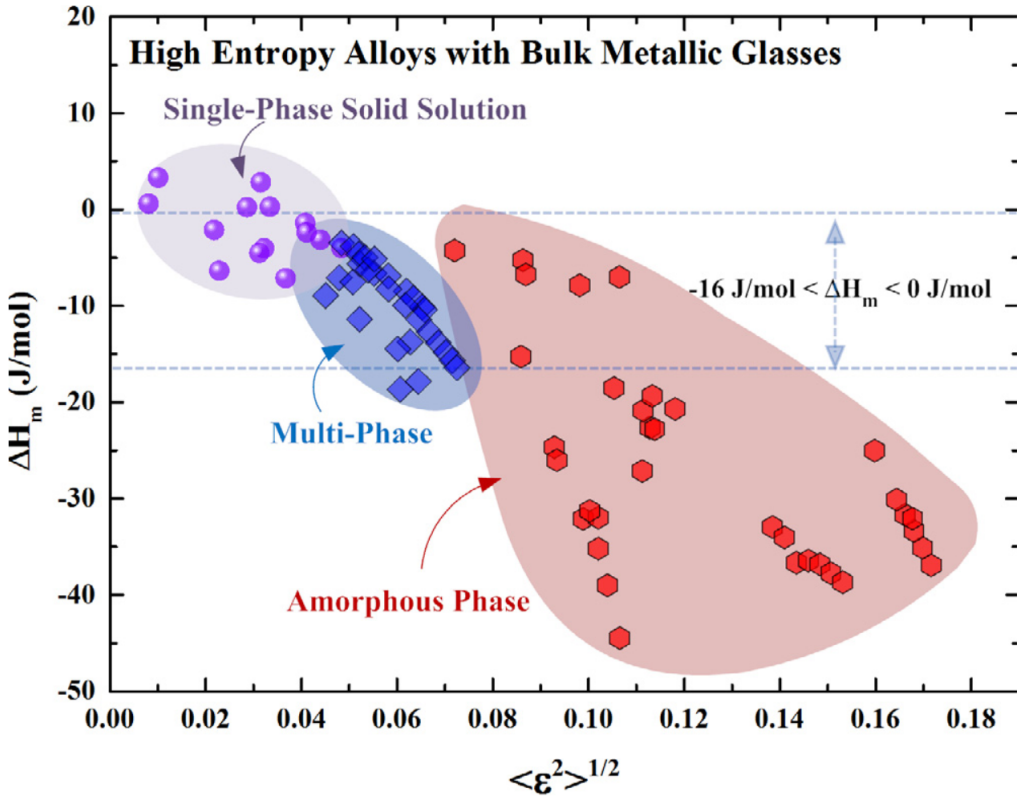


Figure 2.13: The RMS residual strain plotted against the enthalpy of mixing. The shaded regions represent the areas where the labelled phases are found. The data, work and graphs all from Ye et al. [87].

This plot shows the same limits for RMS residual strain as before and uses a $\Delta H$ criteria of -16 $\leq \Delta H \leq$ 0 J/mol. The plot in Fig. 2.13 has regions highlighted for single and multi phase alloys for the same data set that was used in Fig. 2.12.

### 2.3.2 Predicting HEA Formation with Gibbs Energy Based Rules

#### Enthalpy of Mixing

The enthalpy of mixing, $\Delta H_{mix}$, is frequently used as a formation criteria for both HEAs and BMGs. There are different ways of calculating $\Delta H_{mix}$ available but by far the most commonly used is the Miedema method [82]. This method estimates the

overall enthalpy of an alloy by assigning a coefficient to each binary pair and using a weighted average to analyse the whole system. This is expressed in an equation as

$$\Delta H_{mix} = 4 \sum_{i=1,i<j}^{n} c_i c_j \Omega_{ij} \tag{2.15}$$

where $c_i$ and $c_j$ are the atomic fractions of elements $i$ and $j$ respectively and $\Omega_{ij}$ is the enthalpy coefficient for elements $i$ and $j$. The coefficients used for the binary pairs are calculated using first principles and are confirmed with experimental data [82]. Usually in publications that feature HEA predictions these values are not recalculated and instead are found from tabulated values. An example section of the Miedema table is shown in Fig. 2.14 from Takeuchi and Inoue [82]. A full version of the Miedema table is shown in Appendix A.

| 1 | 3 | 4 | 5 | 6 | 7 | 11 | 12 |
|---|---|---|---|---|---|---|---|
| H | Li | Be | B | C | N | Na | Mg |
| H | -25 | 2 | 5 | -3 | -18 | -16 | -19 |
| | Li | -5 | -6 | -61 | -145 | 4 | 0 |
| | | Be | 0 | -15 | -39 | 18 | -3 |
| | | | B | -10 | -28 | 18 | -4 |
| | | | | C | -2 | -45 | -55 |
| | | | | | N | -141 | -134 |
| | | | | | | Na | 10 |
| | | | | | | | Mg |

Figure 2.14: A sample from a Miedema table. Table taken from Takeuchi and Inoue [82] who used values from an earlier paper by Takeuchi and Inoue [82].

The HEA formation limits for the $\Delta H_{mix}$ vary significantly between sources. Table 2.3 shows some of the various limits that have been published on HEA formation. The $\Delta H_{mix}$ formation limits are usually used with some another variable. The other limits used are shown also in Table 2.3.

Table 2.3: A variety of different enthalpy limits from HEA publications with the other limits that accompany them.

| Enthalpy limits (kJ/mol) | Other limits | Year | Reference |
|---|---|---|---|
| -22 $\leq \Delta H_{mix} \leq$ 7 | $\delta < 8.5$<br>11 $\leq \Delta S_{mix} \leq$ 19.5 J/(Kmol) | 2011 | Guo & Liu [81] |
| -12 $< \Delta H_{mix} <$ 10 | $\delta < 6.5$ | 2013 | Guo et al.[84] |
| -16 $< \Delta H_{mix} <$ 0 | $\langle \epsilon^2 \rangle^{0.5} < 10\%$ | 2015 | Ye et al.[87] |

The enthalpy limits in Table 2.3 are assumed to be independent of the other limits included. For example, if the $\delta$ value in an example from Table 2.3 is close to zero or close to the limit (highly favourable or borderline unfavourable respectively), then the enthalpy limits remain the same. There are however, some publications that use enthalpy limits that are dependent on other variables. This was shown already in Fig. 2.11 where the enthalpy limit changes with the delta value. This plot by Zhang et al. was seemingly created by manually fitting the HEA formation region around the data. The trend shows that for alloys with a larger delta value then a more negative enthalpy is required but there is no mention of a physical reason for this.

Another example of a variable enthalpy limit is by Toda-Caraballo and Rivera-Diaz-del-Castillo [89]. They use a variable, $s_m$, that is discussed in more detail later in this section, is roughly equivalent the $\delta$ value. The HEA formation for $s_m$ and $\Delta H_{mix}$ is shown in Fig. 2.15.

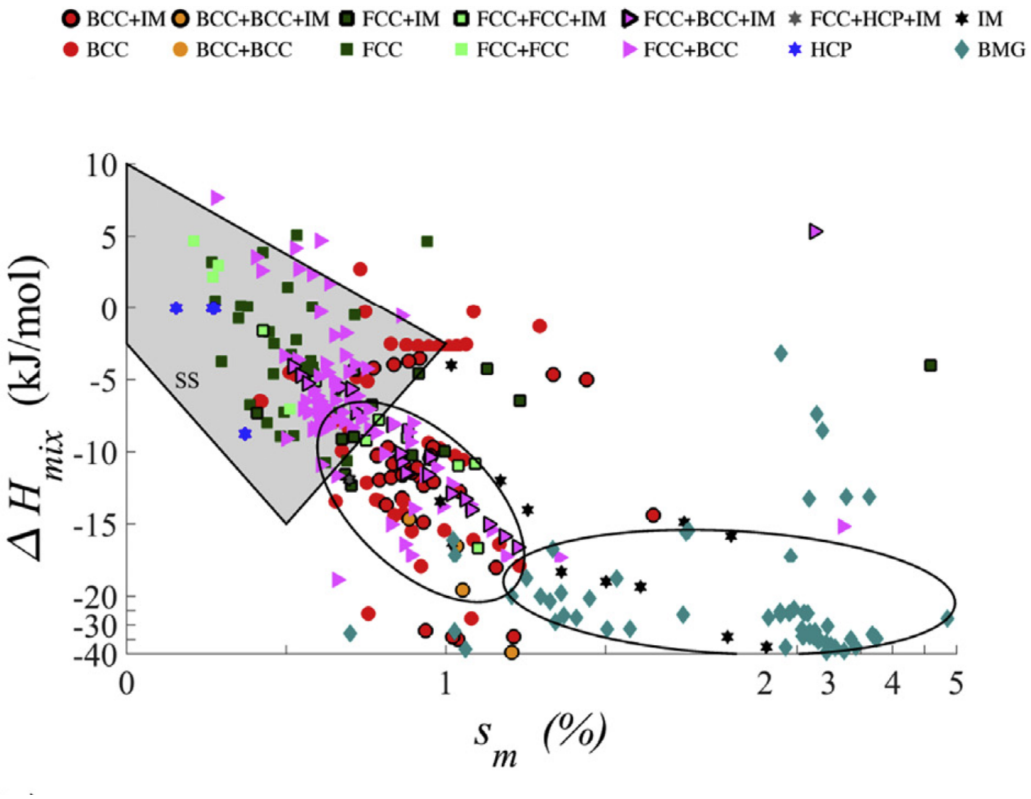


Figure 2.15: A plot of $s_m$ and $\Delta H_{mix}$ showing the HEA region shaded in grey and the various phases indicated by different symbols. The work, data and image are taken from Toda-Caraballo and Rivera-Diaz-del-Castillo [89].

### Entropy of Mixing

The entropy of mixing is the configurational entropy that occurs due to Boltzmann's Law [81]. The large values of entropy account for the naming of HEAs but the significance of entropy in defining their structures is not agreed upon. There are many HEA formation rules that simply ignore entropy and some papers also point out that the formula only works in random solutions which is often not the case [52].

The entropy values can be calculated using equation 2.4. Using this formula it is apparent that increasing the number of elements will increase the entropy. The increase of entropy with number of elements is shown in Fig. 2.16. The maximum entropy (achieved with equiatomic compositions) is shown along with the minimum

entropies that still meet the common HEA composition requirements (5 at% minimum and 35 at′% maximum).

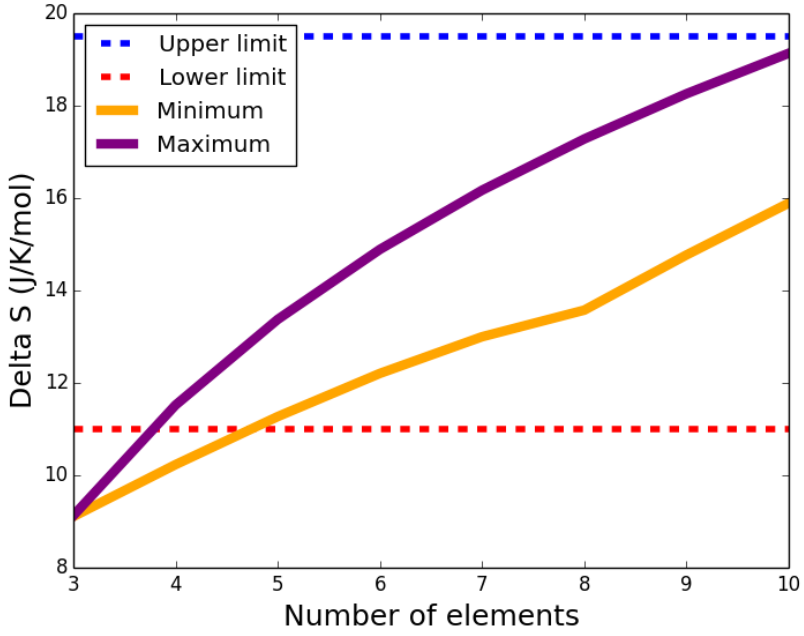


Figure 2.16: The maximum and minimum entropies possible for alloys with a given number of elements. The compositions are limited by the composition limits of HEAs, that no element is below 5 at.% and no element above 35 at.%.

The limits shown in Fig. 2.16 are from Guo et al. who used limits of 11 $< \Delta S_{mix} <$ 19.5 kJ/mol [81]. Using these limits all HEA compositions that have between five and ten components pass this test. Only a portion of four component would fail below this limit and a system of eleven or more components would be required to have an entropy above the upper limit. These limits are so broad that they do not really remove any compositions that could be considered as a HEA.

### Yang Thermodynamic Parameter

The Yang thermodynamic parameter was first published by Yang and Zhang in 2011 [90]. They derived a parameter, $\Omega$, to use as a HEA formation predictor to be

used in conjunction with the delta parameter. Starting with the standard Gibbs energy equation, equation 2.5, the origin of the Yang parameter can be seen. If the requirement is that Gibbs energy needs to be negative then the Gibbs equation looks like

$$0 > \Delta H_{mix} - T\Delta S_{mix} \tag{2.16}$$

this can then be rearranged to give the expression

$$\frac{T\Delta S_{mix}}{\Delta H_{mix}} > 1 \tag{2.17}$$

with the left hand term now equalling approximately the Yang parameter.

There are a few changes to get to the exact form of the Yang parameter though. Due to the change in sign negative enthalpies (even if close to zero) would violate the condition in equation 2.17. To address this the modulus of the $\Delta H_{mix}$ is used rather than the value.

The temperature that is used for T is the melting temperature of the alloy, $T_m$. As these alloys tend not to have phase diagrams or known melting temperatures an approximate melting temperature is calculated using,

$$T_m = \sum_{i=1}^{n} c_i (T_m)_i \tag{2.18}$$

to take a weighted average of the pure element melting temperatures of the alloy. The melting temperature is used as this is considered to be close to the temperature where the solid solution phase transformation to the HEA structure will take place. Finally, instead of comparing to the value 1, once the values are plotted a value of 1.1 is used instead [90]. This leaves the Yang parameter as

$$\Omega = \frac{T_{melt} S_{mix}}{|H_{mix}|} \tag{2.19}$$

with the requirement for HEA formation set at $\Omega$ >1.1.

In the paper that used this derivation the $\delta$ limit imposed was $\delta$<6.5%. As mentioned earlier there are other limits that other papers have used when using delta.

The plot of $\Omega$ and $\delta$ is shown in Fig. 2.17. Other phases are also identified in this plot with regions highlighted by differently coloured regions.

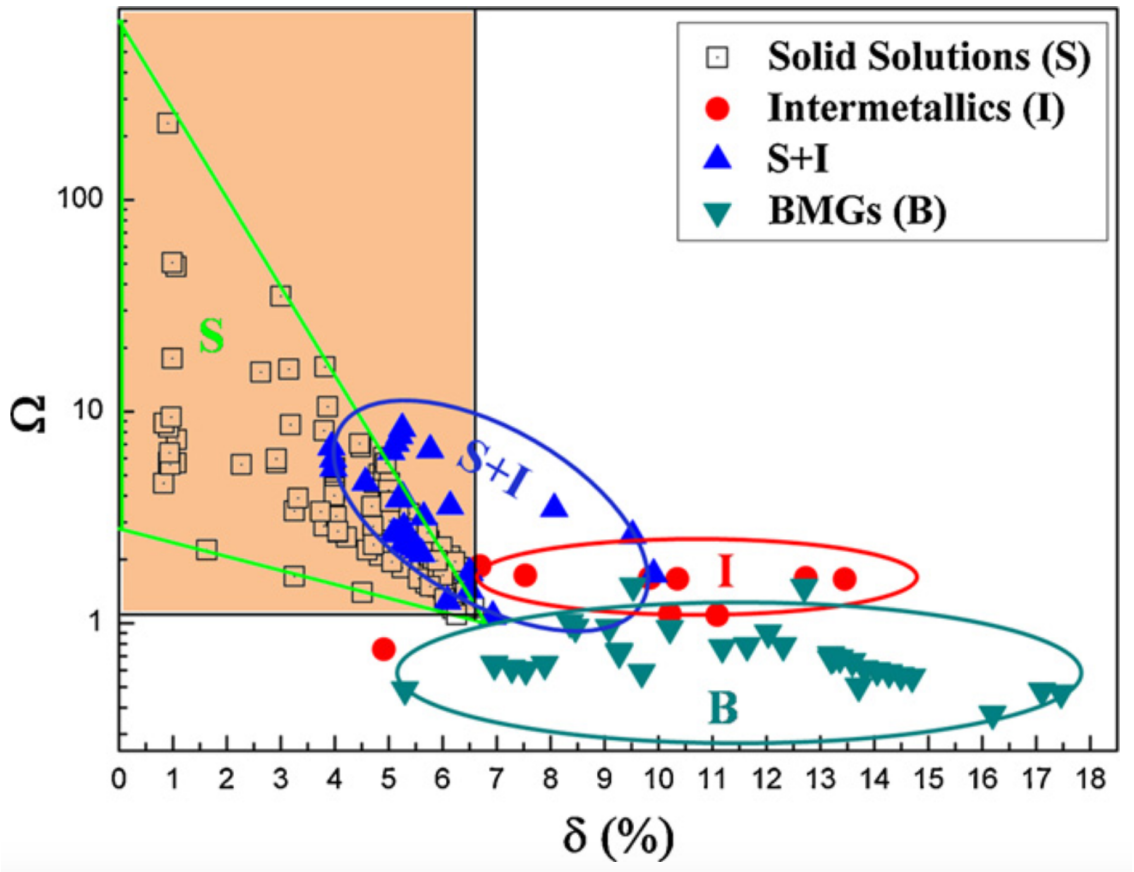


Figure 2.17: Results for $\Omega$ plotted against $\delta$. The orange region indicates the HEA formation region. The data and plot are from Yang and Zhang [90].

In Fig. 2.17 the HEA formation region shows the area indicated using the limits for $\Omega$ and $\delta$ previously mentioned. This is not in perfect agreement with the results, as can be seen by the regions that are drawn onto Fig. 2.17.

### Poletti Thermodynamic Parameter

The Poletti thermodynamic parameter, $\mu$, was first published by Poletti and Battezzati in 2014 [91]. The work follows on from Yang and Zhang [90] and uses some similar concepts and significant portion of the derivation. The paper has three temperature

variables and it is important to be clear about all of them.

The first variable, $T_c$, refers to the critical temperature. This is the temperature at which a solid solution forms in a composition [91]. The second variable, $T_Z$, is defined as the ratio between the $\Delta H_{mix}$ and the configurational entropy. This can expressed in an equation as

$$T_Z = \frac{|\Delta H_{mix}|}{\Delta S_{conf}} \tag{2.20}$$

with $\Delta S_{conf}$ is the configurational entropy. Poletti and Battezzati note that the configurational entropy is essentially the same as the mixing entropy that was used earlier. The $T_Z$ can be used to express the Yang parameter as

$$\mu = \frac{T_m}{T_Z} \tag{2.21}$$

with the other variables remaining the same as the original Yang equation.

The final temperature variable is $T_{sc}$ which is the critical temperature as calculated using spinodal points. The Poletti variable is defined as the ratio between the melting temperature and the new critical temperature, or

$$\mu = \frac{T_m}{T_{sc}} \tag{2.22}$$

with the terms as previously defined. The basis of the calculations for $T_{sc}$ uses Gibbs energy equations and the derivatives of those equations. By looking at the gradients of the Gibbs energy curves and critical points then the stable regions can be calculated, in terms of composition and temperature. The full derivation of $T_{sc}$ is explained in the original paper by Poletti and Battezzati [91].

One final change to this equation is the method for estimating the melting temperature. As with Yang and Zhang [90] the melting temperature for these HEAs is not known but instead of using the approximation in equation 2.18 a new equation is used. Melting temperature, $T_m$, is defined as

$$T_m = \frac{\sum_i c_i \Delta H_i^{fusion}}{\sum_i c_i \Delta S_i^{fusion}} \tag{2.23}$$

with $\Delta H_i^{fusion}$ being the enthalpy of fusion and $\Delta S_i^{fusion}$ being the entropy of fusion both for element $i$.

The Poletti and the Yang parameters are used in similar ways. Both parameters have the HEA formation at high values, with Poletti and Battezzati stating that for $\mu < 1$ the alloy would be multiphase. The Poletti parameter is also used in conjunction with the delta value. The data for the Poletti parameter and $\delta$ are shown in Fig. 2.18.

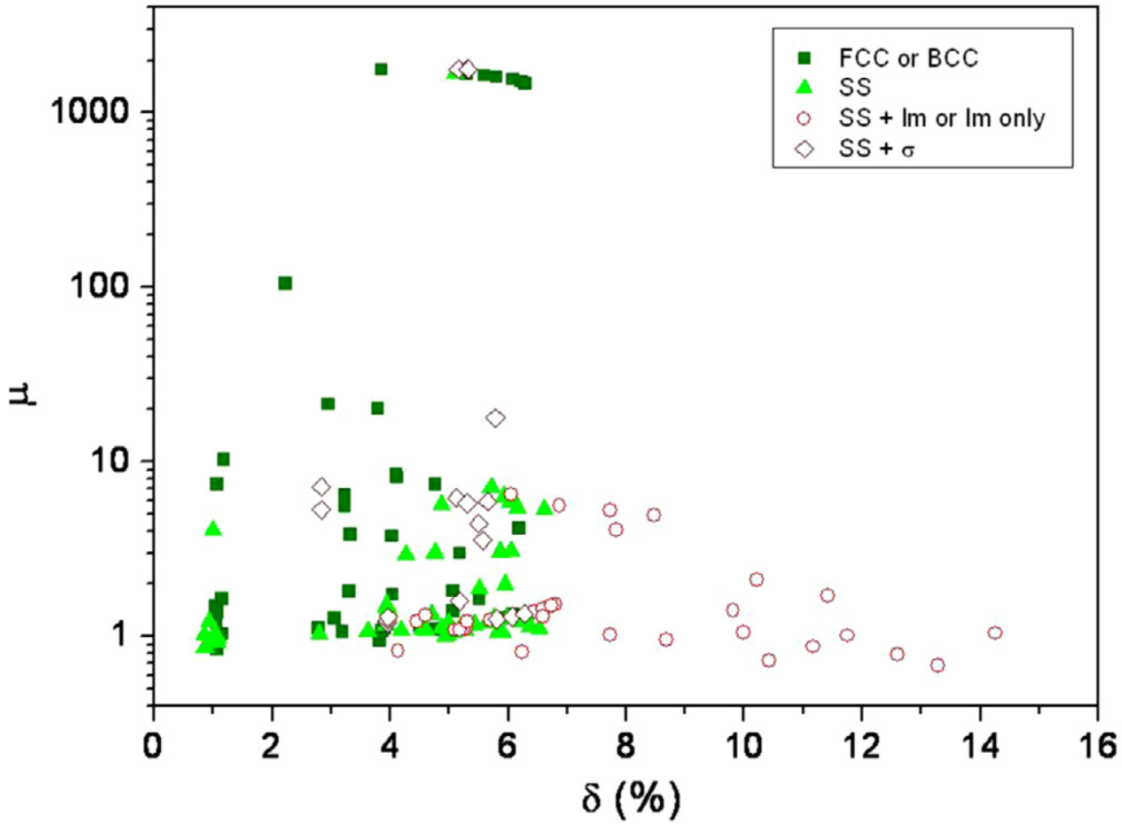


Figure 2.18: Results for $\mu$ plotted against $\delta$ for a variety of HEAs. The solid green markers refer to HEAs and are found in the HEA formation region as described in the publication. The data and plot are from Poletti and Battezzati [91].

The results in Fig.2.18 show a similar trend to the results by Yang and Zhang (see Fig. 2.17). HEAs form at $\delta$ values lower than 6.5% and $\mu$ values larger than 1.

### 2.3.3 Predicting HEA Formation with Electron Orbital Based Criteria

#### Valence Electron Concentration

The valence electron concentration (VEC) is used by a number of papers as part of developing a HEA criteria. The formula is relatively simple with the VEC of the alloy found by simply taking an average of the VEC of the elements, $VEC_i$, defined as

$$VEC = \sum_i c_i (VEC)_i \tag{2.24}$$

There are some studies which found that VEC had an effect on phases that were formed. The third Hume-Rothery rule refers to the valence of the metals that mix and how that effects conventional alloys [83]. For HEAs, research found that high VEC values tended to form face-centred cubic (FCC) structures and low VEC values tended to form body-centred cubic (BCC) structures. The numbers that are often quoted are that for VEC $> 8$ an FCC will form and for VEC $< 6.7$ a BCC will form. For VEC values in between, $6.7 <$ VEC $< 8$, then a mixture of FCC and BCC will form [81].

However, there is evidence to support that these VEC rules can only be applied to a limited number of situations. There are review papers that find when a large number of HEAs are analysed across a wide range of compositions then there is no correlation [52]. There are also some specific examples of VEC predictions being incorrect [45].

Guo et al. found that manganese can make the predictions unreliable [92]. Also, as will be discussed later, there are other models that are used to predict whether HEAs are single phase or multi-phase and does not use VEC in the calculations [80]. This formula is covered in more detail later in this section.

### Electronic Structure Analysis

A recent publication by Leong et al. [93] created a method that used a form of Density Functional Theory (DFT) that could be used to predict the formation of HEAs. The method used a Rigid Band Approximation (RBA) to allow for simpler calculations as DFT of even a single potential composition and structure is very time consuming. Using this approximation the energies of different structures could be calculated and then compared in order to find the structure that would most likely form.

The difference in energies between two structures, (labelled 1 and 2), can be expressed as

$$\Delta E^{(1-2)} = \Delta E_B^{(1-2)} + \Delta E_{e-e}^{(1-2)} \tag{2.25}$$

where $\Delta E^{(1-2)}$ is the overall difference in energy, $\Delta E_B^{(1-2)}$ is the energy difference in band energy and $\Delta E_{e-e}^{(1-2)}$ is the energy difference due to electron-electron interactions.

Once the values in equation 2.25 have been calculated they can then be used to predict a structure for a given composition. The paper does go onto consider changes in composition and other variables to examine the effect the changes have on the phases that are formed. This is achieved by considering the change of energy as a function of VEC and carrying out an integration over the density of states for an atom [93].

The results presented show good agreement, with various CoCrFeNi-based HEAs that were predicted using the method and analysed experimentally. The publication proposes that this method can be used in future as a HEA prediction method. The VEC method used earlier in this section with equation 2.24, has had doubts expressed over whether it could be used consistently for HEA prediction. This method does not contradict this however, as the VEC data and results are handled in a different way entirely.

In this method the use of the RBA along with other simplifications manage to make the DFT calculations necessary significantly simpler. However, the computational steps required are still too intensive and complicated for the broad scale trials

that will form part of the HEA selection of this research.

### 2.3.4 Predicting HEA Formation with Other Rules

#### Interatomic Spacing and Bulk Modulus Mismatches

A criterion for HEA formation was developed by Toda-Caraballo and Rivera-Diaz-del-Castillo based on the lattice distortion in HEAs [89]. The work created two new parameters, $s_m$ and $k_m$, that represent the interatomic spacing mismatch and bulk modulus mismatch respectively. The two parameters are calculated in similar ways and have some common theories with earlier work by Toda-Caraballo and Rivera-Diaz-del-Castillo on modelling the hardness of HEAs [94].

The $s_m$ parameter, which has similarities with the $\delta$ parameter, and the $k_m$ have similar derivations. Both derivations use the same input variables and formulae that are loosely alike. For clarity and efficiency both derivations will be shown simultaneously. To start with the unit cell parameter, $a_{ij}$, and the bulk modulus, $K_{ij}$ for a binary system of elements $i$ and $j$ are defined by,

$$a_{ij} = \frac{a_{ii}^2 K_{ii} + a_{jj}^2 K_{jj}}{a_{ii} K_{ii} + a_{jj} K_{jj}} \qquad k_{ij} = \frac{1}{2} \frac{(a_{ii} K_{ii} + a_{ii} K_{ii})^2}{a_{ii}^2 K_{ii} + a_{jj}^2 K_{jj}} \tag{2.26}$$

where $a_{ii}$, $a_{jj}$, $K_{ii}$ and $K_{jj}$ are the unit cell parameters and the bulk moduli for elements $i$ and $j$ in pure forms. These same variables can be used to calculate the average unit cell parameter $a_{lat}$ and average bulk modulus $K_{lat}$, as

$$a_{lat} = \frac{\sum_i^n a_{ii}^2 K_{ii} c_i}{\sum_i^n a_{ii} K_{ii} c_i} \qquad K_{lat} = \frac{\sum_i^n (a_{ii} K_{ii} c_i)^2}{\sum_i^n a_{ii}^2 K_{ii} c_i} \tag{2.27}$$

where $c_i$ is the atomic fraction of element $i$. This can be used to generate two matrices for the interatomic spacing, $s_{ij}^d$ and the bulk modulus $K_{ij}^d$ that are both used in the final equations for $s_m$ and $K_m$. The formulae for each elements in the two matricies are given by

$$s_{ij}^d = f \frac{a_{ij}^2 K_{ij} + a_{lat}^2 K_{lat}}{a_{ij} K_{ij} + a_{lat} K_{lat}} \qquad K_{ij}^d = \frac{1}{2} \frac{(a_{ij} K_{ij} + a_{lat} K_{lat})^2}{a_{ij}^2 K_{ij} + a_{lat}^2 K_{lat}} \tag{2.28}$$

where $f$ is the atomic packing factor, the number that connects the lattice parameter to the interatomic distance, and all the other terms are as previously labelled. These formulae can be arranged to form a matrix and recalculate the average lattice values but now with the updated model. The final parameters can be calculated as such,

$$s_m = \sum_i^n \sum_j^n c_i c_j \left| 1 - \frac{s_{ij}^d}{s_{lat}} \right| \qquad K_m = \sum_i^n \sum_j^n c_i c_j \left| 1 - \frac{K_{ij}^d}{K_{lat}} \right| \tag{2.29}$$

The $s_m$ parameter is equivalent to and used in the same way as the $\delta$ parameter. The paper states that 1% $s_m$ is the equivalent of 6% using the $\delta$ parameter. The similarity between the parameters is shown in the paper with a plot of the two variables showing a strong correlation, as shown in Fig. 2.19.

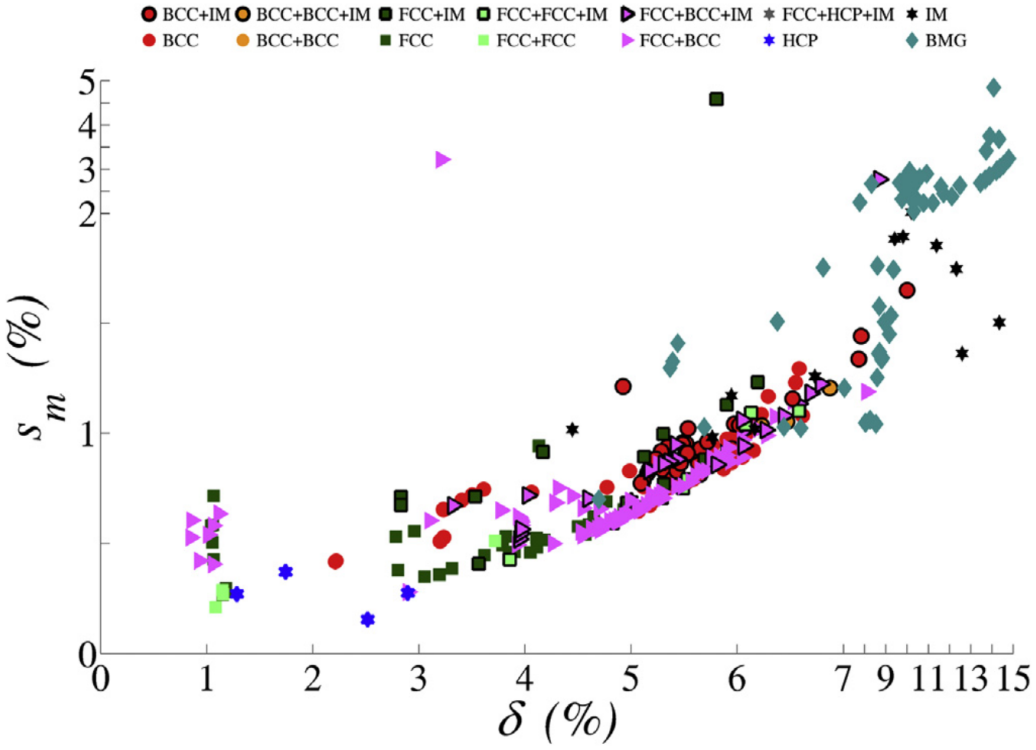


Figure 2.19: A comparison of the similar $s_m$ and $\delta$ variables. Work and image from Toda-Caraballo and Rivera-Diaz-del-Castillo [89].

The publication also shows $s_m$ plotted against the various parameters that $\delta$ would typically be plotted against. One example is a plot against $\Delta$H that has already been

shown in Fig. 2.15. The $K_m$ parameter does not have an equivalent like the $s_m$ parameter does. The two new parameters are plotted against each other in Fig. 2.20. The plot shows a HEA formation region, non-HEA formation regions and also indicates the likely phases within the HEA region.

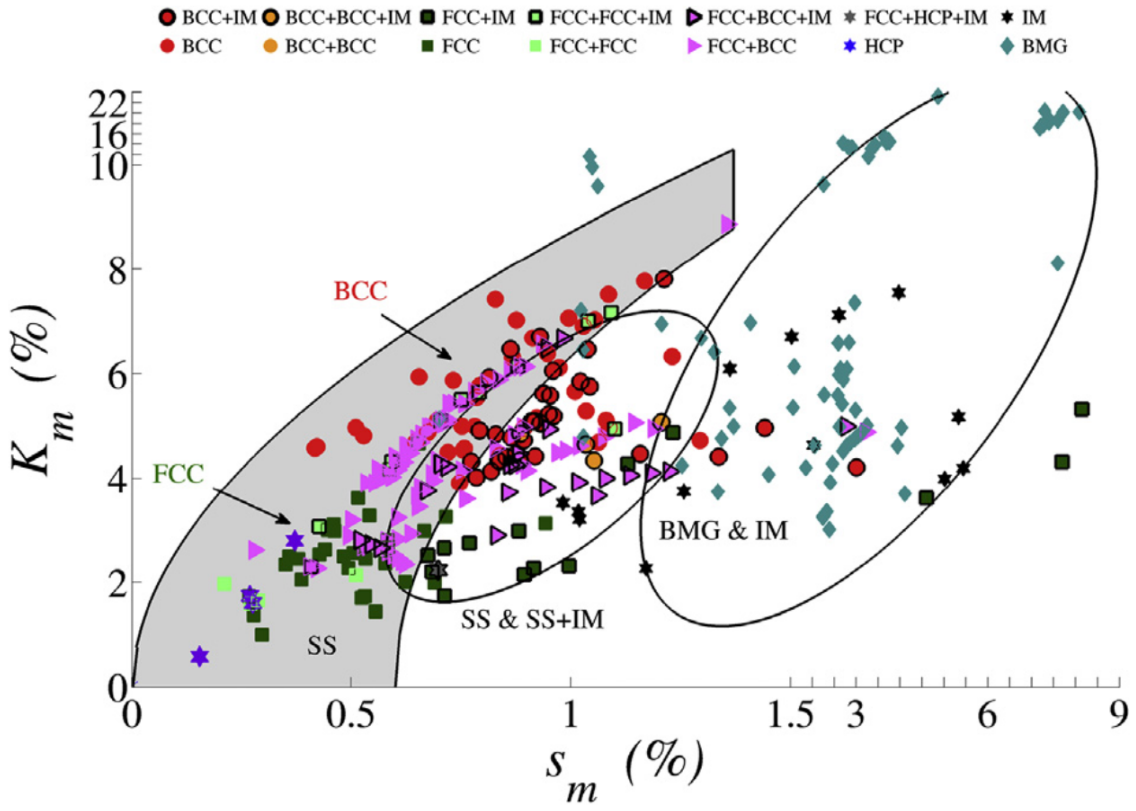


Figure 2.20: The parameters of $s_m$ and $K_m$ are shown to show HEA prediction regions. The blue region indicates HEA formation and other phase regions are indicated with the circled areas. FCC and BCC phase regions with the HEA region are also indiated. The alloy phases are indicated by the marker. Work and image from Toda-Caraballo and Rivera-Diaz-del-Castillo [89].

The criteria outlined in this method appears to be effective and can be used to predict HEA formation as well as the likely structure (both in terms of lattice as well as numbers of phases) of any HEA. There are some difficulties in adapting this method for large scale use, such as that adopted as part of this research. The computer

calculations required are relatively intensive compared to the other models and there are some inputs that may be problematic to input, especially in alloy systems that where is scant HEA data available.

### HEA Single Phase Predictions

So far most of the predictions are primarily focussing on whether a HEA or a non-HEA will form according to certain criteria. This method, based on work by Troparevsky et al. [80], instead looks at the number of phases that will form within a HEA. As discussed previously, most definitions of a HEA will allow for more than one solid solution phase, but it still of significant interest to be able to predict whether an alloy is a single-phase HEA or a multi-phase HEA as this can have a major impact on the properties.

The method has some similarities with the $\Delta H_{mix}$ variable that was covered previously. For a given alloy the enthalpy coefficients for each binary pair of elements are collated from a reference table, in a similar way to the Miedema method. If all the values fall within set limits then the prediction is that the HEA will be single phase. The alternative is that if one or more of the values is too positive or too negative then the prediction is that the HEA will be multi-phase.

While the enthalpy values are presented in a table that appears similar to the Miedema values, however the values are calculated in a different way. The values are calculated by first finding all the formation enthalpies for all the possible lattices in order to find the most likely to form lattice. This enthalpy value is then compared to enthalpy of formation of no structure forming, (i.e. remaining as pure elements), and this value is then used in the reference table. An example of the table is shown in Fig. 2.21. The $\Delta \mathrm{H}_f$ were calculated using "first-principles high-throughput density-functional-theory (DFT) calculations" [80].

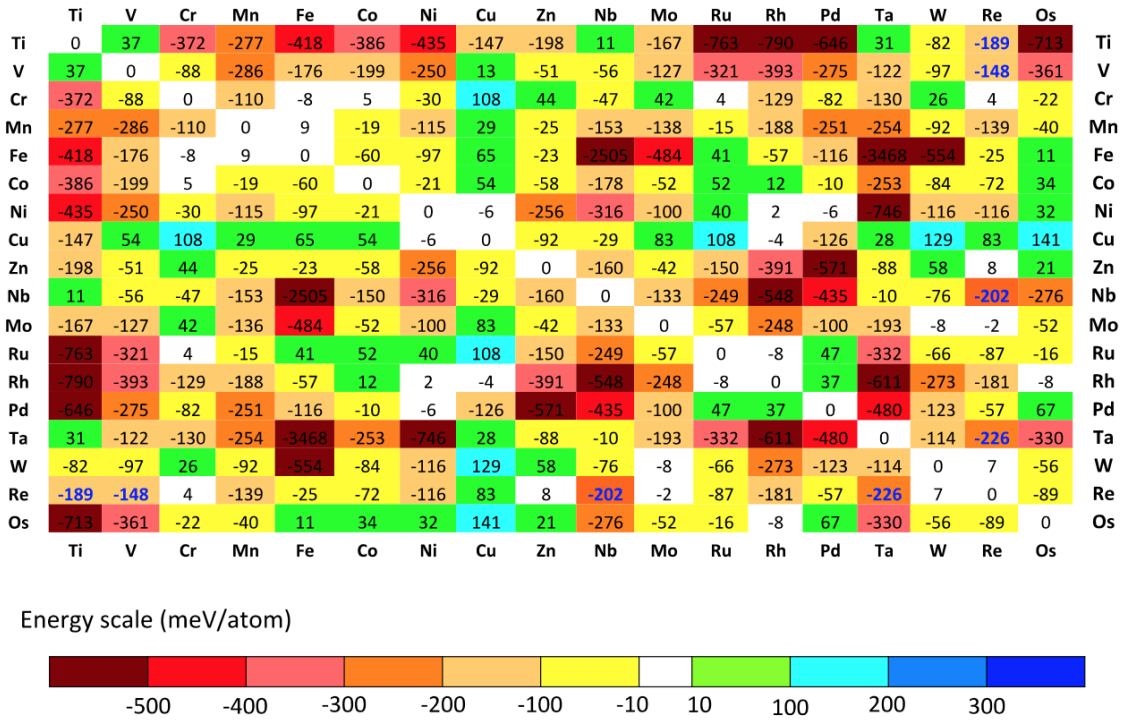


Figure 2.21: The $H_f$ values for a number of elements that can be used to find single phases. Calculations and image from Troparevsky et al. [80].

The limits for single phase formation are set at (-138 < $\Delta H_f$ < 37) meV/atom. However, they also included a second, extended range set at (-232 < $H_f$ < 37) meV/atom. An example of this modelling is the alloy from Cantor, CrMnFeCoNi. These five consecutive elements refer to a five by five square on the grid in Fig. 2.21. The maximum value is the Mn-Fe pair with 9 meV/atom and the minimum value is the Mn-Ni pair with -155 meV/atom. This is in agreement with most published result that CrMnFeCoNi is single phase, although some reports show some metastability [95]

The method does not account for whether a HEA will form or a non-HEA structure. It is possible that a composition could meet the criteria for single-phase set out in this method but not form a HEA due to large atomic size difference or some other reason.

### Other HEA Formation Prediction Methods

There are many other HEA prediction methods that have been used and published by different research groups in recent years. Some of these methods are similar to techniques already detailed in this section, but there are still many that are unlike any previously discussed, and to compere them all would be a lengthy process. Many of the methods have not been widely used but there are some methods of note though that are worth detailing.

A frequently used method is Ab initio modelling. The term, 'Ab initio', does not refer to a particular method, but an approach that is used in many different contexts. The term literally translates as 'from the beginning', and this is reflected in the modelling techniques, as they use the most fundamental physics and material laws. Density Functional Theory (DFT) and Korringa-Kohn-Rostoker Coherent Potential Approximation (KKR-CPA) are two prominent examples of ab initio modelling techniques [96, 97]. There are many widely-cited papers that use Ab initio modelling but none of the techniques are suitable for the HEA modelling that will be used in this research. The methods are far too complicated and computationally intensive to be used in large scale trials.

In terms of empirical-based criteria for HEA prediction most of the techniques have been covered already in the previous subsections. There are still a few more methods that are worth highlighting. One example is a parameter developed by Miracle and Senkov, $k_1^{cr}(T_A)$, that is used by analysing the competing phases in terms of entropy and enthalpy [98]. One other example was a parameter, $\phi$, that was developed by Ye et al. This method is based on aspects of Gibbs equations and is focussed around maximising the entropy of the alloy [99].

There are also many papers that use thermodynamic modelling to help predict HEAs. Some of the techniques are conventional methods, which are usually applied to conventional alloy types, such as stainless steels or nickel superalloys, but instead directed at HEA compositions. There are also methods that are designed to support

other HEA models with information for formulae. Thermodynamic modelling of HEAs is covered in more detail later in this chapter.

### 2.3.5 Suitability of the HEA Modelling Methods

The main method selected for use was to model $\delta$ and $\Delta H$. The intended use of the HEA modelling in this research is to incorporate it into a system that can model extremely large numbers of compositions and then find ideal HEA conditions. As seen in this section there are many options to choose from for HEA modelling but many of them are unsuitable for practical reasons.

The requisites for the method are that the calculations must be relatively simple, the input variables need to be easy to find for all the key elements and the results must be as accurate as possible. Most of these methods are excluded as they would involve too many complex computations. It would simply require too much time for the scale that this method would be used on. A few are also excluded as they are not suitably accurate and would not be useful for finding HEA alloys. More detail on why $\delta$ and $\Delta H$ were selected, and then how they were implemented, is covered in Chapter 3.

## 2.4 CALPHAD Thermodynamic Modelling

CALPHAD is a thermodynamic modelling method that is widely used in academia and industrial research and development and anywhere else that requires modelling of materials. The method uses thermodynamic equations to describe experimental data from simple alloy systems. From these descriptions of simple systems the method can then model higher order systems from this data. The method can be used to describe many types of materials including metals, composites and magnetic systems [100, 101].

## Origins

The name CALPHAD derives from the acronym CALculation of PHAse Diagrams. It is also used as the subtitle from the journal, The Computer Coupling of Phase Diagrams and Thermochemistry [102], which describes use of computers that is integral to this modelling method.

Prior to World War II phase diagrams were determined by manual calculations with Gibbs energies and inexact experimental methods. After World War II the demand for accurate phase diagrams skyrocketed. There were many new industrial, civilian and military applications that required novel alloys and novel alloy systems. Developing a method to rapidly model and investigate new alloys became a very desirable objective [100, 101].

In the 1950s there were a number of groups independently working on modelling techniques. The next major step in the development of CALPHAD was the onset of computing and how it could be used to carry out large numbers of calculations. As computing power gradually increased through over the decades so did the accuracy and the amount of detail CALPHAD could achieve. Sometime around the 1970s-1980s CALPHAD had become accurate and useful enough for it to be recognised as a valid modelling method and a useful alloy development tool [100, 101].

Today CALPHAD is widely used across industry and academia for a wide variety of applications. The method has been incorporated into easy to use commercial programs with large databases. Some of the most commonly used CALPHAD programs are OpenCalphad, CompuTherm and Thermo-Calc [103]. These programs are designed to allow use of CALPHAD without detailed understanding of the methods or techniques that are involved in the calculations, though these will be outlined here.

## Method

### Basic Thermodynamics

The principle of the CALPHAD method is to build up large and complex models for high order systems from the thermodynamic data of smaller (binary and ternary) systems. Using calculated high-order models, phases can be calculated for inputted conditions such as composition, temperature, pressure and so on. The phase prediction part of the calculations is based on the minimisation of Gibbs energies. The approach is to analyse all the potential phases that could form, as well as potential combinations of phases that could exist, and to optimise the amounts of each phase to find the lowest Gibbs energy [100, 101].

This method is useful as it means databases only need to store a few coefficients for each phase and this can be used to generate the phases that could potentially form both quickly and efficiently. The complication to this method, and the main reason why the calculations cannot be done manually, is the modelling of the interactions between the different elements and phases.

The thermodynamic modelling of phases starts with modelling of the Gibbs energies. One of the most general Gibbs energy, $G$, equations can be expressed as

$$G = G^0 + G^{ideal}_{mix} + G^{xs}_{mix} \tag{2.30}$$

where $G^0$ is Gibbs energy of the pure element, $G^{ideal}_{mix}$ is the Gibbs energy due to ideal mixing and $G^{xs}_{mix}$ is the excess mixing Gibbs energy. In a multicomponent system this equation can be expanded and expressed as

$$G = \sum_i x_i G^0_i + RT \sum_i x_i ln x_i + \sum_i \sum_{j>i} x_i x_j \Omega_{ij} \tag{2.31}$$

where $x_i$ and $x_j$ are the molar fractions of elements $i$ and $j$ respectively, $G^0_i$ is the Gibbs energy of the pure element $i$ and the $\Omega_{ij}$ is the interaction parameter of elements $i$ and $j$. The first term, with $G^0_i$, is the Gibbs contribution from pure elements. The second term is the equivalent of $G^{ideal}_{mix}$ and is found by multiplying the entropy with

the universal gas constant, $R$ and the temperature, $T$. The final term, the equivalent of $G^{xs}_{mix}$, uses the $\Omega_{ij}$ term to describe the binary pairs in the alloy. These terms are calculated from an expression called the Redlich-Kistler polynomial [100].

These terms can then be calculated accordingly. The $G^i_0$ can be expressed as a polynomial in terms of the temperature, $T$,

$$G^0_i = a + bT + cT.ln(T) + \sum dT_n \tag{2.32}$$

where $a$, $b$, $c$ and $d$ are all coefficients. There are other forms of this equation with further terms in the polynomial expansion and other contributions to the energies (e.g. magnetism) [100]. Calculations and data storage can be made even more efficient using the heat capacity which replaces the latter half of equation 2.32 [100]. The remaining terms in equation 2.32 can then be calculated. The $G^{ideal}_{mix}$ terms can be calculated easily and are independent of which elements are in the system. The final term is calculated using the Redlich-Kister values that are saved in a database.

In higher order systems there are additional interaction terms to consider. There needs to be ternary interaction terms $\Omega_{ijk}$ to accompany the binary interaction terms, $\Omega_{ij}$, which is found in equation 2.31. For most calculations this level of detail is sufficient. The evidence shows that quaternary or higher interaction terms do not have much effect on the modelled data [100]. Not calculating beyond ternary interactions has a drastic impact on calculation times and data storage, simplifying the process and making very high order systems possible.

### Computational Method

Databases for CALPHAD are often proprietary with the CALPHAD software (in this case Thermo-Calc). The ideal scenario would be that for a given set of elements the database has all the elemental data, all of the binary phase diagrams and all of the ternary phase diagrams. However, CALPHAD can work with some data missing although the amount of data available relates to the reliability of the predictions.

Programs usually have a wide variety of databases to chose from. Some databases are general and cover a wide selection of the periodic table, for example SSOL4 (or solid solution 4). Many of the other databases are grouped according to research areas. Specialist areas such as regular steels, superconducting alloys and nickel superalloys have their own dedicated databases available. Examples of these databases within Thermo-Calc are TCFE9, TCSC1 and TCNI8 respectively [103]. There is also a HEA database, TCHEA2, that has 20 of the most commonly used HEA elements. These elements are Al, Co, Cr, Cu, Fe, Hf, Mn, Mo, Nb, Ni, Ta, Ti, V, W, Zr, C, N, Re, Ru and Si [103].

For researchers heavily involved in the CALPHAD method there is the opportunity to improve the database. Part of the advanced CALPHAD method is for users to include contemporary experimental data to improve the model. New data can be used to fit a more accurate model and so better predictions in the future. This is of particular use with relatively unexplored high order systems, such as superalloys.

The actual computing method is difficult to describe succinctly. There is often high level computer programming and there is a degree of secrecy about the exact calculations that are used by commercial CALPHAD programs. Generally speaking there are three parts to the process. Firstly the degrees of freedom must be reduced so the code can more easily hone in on a minimisation value. Secondly the actual Gibbs energy calculations for the phases must be carried out. Finally there needs to be an iterative process that minimises the Gibbs energy to find the final modelled values.

### Extra considerations

There are many further considerations that are used in many CALPHAD programs. Considerations need to be made about the solubilities of elements in phases, short and long range ordering and the effects of pressure [100].

There are also other considerations that can be included in calculations but may

not be necessary for all systems. The most significant example of this is the modelling of magnetism and magnetic materials. For paramagnetic materials the magnetism based Gibbs energy terms are usually not needed. For other magnetic effects though; ferromagnetism, anti-ferromagnetism and ferri-magnetism, the spin alignment and polarisation are important considerations [100, 101].

## CALPHAD Modelling of High Entropy Alloys

CALPHAD based modelling has two roles in HEA prediction. The method is used to support other HEA modelling techniques and as a prediction technique on its own. CALPHAD can support other HEA prediction methods by providing a way to calculate some of the values that are needed in the calculations. CALPHAD can provide Gibbs energies, enthalpies, melting temperatures and many other parameters that may be difficult to describe with a simple formula.

The versatility of CALPHAD modelling means that predictions involving HEA-type composition operates in much the same way that predictions of conventional alloys are carried out. While the practicality of setting up a CALPHAD prediction for a HEA is straight forward, the issue that needs to be addressed is the accuracy and the reliability of the HEA predictions.

There are some large scale analyses of CALPHAD predictions for HEA [104, 105]. Predictions of 130,000 equiatomic alloys were made to assess the structures that were present. The trends across the alloys were as expected. Increasing the number of elements reduced the likelihood that the alloy would form a solid solution. Also, prediction using the melting temperature of the alloys meant more solid solution predictions than measurements taken at (the colder temperature) 600°C [104, 105].

The same studies also looked at the veracity of the predictions. The main factor affecting the credibility of the results was the amount of data for the particular system. The amount of data is expressed in terms of the number of binary and ternary systems that are saved in the database. The fraction of binary systems included in

the database out of all the possible binary systems for a composition is labelled as, $f_{AB}$. The same is also applied to the ternary systems with the label $f_{AT}$. The results found good agreement when $f_{AB}$=1 and agreement between model and prediction even as low $f_{AB}$=0.6 [104, 105].

Uncertainty about the data is potentially a significant problem for using CALPHAD HEA modelling in this research. The alloy systems involved feature atypical elements for HEAs and so it is unlikely that the $f_{AB}$ and $f_{AT}$ values will be good. As silver features prominently in the majority of these alloys using the HEA specific database is not possible. Other databases have better coverage but it is not clear how accurate these measurements will be.

Another problem with the thermodynamic modelling is the computational time required. In the CALPHAD HEA investigations 130,000 were put through a high-throughput method. For the modelling in this project orders of magnitude more alloys will require modelling. This makes the modelling process prohibitively lengthy unless significant detail is lost from composition scans.

**Literature Review Summary**

Following the survey of the literature it is clear that there are unexplored theories and unused or underutilised methods that can be applied to brazing alloys and novel HEAs. Thermodynamic modelling offers the potential to refine compositions to offer improved overall properties. There are many HEA techniques available and there are some that can be incorporated into a large scale modelling method. This method can be used to predict HEAs that would be difficult to create without modelling. This method can be adapted further to model other properties, in particular brazing related properties, and can be used to find HEA-type brazing alloys.

# Chapter 3

# Thermodynamic Assessment of Brazing Alloys

This chapter is split into 3 sections. The first section looks at the thermodynamic modelling of the existing commercial brazing alloys and the insights that might explain observed brazing behaviour. The second section refers to the use of thermodynamic modelling for finding new alloys, looking at how it can be implemented and what properties need to be considered. The final section is an application of the thermodynamic modelling method to a case study on finding a replacement for an existing alloy.

The main goal of this thermodynamic modelling method was to find superior brazing alloys. To achieve this there were different ways to utilise the thermodynamic modelling predictions. The main method was to model as many different brazing relevant properties as possible then to filter out poor compositions and to hone in on the best compositions. Other work in this area was focussed in gaining a greater appreciation of specific details. Information such as knowledge of phases and the roles each element plays are interesting and worth looking into. New knowledge in this area is useful in its own right as well as helping to direct the search for new alloys.

## 3.1 Using Thermodynamics to Predict Brazing Properties of Existing Brazing Filler metals

CALPHAD techniques have the ability to model many different properties depending on the information required within a trial. Depending on the property the CALPHAD software can be used independently or as part other predictive work. On its own the software can predict values such as melting temperatures and phase information which can be plotted graphically. Other times CALPHAD may only provide part of the information that is an input for another model. Examples of this include enthalpy and Gibbs energy values that are involved in many formulae for materials calculations.

One of the most commonly used features in CALPHAD modelling are the functions that can produce a variety of graphs. These include classic phase diagrams, modified phase diagrams, Scheil graphs and many others depending on the specific program that is being used. However, for higher order systems displaying phase diagrams may not be possible as there are not enough dimensions to display the information. If only one element is being varied then these can be displayed (e.g. looking at variation in the carbon content in a multicomponent stainless steel), but if all elements are varying then there are not enough dimensions on a graph to display it properly.

An alternative to modelling an entire phase diagram is to model a single composition for a set of conditions. A single modelled equilibrium displays a wide range of phase information, Gibbs energy data and other properties, such as activity and potential. The text output from a modelled equilibrium state is shown in Fig. 3.1.

```
Output from POLY-3, equilibrium =     1, label A0  , database: SSOL4

Conditions:
 P=1E5, N=1, W(CU)=0.21, W(ZN)=0.22, W(SN)=2E-2, T=300
 DEGREES OF FREEDOM 0

Temperature    300.00 K (    26.85 C),  Pressure  1.000000E+05
Number of moles of components  1.00000E+00,  Mass in grams  8.37779E+01
Total Gibbs energy -1.91553E+04,  Enthalpy -5.76964E+03,  Volume  0.00000E+00

Component               Moles       W-Fraction  Activity   Potential  Ref.stat
AG                      4.2716E-01  5.5000E-01 2.7467E-03 -1.4710E+04 SER
CU                      2.7686E-01  2.1000E-01 1.4978E-03 -1.6223E+04 SER
SN                      1.4115E-02  2.0000E-02 6.3102E-06 -2.9866E+04 SER
ZN                      2.8186E-01  2.2000E-01 1.2128E-05 -2.8236E+04 SER

FCC_A1#1                    Status ENTERED     Driving force  0.0000E+00
Moles 5.4067E-01, Mass 5.4174E+01, Volume fraction 0.0000E+00  Mass fractions:
AG  8.50472E-01  ZN  1.21744E-01  SN  2.77691E-02  CU  1.44002E-05

FCC_A1#2                    Status ENTERED     Driving force  0.0000E+00
Moles 4.3049E-01, Mass 2.7669E+01, Volume fraction 0.0000E+00  Mass fractions:
CU  6.00580E-01  ZN  3.99248E-01  AG  1.38323E-04  SN  3.36661E-05

BCC_A2                      Status ENTERED     Driving force  0.0000E+00
Moles 2.8842E-02, Mass 1.9343E+00, Volume fraction 0.0000E+00  Mass fractions:
CU  5.04043E-01  ZN  4.07802E-01  SN  8.80208E-02  AG  1.33518E-04
```

Figure 3.1: A text output from a Ag-Cu-Zn-Sn composition that was modelled using the SSOL4 database from Thermo-Calc. The input conditions, listed towards in the fourth line, for this trial have been set at standard room temperature and pressure. The outputs are listed in the rest of the text with the element data, phases present and phase data.

There is a tremendous amount of information available from one single equilibrium, although ultimately a great deal of this data will not be used in this chapter. The data available from this output fell into three categories; data that can be used to filter prospective alloys, data that is worthwhile investigating but cannot be used to discriminate between alloys and data that was irrelevant for this research.

As discussed in the literature review there are a vast array of brazing alloys available with many different elements. The analysis and discussion of brazing alloys from all these systems would be too lengthy, so the remainder of this section will focus on one of the most widely used and versatile alloy systems, Ag-Cu-Zn-Sn.

### 3.1.1 Melting Temperatures

One property that is of obvious prominence and importance is the melting temperature. The most important melting temperature is the liquidus, which is desired to be as low as possible. However, it is also worth modelling the solidus and the melting range of the alloys. The low liquidus temperature is desirable as it saves on heating costs when brazing, it means less heat is imparted onto the parent material and a wider variety of parent materials can be used. A good melting range is small (a eutectic would be ideal) to prevent problems with liquation and partial melting. The effect of the melting temperatures are discussed later in this chapter.

Most commercial brazing alloys are given a International Organization for Standardization (ISO) designation but are then sold by multiple companies each with different brand names. The brazing data that is associated with each alloy is associated with ISO number and so is the same regardless of alloy supplier.

An early test of the thermodynamics was to check the quoted melting ranges of brazing alloys against what was predicted using CALPHAD. Seven alloys were selected from the Ag-Cu-Zn-Sn system, the details are shown in Table 3.1.

Table 3.1: A selection of Ag-Cu-Zn-Sn brazing alloys with the quoted melting temperatures. Values sourced from Johnson Matthey [14] and Lucas Milhaupt [14].

| ISO code | Composition (wt%) | Melting (°C) |
|---|---|---|
| ISO 17672 Ag 156 | Ag56-Cu22-Zn17-Sn5 | 618-652 |
| ISO 17672 Ag 155 | Ag55-Cu21-Zn22-Sn2 | 630-660 |
| ISO 17672 Ag 145 | Ag45-Cu27-Zn25.5-Sn2.5 | 640-680 |
| ISO 17672 Ag 140 | Ag40-Cu30-Zn28-Sn2 | 650-710 |
| ISO 17672 Ag 138 | Ag38-Cu31-Zn29-Sn2 | 660-720 |
| ISO 17672 Ag 134 | Ag34-Cu36-Zn27.5-Sn2.5 | 630-730 |
| ISO 17672 Ag 130 | Ag30-Cu36-Zn32-Sn2 | 665-760 |

The predicted melting temperatures were calculated using the Thermo-Calc software and SSOL4 database. The results are plotted in Fig. 3.2.

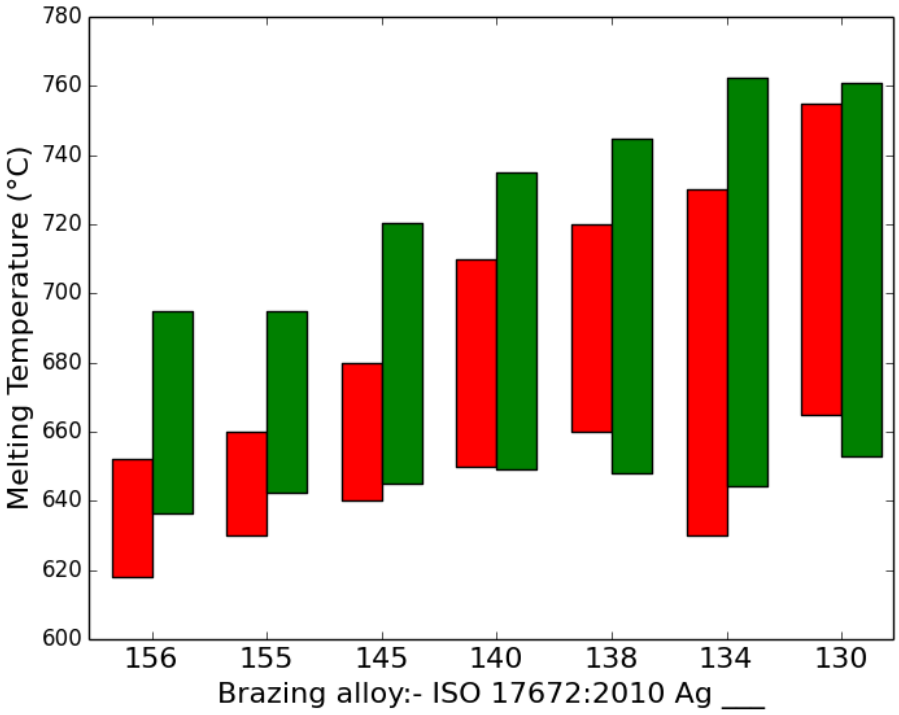


Figure 3.2: The quoted melting temperatures of the Ag-Cu-Zn-Sn alloys and Table 3.1 are in red. These are compared to the values found using Thermo-Calc (in green).

The results show varying levels of agreement between the two sets of melting temperatures. Out of the seven alloys the higher melting alloys tend to have closer agreement than the lower melting alloys. Also, the solidus temperatures are in closer agreement than the liquidus temperatures. The modelled liquidus temperatures tend to predict higher melting temperatures.

There were a number of possible reasons why the results differed. One theory was that the higher melting phases in the alloy might be predicted in small quantities that are then not detected by the experimental methods. One plausible explanation was that the higher melting phase might not actually form at all. To investigate the effect and to see if there was a possible explanation amongst the finer detail,

a temperature scan trial was programmed. Instead of just looking at 0% molten stage (the solidus) and 100% molten stage (the liquidus) the progression of the liquid phase, as temperature increases, was analysed through the range. Using a narrow temperature interval a scan could make predictions across the melting range and record the atomic percentage that had melted. An example of this type of scan is shown in Fig. 3.3 with the temperature spanned from entirely solid at 630°C to entirely liquid at 700°C.

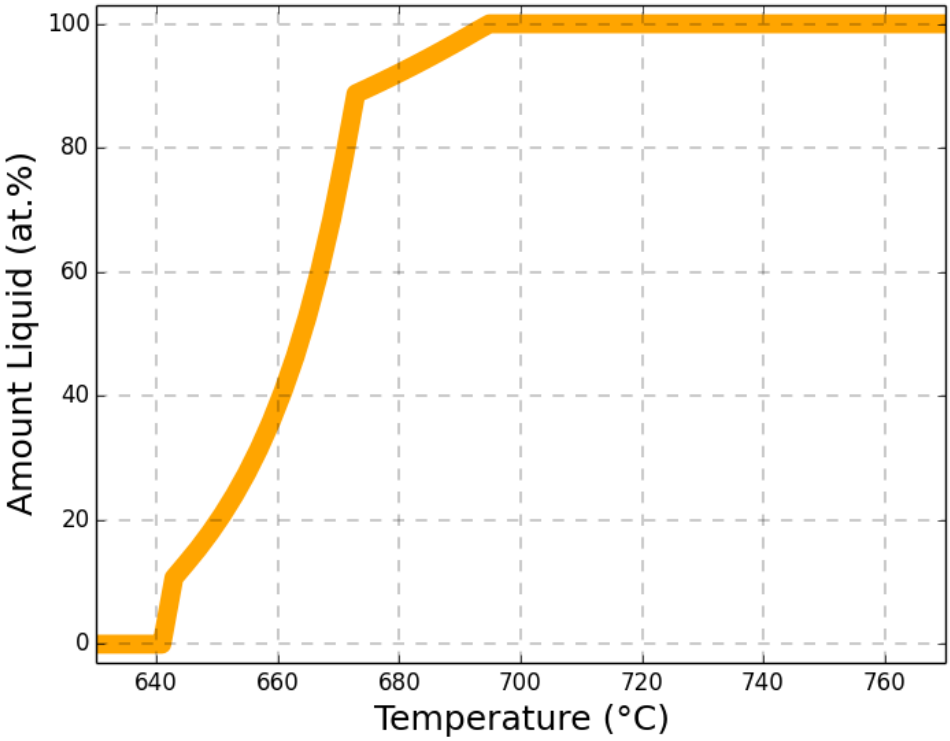


Figure 3.3: The CALPHAD modelled progression of the liquid phase with increasing temperature. The alloy modelled is ISO 17672:2010 Ag 155 with the composition Ag55-Cu21-Zn22-Sn2 wt.%.

The results Fig. 3.3 are a result of different phases melting at different temperatures. Some of the first stages of melting are steep, indicating an entire phase melting at about the same temperature. Some later stages of melting have shallow

gradients, indicating a gradual melting as temperature is increased. A more complete explanation of this is shown in the next subsection with a full phase analysis.

The temperature scan approach in Fig. 3.3 was carried out on all the alloys in Table 3.1. The results are shown in Fig. 3.4.

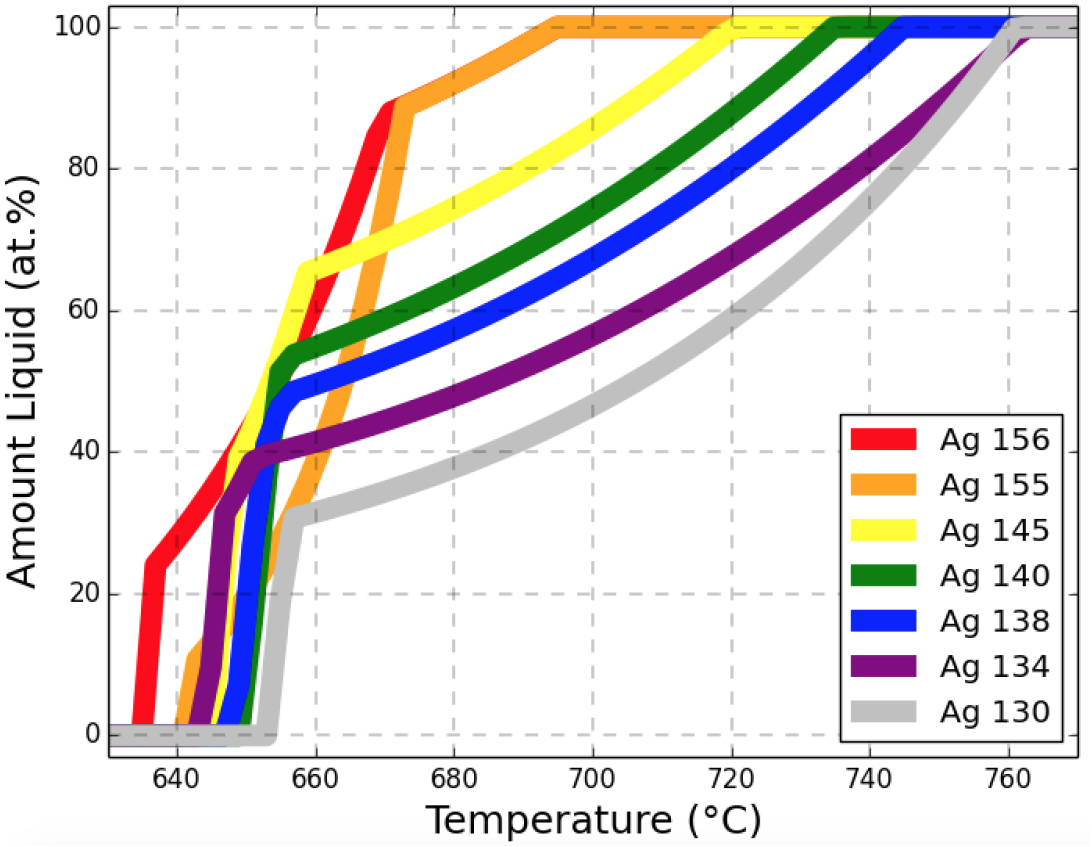


Figure 3.4: The CALPHAD modelled progression of the liquid phase with increasing temperature. The results are for the seven alloys featured so far. The full ISO names of these alloy are ISO 17672:2010 followed by the label in the legend.

These data in Fig. 3.4 were created to investigate the difference in the results in Fig. 3.2 between the quoted and the modelled melting temperatures. One proposed theory was that the trace amounts of high-melting phases may be affecting the modelled data (increasing the liquidus) but would be present in such a small amount that it would not effect the melting temperature in experimental or practical scenarios.

The data in Fig. 3.4 supports this theory to a limited extent. Alloys Ag 156 and

Ag 155 show the trend that would be expected for this theory to be true. Both alloys reach 90% liquid at approximately 670°C and then both alloys require approximately 25°C higher temperatures to fully melt. However, even if this 90% liquid temperature was used as the modelled temperature instead of the liquidus it is still not in agreement with the quoted values. The other alloys in Fig. 3.4 do not show the same trends as Ag 156 and Ag 155, so the agreement with the theory may just be coincidental.

There are other explanations of the discrepancies between the melting temperatures. It is possible that the results are just an inherent problem with the modelling. If there are missing alloy systems in the data then the results may be as accurate as could be hoped for. The problem may also lie with the quoted values. They may be inaccurate or may be expressing some sort of practical brazing temperature rather than the most rigorous scientific measurement of temperature. This will be investigated further later in this chapter as part of the search for new brazing alloys.

### 3.1.2 Phase Modelling

The next level of detail from the temperature scan in Fig. 3.4 is to not just record the liquid phase but to identify all the solid phases as well, including solid solution transformations.Also, each phase predicted has the elements within each phase. This information is useful for identifying phases, for example whether an FCC phase is Ag or Cu based, and also for showing more subtle information like solubilities.

#### Phase Modelling with Temperature Scan

Predictions of the phases at room temperature can be very useful for ductility predictions. Analysis of the phases that are present, particularly IMC, will be returned to later in the case study at the end of this chapter. In this part of the modelling though the phases are tracked from room temperature to above the liquidus temperature.

The main reason to investigate this was to look at the differences in temperature between the quoted and the predicted melting temperatures. The discrepancies

between the two may have arisen as the predicted results are at equilibrium and the quoted values were not. Also, to support the results in Fig. 3.4, knowing what phase requires the highest melting temperature may help guide efforts for finding lower melting brazing alloys. An example temperature scan from room temperature to fully liquid is shown in Fig. 3.5.

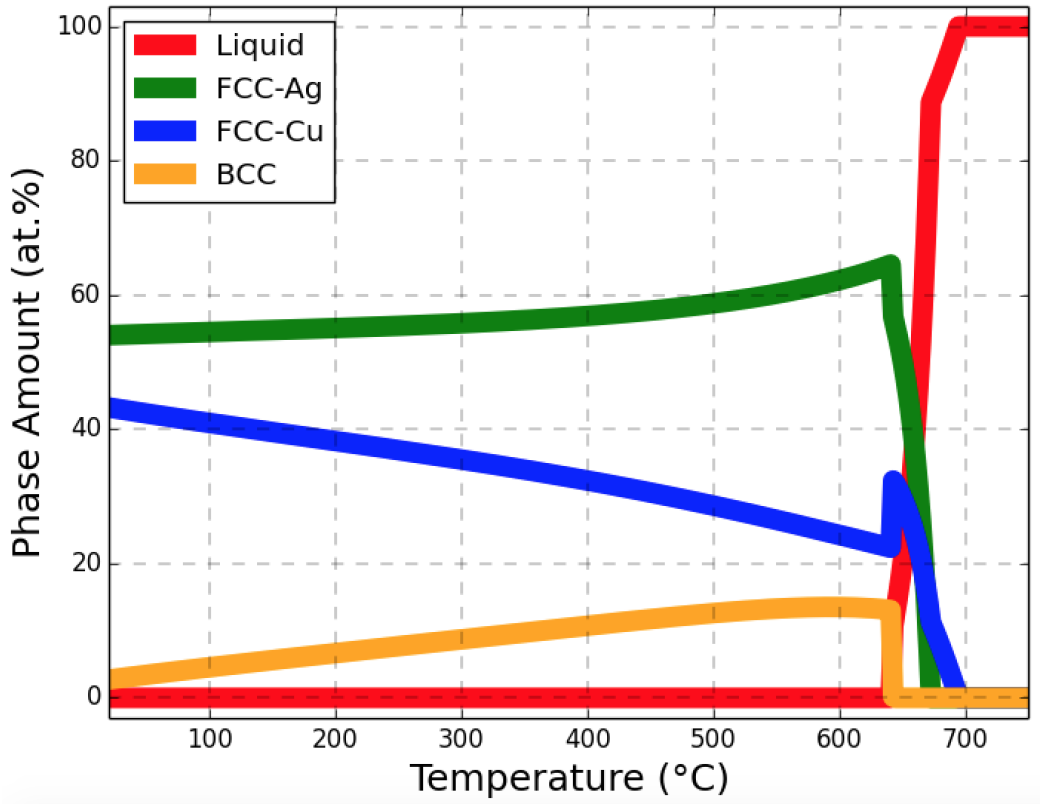


Figure 3.5: The CALPHAD modelled progression of the all phases with increasing temperature. The temperature spanned from room temperature to entirely liquid at 700°C. The alloy modelled is ISO 17672:2010 Ag 155 with the composition Ag55-Cu21-Zn2-Sn2 wt.%.

The results in Fig. 3.5 show that three phases are present at room temperature, FCC-Ag, FCC-Cu and a BCC phase. There remains three phases up to the solidus temperature where the BCC melts. After the solidus the FCC-Ag melts next with the FCC-Cu melting last.

In this example, and many of the other brazing alloys that were trialled, there are phase transformations within the solid solution. As mentioned, this may be useful in the alloy development process as it would explain the phases that are present in alloys that have been rapidly cooled. Usually this sort of high-temperature phase information would be displayed on a binary phase diagram, but as these alloys are multi-component this is not possible.

As previously stated the theory about trace amounts of high melting phases affecting the modelled melting temperature is only supported to a limited extent. The results from Fig. 3.5 do fall in line with what is expected though. The highest melting phase is FCC-Cu which is the highest melting element. From a design point of view this would indicate that reducing the copper content would be a potential route to reducing the liquidus temperature.

A difficulty with this method is confirming it experimentally. Phase measurements at elevated temperature, with a partially melted sample, are difficult to measurement and would require equipment capable of high temperature XRD measurements. It may be possible to quench or rapidly solidify the sample to analyse the phases at high temperature but this again is difficult to carry out reliably.

### Ductility and IMC modelling

An obvious reason for brazing alloys requiring ductility is that brazed joints are required to have ductility and to not fail due to high brittleness. The other main reason is that brazing alloys are usually sold in rod, foil or some other form that requires processing of the alloy down to narrow dimensions. This process is heavily dependent on the alloy being ductile enough to be processed down. A novel alloy that offered marginally improved properties but could not be processed to a useable form will struggle to be a economically viable product.

The modelling of the ductility is an intensive process and it is difficult to infer exactly from just from the phase information. The structure type and quantity of each

phase is useful for ductility estimates, as is the element distribution for estimating the solid solution hardening in an alloy. However, this information may be irrelevant without knowledge of the microstructure of the alloy. Grain size has a critical effect on the ductility, as described by Hall-Petch [106]. Other factors like the shape and orientation of the grains and the dislocation density are also important [106].

The complexity of the ductility modelling prevents the method being applied on the large scale that is planned. However, some useful information about the ductility can be inferred from the phase information available with relatively quick and simple programming. One particular trait that can be looked for is the presence of intermetallic compounds (IMCs). These have a tendency to be brittle [106, 107] and the presence of even a small amount can cause the whole alloy to be brittle [107].

Evidence that IMC content is a useful approximation of ductility can be found by analysing existing brazing alloys. If IMC is as problematic for alloys as expected then there should be very little present in the already commercial alloys [106, 107].

The simplest approach for improving the melting temperature of these alloys would be to increase the amount of the lower melting elements. This is known from experiments to embrittle alloys and was likely a factor in the original design of the alloys (i.e. metallurgists increasing the low melting temperature elements until the alloy became brittle). It would be expected that the increase of the low melting temperature elements would also produce a larger amount of IMCs. If this were to be found this would support the idea that using IMC to predict ductility is a reasonable estimation and a worthwhile approach. Lower melting elements were either added (in the case of zinc and tin) or increased (in the case of indium) to the seven previously used alloys, with the predicted results shown in Table 3.2.

Table 3.2: A selection of Ag-Cu-Zn-Sn brazing alloys with predicted IMC content. Additions of elements were done by adding the percentage of the extra element and then normalising the new composition to 100%.

| | IMC At.% | | | | | | |
|---|---|---|---|---|---|---|---|
| ISO Code | Original | 5% Zn | 10% Zn | 5% Sn | 10% Sn | 5% In | 10% In |
| Ag 156 | 8.44 | 7.40 | 3.45 | 1.60 | 14.36 | 17.00 | 53.07 |
| Ag 155 | 0.00 | 5.14 | 13.24 | 28.07 | 1.78 | 4.59 | 53.61 |
| Ag 145 | 0.00 | 5.82 | 13.54 | 27.72 | 1.36 | 4.05 | 61.69 |
| Ag 140 | 2.88 | 10.71 | 18.10 | 31.69 | 0.00 | 1.95 | 47.71 |
| Ag 138 | 0.00 | 7.21 | 14.62 | 28.28 | 0.85 | 3.45 | 8.20 |
| Ag 134 | 2.53 | 0.00 | 4.97 | 18.92 | 5.10 | 7.59 | 10.66 |
| Ag 130 | 6.64 | 14.00 | 20.98 | 33.86 | 0.00 | 0.38 | 13.72 |

The predicted IMC content for the majority of these alloys is low, at less than 3 at.%. The only exceptions are the alloy with the lowest silver, Ag130, and the high tin alloy, Ag 156. The predicted intermetallics that formed in the alloys were either CuZn gamma, $Cu_3Sn$ or both occurring in the same alloy.

The effect of adding extra zinc and tin is not uniform and the effect varies depending on the original composition, in particular the original zinc and tin concentrations. In most cases, but not all, the additional zinc and tin increased the amount of IMC. The results in Table 3.2 are plotted in Fig. 3.6 with the predicted liquidus temperatures.

The potential positive effect to adding zinc and tin was to reduce the melting temperature. This can be seen in Fig. 3.7 where additional tin reduces the liquidus melting temperature of all the alloys. The effect is not seen as consistently though with the additional zinc. This is likely due to the zinc moving a composition away from a eutectic, which counters the low melting point of the zinc.

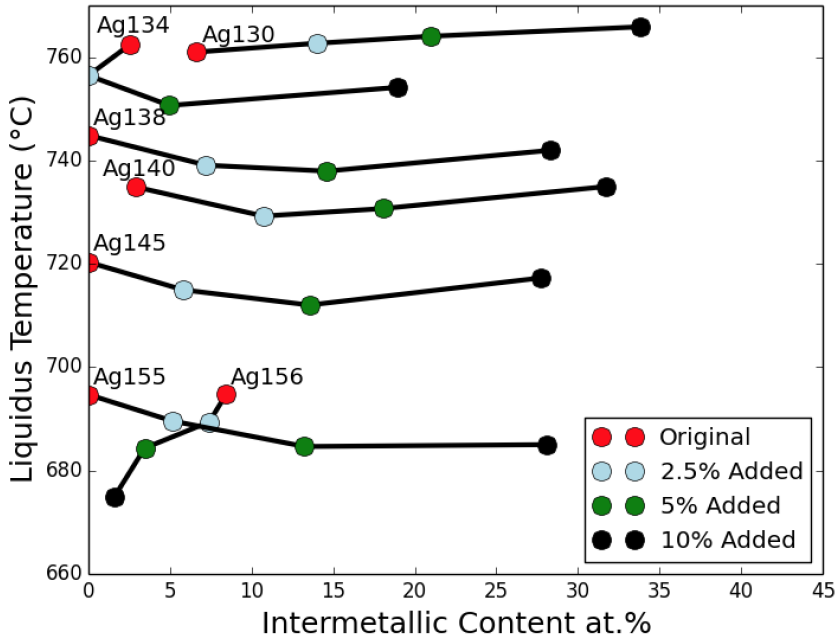


Figure 3.6: The plotted effects of adding zinc to various ISO 17672 (Ag-Cu-Zn-Sn) alloys. The colours of points represent the addition to the alloy, in weight percentage.

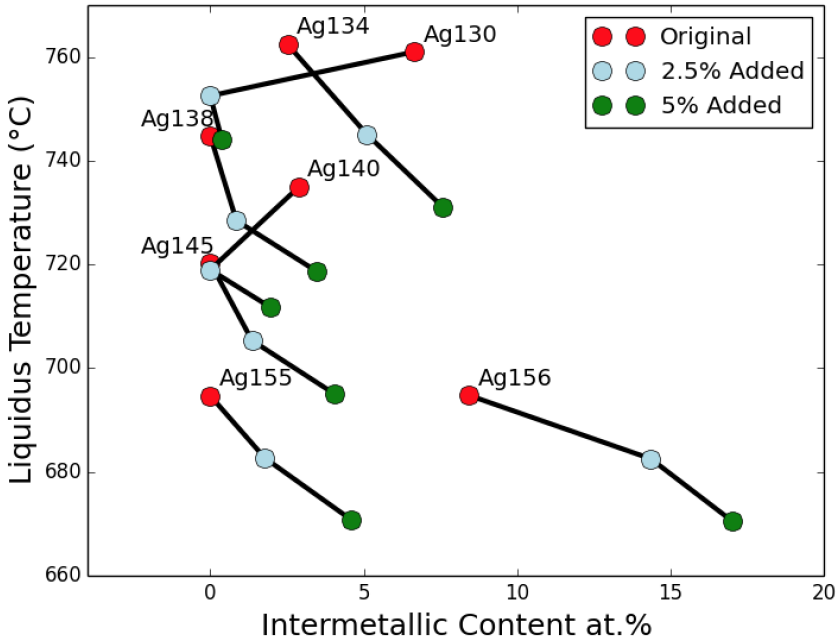


Figure 3.7: Effects of adding tin to various ISO 17672 (Ag-Cu-Zn-Sn) alloys. The colours of points represent the addition to the alloy, in weight percentage. The 10% results have not been included so the other points to be seen in greater detail.

There are two main conclusions from this phase modelling. Firstly that the use of IMC seems to be a indicator of a ductile alloy or at least as suitable for use. This is seen from the low values for the existing brazing alloys and the frequent increase shown when the composition is altered with low melting temperature elements.

The second point is that it is unlikely that alloy improvements can be made by the simple addition of an element. As seen in Fig.3.7, increasing an element produces different changes depending on the original composition. This leads to the conclusion that all elements need to be controlled at the same time to find new compositions with optimised properties.

### 3.1.3 Other Modelling - Surface Energy

As mentioned briefly in the literature review there are many formula that can be used for surface energies. The Butler equation (equation 2.3) has many formulae and can be used to calculate binary or multicomponent alloys. The Butler equation employed in this modelling uses the activity of the elements, so that

$$\sigma_i = \sigma_i^0 + \frac{RT}{A_i} ln \frac{a_i^*}{a_i} \tag{3.1}$$

where $\sigma_i$ and $\sigma_i^0$ are the surface energies of element i in the alloy and the pure form respectively. $A_i$ is molar surface area of element $i$, $a_i$ is the activity and $a_i^*$ is the activity in the surface, all for element $i$. $R$ is the universal gas constant [22].

The surface energies of the pure elements and the molar surface area for elements can be found [108, 109, 110]. The activity of the bulk can be modelled using CALPHAD. The only remaining value is the activity in the surface, which can not be found easily. To calculate this value two formulae were used to substitute in for this. These formulae were,

$$a_i = \gamma_i x_i \tag{3.2}$$

$$ln\gamma_i^* = \beta ln\gamma_i \tag{3.3}$$

where $\gamma_i$ is the activity coefficient and $\beta$ is a coefficient that relates the activity coefficient in the surface to the activity coefficient in the bulk. There are a number of values for $\beta$, ranging from 0.5 to 0.84 [111]. The value selected for $\beta$ was 0.83 from Tanaka et al. [112] that has also been used elsewhere [113].

Using the two equations, as well as the surface equivalent of equation 3.2, the original Butler equation can be arranged as

$$\sigma_i = \sigma_i^0 + \frac{RT}{A_i} ln \left( \frac{\left(\frac{a_i}{x_i}\right)^{\frac{1}{0.83}} x_i^*}{a_i} \right) \tag{3.4}$$

using 0.83 as the $\beta$ value. The only unknown input variable in this equation is the concentration of each component in the surface, $x_i^*$. There are no direct measurements or calculations of these values but they can be found using regression and the knowledge that all the $x_i^*$ must sum to 1 and the the surface energies of each component must be equal [112].

The method for finding the surface energy could not be solved analytically and was solved using a trial and improvement method. Arbitrary surface concentrations were selected and surface energies of each component were calculated. The surface compositions were there adjust until the surface energies of each component were equal to each other. This surface energy was then used as the modelled value.

The method was checked by measuring a variety of Ag-Cu compositions and comparing them to published values. Compositions were selected at 10% intervals between pure Ag and pure Cu and a temperature range of 1200K to 1600K. The results are shown in Fig. 3.8

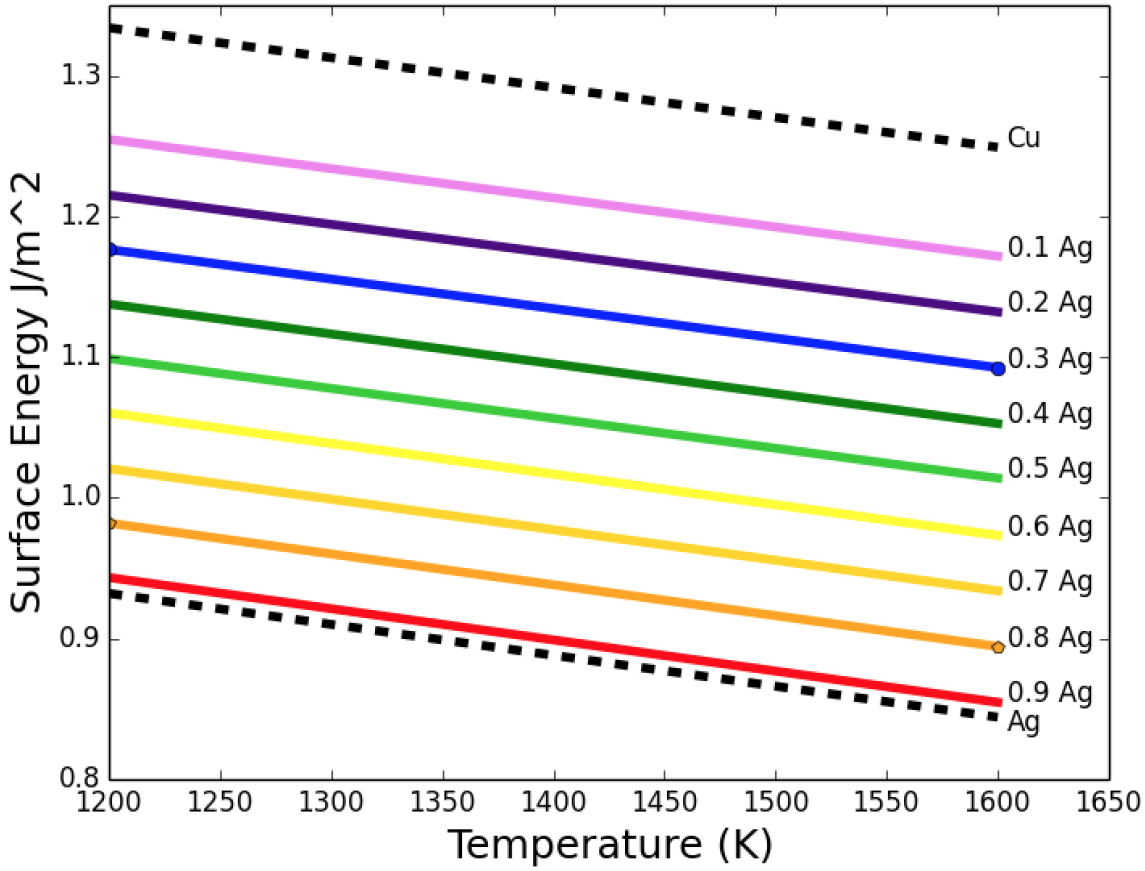


Figure 3.8: The predicted surface energies of Ag-Cu alloys over a range of temperatures. Lines have been labelled with the concentration of Ag in each alloy. Measurements were taken at small intervals, however the results were linear so any interval would provide the same results.

These predicted values seem reasonable as the changes in composition and temperature go according to the expected trends. Direct comparison to published values of Ag-Cu compositions was difficult. There is a large range of in the values of Ag-Cu surface energies. Experimental values [114, 115, 116, 117] and calculated values [118, 115] both had large discrepancies in the reported surface energies. Even measured values for pure Ag and pure Cu had discrepancies between sources [114]. While there is no definitive published set of results, the surface energies predicted in Fig. 3.8 are in the same region as the various published values.

One use of this method that could be potentially useful for brazing alloys is to

look at the effect that small additions have on the surface energy of the composition. Anecdotal reports state that elements like tin are added to brazing alloys to enhance the flow properties. The effect of tin content on a brazing alloy is shown in Fig. 3.9.

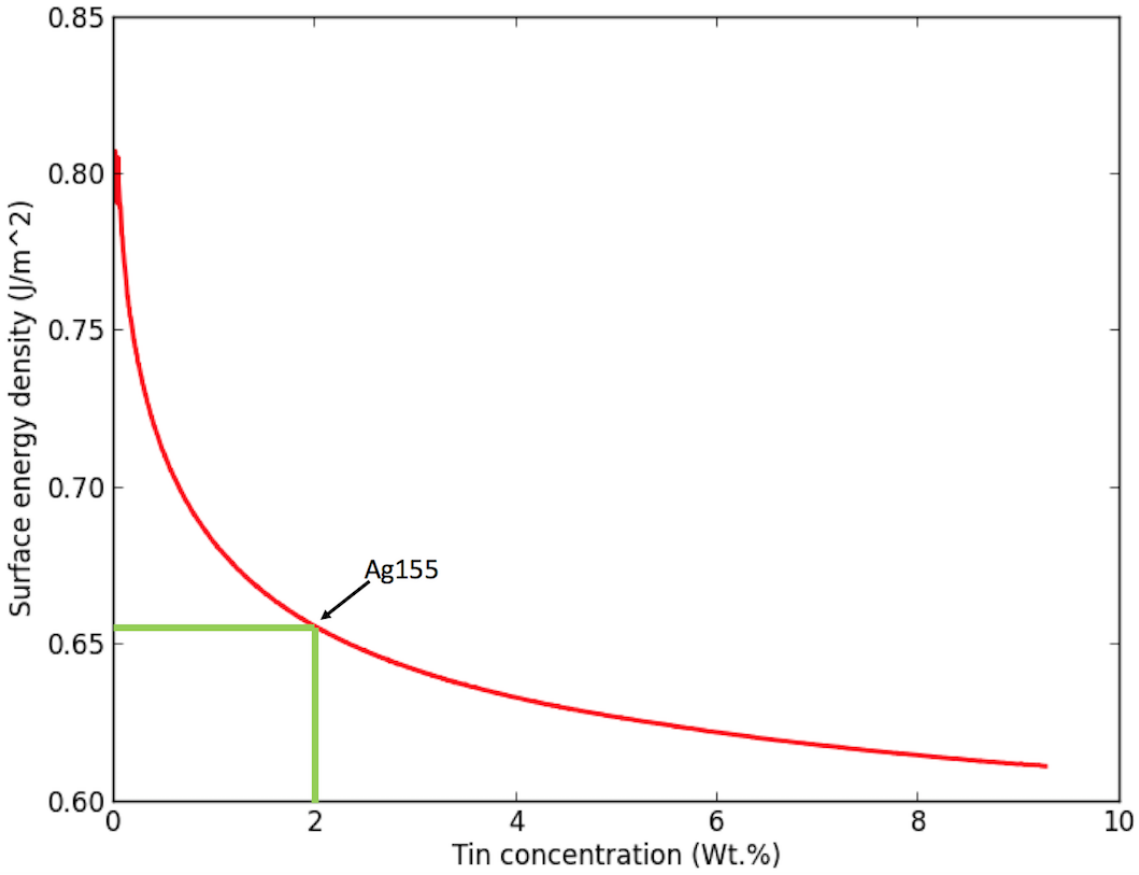


Figure 3.9: The surface energy of ISO 17672 Ag 155 alloy with varying tin content. At 2 wt.% tin the alloy is at the Ag 155 composition. At other tin concentrations the Ag-Cu-Zn contents are scaled proportionately.

The results in Fig. 3.9, and similar trials, were of particular interest. They highlighted how small amounts of some elements can have large effects on the surface energy. This supports the observed phenomenon in the brazing community that the small tin additions are included in alloys to improve the wetting and flow.

There are a number of problems with the surface energy modelling however which prevent it from being a useful modelling tool in this research. The results predicted

here are for ideal situations with uniform, stable temperatures and do not consider the substrate the alloy is on. In practicality the temperature varies and the surface that is being brazed has a significant effect on the results. There are then further problems such as the presence of flux on the surface.

Even if all these problems could be addressed the wetting is not the highest priority property. Melting temperature, cost and joint performance are all more important. The main useful discovery from this modelling though is the supporting modelled data to the effect small element additions can have. This provides an incentive to trial small element additions when looking for new alloys in later searches (see Chapter 6).

## 3.2 Modelling of New Brazing Alloys

### 3.2.1 Modelling Using Thermo-Calc

The CALPHAD program that was used for this research was Thermo-Calc. The Thermo-Calc software has inbuilt functions that can make complex graphs easy to plot. However, due to the coding that Thermo-Calc uses it can also be difficult to get other programs to interact with it.

As this work requires Thermo-Calc to interact with other software and databases it was necessary to create an interface between it and other programs. The other programs that Thermo-Calc needed to interact with were created in Python, with the intention that the code would control both the inputs and the management of the output data.

This process of getting Thermo-Calc and Python to interact was not as straight forward as it might have been. Thermo-Calc is written using Fortran, a computing language originally developed in 1950s. There was an added complication with Thermo-Calc that as a commercial program there are elements of secrecy with the exact workings of the code.

The solution to the problems of getting Python and Thermo-Calc to communicate was not elegant but did allow the full range of measurements to be taken. To get Thermo-Calc to carry out the desired measurements a macro file was used. This macro file acts as a list of commands for Thermo-Calc. The Python code has the job of compiling the desired measurements and then writing them out into a text file in a form that Thermo-Calc will understand. The Python program then saves the text file with the correct extension and executes the file. Once executed Thermo-Calc carries out these instructions as if they were being typed in manually.

As part of the macro file there is information about where to save the various measurements. These measurements are then opened and read using the same Python program. The program reads the text output and extracts the text that correspond to the required data.

### 3.2.2 Python Trials

The Python program has the task of interfacing with Thermo-Calc but it also has the job of generating the list of requests, both in terms of composition and temperatures. Composition lists were sometimes set lists of a handful of alloys. These could just be manually entered into a NumPy (numerical python) array and used from there. If the alloys were from different systems then there would be some extra code required to allow switching between systems (essentially reseting Thermo-Calc before reloading new parameters).

The alternative to this is a spread of compositions across a system. This may be across the entire range of the system (replicating a phase diagram) or is more likely to be focused in on a specific region of alloy space. An appropriate composition increment needs to be set here, one that is not too fine that it takes too long computationally but not so coarse that it misses potentially useful compositions.

The options for selecting the compositions depend on whether the trial is analysing a select few alloys or searching a region of alloy space. The options for temperature

control also depend on which trial is desired. The temperature scan, as seen in Fig. 3.5, is one option. This method is thorough and contains a lot of information, but it is a very time consuming process. The other option is to take only measurements at room temperature, the solidus temperature and the liquidus temperature. This method makes use of "calculate-transition" function that can accurately find the phase transitions for phases, in this case liquid.

In addition to the measurement controls there are some additional data handling methods when searching for new alloys. The main task was to find compositions with the best combinations of properties. This was necessary as often the optimisation of one property was at the detriment of another property. Finding the best compromises and the limits to how far each property can be pushed are necessary steps when exploring new alloys.

There was also some additional code, that will only be covered here briefly, available to ensure trials of new compositions were spread out. There was a risk that all the best alloys, according to whatever criteria is being used, would all have very similar compositions. To avoid this there was a code implemented that would exclude from further selection any alloy that was similar to an alloy already selected. This would ensure that the alloys selected for trials would be somewhat spread out around the alloy space of a system.

The limit on how similar the alloys selected could be changed depending on the trial. A typical limit would be that at least one component of the alloy had to be more than 2 at.% away from the original. On a ternary diagram this can visualised as drawing a circle around a composition that acts as an exclusion zone. Of course in these high order systems the circle cannot be drawn and the exclusion zone becomes a N-dimensional hypersphere.

### 3.2.3 Other considerations

There are a number of other properties that are important for brazing alloys but that will not be a focus of investigation within this research. These include corrosion, the bonding with different parent materials and the flow. These properties were either not considered a priority or were controlled in such a way that they were not likely to vary much or be a factor used for discriminating between alloys.

Corrosion has the potential to have a devastating effect on new alloys that might otherwise have excellent properties. For the most part research into novel alloys avoids this problem by not radically changing the alloy system. Tweaks to compositions within a system are unlikely to develop significantly different corrosion properties. Also, when searches go across multiple systems they tend to focus on elements that are already used in brazing alloys. This means that the corrosion characteristics of each element should be already known.

The bonding between brazing alloys and the parent materials is an important consideration when selecting brazing alloys. Some alloy systems are versatile but many of the systems are tailored for one or two particular applications. Similar to the way corrosion was not a problem, most potential problems with bonding are avoided by staying within systems and only using known elements.

The surface tension, or wetting, refers to the force that draws an alloy along through a joint. The flow properties refer to how easy that alloy is to move along the joint. This can be modelled with formula related to the surface energies and the viscosity [18]. However, flow properties were not explored in much detail as it was a low priority property. A great many brazing alloys have poor flow properties, with cost, melting temperatures and ductility all considered more important.

## 3.3 Case Study on ISO 17672 AG 155

The various modelling techniques can be used to search entire alloy systems, or even multiple systems, to find the alloys with the best overall sets of properties that may offer an improvement on existing alloys. However, filtering through so many results is a tedious process and comparing vastly different compositions and properties is difficult. To make things simpler and easier to manage the search for new alloys is broken down into multiple smaller searches. These searches are often defined by existing alloys, with searches targeted at offering an improvement in some way on a particular alloy. As an example of this process and the results it can generate this case study is focussed on ISO 17672 Ag 155, from now on referred to as just Ag155.

### 3.3.1 Details about Ag155

Ag155 is from the Ag-Cu-Zn-Sn system. It has a composition of Ag 55wt.%, Cu 21wt.%, Zn 22wt.% and Sn 2wt.% with a quoted melting range of 630 °C to 660 °C. Ag155 is a widely-used alloy that is noted for its versatility in its application and material it can join as well as excellent all round properties. As can be seen from Table 3.1 the melting range is low compared to the other brazing alloys. Table 3.1 also shows that the Ag content is the among the highest and it can be assumed so is the cost of the alloy. There are many factors that make up the cost of an alloy but for this particular alloy the cost of the other elements and the production will likely be much smaller than the silver cost.

### 3.3.2 Searching for an Ag155 replacement

There are two main targets for an Ag155 replacement. A replacement alloy can either have better brazing related properties or can achieve similar properties with a reduction in silver content. For the properties the ultimate goal would be a brazing alloy with a lower liquidus melting temperature that still maintains all the other

necessary brazing properties (i.e. ductility, flow, joint strength, etc...). Alternatively, a reduction in silver would also be attractive for companies that use brazing alloys.

As mentioned, there are a number of different approaches that can be taken for modelling new alloys. The most appropriate method for this case study is to use a large number of compositions across a region of alloy space. To accompany this the temperature predictions should only look at the room temperature, solidus and liquidus as the long temperature scan will be too time consuming.

The search for new alloys looked at compositions around the starting composition of Ag155. This search was purposefully set with wide composition limits for a large number of trials, before the results are filtered and optimised. The wide composition limits do cover alloys that would appear to have an obvious problem (e.g. more expensive or high melting) but it is a more thorough approach to include these alloys and then to filter these out later.

The search limits used in this search are shown in Table 3.3. The step size used was 1 wt.%. This step size was chosen as it was fine enough to not miss potential alloys. As this was not a particularly large trial this step size could have been reduced to 0.5% or even smaller if desired. However, this was thought unnecessary as the production methods, both in these experiments and in industrial production, have an error of between 0.5 wt.% to 2 wt.% associated with the amount of each element.

Table 3.3: The range of values that were used in this trial around Ag 155. All the alloys trialled had compositions within these limits at 1% intervals.

| Element | Original value (Wt%) | Range of values (Wt%) |
|---|---|---|
| Ag | 55 | 40 - 60 |
| Cu | 21 | 10 - 40 |
| Zn | 22 | 10 - 40 |
| Sn | 2 | 1 - 5 |

The results of this scan were calculated and were saved to a database. For easy comparison the main data points used were the liquidus temperatures and the amount of IMC present, with some attention paid to the solidus temperature also. The liquidus temperatures and the IMC contents are shown in Figs. 3.10-3.13. In order to see the effect of different elements each figure has the results shaded according to the content of a particular element. There are 3646 compositions in each plot.

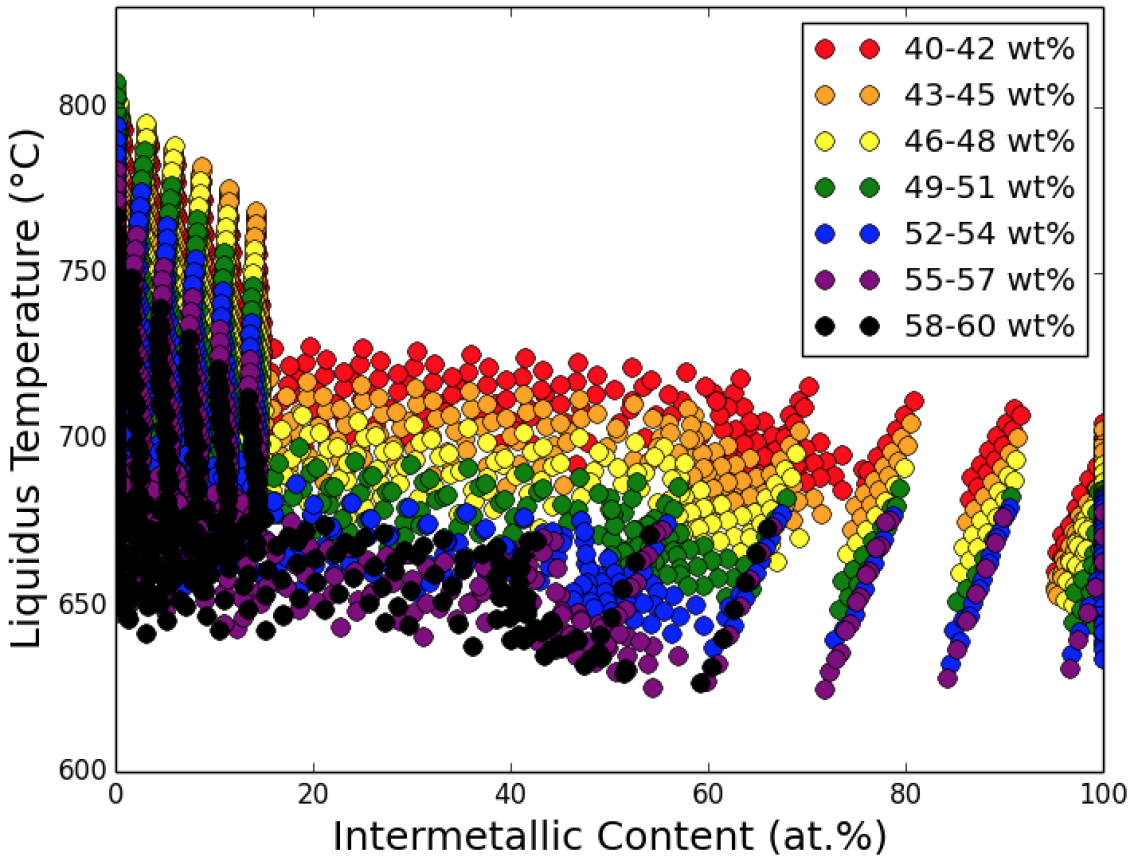


Figure 3.10: The results of the scan to find a replacement to Ag155, across the limits set out in Table 3.3 with points coloured according to silver wt.%.

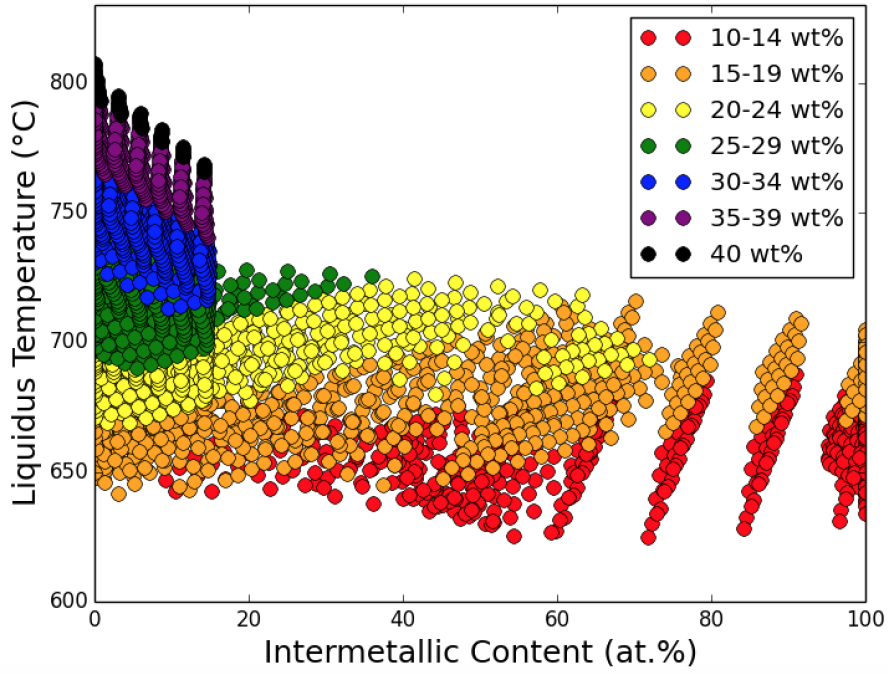


Figure 3.11: The results of the scan to find a replacement to Ag155, across the limits set out in Table 3.3 with points coloured according to copper wt.%.

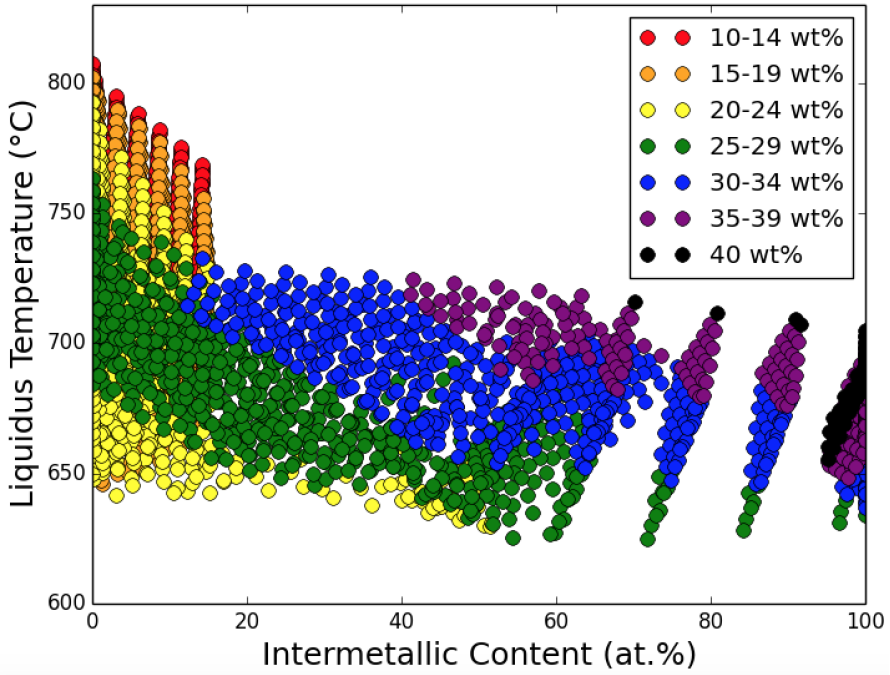


Figure 3.12: The results of the scan to find a replacement to Ag155, across the limits set out in Table 3.3 with points coloured according to zinc wt.%.

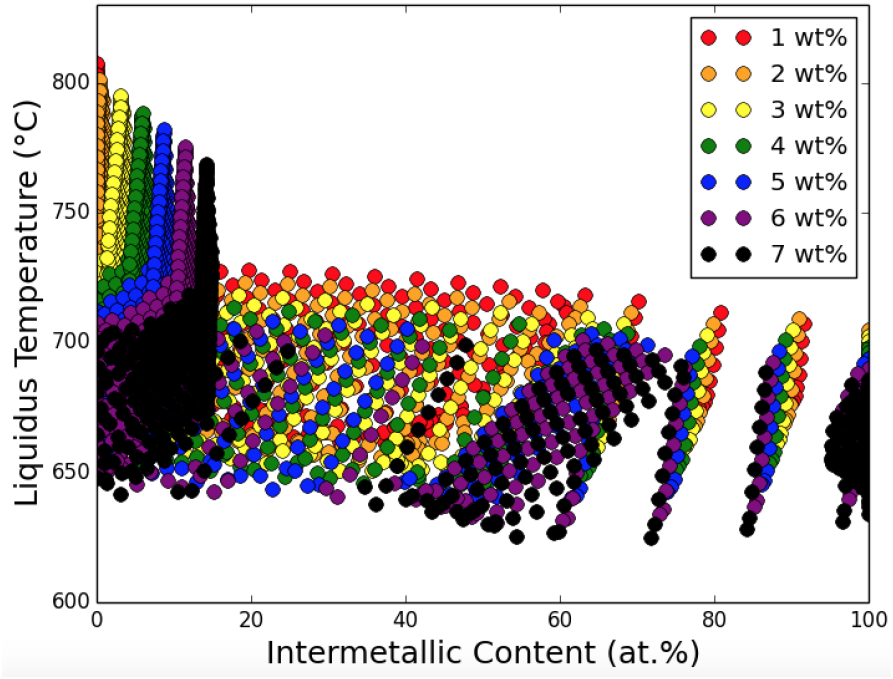


Figure 3.13: The results of the scan to find a replacement to Ag155, across the limits set out in Table 3.3 with points coloured according to tin wt.%.

The main properties used for selection from this range of compositions are the liquidus temperature, silver content and the IMC content. The properties that need to be optimised are the liquidus temperature and the silver content. The IMC content does not need optimising and is likely the limiting factor to the improvements of the others properties.

In this method it was forecast that the IMC amount would act as a limit on the improvement alloys. It was expected that once a certain level of IMC was reached the alloy would become too brittle. The location of this limit was not obvious though. Analysis of the ISO 17672 range of brazing alloys showed that IMC content was low in existing brazing alloys and that keeping the IMC low would likely be a desirable aim for new alloys. However, existing brazing alloys may have been conservative in design. It would mean that using such a low level of IMC content as a limit may be an unnecessarily strict limit that needlessly excludes potentially good alloys.

The decision therefore was to favour alloys with a low amount of IMC but to also

have some alloys with medium and high amounts to confirm that they are brittle as would be expected. For the range of IMC values selected the other properties were then optimised for the other properties. The optimisation process in this case was simple as the lower silver content alloys tended also to have a lower melting temperature.

Table 3.4: The modelled properties of Ag 155 and the 12 new alloys that have been selected, listed from the highest in silver to the lowest.

| Alloy number | Composition (Ag-Cu-Zn-Sn) | Predicted IMC content (at.%) | Predicted melting range (°C) |
|---|---|---|---|
| Ag 155 | 55-21-22-2 | 0% | 642-670 |
| NBA1 | 54-18-23-5 | 2% | 608-662 |
| NBA2 | 52-16-31-1 | 41% | 639-677 |
| NBA3 | 52-25-18-5 | 9% | 636-608 |
| NBA4 | 52-17-29-2 | 31% | 626-675 |
| NBA5 | 52-16-31-1 | 41% | 639-677 |
| NBA6 | 52-17-28-3 | 25% | 613-671 |
| NBA7 | 49-16-34-1 | 52% | 646-687 |
| NBA8 | 49-18-32-1 | 41% | 644-680 |
| NBA9 | 47-19-33-1 | 43% | 645-698 |
| NBA10 | 46-19-34-1 | 43% | 645-698 |
| NBA11 | 45-21-33-1 | 39% | 644-706 |
| NBA12 | 43-16-40-1 | 43.1% | 648-690 |

### 3.3.3 Practical methods

To produce the alloys two methods were carried out, a furnace method and an induction method. The most significant problems that had to be overcome were largely

caused by the zinc. Compared to the other elements in these alloys zinc has a low melting and boiling point. Zinc boils at 907 °C, which is below the melting temperatures of silver, 961.8 °C, and copper, 1085 °C. Even below the boiling temperature zinc has a high vapour pressure and so will readily evaporate. This means that even the eutectic temperature of silver and copper, 780 °C, is liable to cause some evaporation of zinc [36, 33].

The oxidation of zinc is another problem that has to be controlled. In a heated environment exposed to the air the zinc will readily oxidise to a zinc oxide compound. The presence of zinc oxide in a melt is not necessarily problematic, as it will tend to separate from the rest of the molten elements and not form part of the finished alloy. However, the oxidation does mean that some of the zinc intended for the alloy is no longer present, and so the alloy may be significantly different than the intended composition.

### The Furnace Method

The furnace method uses multiple muffle furnaces and an argon gas flow. To limit the zinc evaporation two furnaces are used at different temperatures. The cooler of the furnaces, at 450 °C, melts a crucible of zinc. A hotter furnace melts all the other elements together. This furnace starts at 1000 °C to ensure silver melts. Then due to the eutectic between silver and copper this temperauture can be reduced to approximately 800 °C. The exact temperature of the hotter furnace would vary depending on the composition. Once both the contents of both crucibles are fully molten, the heating time required depends on the composition, then the crucibles are combined and cast into an ingot.

The theory behind this method was that the zinc evaporation could be limited by using a cooler furnace just for the zinc. Also, temperatures were chosen to be just hot enough to mix the alloys, as excess heat would increase zinc evaporation.

### The Induction Heated Method

The alternative method, that was developed after the furnace method, used a small scale induction melter with a borax coating. The induction melter was an Ambrell 2.2kW cooled with a water chiller. This method would place all the elements in a single crucible with significant mixing of the elements. Silver and copper were used in shot form while the zinc and tin were cut up to a similar size. The borax coating was then poured on top of the elements.

This method relied on the protective effect of the borax as well as the rapid temperature changes possible with the induction melter. The borax starts as white powder, similar to coarse salt crystals in appearance. The borax at 743 °C will melt and form a glassy liquid that floats on top of the elements. This liquid acts as a barrier preventing gaseous zinc escaping and preventing oxygen from entering.

The heating procedure with the induction melter is also designed to prevent zinc evaporation. The process attempts to be as quick as possible, to limit the chance for zinc to evaporate, while also avoiding any overheating that will quickly boil the zinc. The stage is to rapidly heat the mixture to the melting point of zinc. The heat is then smoothly increased over approximately 3 to 4 minutes to a temperature where it is entirely molten. This smooth increase in heat is intended to encourage the alloying of the elements and not leaving zinc as an element to get hot and boil. Penultimately there is a brief period of heating and mixing of the alloy to ensure a complete melting and alloying, before finally the alloy is cast into a 6mm rectangular ingot.

The furnace method was developed first and could achieve accurate compositions. However, the method was not reliable. Slight mistakes could result in significant oxidation and zinc loss. It was always apparent when this happened as the oxidation of the zinc left a distinctive yellow stain an the presence of a wispy white material unlike any of the other elements involved.

The induction method though provided slightly more accurate compositions and had a much higher success rate. As long as there was no break in the borax coverage

then the melts would hit the composition reliably. For the main results the induction method was chosen as the principle method for alloy production.

### 3.3.4 Experimental results

The experimental measurements offered opportunities to test the alloys produced from this method but also a chance to verify aspects of the method. This verification of methods, such as melting temperature and phase predictions, will be carried out on the novel alloys and the existing brazing alloys.

#### Compositions of Novel Alloys

The novel alloys outlined in Table 3.4 were produced and the compositions were confirmed using x-ray fluorescence (XRF) analysis. The results of the XRF on these alloys are shown in Table. 3.5. The XRF analysis was carried out primarily using a Panlytical Zentium with a standard element scan for solid samples in a vacuum. Measurements were repeated by sending samples away to London & Scandinavian Metallurgical Co for analysis in a guided microwave spectrometer (GMS). Results matched within 1 wt.% of the intended composition.

Table 3.5: The nominal compositions and the compositions of the as-produced alloys that were measured using XRF and also confirmed externally using guided microwave spectrometer (GMS) techniques.

| Alloy Number | Intended Composition (Ag-Cu-Zn-Sn) | Ag (wt%) | Cu (wt%) | Zn (wt%) | Sn (wt%) |
|---|---|---|---|---|---|
| Ag 155a | 55-21-22-2 | 55.6 | 20.5 | 21.9 | 2.0 |
| Ag 155b | 55-21-22-2 | 54.7 | 20.8 | 22.5 | 2.0 |
| NBA1 | 54-18-23-5 | 53.9 | 18.2 | 23.4 | 4.5 |
| NBA2 | 53-16-29-1 | 53.3 | 16.4 | 29.3 | 1.0 |
| NBA3 | 52-17-29-2 | 52.3 | 17.2 | 28.6 | 1.9 |
| NBA4 | 52-25-18-5 | 51.8 | 24.8 | 18.4 | 5.0 |
| NBA5 | 52-16-31-1 | 51.7 | 16.0 | 31.3 | 1.0 |
| NBA6 | 52-17-28-3 | 51.5 | 16.9 | 28.6 | 3.0 |
| NBA7 | 49-16-34-1 | 49.0 | 16.0 | 33.9 | 1.1 |
| NBA8 | 49-18-32-1 | 49.0 | 18.3 | 31.7 | 1.0 |
| NBA9 | 47-19-33-1 | 46.8 | 18.7 | 33.5 | 1.0 |
| NBA10 | 46-19-34-1 | 46.5 | 18.8 | 33.6 | 1.0 |
| NBA11 | 45-21-33-1 | 44.9 | 20.8 | 33.3 | 1.0 |
| NBA12 | 43-16-40-1 | 43.1 | 16.0 | 39.8 | 1.1 |

### Melting temperatures

The ISO 17672 alloys from earlier and several novel alloys were measured using Differential Thermal Analysis (DTA). The scans were carried out using heating and cooling at a rate of 5 K/min between room temperature and 800°C. An example of scan from a DTA is shown in Fig. 3.14.

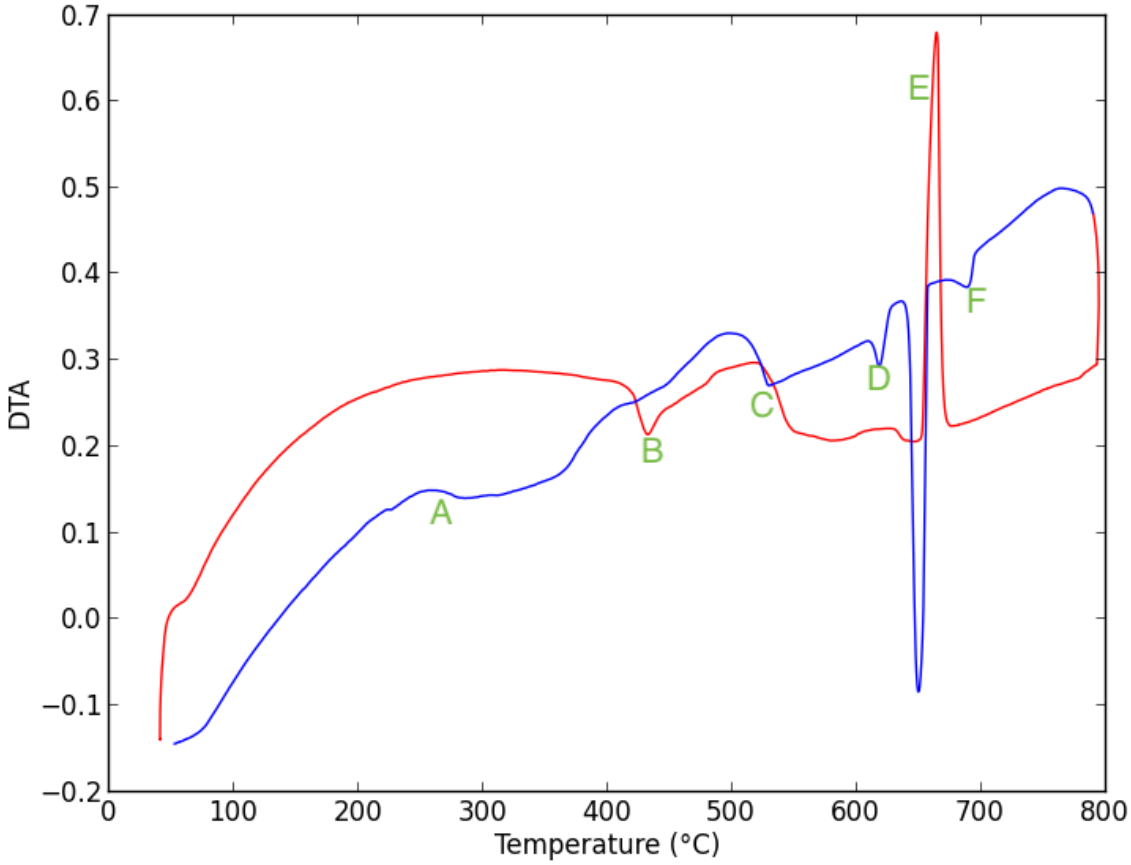


Figure 3.14: The trace from the DTA scan for Ag155. The red line indicates the heating part of the scan and the blue line represents the cooling part of the scan. Various points of interest have been labelled in green.

The results in Fig. 3.14 can be related to the Thermocalc predictions. Points A, B and C relate to solid solution transformations. Points D, E and F refer to liquid-solid transitions, each representing different solid phases melting to liquid (or solidifying when cooling). Point D is the lowest melting phase and corresponds to the Cu-Zn phase that is predicted using Thermo-calc. The largest melting spike, point E, correlates with the FCC-Ag phase that is the largest present phase according to the modelling. The highest melting phase, point F aligns with the FCC-Cu which is predicted to be the last phase to melt.

Results were evaluated by taking average values of the colder side of the each spike (the solidus) and the hotter side of each spike (the liquidus). The results for the ISO

17672 alloys are shown in Fig. 3.15 along with the quoted values and the modelled values.

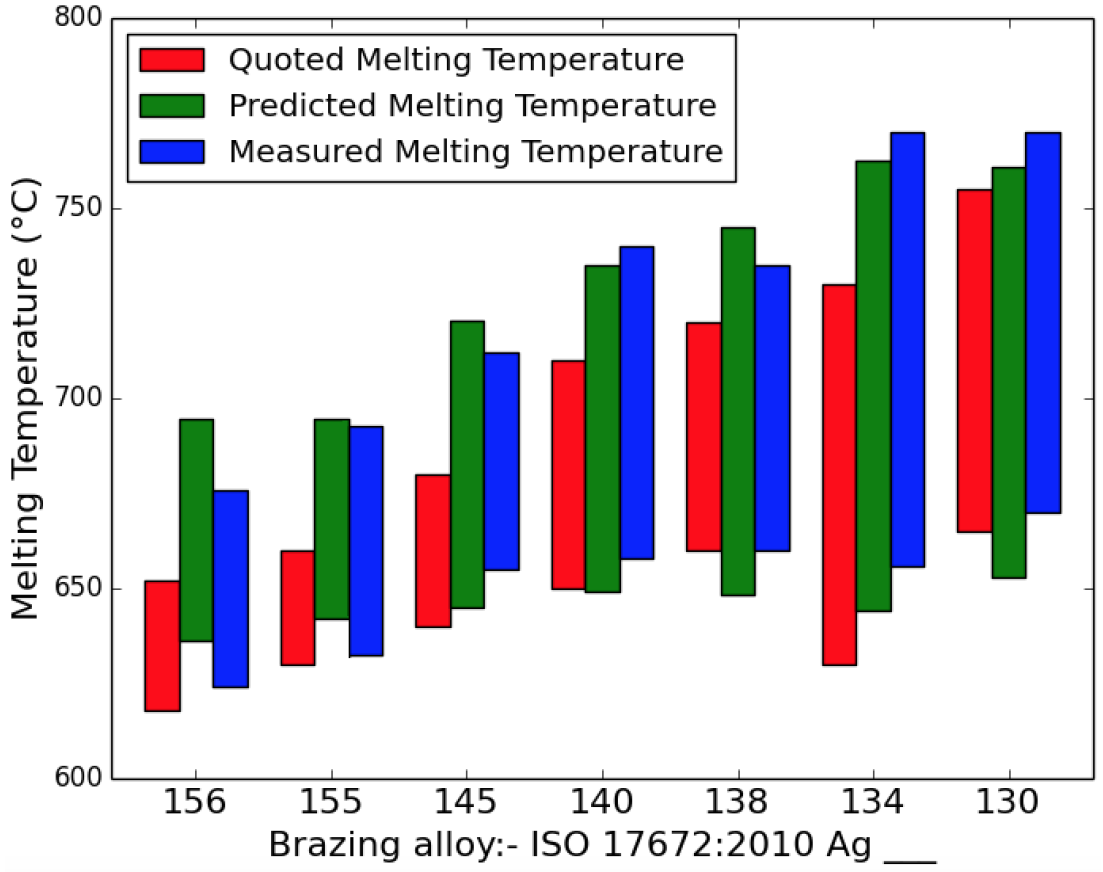


Figure 3.15: The melting ranges for the ISO 17672 alloys. The values shown are the quoted values from literature [14] (in red), the predicted values from CALPHAD modelling (in green) and the measured values from DTA analysis (in blue).

The measured melting temperature values agreed with most of the existing data. For the low melting temperature alloys, where the quoted and predicted melting temperatures were already close, the measured melting temperature was also in reasonable agreement. For the low melting temperature alloys the tended to have melting ranges similar to the quoted values (i.e. a narrow range) but was closer in the value to the modelled values (melting at a slightly higher temperature).

For the novel brazing alloys an initial screening was carried out to find approximate values for the melting temperatures. This was done by placing similarly sized

pieces of alloys (approximately 2g) on copper coupons and subjecting them to the same heating. Comparing novel alloys with each other and with Ag155, along with the subsequent repeat measurements, it became clear which alloys were the lowest melting, around the controlled flame region as Ag155 and which alloys definitely had a higher melting point. These higher melting point alloys were not sent for DTA and not considered as an alloy replacement, but some further experiments were carried out on them. The main point of this initial screening was to save on costly DTA measurements that were clearly unnecessary on alloys that were definitely not going to improve Ag155.

The novel alloys selected for DTA analysis were measured in the same way as the results from Fig. 3.15. The results are plotted with modelled values that were calculated. Also shown for comparison is the manufacturer supplied Ag155 and the two versions of Ag155 that were produced using the same method as the novel alloys. The results are shown in Fig. 3.16.

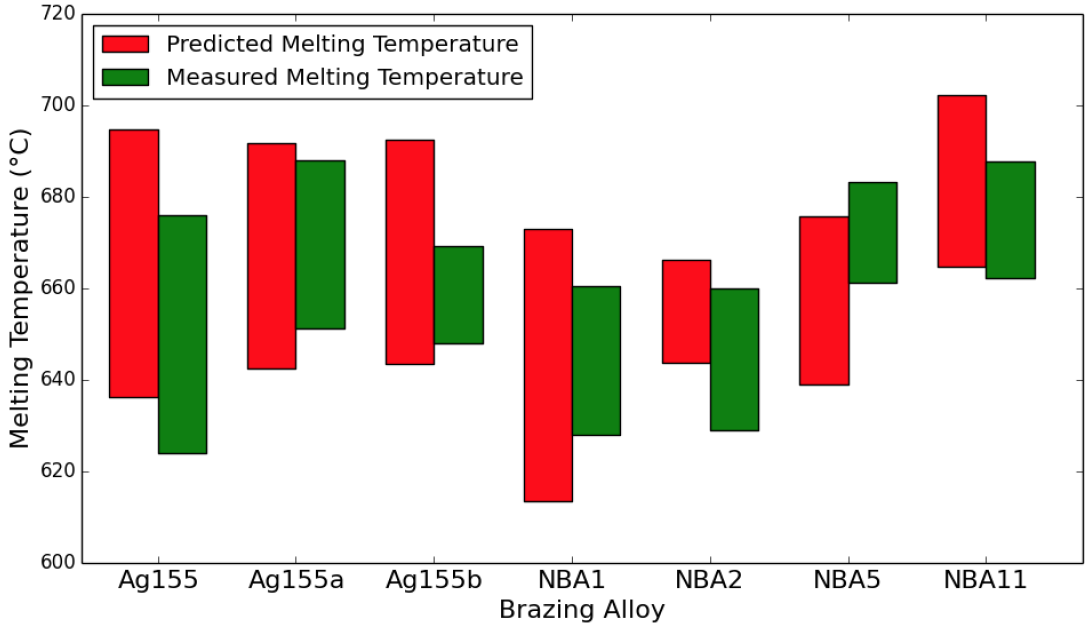


Figure 3.16: The predicted and DTA measured melting ranges for the lowest melting of the novel alloys that were produced.

The results in Fig. 3.16 show that some of the alloys (NBA1 and NBA2) offered improved melting properties over Ag155. However, in order to be considered as an alternative to Ag155 the brazing performance must be suitable and the silver content must justify the overall performance of the alloy.

### Ductility and Brazability

The next stage of alloy development is to test the ductility of the alloys. As the ductility of the alloy is important for the production of the alloy, for example rolling or drawing, a test was devised to replicate this scenario. The alloys were to go through a cold rolling procedure with success and failure judged on whether alloys cracked or held together. The process involved successive passes reducing the roll gap from the original size by 1mm until 1mm is reached. Finally a pass is done at 0.5mm roll gap. Results grouped into distinct brittle and ductile definitions with no alloys having moderate ductility. The results of the test are shown in Table 3.6.

The brazability is a non-standard but widely used test in brazing alloy development [12]. The alloys are brazed using a typical brazing setup so the user can get a gauge on how well the brazing alloy performs in service. There are many properties that are relevant to this test. Some of the properties have already been measured in this research, such as the melting temperature and ductility. The results also helped to confirm the initial screening results about which alloys had a higher melting point than required.

There were other properties involved in the test that had not been measured, such as the wettability, the flow and the strength of the joint. The results are inevitably subjective but efforts were taken to reduce the subjectiveness. Repeat measurements were taken and the heating process used was as standardised as possible. Results were scored in comparison to the Ag155 alloy that has excellent brazing properties. The results of the test are shown in Table 3.6.

Table 3.6: The evaluated properties of the Novel Brazing Alloys (NBA) and the two Ag155 alloys.

| **Alloy** | Ag wt% | **Ductility** | **Brazability** |
|---|---|---|---|
| Ag155a | 55.6 | Ductile | Excellent |
| Ag155b | 54.7 | Ductile | Excellent |
| NBA1 | 54.0 | Ductile | Good |
| NBA2 | 53.3 | Ductile | Good |
| NBA3 | 52.3 | Ductile | Poor |
| NBA4 | 51.8 | Ductile | Average |
| NBA5 | 51.7 | Brittle | Good |
| NBA6 | 51.6 | Brittle | Poor |
| NBA7 | 49.0 | Brittle | Excellent |
| NBA8 | 49.0 | Brittle | Good |
| NBA9 | 47.0 | Brittle | Good |
| NBA10 | 46.5 | Brittle | Excellent |
| NBA11 | 44.9 | Brittle | Poor |
| NBA12 | 43.1 | Brittle | Average |

### Alloy results

The results from the temperature measurements and the ductility measurements showed that there were two alloys that had viable performance in rivalling Ag155 in terms of melting, brazability and ductility, namely alloy NBA1 and NBA2. These alloys are the two highest in silver content out of the the novel alloys, with 54 wt.% and 53.3 wt.% respectively. These values of silver content are so close to that of Ag155 (55 wt.%) that these melts do not offer an overall improvement.

### Phase Analysis of Ag155 and Potential Replacements

The final part of the experimental work is to look at the phases present in the alloys. This was done to assess the accuracy of the phase predictions from earlier and also to see if there are any traits that the best performing and most ductile alloys have in common. X-ray diffraction (XRD) analysis was carried out on the alloys using a Bruker D2 machine and a Cu K$\alpha$ source. The XRD scan that was done Ag155 is shown in Fig. 3.17.

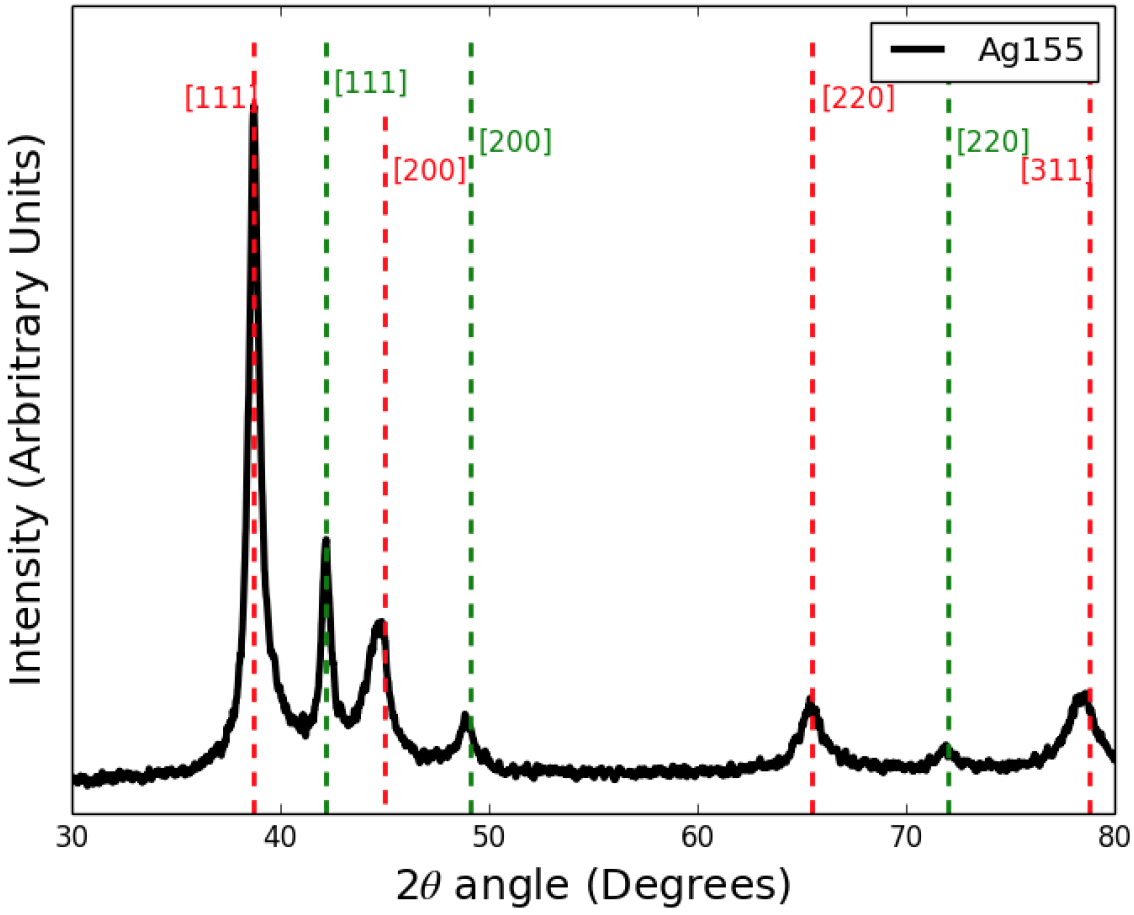


Figure 3.17: The XRD trace for Ag155. The peaks of the two FCC phases are highlighted with the red and green vertical lines. The FCC-Ag is in red and the FCC-Cu phase is in green.

This two phase structure can also be seen when analysed using SEM. Image was

taken using a Philips XL 30S electron microscope. A micrograph of the alloy is shown in Fig. 3.18.

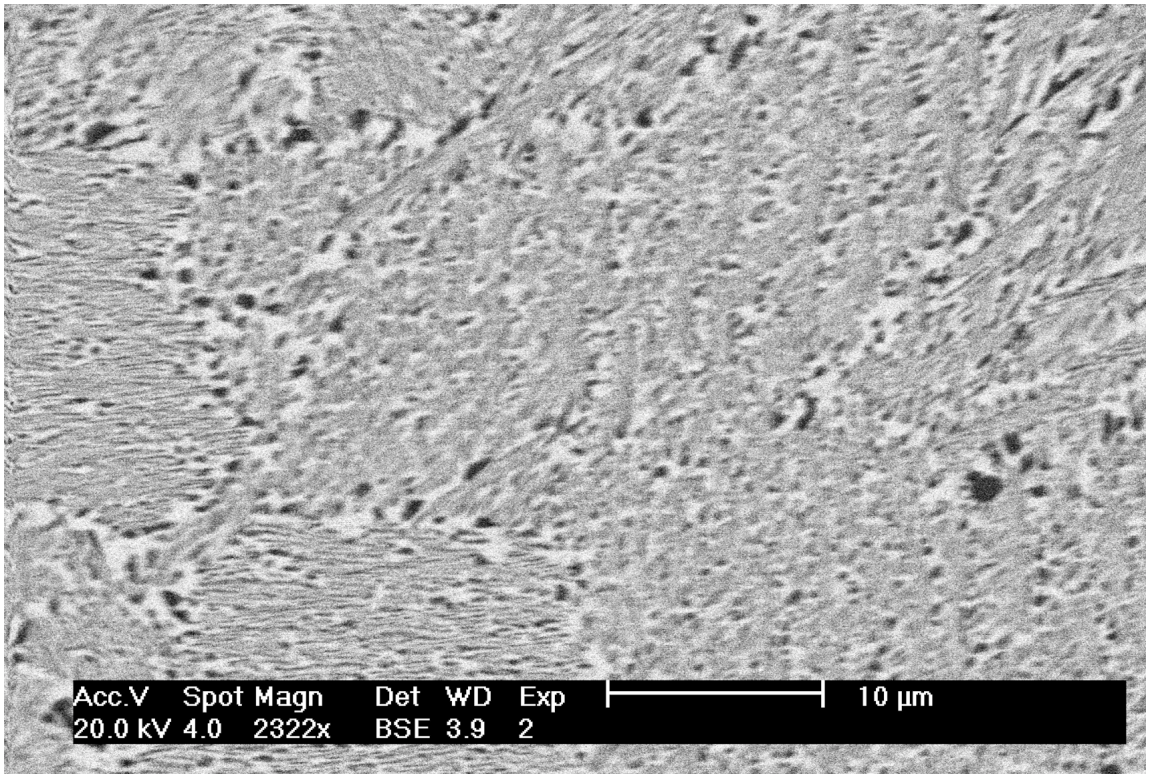


Figure 3.18: A backscattered electron image of Ag155 showing the two phase structure that was predicted using CALPHAD and measured by XRD. The light colour is FCC-Ag and the dark colour is FCC-Cu.

### Phase Analysis of Alloys with IMC

The alloys analysed so far have not contained any IMC content. However, this was expected as the CALPHAD modelling predicted there would be no, or very little, IMCs present. To investigate if the predictions of IMC formation were accurate across the range of predictions some alloys with IMC were made analysed. One example is NBA11 which was produced and found to be extremely brittle. The sample after one pass of the rolling test shattered into many pieces, as seen in Fig. 3.19


Figure 3.19: NBA11 after one pass of the rolling ductility test. The roll gap was less than 1mm smaller than the thickness of the sample.

The XRD analysis of NBA 11 was carried out using the same equipment (Bruker D2 Phaser) and techniques as the other XRD analyses in this chapter and the other chapters. The results are shown in Fig. 3.20

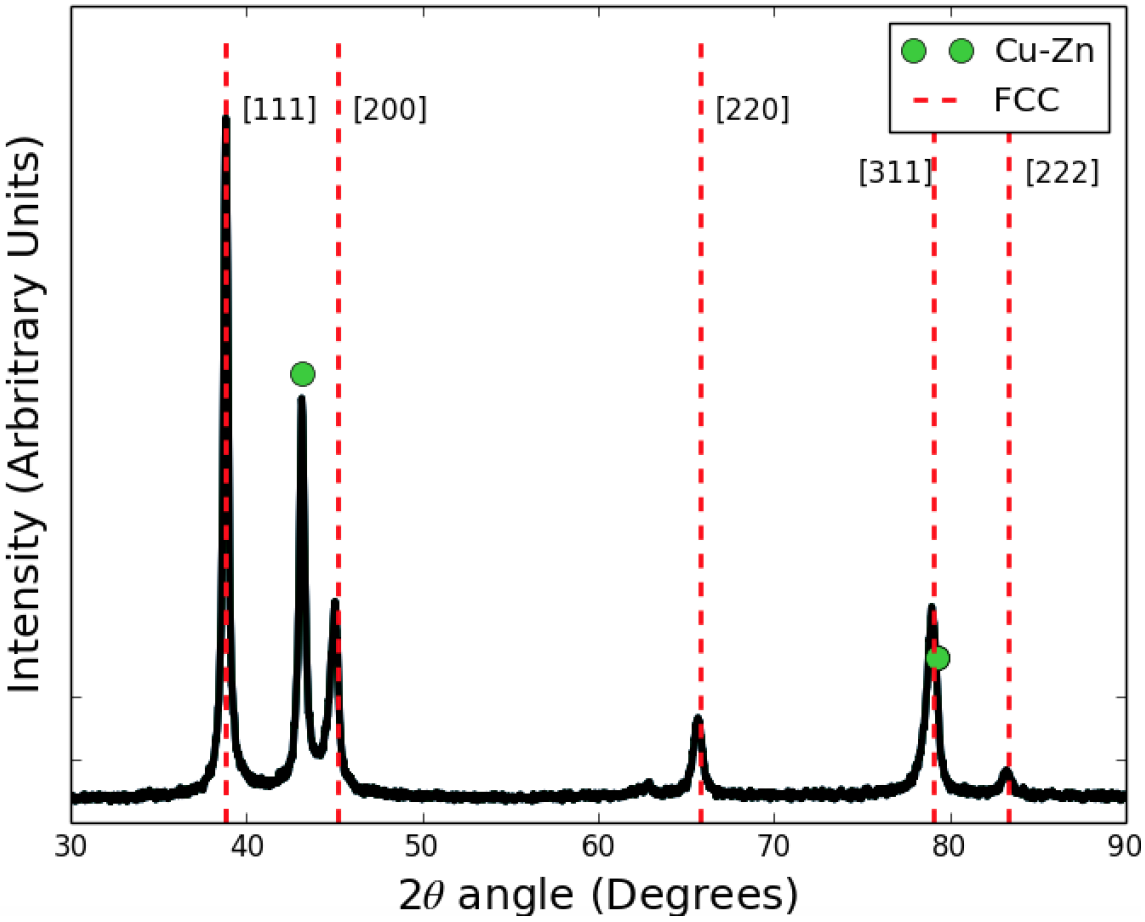


Figure 3.20: The XRD of NBA11. Indicated is a FCC phase with a lattice parameter of 4.015Åand Cu-Zn IMC. The second Cu-Zn marker is hidden within the [311] peak of the FCC.

The XRD of NBA11 found a dominant FCC phase and secondary Cu-Zn IMC phase. This was in approximate agreement with the predictions. More complex analysis, possibly including EDS or repeat XRD measurements would be needed to confirm the ratios of the phases.

## 3.4 Conclusion

The first part of this thermodynamic modelling chapter looked at the details of existing brazing alloys. The thermodynamic modelling of the alloys, in terms of melting

temperatures and phases that formed, were largely in agreement.

The second part of this chapter looked at using the thermodynamic modelling in order to improve a brazing alloy, ISO 17672 Ag 155 (Ag155). Thousands of alloys were modelled and 12 of alloys were produced and tested for their brazing properties. Two of the alloys came close to matching the performance of Ag155 but none were able to offer enhanced brazing properties. The two best alloys were also the alloys that had the highest levels of silver and only offered very modest reductions in silver content.

The case study on Ag155 was an indicator of a larger problem with this method. There are limitations to what can be done by just adjusting compositions. Improvements to certain properties is almost always detrimental to other properties. In the case that any alloys are found with overall improved properties then it is very likely that the improvements will be slight and not worth the cost and effort of standardising and rebranding the new alloys.

The final conclusion from this method is that if significantly improved alloys are desired then a different method must be used. This lead onto the idea of using HEA modelling to develop HEA-type brazing alloys. This offers the opportunity to use radically different compositions that without HEA modelling would not have been considered as a potential brazing alloy. These topics are addressed in the subsequent chapters. Chapter 4 looks at the adaptation of HEA modelling for atypical atoms, Chapter 5 details the finer points of the computing method in more detail and finally Chapter 6 is an investigation into HEA-type brazing alloys.

# Chapter 4

# Silver HEAs

This chapter looks at the inclusion of silver as a one of the components of HEA compositions. As mentioned in the literature review there are a handful of publications that have silver containing HEAs [58, 59, 60, 61]. However, the HEAs in these examples tend to have limited quantities of silver. In this chapter the overall goal is to achieve alloys that conform to the definition of a HEA and also have quantities of silver that are at least 25 at.%.

The chapter is split into three sections. Firstly the addition of silver to existing HEAs is predicted using HEA formation criteria. The next section then produces and tests some of these alloys. The final section in this chapter is the designing HEAs from a selection of elements, systems and compositions to find HEAs with high silver content.

## 4.1 Predictions of HEAs with Additional Silver

The first approach looked at a number of existing and published HEAs and attempted to add silver to the composition. This was done by either adding silver in an equiatomic ratio or by substituting silver in for one of the components. The calculations was carried out for two main reasons. Firstly, it helped with the search

for the most promising alloys, the ones most likely to form a Ag-containing HEA. The secondary reason was to investigate the effect of silver on the HEA formation criteria. This could begin to reveal why silver is compatible or incompatible with the HEAs.

A list of ten HEAs was made to serve as the basis for investigating the effect that silver has on typical HEAs. This list was formed based on whether the alloy had been featured in published work, whether the alloy could be easily produced and trying to select a variety of elements and systems. There are countless HEAs that could be on this list but it was capped at ten to save time and as this was thought to be sufficient to see the trends with the data. These HEAs are not of use for brazing. The list of the alloys with the references are shown in Table 4.1.

Table 4.1: The details of Existing HEAs (EHEA) selected for trialling. As well as in the references listed all of these alloys can be found in the book, "*High Entropy Alloys*" by Murty et al. [45]. Most of the alloys can also be found in other review papers and other publications as well.

| Alloy code | Alloy | Ref. | Year |
|---|---|---|---|
| EHEA1 | CoCrFeNi | He et al. [119] | 2017 |
| EHEA2 | AlTiFeCoNi | Vaidya et al. [120] | 2017 |
| EHEA3 | AlTiCrFe | Varalakshmi et al. [121] | 2008 |
| EHEA4 | CoCuFeNi | Singh et al. [122] | 2014 |
| EHEA5 | $CrMn_2FeNi_2Cu$ | Ren et al. [123] | 2012 |
| EHEA6 | CrFeNiCu | Diao et al. [124] | 2015 |
| EHEA7 | $Al_{0.5}CrFeCoNi$ | Zhang et al. [85] | 2008 |
| EHEA8 | AlCoNiCu | Yeh et al. [125] | 2007 |
| EHEA9 | AlCoCrNiCu | Lin and Cho [126] | 2009 |
| EHEA10 | CoCrFeMnNi | Cantor et al. [127] | 2004 |

The criteria used for HEA formation here was based on measurements of the $\delta$ (the atomic size difference, using metallic radius) and the $\Delta H_{mix}$ (the enthalpy of mixing). These were selected from the list of other possible methods as the calculations were simple but still offered an effective way of discriminating between HEAs and non-HEAs. There are many publications that use different limits for selection. Shown in Fig. 4.1 are limits by Guo et al. [81], Guo et al. [84] and Zhang et al. [85]. In Fig. 4.1 the results of the ten HEAs in Table 4.1 are plotted.

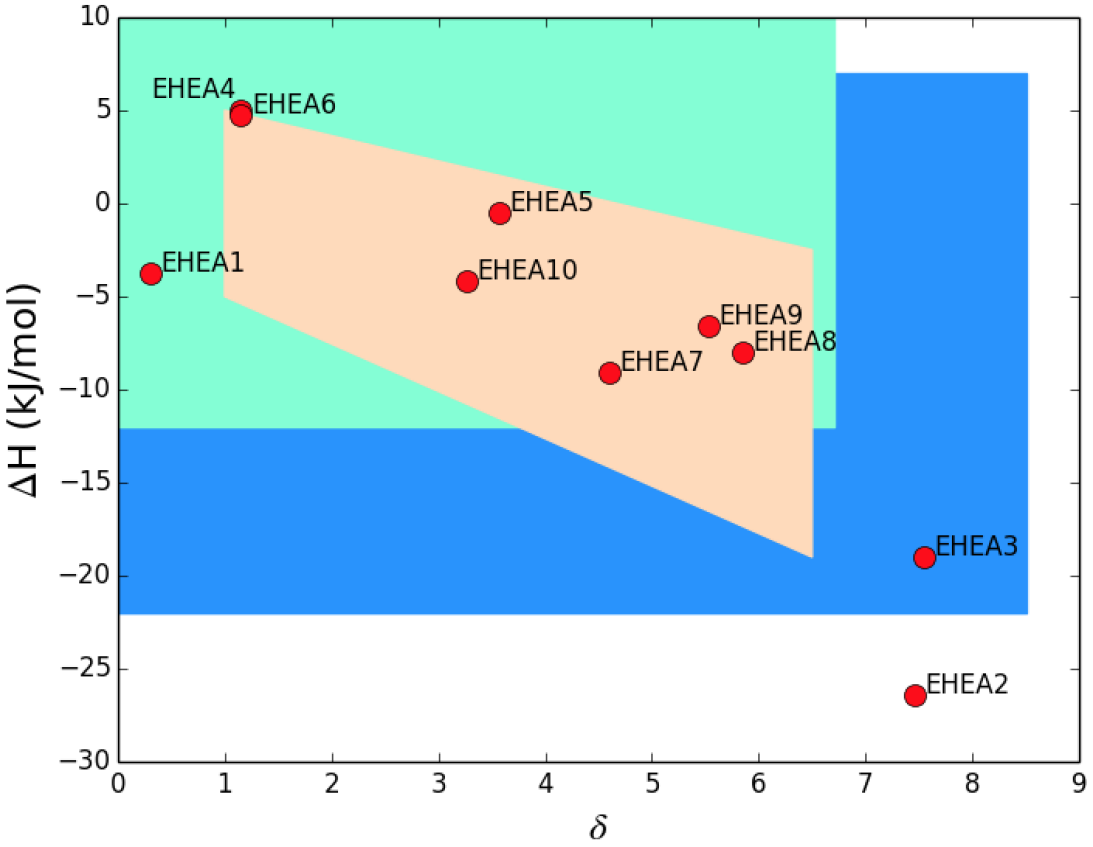


Figure 4.1: The largest blue region is from Guo et al. [81], the aquamarine region is from Guo et al. [84] and the peach region is from Zhang et al. [85].

Partly from the data shown in Fig. 4.1, but also from other research taking place in the research group, it was decided that the limits set out by Zhang et al. (the peach trapezoid) were the best to use. As these limits were the most constrictive they were thought to offer the strongest agreement between positive HEA predictions

and results.

The predictions of the EHEAs in Fig. 4.1 also show the approximate nature of this method. There are positive results (HEAs) that form outside the HEA formation regions. This is an unavoidable aspect of this method. Two relatively simple formulae cannot be expected to perfectly describe complex alloy systems with many elements. This could be a justification for using a more complex model that has a better success rate. However, as can be seen from earlier examples in the literaturere review, even the very complicated HEA models are not fully accurate, with models showing both false positives and false negatives. The first set of predicted data to use Ag used the EHEAs in Table. 4.1 and simply added silver to the composition.

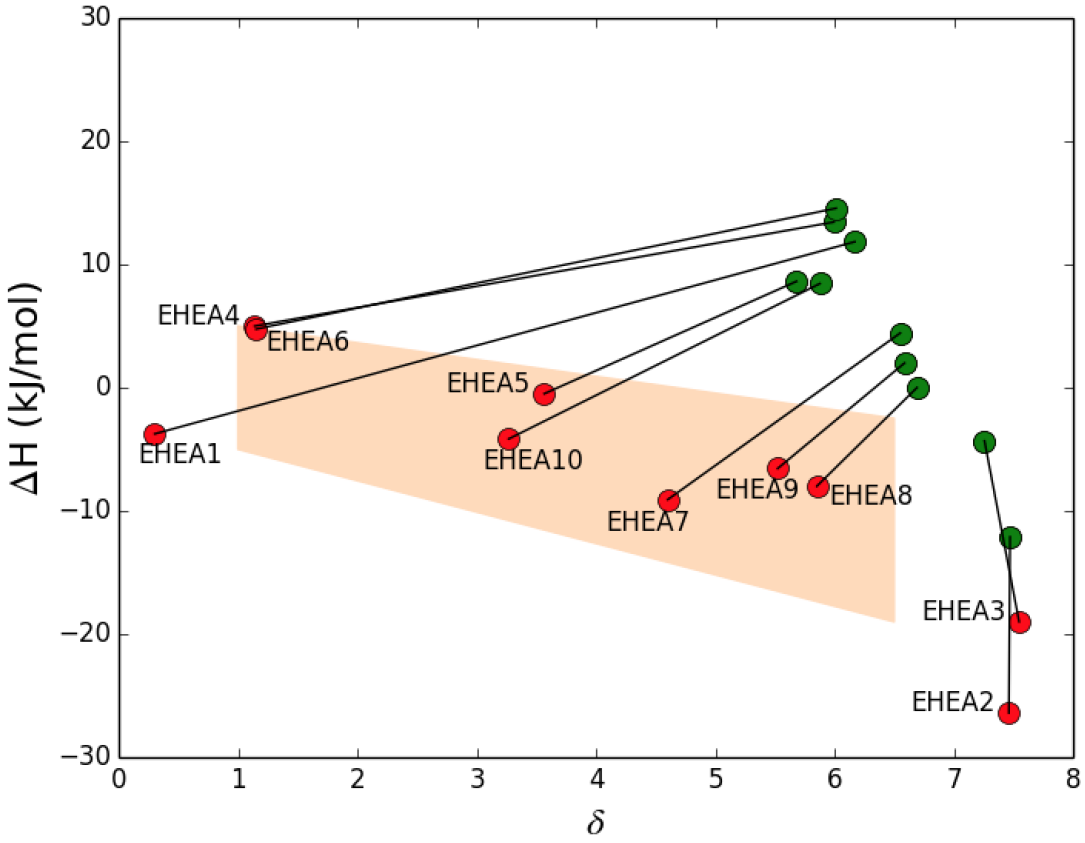


Figure 4.2: The HEA predictions for the EHEA range of alloys and the composition once silver has been added. The silver concentration in the adjusted compositions (the green data points) is equal to the average composition of the alloy.

The results in Fig. 4.2 show that silver has significant effects on the HEA criteria values. For most of the HEAs silver increases both $\delta$ and $\Delta H_{mix}$ (calculated using Miedeme), moving both away from the HEA forming region. The two exceptions (EHEA2 and EHEA3) already have large $\delta$ values. The values remain approximately the same, although the $\Delta H_{mix}$ does increase to a better value. None of the silver containing predictions in Fig. 4.2 would be more likely to form a HEA.

The other simple method for including silver is to substitute silver for one of the existing components in a HEA. This method again uses the same range of EHEAs as a base to swap silver in. The results are shown in Fig. 4.3.

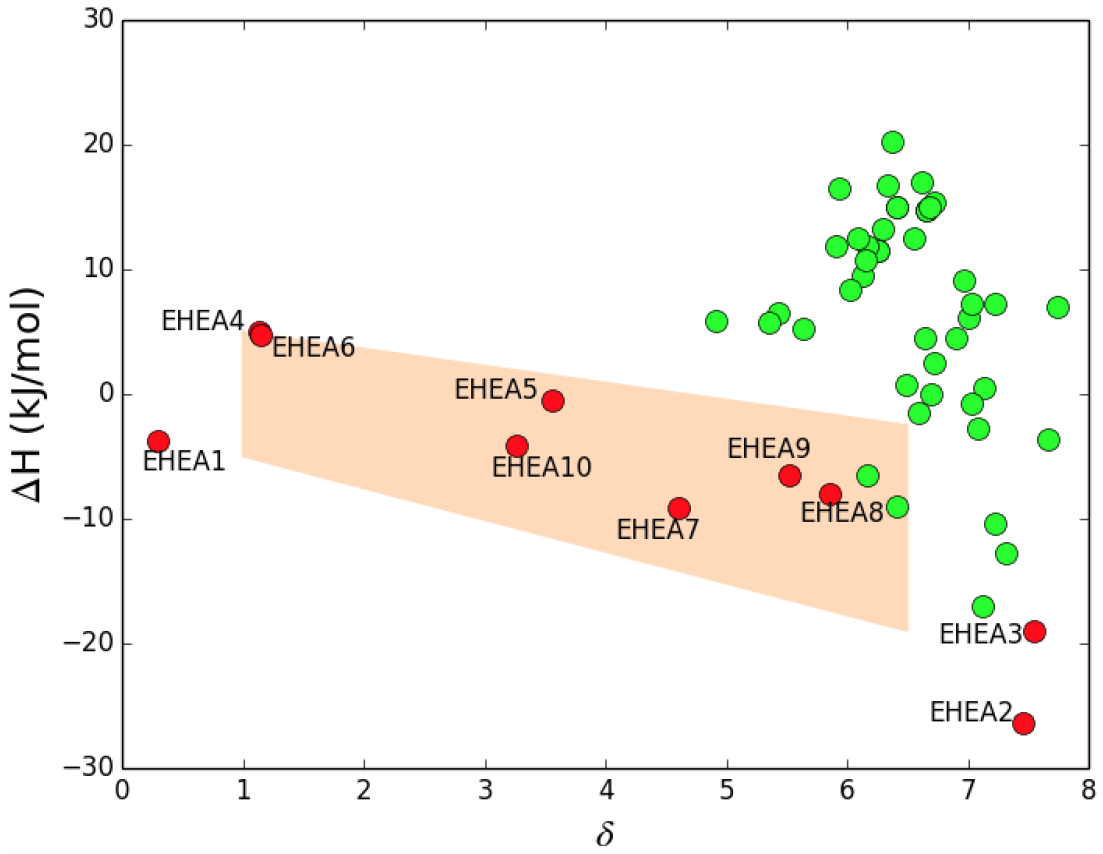


Figure 4.3: The EHEA range of alloys (red) plotted with the alloys that can be found by substituting silver for each component (green). The silver content matched the amount of component it replaced, so silver contents varied between 11.1 at.% and 25.0 at.%.

The results shown in Fig. 4.3 shows similar results to Fig. 4.2. Although not all silver containing alloys fall outside the HEA region in this case similar trends can be seen in terms of $\delta$ and $\Delta H_{mix}$.

### 4.1.1 Elemental Interactions with Silver

The results in Fig. 4.2 and Fig. 4.3 are expected and can be explained by looking at the input values that go into the parameters ($\delta$ and $\Delta H_{mix}$) that are plotted in the graphs. The $\delta$ value is a measure of how much each atomic radius is different from the average. As the intention is to include a large amount of silver it would be preferential for the other elements to have atomic radii similar to the atomic radius of silver. The value for silver compared to the other atomic radii in the HEAs, is shown in Table 4.2.

Table 4.2: The atomic radii of the commonly used HEA elements with a comparison to the radius of silver. Values for the atomic radii are from Guo et al. [81].

| Element | Atomic Radius (Å) | % Difference with Ag |
|---|---|---|
| Ag | 1.445 | 0.0% |
| Al | 1.432 | -0.9% |
| Ti | 1.462 | +1.2% |
| Cr | 1.249 | -14.6% |
| Mn | 1.350 | -6.8% |
| Fe | 1.241 | -15.2% |
| Co | 1.251 | -14.4% |
| Ni | 1.246 | -14.8% |
| Cu | 1.392 | -12.3% |

The data in Table 4.2 show why the addition of silver increases the $\delta$ in all the HEAs. For many of the elements listed the atomic radii are significantly smaller than

the silver radius. The exceptions are aluminium and titanium that are very close to silver and manganese that is relatively close. It is likely that these elements will feature prominently when designing silver HEAs.

For $\Delta H_{mix}$ the input numbers can be found in the large Miedema enthalpy table found in Appendix A. A condensed version, showing only the pairs relevant to the HEAs is shown in Table 4.3.

Table 4.3: The Miedema enthalpy values for the elements involved in this silver HEA alloy search. All values are in units of kJ/mol. Values are from Takeuchi and Inoue [82] and can be found in the complete table in Appendix A.

| | Miedema Enthalpy Values (kJ/mol) | | | | | | | | |
|---|---|---|---|---|---|---|---|---|---|
| Elements | Ag | Al | Ti | Cr | Mn | Fe | Co | Ni | Cu |
| Ag | 0 | -4 | -2 | 27 | 13 | 28 | 19 | 15 | 2 |
| Al | -4 | 0 | -30 | -10 | -19 | -11 | -19 | -22 | -1 |
| Ti | -2 | -30 | 0 | -7 | -8 | -17 | -28 | -35 | -9 |
| Cr | 27 | -10 | -7 | 0 | 2 | -1 | -4 | -7 | 12 |
| Mn | 13 | -19 | -8 | 2 | 0 | 0 | -5 | -8 | 4 |
| Fe | 28 | -11 | -17 | -1 | 0 | 0 | -1 | -2 | 13 |
| Co | 19 | -19 | -28 | -4 | -5 | -1 | 0 | 0 | 6 |
| Ni | 15 | -22 | -35 | -7 | -8 | -2 | 0 | 0 | 4 |
| Cu | 2 | -1 | -9 | 12 | 4 | 13 | -6 | 4 | 0 |

In Table 4.3 there is some insight as to why silver increases $\Delta H_{mix}$ in the HEAs. While the calculations are more complicated, as a general rule of thumb a slightly negative $\Delta H_{mix}$ is approximately the best value. Analysis of Table 4.3 without the Ag row and column would show elements which are commonly used in HEAs. Most values are negative, and for the few values that are positive there are some large negative values to balance them. It would very easy to design alloys with appropriate

$\Delta H_{mix}$ from this element set.

When Ag is added though there some difficulties are evident. Ag has large positive values with many of the elements and those that are negative are only slightly negative. This would explain why $\Delta H_{mix}$ usually becomes more positive when Ag is added to the compositions in Fig. 4.2 and Fig. 4.3 . It would also indicate that when designing silver HEAs keeping $\Delta H_{mix}$ at a suitably negative (or close to zero) value may be problematic. The solution would likely be to include elements that have low values with Ag and have low values with the other elements to reduce the overall number. This would drastically limit the number of systems that could be used though and may produce effects beyond those anticipated in the prediction, promoting specific interactions between particular elements.

## 4.2 Experimental Method

This chapter will cover a number of different alloys from many alloy systems. Regardless of the system or composition the melting method used for every alloy was arc-melting. This was then followed by analysis using XRF, XRD and SEM, which was done on the same pieces of equipment for every alloy in this chapter.

The melting of these alloys was done using a Edmund-Buehler MAM1 arc-melter. The melt used a copper hearth and an argon atmosphere. There were some complications to the method however. There would on occasion be a melt that failed to meet the intended composition. Any number of possible reasons could cause a melt to go wrong, common arc-melter problems include porous materials and problems removing all of the oxygen from the chamber. The most likely problem in these melts though was the presence of manganese. All of these problems may cause elements to get dislodged from the melting area.

Manganese has a relatively high boiling point (2061 °C [36]) which is a necessity for elements in the arc-melter, as otherwise they are liable to boil and escape the

alloy. However, manganese has a relatively high vapour pressure, which is especially problematic in the low pressure setting of the melting chamber. Manganese in the arc-melter is liable to violent eruptions which can push itself and other elements out of the individual bowls in the copper hearth.

The most reliable way to include manganese in these alloys was to melt everything else together first. Then, after the arc-melter had been cleaned and reset, to add the manganese to the melt. It also helped to not let the arc of the arc-melter directly interact with the manganese. Instead the button with all the other elements should be melted and as the liquid flows it incorporates the manganese. Once the manganese is in the solid sample, then normal heating procedures can be resumed until the alloy is properly mixed and uniform.

Compositions were confirmed using XRF analysis using a Panalytical Zetium. Phases were analysed using XRD on a Bruker D2 Phaser using Cu k$\alpha$ source. SEM was used as a supplementary tool to look at compositions, phases and to confirm alloys were mixed properly. This was done on a Philips XL30S electron microscope.

## 4.3 Experimental Results for Existing HEAs with Additional Silver

### 4.3.1 Cobalt-Chromium-Iron-Nickel with Additional Silver

The first alloys produced sought simply to include any amount of silver in a HEA. As the previous section described, the predicted results for alloys with equiatomic levels of silver were not promising. This example predicted the HEA with increasing amounts of silver, from 0 at.% up to 35 at.% before going on to make and test some of the alloys. The HEA used was CoCrFeNi (referred to as CCFN). The plot of CCFN and CCFN with Ag can be seen in Fig. 4.2.

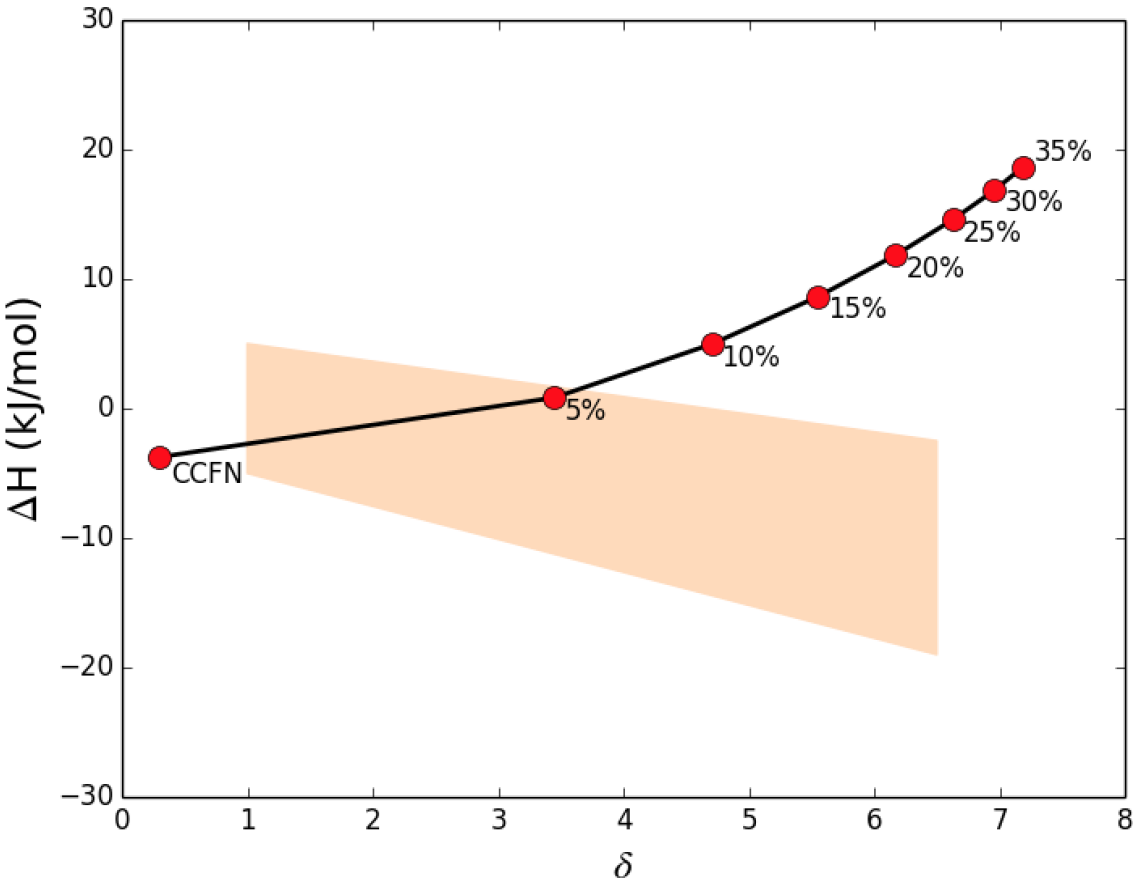


Figure 4.4: The results for CCFN with increasing amounts of Ag, that are labelled in at%.

Alloys with 0, 5, 10 and 20 at.% Ag were then produced, with CCFN making the balance of the composition. The alloys were arc-melted using the method described previously. The elements were of at least 99.9% purity with the elements from Johnson Matthey (Ag) and Alfa Aesar (all other elements). All the analysis of the alloys were carried out using the XRD, XRF and SEM techniques described earlier.

The results from the CCFN with Ag alloys were as expected. CCFN formed a single FCC phase as has been reported previously [119]. The 5 at.% Ag alloy formed a HEA with a single FCC phase. Visual checks were carried out to ensure that the silver had mixed with some of the other elements and it was not a case of incomplete melting. The XRD trace of the 5 at.% Ag alloy is shown in Fig. 4.5.

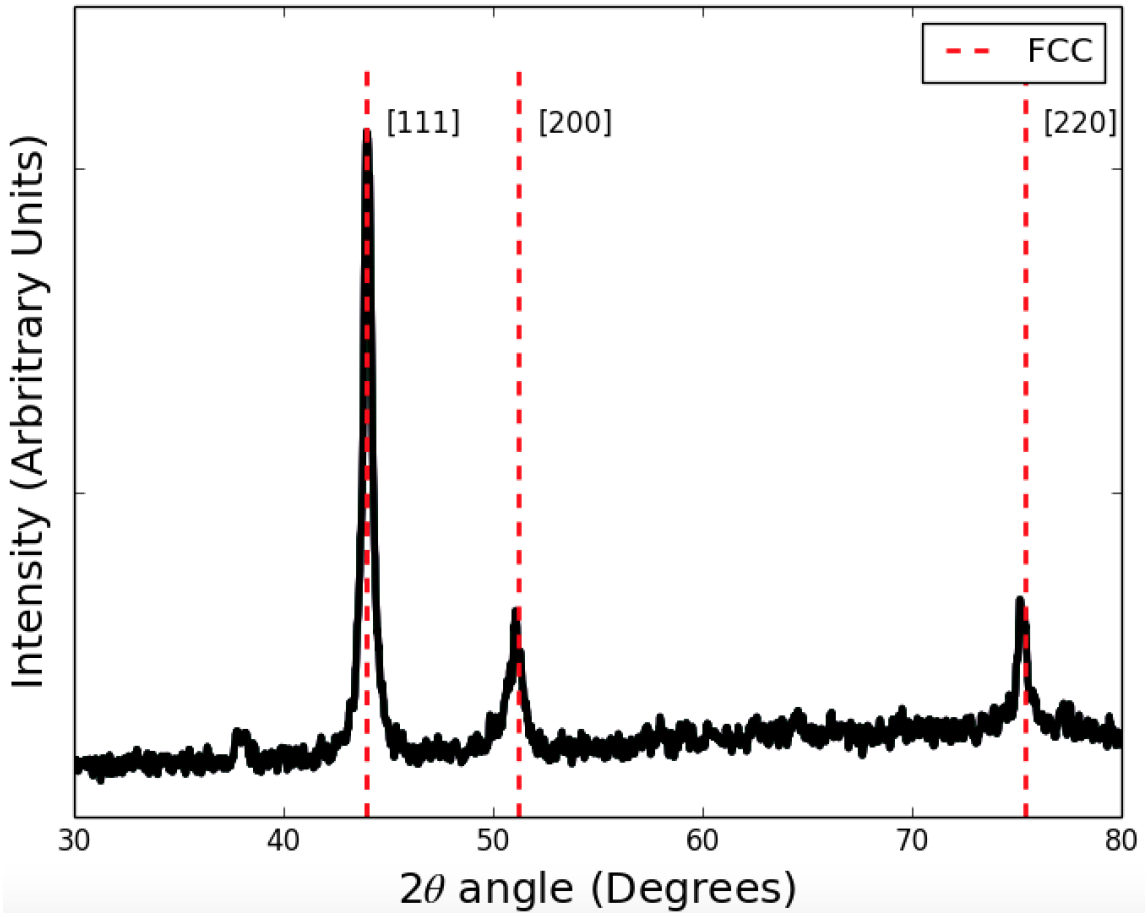


Figure 4.5: The XRD of the CCFN with 5 at.% Ag. The primary phase shown corresponds to FCC.

The 10 at.% Ag alloy and the 20 at.% Ag alloy did not form a HEA. The alloy, despite multiple attempts and increased heating, would not mix and form an alloy. Macro-segregation would always occur, leaving the elements unalloyed.

### 4.3.2 The Remaining HEAs with Additional Silver

This subsection produced and analysed the EHEAs with additional silver that had been plotted in Fig. 4.2 and Fig. 4.3. Although positive results (HEAs forming) were not expected in most cases it was necessary to confirm this was the case by producing the alloys and confirming their non-HEA status. The production and testing methods were exactly the same as were used for CCFN with Ag alloys as

described in the previous subsection. Including the alloys with silver addition and with silver substitution there are 55 possible compositions that could be made. Out of those alloys six were produced as well as the three CCFN with Ag alloys that had already been made. The alloys that were selected and produced are shown in Table 4.4.

Table 4.4: The range of alloys that were selected for trials. These were chosen using the original HEA as a base and with some effort to select alloys from a variety of systems.

| Alloy Code | Base HEA(s) | New Alloy | Ag (at.%) |
|---|---|---|---|
| AddedAg1 | CoCrFeNi | AgCoCrFeNi | 5 |
| AddedAg2 | CoCrFeNi | AgCoCrFeNi | 10 |
| AddedAg3 | CoCrFeNi | AgCoCrFeNi | 20 |
| AddedAg4 | AlTIFeCoNi | AgAlTIFeCoNi | 16.66 |
| AddedAg5 | AlTiCrFe | AgAlTiCrFe | 20 |
| AddedAg6 | $CrMn_2FeNi_2Cu$ | $AgCrMn_2FeNi_2Cu$ | 12.5 |
| AddedAg7 | CrFeNiCu | AgCrFeNiCu | 20 |
| AddedAg8 | $Al_{0.5}CrFeCoNi$ | Ag $Al_{0.5}CrFeCoNi$ | 18.18 |
| AddedAg9 | AlCoNiCu | AgAlCoNiCu | 20 |

The predicted results for the AddedAg alloys, the $\delta$ and $\Delta H_{mix}$, are shown in Fig, 4.6.

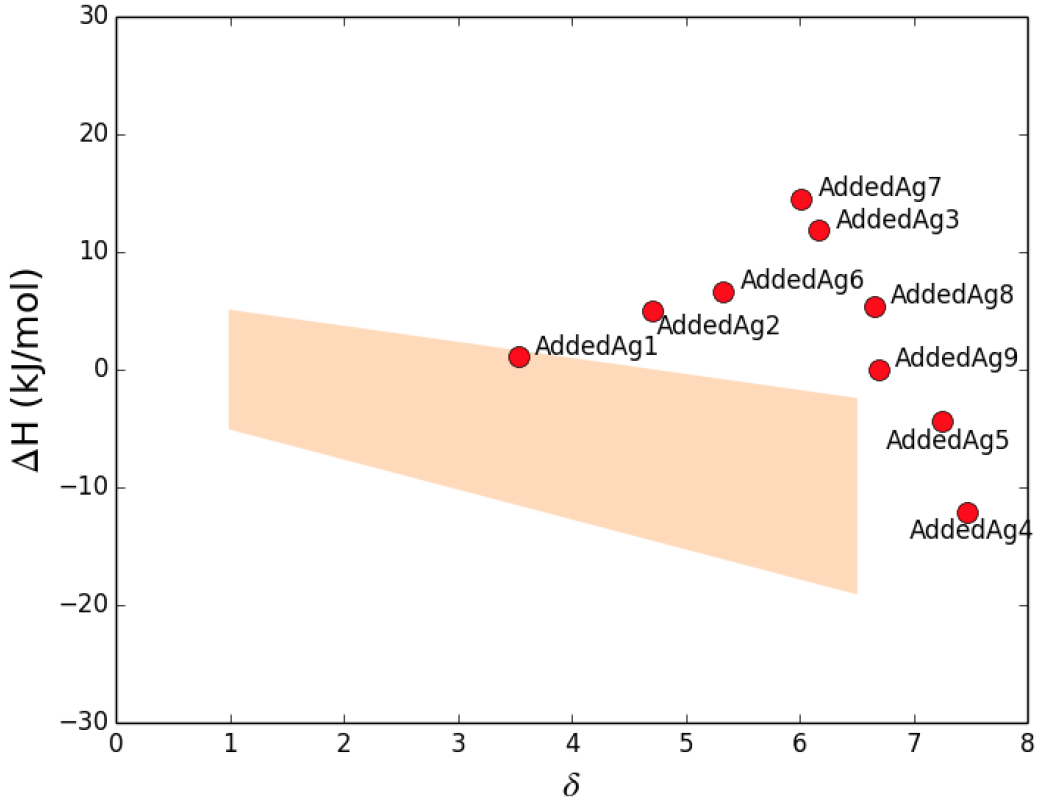


Figure 4.6: The plotted calculated parameters for the alloys from Table. 4.4.

The experimental results of these alloys were as expected, with all alloys failing to form a HEA apart from the CCFN with 5 at.% Ag. Most failures occurred due to macro-segregation, with the existing HEA rejecting the silver atoms. However there were some alloys that formed IMCs or multiple (three or more) phases and so were non-HEA. An example of an AddedAg alloy that did not form a HEA is shown in Fig. 4.7.


Figure 4.7: A photograph of the macro-segregation that has occurred in AddedAg5. There are three phases present as well as macro-segregation.

The results of adding silver to existing HEAs showed that silver cannot be easily added to HEAs without macro-segregation or some other breakdown of the HEA structure. There was one exception to this as silver could be added in a small quantity (although enough to fulfil the HEA composition limit of 5 at.%). However, as it is desired to find HEAs with high levels of silver it is therefore necessary to take a more thorough approach that can analyse a high number of compositions.

## 4.4 Designing Silver HEAs

### 4.4.1 Computing Method

The designing of silver HEAs includes a method of finding novel compositions that will feature heavily in this research. The method is explained in more detail in Chapter 5 and is also used in Chapter 6. The method is to use a large scale approach to

composition modelling before then applying a filtering process on the results. The principle is to model every possible composition before then filtering out alloys that do not meet the criteria and honing in on the best ones, judged by a set of criteria that can be changed depending on each trial, set of modelled data and the desired properties of the alloys.

In this section the only objective is to achieve Ag-HEAs, with no other properties considered. In later versions of this method there are additional properties that are modelled, such as melting temperature, which are used to find alloys that can fulfil certain requirements (e.g. low melting brazing alloys). The only criterion needed here is that there is a minimum amount of silver. This meant that optimisation of the alloy results could be judged solely on the HEA formation values.

Optimisation based on HEA formation values ($\delta$ and $\Delta H_{mix}$) is a process of selecting the alloys that are far away from the limits of HEA formation and are therefore, in theory, the most likely to form a HEA. This meant reducing the value of $\delta$ to as low as possible and ensuring the $\Delta H_{mix}$ value was in the acceptable range of values and ideally towards the middle of the acceptable range.

This trial covered alloy systems that had Ag plus an additional three, four or five elements. These elements were selected from some of the most commonly used HEA elements; Al, Cu, Ti, Cr, Mn, Fe, Co, Ni and Cu. All the possible combinations of these elements mean a total of 182 systems are available. This is calculated as follows using the mathematical 'Choose' function

$$Alloy\ systems = \binom{8}{3} + \binom{8}{4} + \binom{8}{5} \tag{4.1}$$

where the values in the choose functions are one lower than if this was a complete scan of the elements. This is because the Ag is included in all the alloys so there are then only eight other elements to chose from and they make one less than the orders of each alloy system.

For examining the compositions within each system a step size is required to control how many compositions will be measured. The decision for what step size

to use is based on two competing factors. A small step size is the equivalent of a fine mesh across a phase diagram, it is much more likely to capture any compositions of interest and to find the absolute optimum alloy in a system with a higher degree of accuracy. The opposing factor is the number of calculations involved and the computational time necessary.

The number of calculations, $N$, for each system can be found using equation

$$N = \frac{(A+B-1)!}{A!(B-1)!}, \quad A = \frac{100}{Step\ Size} \tag{4.2}$$

where $A$ is the number of times the step size goes into the whole composition. As the step sizes in this example are in at.% the equation for $A$ uses 100, but it could work using molar fractions and a value of 1 instead of 100. $B$ is the number of elements in the system. Some examples of calculation from this equation are shown in Table 4.5.

Table 4.5: A table showing the number of combinations a brute force process would have to trial based on the composition interval in weight percentage and the number of elements in the alloy.

| | | Step Size | | | |
|---|---|---|---|---|---|
| | | 1 | 2 | 4 | 5 |
| Number of elements | 3 | 5151 | 1326 | 351 | 231 |
| | 4 | 176,851 | 23,426 | 3276 | 1771 |
| | 5 | 4,598,126 | 316,251 | 23,751 | 10,626 |
| | 6 | 96,560,646 | 3,478,761 | 142,506 | 53,130 |

The numbers in Table 4.5 are for full composition scans. The composition limits of a HEA scan reduce these values and make the numbers more manageable, although it is worth noting that these limits (each component is between 5 at.% and 35 at.%) are arbitrary. Later uses of this method look for HEA-type properties using HEA

prediction methods but are focussed on certain properties and so can look in alloy space that would not usually be classed as HEA.

It can also be seen in Table 4.5 that there is a substantial difference between four element systems and six element systems. It was decided that the best approach was to use different step sizes for differently sized systems. A 1% step size would be far too fine to be used on a six element system, but equally a 4% step size is needlessly coarse for a four element system that is quick to run. The step size, limits and total number of alloys that were used for each system are shown in Table. 4.6.

Table 4.6: The details of the composition searches that were carried out for each system, based on the order of the system.

| System Order | Number of Systems | Step Size (at.%) | Composition Limits (at.%) | Alloys per System |
|---|---|---|---|---|
| 4 | 56 | 1 | 5 - 35 | 8803 |
| 5 | 70 | 2 | 6 - 34 | 22,301 |
| 6 | 56 | 4 | 6 - 34 | 8652 |

This means a grand total of 2,538,550 compositions were analysed as part of this trial.

### 4.4.2 Predicted Results

#### Equiatomic Compositions

Before investigating the results of the full range of alloy systems and compositions a preliminary trial was done using the equiatomic values of each system. There were two main reasons for doing this. Firstly to look at the best results, those within the HEA region with the lowest $\delta$, and to see if any of those alloys could form a HEA. The second reason was to provide a comparison for the compositions that will be

generated later that do not have equiatomic values. The results of the equiatomic values for the each alloy system are shown in Fig. 4.8.

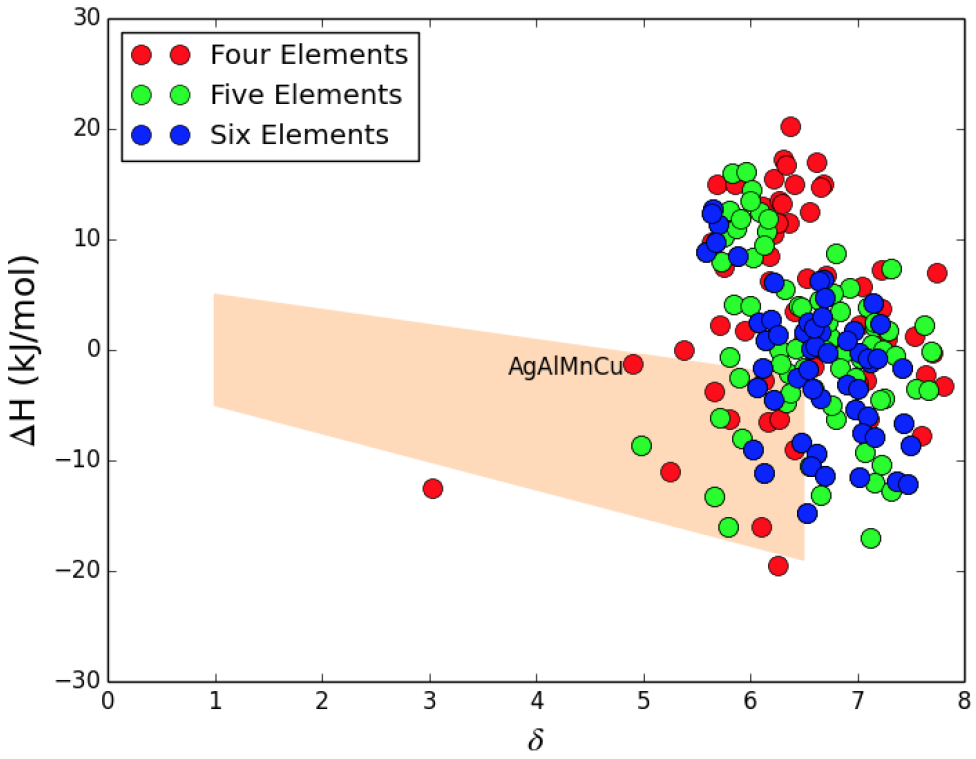


Figure 4.8: The results of looking at the equiatomic compositions for the 182 systems that had been modelled. Data points have been coloured based on the number of components. The alloy that was made, Ag-Al-Mn-Cu, has been labelled also.

There are 182 data points in Fig. 4.8 with some of the compositions already made and trialled as part of the AddedAg series of alloys. The majority of the points fall outside the HEA formation region. There are a handful of compositions that do fall within the the region but most are towards the higher values of delta. From this data set the best composition was selected for production. This was Ag-Al-Mn-Cu which had the lowest $\delta$ of the points that had a suitable $\Delta H_{mix}$ value as detailed by the limits by Zhang et al. in the peach trapezoid.

### Non-Equiatomic Compositions

Once all the composition had had their $\delta$ and $\Delta H_{mix}$ values calculated, the next stage of the process was to filter results down to the best systems and ultimately best compositions that could form HEAs with high concentrations of silver.

Many of the systems could be removed from consideration entirely as all compositions fell outside of the HEA formation region. These tended to be systems made up of elements that had mixtures of large and small atomic radii causing large $\delta$ values. Some examples of these systems can be seen in Fig. 4.9 along with a system that had suitable compositions.

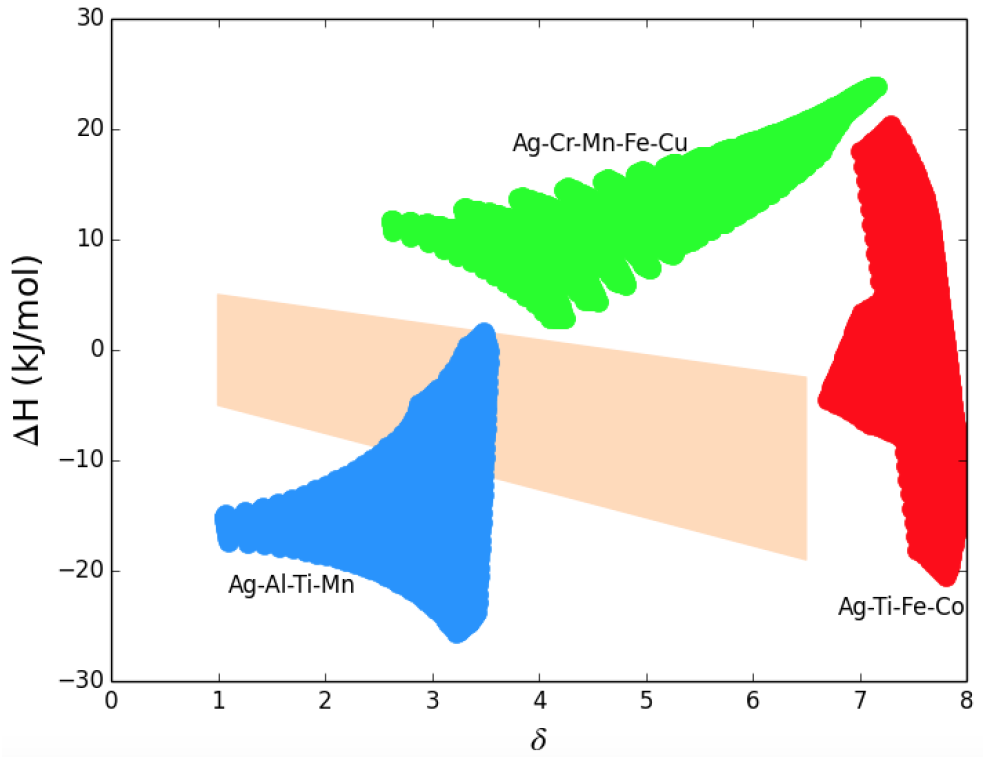


Figure 4.9: Some example plots of alloy systems. The three coloured regions each represent an alloy system (as labelled). The data points for the compositions overlap each over within each region. No six component systems were included in the examples as these ranges often take up a large area and displaying multiple systems on the same plot would be difficult.

There were however many systems that did have compositions within the HEA formation region. These compositions were then optimised using $\delta$ and $\Delta H_{mix}$ values to find the compositions furthest away from the HEA limits. For research purposes and to mitigate against unknown problems with elements or alloy systems, it was decided at this stage that the trial should attempt to cover as many different systems and elements as possible. Selecting the best alloys from the whole trial would have likely meant all the alloys originating from the same system and with similar compositions. 20 alloys were selected from 11 systems using all the elements in this trial. There were 13 alloys that formed HEAs, these are detailed in Table 4.7.

Table 4.7: The compositions that were made to form HEAs with a high silver content and successfully formed a HEA structure.

| | Element at.% | | | | | | | | |
|---|---|---|---|---|---|---|---|---|---|
| Alloy | Ag | Al | Ti | Cr | Mn | Fe | Co | Ni | Cu |
| AgHEA1 | 35 | 30 | 5 | | 30 | | | | |
| AgHEA2 | 30 | 35 | 10 | | 15 | | | | 10 |
| AgHEA3 | 20 | 35 | | | 30 | | 10 | 5 | |
| AgHEA4 | 30 | 35 | 15 | | | | | | 20 |
| AgHEA5 | 30 | 35 | 20 | 10 | | | | | 5 |
| AgHEA6 | 27 | 35 | 28 | 10 | | | | | |
| AgHEA7 | 30 | 34 | 22 | 6 | 8 | | | | |
| AgHEA8 | 25 | 25 | | | 25 | | | | 25 |
| AgHEA9 | 30 | 30 | 20 | 10 | | | | | 10 |
| AgHEA10 | 25 | 25 | | | 25 | | | | 25 |
| AgHEA11 | 30 | 30 | 10 | | 30 | | | | |
| AgHEA12 | 30 | 30 | 15 | | 15 | | | | 10 |
| AgHEA13 | 30 | 30 | 20 | | | | | | 20 |

The 13 compositions in Table 4.7 were all produced and experimentally verified as being HEA out of the 20 originally planned. Compositions were checked with XRF and phase analysis was done with XRD. Alloys that were found to have an incorrect composition were remade. Incorrect compositions were usually caused by the volatility of the manganese, either losing manganese or physically removing another element from the hearth before mixing.

The 13 successfully made silver containing HEAs were from a variety of systems and had a reasonably wide spread of $\delta$ and $\Delta H_{mix}$ values. By design all values were within the Zhang et al. alloy formation region, but the values varied around the region. The $\delta$ and $\Delta H_{mix}$ values of the 13 successful HEAs (the AgHEA range) are plotted in Fig. 4.10.

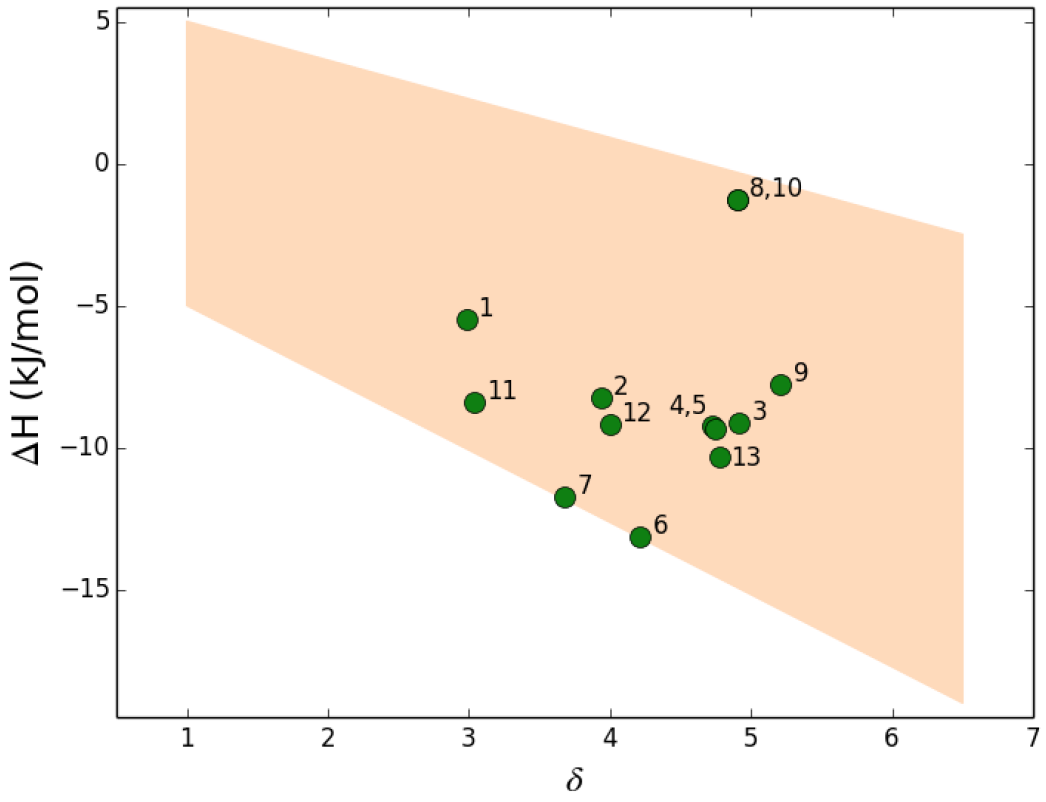


Figure 4.10: The high silver content alloys that formed a HEA. Alloys are labelled with the number that corresponds to the AgHEA range of alloys. Alloys four and five have different compositions but happen to have similar values.

Out of 20 there were seven alloys that did not form HEAs. These were classed as non-HEAs for a variety of reasons. The most common reason was macro segregation within the alloy. There were also alloys that formed IMCs and an alloy that formed three FCC phases. The details of the compositions for the alloys that did not form HEAs is shown in Table 4.8. Although these alloys have been listed separately from the alloys that did form a HEA (those in Table 4.7 and Fig. 4.10) they were designed and predicted in the same way.

Table 4.8: The compositions that were made to form HEAs with a high silver content and did not form a HEA structure.

| | Element at.% | | | | | | | | |
|---|---|---|---|---|---|---|---|---|---|
| Alloy | Ag | Al | Ti | Cr | Mn | Fe | Co | Ni | Cu |
| NonHEA1 | 30 | 30 | 10 | | 25 | 5 | | | |
| NonHEA2 | 30 | 25 | 15 | 5 | 25 | | | | |
| NonHEA3 | 35 | 35 | 20 | | | | | | |
| NonHEA4 | 34 | 34 | 20 | | | 6 | 6 | | |
| NonHEA5 | 25 | 30 | 29 | 16 | | | | | |
| NonHEA6 | 30 | 29 | 29 | | | 12 | | | |
| NonHEA7 | 30 | 30 | 20 | | | 10 | 10 | | |

The $\delta$ and $\Delta H_{mix}$ values for the compositions in Table 4.8 are plotted in Fig. 4.11.

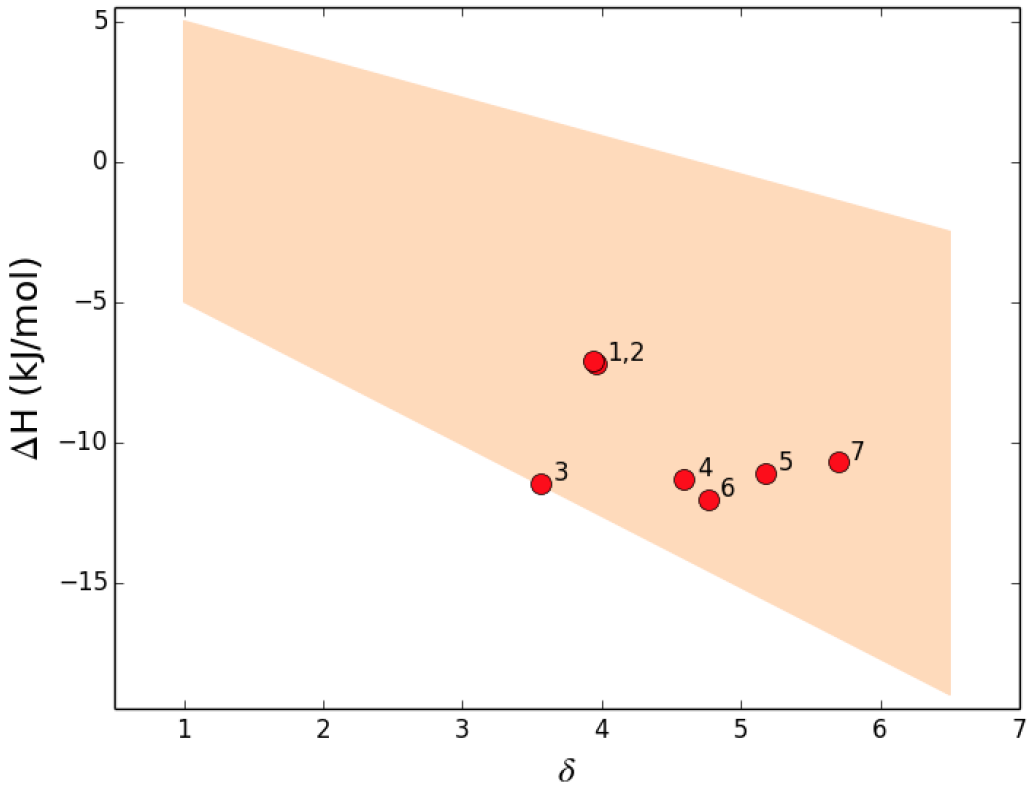


Figure 4.11: The plotted data for the HEAs with high silver content that did not form a HEA. Alloys are labelled with the number that corresponds to the NonHEA range of alloys.

### 4.4.3 Further Analysis

#### HEA Prediction Success

There were seven alloys that failed to form HEAs, which is a significant fraction of the 20 that were attempted. However, many of these alloys may be explained by looking at the elements involved in the melts. There were four alloys that contained iron and all four failed to form a HEA. It could be that iron is inherently incompatible with silver in HEAs. Analysis of the Ag-Fe phase diagram shows a large temperature range where the two liquids are immiscible [128].

Once the iron containing alloys have been removed the ratio of HEAs to non-HEAs appears much better. Instead of 13 out of 20 (65%) the results become 13 out of 16

(81%). Of course removing results that contradict after they have been measured will always improve the results but there is some justification for excluding iron. Iron and silver is immiscible to a high temperature, they have the largest difference in terms of atomic size difference out of the alloys trialled and they the largest positive enthalpy of the all the alloy pairs. If this alloy search was to be repeated then removing iron from the search and replacing it with a different element would be a sensible step.

### Phase Analysis

The successful HEAs all had two phases, which still counts as a HEA [45]. A typical XRD scan from one of these alloys is shown in Fig. 4.12.

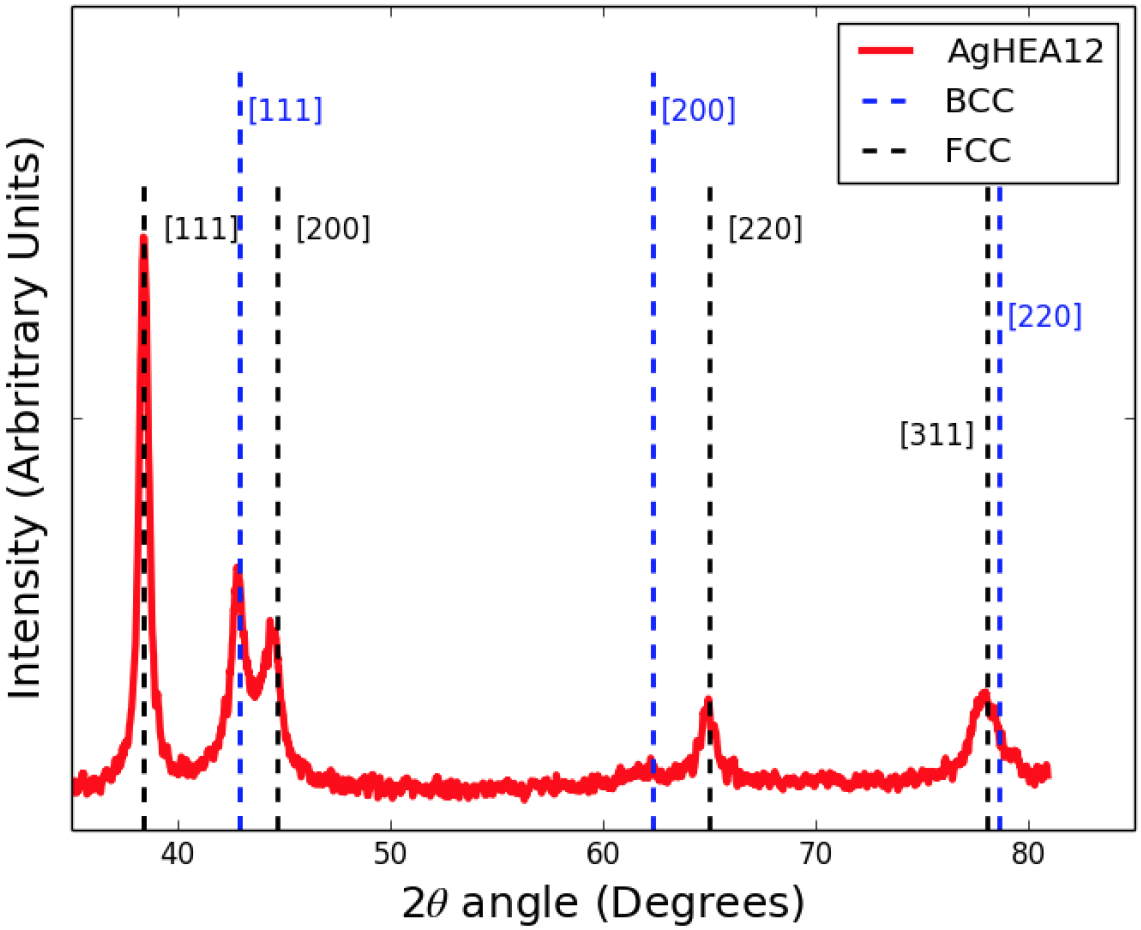


Figure 4.12: The XRD trace of alloy AgHEA12 showing an FCC and BCC structure. The FCC is Ag-FCC based and BCC is a novel mixture.

The two phase nature of this HEA was also confirmed using SEM analysis. A micrograph of the two phase structure is shown in Fig. 4.13.

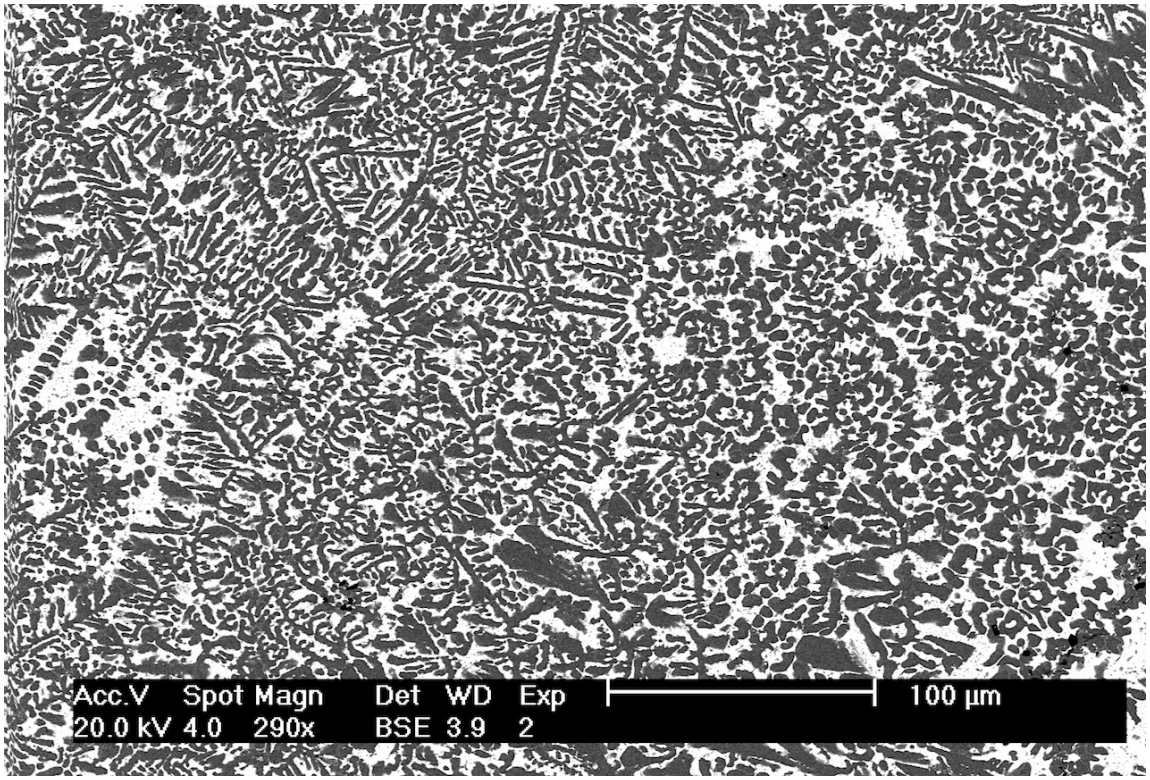


Figure 4.13: An SEM micrograph of alloy AgHEA12 showing the two phases present in the structure.

The dark phase in Fig. 4.13 is deficient in silver (Ag4-Al26-Ti27-Mn25-Cu18), while the light phase is dominated by silver and aluminium (Ag65-Al30-Ti1-Mn2-Cu2).

### Number of Phases

The 13 high-silver HEAs that were found in this chapter were two phase. Although doubted by some sources [52] there are still many publications that use valence elecrtron concentration (VEC) to calculate the phases that are present. The VEC rules state that alloys with VEC values above 8.0 will be FCC, below 6.7 will be BCC and a mixture when between the two. In this example the successful alloys that form have

values between 5.77 and 8.0.

This means that for some alloys, like AgHEA12, the VEC value (6.94) leads to a phase prediction that is in agreement with the measured phases. However, for alloys that have VEC values below the 6.7 and above 8.0 then the prediction does not work. Testing the validity of the VEC method is difficult though due to the limitations on the elements available. Compositions that have very low or very high VEC values, and so should form a single phase, cannot be easily found without violating the HEA formation rules.

Another explanation for the measured phases can be found using the method developed by Troparevsky et al. [80], as detailed earlier in the literature review. This method used a table of values for all the binary pairs in an alloy. The values in the table are found by considering the energy levels of the phases that could potentially form and could disrupt the single phase structure. If the values fall within a certain range ($-232 < H_f < 37$) meV/atom then the alloy would be single phase. Many of the values in the alloys that were made were significantly out of this range. For example, Al-Ti is -428 meV/atom, Ag-Fe is 176 meV/atom and Al-Co is -629 meV/atom. This could be an explanation for why these alloys always formed two phases. This method is returned to in the Chapter 5 for further investigation and to see if a single phase silver HEA is possible.

### Heat Treatment

The silver HEAs were given a heat treatment to examine if the alloys were metastable. This was done to see if the formation of the HEA structure depends on the heat history of the alloy. The alloys were held at 500°C for 72 hours. Most alloys showed some changes but still maintained most of the peaks between the as-cast and the annealed versions. A typical change in XRD peaks is shown in Fig. 4.14.

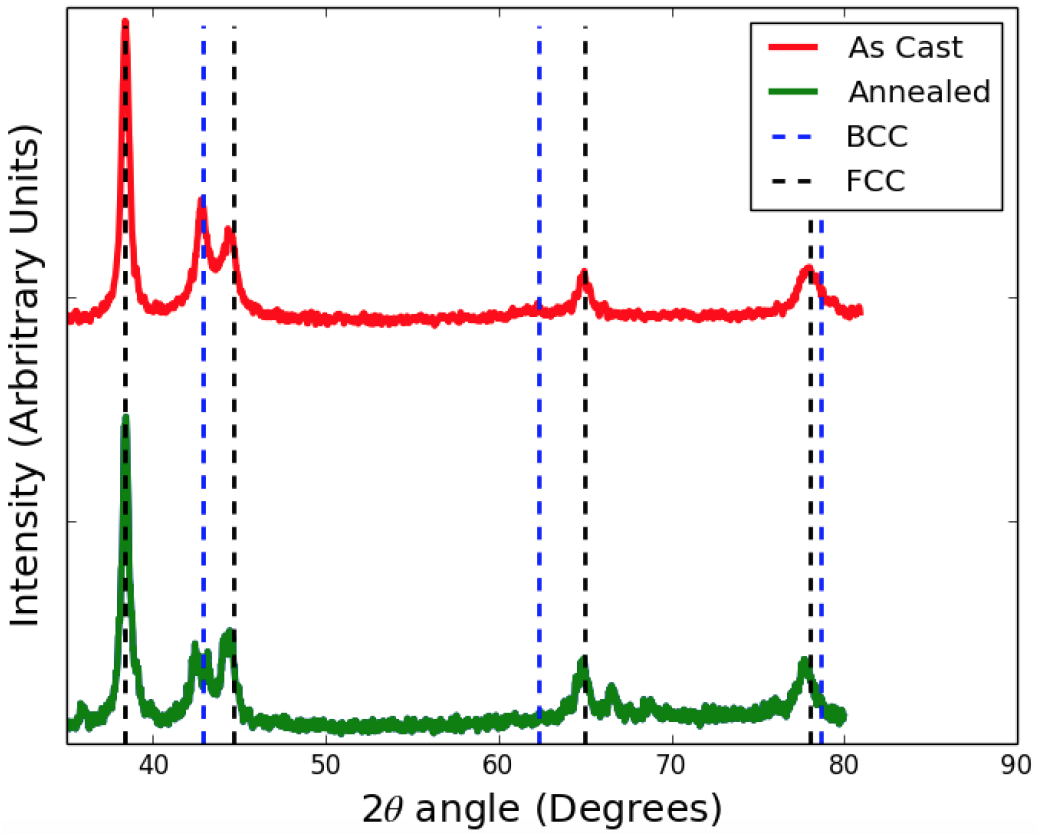


Figure 4.14: The XRD trace of alloy AgHEA12 before and after heat treatment.

The changes due to the heat treatment showed some minor changes but most of the structure remained the same. The two phases that were present in the as-cast are still present in the annealed. There are some additional peaks in the annealed alloy. There appears to be an additional peak around 44° $2\theta$ and possibly two extra peaks between 65° and 70°. These could not be identified as a simple structure and are likely indicate the formation of one, or more, IMC structure.

## 4.5 Conclusions

The goal of this chapter was to create HEAs with high levels of silver. This was achieved with 13 alloys having silver contents of at least 25 at.% Ag and having the simple XRD trace associated with HEAs. These alloys were found by using a large

scale modelling method that could trial millions of compositions before filtering and optimising to find the best possible alloys.

The chapter also investigated the problems associated with silver inclusion in HEAs and why silver could not simply be added to existing HEAs. The modelled results showed that for most alloys there were significant increases in both $\delta$ and $\Delta H_{mix}$ when silver was added. For most HEAs only modest amounts of silver can be added before the HEA structure was corrupted in some way.

# Chapter 5

# Large-Scale Modelling Method

This chapter looks in more detail at the large-scale modelling method that features heavily in this work. The strength of this modelling approach is its relative simplicity which allows it to be easily adapted for a wide variety of materials and properties. The part that is consistent throughout the different applications is the consideration of HEAs. The reason HEA modelling is of interest in a wide variety of materials is that HEA-type alloys explore compositions and systems that are relatively unexplored.

This chapter starts by reexamining the large scale modelling method that was introduced in the previous chapter. The methodology is shown in more detail with some explanation of the coding and data management that goes into the method. To demonstrate the flexibility and adaptability of the code this chapter then features two examples of adaptations for different purposes. The examples look at single phase HEAs, with one looking at single phase silver HEAs and the other looking at high order single phase HEAs. Entirely different element sets are used in these examples. This method is used again in Chapter 6 looking for HEA-type brazing alloys.

## 5.1 Method

The computing method as a concept is relatively simple. The program models all the compositions for a set of parameters, filters out the bad compositions and then focuses in on good compositions. The limiting factor in this approach is the time required to model all the compositions. Deciding on the level of detail, the scope and scale of any alloy search, and the data processing required are all factors that control how long a trial will take to complete.

Before the calculations can be carried out two arrays need to be generated that control what compositions are to be used. The first array controls which elements are in composition and the second array controls the amounts of each element. As this program was written using the Python programming language these arrays used the Numerical Python package (NumPy). The arrays are similar in appearance to spreadsheets but they can be manipulated much more easily and with much greater speed than spreadsheet-based software, such as Microsoft Excel, possibly could.

The first array, the one that controls the elements, has a column for each element and a row for each system that is to be measured. Each row then contains a binary series of numbers, which control whether an alloy is present in the system (represented by 1) or is not present in the system (represented by 0). An annotated example of this array is shown in Fig. 5.1.

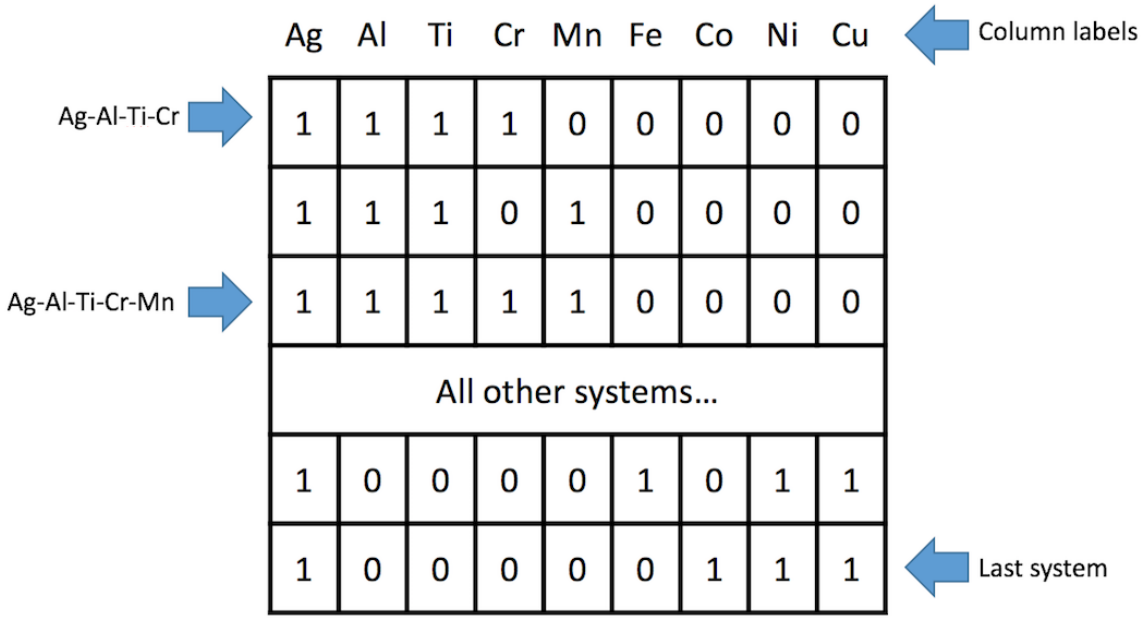


Figure 5.1: An example array of values for determining which systems are to be measured in a trial.There are are nine columns which represent nine elements, as labelled. The array in this example features both four and five element systems. This trial, from the silver HEA investigation, varies all the elements, except Ag, which is included in every alloy system.

The second type of array, that controls the compositions, is calculated separately. An example of this array is shown in Fig. 5.2. These arrays are generated using minimum and maximum values for each component along with a step size. The number of arrays that need to be saved depend on the range of system sizes that are being used, with one array necessary for each order of system in the trial.

In the example in Fig. 5.2 there are five elements in the system. The column labels are not for specific elements as this array can be used for any five element systems in a trial. There is also the option to have these values represent either at.% or wt% if there was a preference for one or the other. HEA calculations though tend to use at.% so this used the vast majority of the time.

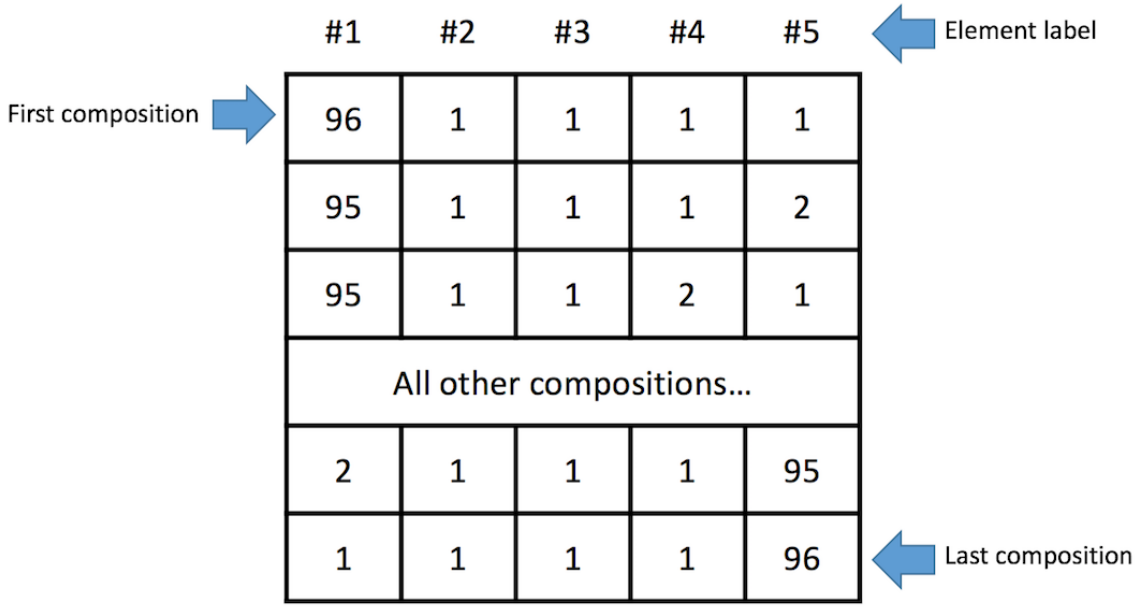


Figure 5.2: An example array for determining the compositions that are to be measured within each system in a trial. The numbers in each column correspond to the atomic value for each component.

The arrays in Fig. 5.1 and Fig. 5.2 provide the details for the two main programming loops that control the calculations in a trial. The alloy system loop is the outer loop with the composition loop being the inner loop that cycles for every system. This method ensures that every composition from one array is applied to every system from the other array. A simplified version of the loop within a loop setup is shown in Fig. 5.3.

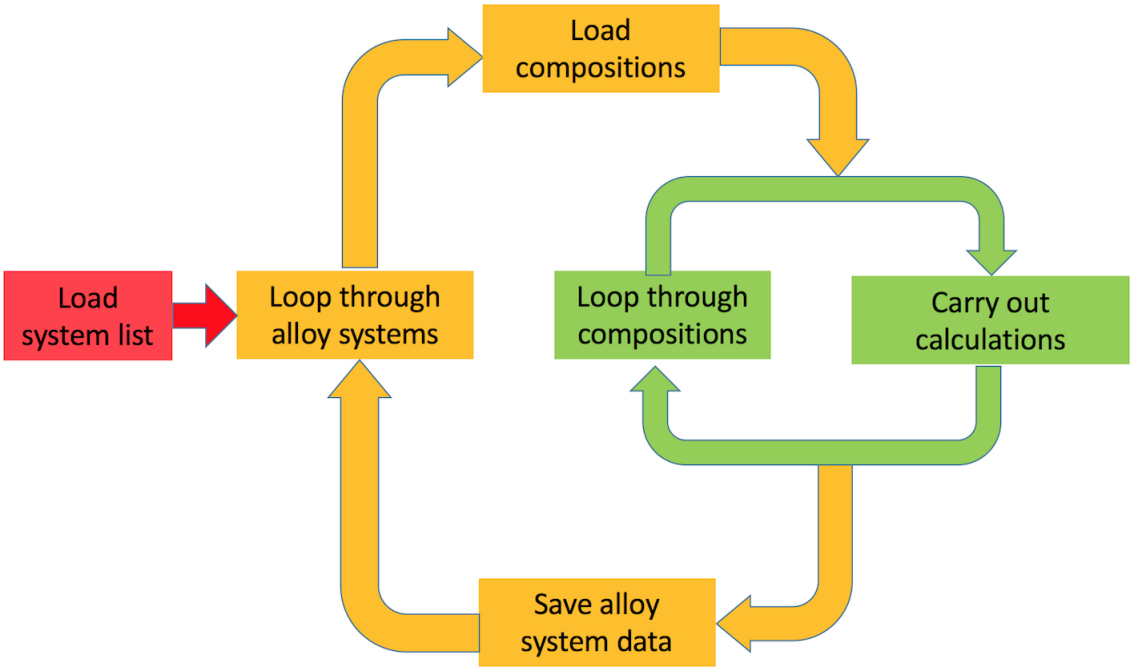


Figure 5.3: A simplified diagram of the loop structure for this large-scale modelling method. The red part represents the initialisation, as the alloy array (Fig. 5.1) is loaded. The orange parts represent the alloy system loop. This includes loading the composition array for each alloy system and exporting the data once measured. The green section is the composition loop that is within the alloy system loop. This loop actually carries out the calculations on the compositions.

Once the calculations have been carried out the results are saved in a database. When accessing the data the structure of the program is very similar to the structure in Fig, 5.3. The loop within a loop structure is repeated to ensure that every composition and system is covered. The difference this time though is that values are read from a database rather than any calculations carried out.

There is the added function to filter out systems. This might be based on the presence of an element or on a material property that is true for every value in a system regardless of the composition (e.g. magnetic atoms). The system filtering function can save significant processing time as it means that a whole alloy system can be filtered out without the need to go through each composition.

The overall loop structure in Fig. 5.3 remains constant throughout the various versions of this method. The changes arise in the inputs to the system and the calculations that are carried out. The inputs vary by what elements are included, the size of alloy systems and the range of compositions. The calculations can include HEA formation rules as well as other properties. In the examples here the HEA formation is judged using $\delta$ and $\Delta H_{mix}$, but other options could be calculated if they were required. The other calculations could be anything that can modelled easily.

## 5.2 Single Phase Silver HEA

### 5.2.1 Modelling

This section looked to use modelling from Troparevsky et al. [80] combined with standard HEA formation modelling to find a single phase silver HEA. The method uses a table of values, similar to the Miedema enthalpy table. Examples can be found in Fig. 2.21 and the fuller version in Appendix B. For each binary pair in an alloy the values are found and recorded. If all the values fall within a certain range (-232 $<$ $H_f$ $<$ 37 meV/atom) then according to the theory the alloy will be single phase.

The data found using the Troparevsky et al. method provides an explanation for the findings that all the silver HEAs created in Chapter 4.5 are not single phase. Many of the values for the binary pairs fall significantly out of the single phase range. The successful silver HEAs and the unsuccessful HEAs were analysed using this method. The details of these alloys are shown in Table 5.1 along with the minimum and maximum $H_f$ values from the Troparevsky et al. method.

$H_f$ used Troparevsky et al. represents the enthalpy of formation. These are calculated using DFT and represents the lowest energy structure of the two elements relative to the separate pure elements [80]. A large negative value indicates an IMC is likely to form between those two elements and a large positive value indicates segregation of the two elements [80].

Table 5.1: The results for single phase predictions using the Troparevsky et al. method for the alloys from Chapter 4.5. The $H_f$ minimum values and maximum values for the alloys. The compositions of the alloys can be found in Tables 4.7 and Table 4.8.

| Alloy Name | Alloy System | Low $H_f$ (meV/atom) | High $H_f$ (meV/atom) | Within Limits |
|---|---|---|---|---|
| AgHEA1 | Ag-Al-Ti-Mn | -428 | 97 | No |
| AgHEA2 | Ag-Al-Ti-Mn-Cu | -428 | 97 | No |
| AgHEA3 | Ag-Al-Mn-Co-Ni | -677 | 154 | No |
| AgHEA4 | Ag-Al-Ti-Cu | -428 | 47 | No |
| AgHEA5 | Ag-Al-Ti-Cr-Cu | -428 | 129 | No |
| AgHEA6 | Ag-Al-Ti-Cr | -428 | 129 | No |
| AgHEA7 | Ag-Al-Ti-Cr-Mn | -428 | 129 | No |
| AgHEA8 | Ag-Al-Ti-Cu | -428 | 47 | No |
| AgHEA9 | Ag-Al-Ti-Cr-Cu | -428 | 129 | No |
| AgHEA10 | Ag-Al-Ti-Cu | -428 | 47 | No |
| AgHEA11 | Ag-Al-Ti-Mn | -428 | 97 | No |
| AgHEA12 | Ag-Al-Ti-Mn-Cu | -428 | 97 | No |
| AgHEA13 | Ag-Al-Ti-Cu | -428 | 47 | No |
| NonHEA1 | Ag-Al-Ti-Mn-Fe | -428 | 176 | No |
| NonHEA2 | Ag-Al-Ti-Cr-Mn | -428 | 176 | No |
| NonHEA3 | Ag-Al-Ti-Cu | -428 | 47 | No |
| NonHEA4 | Ag-Al-Ti-Fe-Co | -629 | 176 | No |
| NonHEA5 | Ag-Al-Ti-Cr | -428 | 129 | No |
| NonHEA6 | Ag-Al-Ti-Fe | -428 | 176 | No |
| NonHEA7 | Ag-Al-Ti-Fe-Co | -629 | 176 | No |

The values in Table 5.1 show that none of the alloys already produced meet the requirements to be single phase. All of the alloys have minimum $H_f$ values below the lower limit and maximum $H_f$ values above the upper limit. For most of the alloys the values are not even close to the the single phase limits. The extent to which the alloys miss the single phase limits is shown in Fig. 5.4, with the minimum and maximum $H_f$ for each alloy. Also shown for comparison are the $H_f$ limits of -232 to 37 meV/atom that the alloys would have to conform to to be single phase.

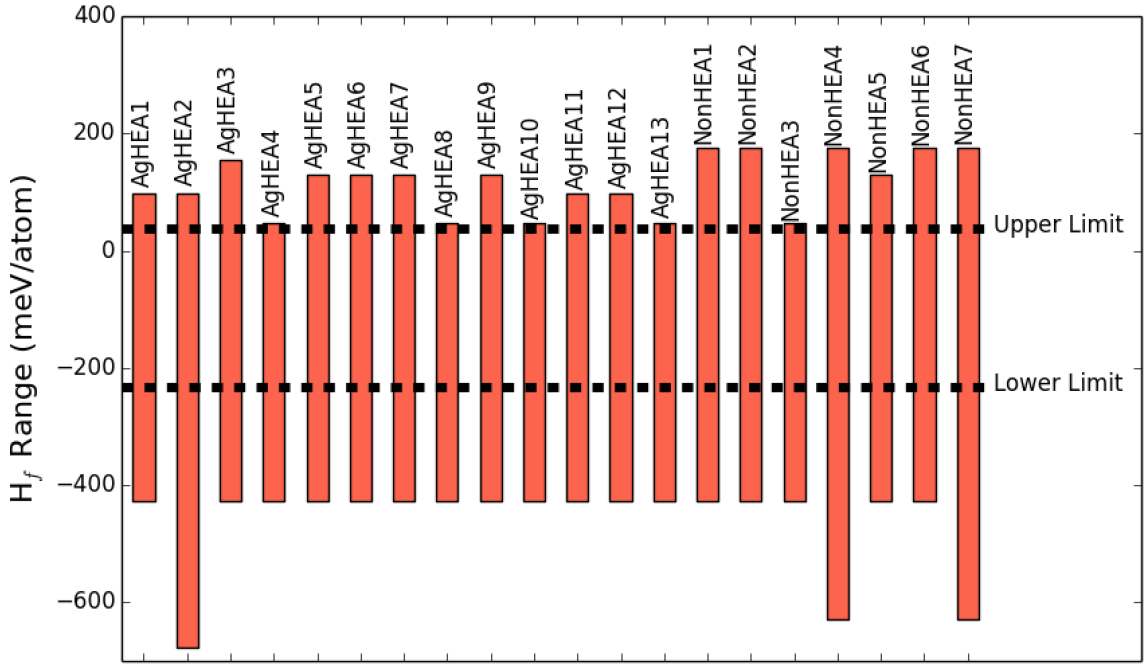


Figure 5.4: The single phase values for the alloys already produced in Chapter 4.5. The dashed lines represent the upper and lower limits that all the values should fall within for the alloy to be single phase. The plotted bars represent the maximum and minimum values of $H_f$ for each alloy.

The minimum and maximum $H_f$ values for the alloys in Table 5.1 are shown in Fig. 5.4. There are many $H_f$ values though that do not appear in Fig. 5.4 as they are either in the middle of the range or are from an element pair not used in the alloys. The full results for all the binary pairs from the elements in this trial are shown in Table 5.2.

Table 5.2: The single phase values for the elements in the silver HEA trial. The numbers in red are values that fall outside the limits for single phase formation.

| | $H_f$ Values (meV/atom) | | | | | | | | |
|---|---|---|---|---|---|---|---|---|---|
| | Ag | Al | Ti | Cr | Mn | Fe | Co | Ni | Cu |
| Ag | 0 | -254 | -65 | 129 | 97 | 176 | 154 | 98 | 47 |
| Al | -254 | 0 | -428 | -138 | -278 | -369 | -629 | -677 | -224 |
| Ti | -65 | -428 | 0 | -372 | -277 | -418 | -386 | -435 | -147 |
| Cr | 129 | -138 | -372 | 0 | -110 | -8 | 5 | -30 | 108 |
| Mn | 97 | -278 | -277 | -110 | 0 | 9 | -19 | -115 | 29 |
| Fe | 176 | -369 | -418 | -8 | 9 | 0 | -60 | -97 | 65 |
| Co | 154 | -629 | -386 | 5 | -19 | -60 | 0 | -21 | 54 |
| Ni | 98 | -677 | -435 | -30 | -115 | -97 | -21 | 0 | -6 |
| Cu | 47 | -224 | -147 | 108 | 29 | 65 | 54 | -6 | 0 |

Table 5.2 shows that many of the values fall outside the limits but not all of them. There are many values that fall within the limits and if silver was not part of the trial single phase HEAs would be achievable, under these limits. However, this trial does of course feature silver and analysis of the silver values in Table 5.2 show only titanium within the limits. Furthermore, there needs to be consideration of which elements can be included that will still allow a HEA to form. If the alloy was to fail to be a HEA, by having IMCs or macro-segregation, then would be no chance of a single phase regardless of the $H_f$ values.

The clash between how elements model in HEA formation predictions and in single phase predictions demonstrate is another reason why single-phase silver HEAs are difficult to find. Aluminium and titanium are the closest elements in terms of atomic size difference to silver, and have reasonable enthalpy values, hence why both elements feature prominently in the AgHEA range of alloys. These elements though

are particularly bad in the single phase modelling with large negative values that will prevent single phase formation. The best systems, in terms of most likely to form a single phase, are shown in Table 5.3.

Table 5.3: The alloy systems that are have the best single phase values for Ag-containing HEAs. There are nine elements included in this search can be found in Table 5.2.

| System Order | Rank | Alloy System | Min. $H_f$ (meV/atom) | Max. $H_f$ (meV/atom) | Within Limits |
|---|---|---|---|---|---|
| 4 | $1^{st}$ | Ag-Al-Mn-Cu | -278 | 97 | No |
| 4 | $2^{nd}$ | Ag-Al-Mn-Fe | -369 | 176 | No |
| 4 | $=3^{rd}$ | Ag-Ti-Mn-Co | -386 | 154 | No |
| 4 | $=3^{rd}$ | Ag-Ti-Co-Cu | -386 | 154 | No |
| 4 | $5^{th}$ | Ag-Ti-Fe-Co | -418 | 176 | No |
| 5 | $1^{st}$ | Ag-Al-Cr-Mn-Fe | -369 | 176 | No |
| 5 | $=2^{nd}$ | Ag-Ti-Cr-Mn-Co | -386 | 154 | No |
| 5 | $=2^{nd}$ | Ag-Ti-Mn-Co-Cu | -386 | 154 | No |
| 5 | $=4^{th}$ | Ag-Ti-Cr-Fe-Co | -418 | 176 | No |
| 5 | $=4^{th}$ | Ag-Ti-Mn-Fe-Co | -418 | 176 | No |
| 5 | $=4^{th}$ | Ag-Ti-Fe-Co-Cu | -418 | 176 | No |
| 6 | $1^{st}$ | Ag-Ti-Cr-Mn-Co-Cu | -386 | 154 | No |
| 6 | $=2^{nd}$ | Ag-Ti-Cr-Mn-Fe-Co | -418 | 176 | No |
| 6 | $=2^{nd}$ | Ag-Ti-Mn-Fe-Co-Cu | -418 | 176 | No |
| 6 | $4^{th}$ | Ag-Al-Ti-Cr-Mn-Cu | -428 | 129 | No |
| 6 | $=5^{th}$ | Ag-Al-Ti-Cr-Mn-Fe | -428 | 176 | No |
| 6 | $=5^{th}$ | Ag-Al-Ti-Cr-Fe-Cu | -428 | 176 | No |
| 6 | $=5^{th}$ | Ag-Al-Ti-Mn-Fe-Cu | -428 | 176 | No |

None of the alloy systems modelled pass the single phase limits set out by Troparevsky et al. Furthermore, all of the alloys shown in Table 5.3 violate not just one of the limits, but both the upper and lower boundaries. The values of the best performing systems offered only modest improvements, in terms of single phase likelihood, on the systems that were tested as part of the silver HEAs in Table 4.7.

### 5.2.2 Experimental Results

Ideally alloys would be selected that have HEA formation properties with the HEA formation region and have single phase values that meet fall within the range needed for single phase. The results from the modelling so far though show that this ideal scenario is not possible and some rules will have to be violated. To help decide which rules are more important the results from Chapter 4.5 can be used.

The results in chapter 4.5 showed the importance of the $\delta$ and $\Delta H_{mix}$ in HEA formation. All the alloys that had values outside of the HEA formation region failed to form a HEA (see Fig. 4.1). Even for alloys within the HEA formation region most compositions did form HEAs, but not all of them (see Fig. 4.11). Although results were not in perfect agreement it does suggest quite strongly that the HEA formation criteria should be adhered to for new alloys in this trial. This was the case for four of the five new alloys that were trialled. The HEA formation values of the alloys made in this trial are shown in Fig. 5.5. The exact compositions are shown in Table 5.4.

Table 5.3 shows that no system has been selected that can meet either the lower limit or upper limit for single phase formation. Alloys could have been selected based on how close they came to the limits, as was used to judge the best systems in Table 5.3. However, once the HEA formation limits have been applied and the compositions that failed had been removed, only a few systems remained. Using the best systems that passed the HEA formation limits would have been essentially repeat measurements of the alloys in Chapter 4.5. Many of these alloys were found to have two phases, making additional experimental verification redundant.

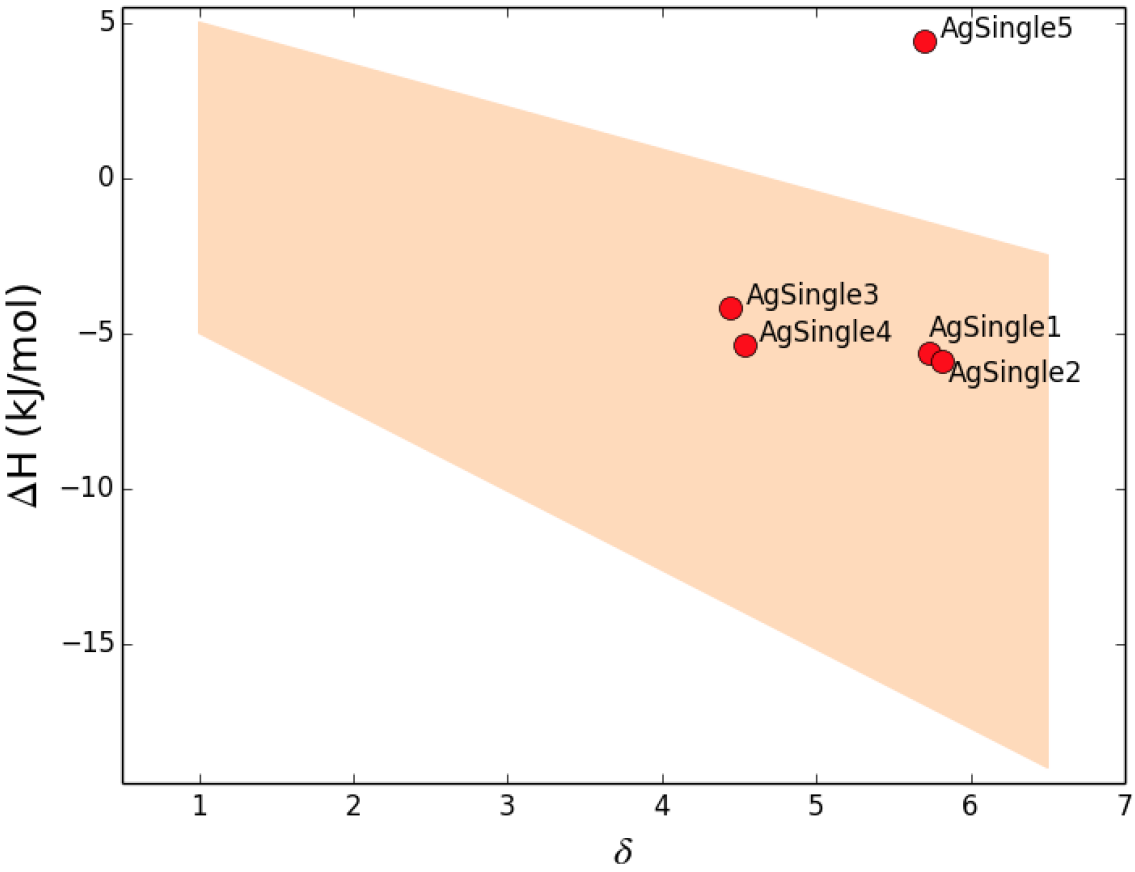


Figure 5.5: The HEA formation properties for the alloys selected as part of the single phase silver HEA trial.

Instead compositions were selected based on whether they had the best values on either the upper limit or the lower limit of the single phase range, even if the other value was especially poor, to investigate if this had any effect on the resultant alloy. The alloys selected for trialling are shown in Table 5.4. AgSingle1 and AgSingle2 were closest on the lower $H_f$ limit. AgSingle3 was closest on the upper $H_f$ limit. AgSingle4 was the closest on the upper $H_f$ limit from the remaining systems, even though it had the same upper $H_f$ value as AgSingle2. AgSingle5 was selected as it had $H_f$ at the detriment to the HEA formation properties (see Fig. 5.5).

Table 5.4: The compositions of the five alloys that were produced as part of the silver single phase HEA trial.

| | Element at.% | | | | | | | | | $H_F$ (meV/atom) | |
|---|---|---|---|---|---|---|---|---|---|---|---|
| Alloy Name | Ag | Al | Ti | Cr | Mn | Fe | Co | Ni | Cu | Low | High |
| AgSingle1 | 22 | | 30 | | 30 | | 8 | 10 | | -435 | 154 |
| AgSingle2 | 20 | | 30 | | 28 | | | 14 | 8 | -435 | 98 |
| AgSingle3 | 30 | 30 | | | 30 | | 10 | | | -629 | 97 |
| AgSingle4 | 30 | 30 | | | 30 | | | 10 | | -677 | 98 |
| AgSingle5 | 17 | | | | 30 | | 23 | 30 | | -115 | 154 |

All of the alloys in Table 5.4 failed to form a HEA. All alloys had macro-segregation, so could not even be classed as an alloy. The extent of the macro-segregation in these alloys is so large that it can be seen easily with the naked eye, as seen by the photographs in Fig. 5.6.


Figure 5.6: The significant macro-segregation that is found in the alloys as part of the silver single phase HEA search. The sample on the left is AgSingle2 and the sample on the right is AgSingle3. Scale shown is in cm.

Through a combination of the alloys produced here and in Chapter 4.5 there are no further options to explore in this trial. Alloys that were selected with no regard for the single phase properties were all found to be multi-phase. Alloys that compromised on the HEA formation properties to achieve better single phase properties all failed to form HEAs. The only way to improve the single phase properties any further would be to use alloys with even poorer HEA formation properties. All results so far would suggest that any alloy found that way would fail to form a HEA.

### 5.2.3 Discussion and Further Work

The search for single phase Ag-containing HEAs was not successful with no alloys found that meet the criteria. The negative experimental results though were expected as the modelled results indicated that that the alloys were unlikely to form for a number of reasons.

The multiple phases of the alloys in Table 5.4 were expected but the non-HEA status of all the alloys was somewhat unexpected. There are many reasons why the alloys may not have formed HEAs. Alloy AgSingle5 was outside the HEA formation region, while alloys AgSingle1 and AgSingle2 were towards the edge of the HEA region with high $\delta$ values. Four of the alloys contained nickel which could have similar problematic tendencies like iron did in Chapter 4.5. Of course the imperfections of the model mean there may be no specific reason the alloys fail to form HEA.

The various modelled and experimental results suggest that single phase silver HEAs with the elements from chapter 4.5 are very unlikely to form, verging on impossible. The next step would be to change the element set for the alloy search to one with elements that have more favourable single phase properties. This, however, is not an easy process as many of the elements included in the single phase data table (see Appendix B) fall outside of the limits. Of the 29 element pairs that include silver only seven of the elements had values within the limits.

Out of these seven elements three have a high cost (Pd, Pt and Au), one is toxic

(Cd) and one cannot be used in the arcmelter due to a low boiling point (Zn). This leaves just Ti and Zr as affordable and useable elements for finding a suitable alloy. Of course there are many elements that are not included in the single phase data. The suitability of the elements not included in the data set is unknown. The only way to find out would be to replicate the complicated and time consuming work that went into producing the original data by Troparevsky et al. and the other research groups that contributed to the values (referenced within the paper). The issue of single phase formation in silver HEAs will be revisited in the chapter 6 as part of the HEA-type brazing alloy work.

## 5.3 High Order Single-Phase HEA

### 5.3.1 Modelling

In the original publication by Troparevsky et al. one of the original intentions for the modelling was to be able to find high-order single-phase HEAs (referred to as HOSP HEAs from now on). In the supplementary information [129] to accompany the paper by Troparevsky et al. [80] 30 elements are analysed. In the same document the most likely to be single phase systems are shown for five, six and seven element systems. These systems are detailed in Table 5.5.

Table 5.5: The high order systems most likely to be single phase, from Troparevsky et al. [129] supporting the paper also by Troparevsky et al. [80].

| Best Alloy Systems | | | |
|---|---|---|---|
| Rank | Five elements | Six Elements | Seven Elements |
| 1st | Co-Ni-Rh-Os-Ir | Ni-Ru-Rh-Os-Ir-Pt | Cr-Mn-Fe-Co-Ni-Rh-Os |
| 2nd | Co-Ni-Rh-Pd-Ir | Co-Ni-Rh-Os-Ir-Pt | Cr-Fe-Co-Ni-Rh-Re-Os |
| 3rd | Mg-Sc-Ti-Zr-Hf | Fe-Co-Ni-Rh-Os-Ir | Mn-Fe-Co-Ni-Rh-Os-Ir |
| 4th | Ru-Rh-Os-Ir-Pt | Co-Ni-Rh-Pd-Ir-Pt | Cr-Mn-Fe-Co-Ni-Re-Os |
| 5th | Ni-Ru-Rh-Os-Ir | Co-Ni-Rh-Pd-Ir-Pt | Cr-Fe-Co-Ni-Rh-Pd-Re |
| 6th | Ti-V-Zr-Nb-Hf | Cr-Fe-Co-Ni-Rh-Os | Cr-Mn-Fe-Co-Rh-Re-Os |
| 7th | Co-Rh-Os-Ir-Pt | Fe-Co-Ni-Rh-Pd-Ir | Cr-Mn-Ni-Ru-W-Re-Os |
| 8th | Ni-Rh-Os-Ir-Pt | Cr-Mn-Fe-Co-Ni-Os | Cr-Mn-Co-Ni-W-Re-Os |
| 9th | Fe-Co-Rh-Os-Ir | Cr-Fe-Co-Ni-Re-Os | Mn-Fe-Co-Ni-Rh-Re-Os |
| 10th | Ni-Ru-Rh-Os-Pt | Mn-Fe-Co-Zn-Re-Os | Cr-Mn-Co-Ni-Rh-Re-Os |

The easiest route in terms of programming would be to analyse these systems listed in Table 5.5 for their HEA formation properties and then to make the most stable of these alloys. However, almost all of the systems highlighted in the supplementary information feature very high cost elements. The one exception is the Ti-V-Zr-Nb-Hf which, compared to the other systems listed, is relatively low cost.

For this trial the elements were restricted to those that could be acquired and melted easily from the 30 elements featured in the full data. Expensive elements like Ru, Re and Ir are removed as they are too costly. Elements that are impractical to melt are also removed. These impractical elements include Cd that is toxic and Mg that requires specific handling and safety considerations. Zn was allowed to remain as part of the alloy search, as it can be melted in an induction melter.

After the various elements have been excluded there are 17 that remain for select-

ing alloys. These 17 are; Al, Ti, V, Cr, Mn, Fe, Co, Ni, Cu, Zn, Zr, Nb, Mo, Ag, Hf, Ta and W. For four, five, six and seven component alloy systems there are 110, 41, 5 and 0 alloy systems respectively that pass the single phase limits with the reduced set of elements. This would indicate that six and seven element single phases alloys may be difficult to produce, however, there are many alloy systems that are close to the single phase limits and so are worth investigating. This research will focus on the higher order systems, specifically the six and seven element alloy systems. The five best systems for the six and seven element systems are shown in Table 5.6. These systems are different from Table 5.5 as this is using the reduced set of 17 elements with alloy systems ranked according to how close they meet the single phase limits.

Table 5.6: The five systems most likely to form a single phase, for the six and seven component systems, from the reduced set of elements. The results were judged using the method by the Troparevsky et al. method.

| Number Of Elements | Ranking | Alloy System | Low $H_f$ (meV/atom) | High $H_f$ (meV/atom) |
|---|---|---|---|---|
| 6 | 1st | Ti-Zr-Nb-Mo-Hf-W | -171 | 24 |
| 6 | 2nd | V-Zr-Nb-Mo-Hf-W | -171 | 26 |
| 6 | 3rd | V-Cr-Zr-Nb-Ta-W | -150 | 36 |
| 6 | =4th | Ti-Zr-Nb-Mo-Ta-W | -193 | 36 |
| 6 | =4th | V-Zr-Nb-Mo-Ta-W | -193 | 36 |
| 7 | 1st | Ti-V-Zr-Nb-Mo-Hf-W | -171 | 37 |
| 7 | 2nd | Ti-V-Zr-Nb-Mo-Ta-W | -193 | 37 |
| 7 | 3rd | V-Cr-Zr-Nb-Mo-Ta-W | -193 | 42 |
| 7 | 4th | Ti-V-Zr-Nb-Hf-Ta-W | -171 | 12 |
| 7 | 5th | Ti-V-Zr-Nb-Mo-Hf-Ta | -193 | 12 |

The single phase values in Table 5.6 are significantly better than the single phase

results in the silver trial in the previous section. All of the six component systems listed passed both limits and there were many other systems that had values that were close to the limit. None of the seven alloy systems passed, but as the systems listed show, there were many that were close to the limits. Unlike in the previous trial using silver there is now the opportunity to be more selective with the compositions.

As seen previously from the single-phase silver HEAs, there needs to be consideration of the HEA formation values. As an initial scan of the data, the equiatomic compositions for the six and seven element systems were modelled for their HEA formation properties. These could then be plotted to give an indication of how many systems are in or are close to the HEA formation region.

Plotting all the modelled properties of the each equiatomic composition would be difficult to display clearly on a graph. The equiatomic compositions from the alloy systems with the most likely to form single phase properties are plotted in Fig. 5.7 and Fig. 5.8, with the alloy systems that are far away from being single phase not plotted at all. Using the limits in the figures there are 230 six component systems and 73 seven component systems. Alloys that were within 60meV/atom of both limits were included in the plots. The results for the six element systems are shown in Fig. 5.7.

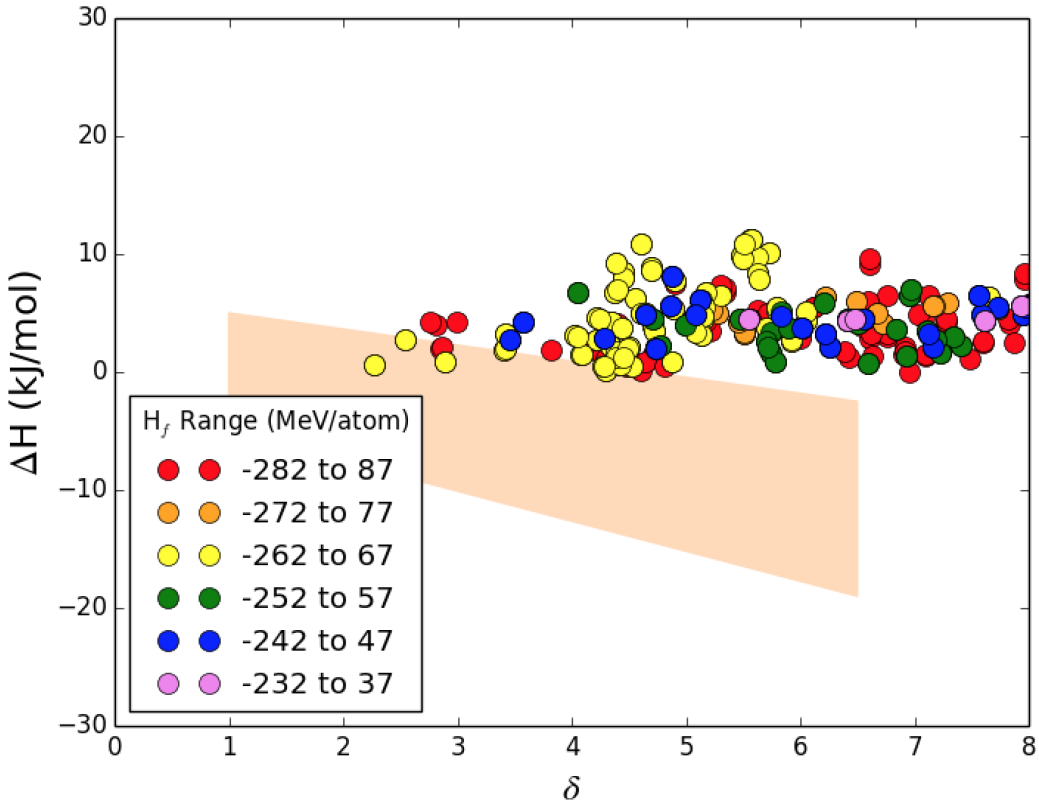


Figure 5.7: The HEA formation properties for 230 equiatomic compositions with six components. These compositions are from alloy systems using the reduced set of elements in this trial. The points are coloured according to the single phase limits, shown in the legend. The HEA formation regions shown is by Zhang et al. [85]

The results in Fig. 5.7 show that there are many systems that have single phase properties close to the limits set out by Troparevsky et al. There are also some compositions that fall within the HEA region set out by Zhang et al., although these data points are largely from the extended range of the single phase properties (the red, orange and yellow coloured data points). The systems that will likely be of most interest will be the those with data points that are close to the single phase region (blue or violet) and are near the HEA formation region. These compositions can be optimised (i.e. changing the level of the each element from equiatomic) to find alloys that have better HEA formation properties and the same single phase properties. This is because changes to the composition within an alloy system has no effect on

the single phase formation properties, according to the Troparevsky et al. model. This seems reasonable, as any element pair will make up at least 10 at.% of the alloy. 10 at.% of IMC or macro segregation would be more than enough to corrupt a HEA structure. The results for the seven element systems are shown in Fig. 5.8.

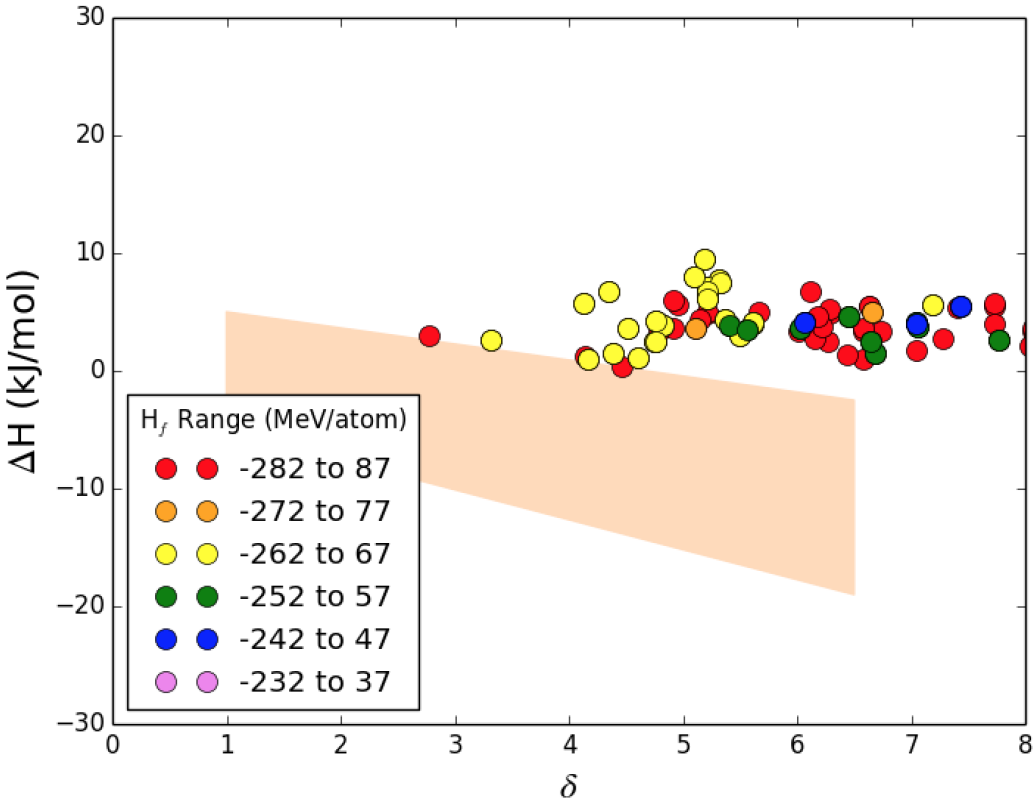


Figure 5.8: The HEA formation properties for 73 equiatomic compositions with seven components. These compositions are from alloy systems using the reduced set of elements in this trial. The points are coloured the same as Fig. 5.7. The HEA formation regions shown is by Zhang et al. [85]

The results in Fig. 5.8 show some similar trends to the results in Fig. 5.7 but with some distinct differences also. The most noticeable difference is the reduction in the number of points plotted. This is simply because fewer systems meet the single phase requirements. This is understandable as even though there are more systems in the seven element trial each system has an additional six element $H_f$ values to consider. This significantly increases the changes that the system will have a $H_f$ value outside

of the single phase limits.

Similar to Fig. 5.7 though there are some data points around the HEA formation region and again these tend to be the systems that only meet the extended single phase limits. As with the six element systems the ability to change compositions will be vital for finding alloys that have good HEA formation values as well as good single phase values.

The silver HEA modelling work in the previous chapter showed moving away from equiatomic compositions can find alloys with significantly improved HEA formation values. The same composition search parameters could be repeated in this search. However, that approach would be very time consuming. There are many more systems available in this trial as there are more elements, no element is always present (like Ag was previously) and the systems are of a higher order.

The reduction in calculations used in this trial was to use relatively large step size of 5 at.% when scanning through the compositions. The lower and upper limits for each component was 10 at.% and 30 at.% rather than the 5 at.% and 35 at.% typically associated with HEAs. This reduction of the composition range saved some calculations although it was implemented primarily as a safeguard against inaccurate melting. There was a concern that these high order and high melting point alloys might have problems with composition accuracy. The tightening of the limits meant that alloys could miss their composition target and still be classed as a HEA. For example, an element with an intended composition of 35 at.% might increase slightly and so push the alloy outside the definition of a HEA. Using 30 at.% as the upper limit helps to avoid this problem.

### 5.3.2 Preliminary Experimental Work

As a small trial of potential HOSP HEAs were selected to form a preliminary search for these alloys. This consisted of three six-element HEAs and three seven-element HEAs were modelled, produced and tested. These were selected based on the $H_f$

values as well as the $\delta$ and $\Delta H_{mix}$ HEA formation values. The comprehensive search of compositions was carried out, trialling every available system and every composition within the system using the (10 at.% to 30 at.% described previously).

The results in Fig. 5.7 and Fig. 5.8 show that the systems that had the best single phase properties (the blue and violet data points) had equiatomic compositions that did fall in the HEA formation region. The composition scan allowed for compositions to be found from these systems but with suitable HEA formation values. This happened for many of the systems but not for all. Some of the systems (e.g. Ti-V-Zr-Nb-Mo-Hf and Ti-V-Zr-Nb-Mo-Ta from Table 5.6) had very good single phase values but there were no compositions in the scan that fell in the HEA formation region.

The results in Table 5.6 showed that there were only a handful of six element systems met the single phase limits and none from the seven element systems. Inevitably this meant that some of the alloys selected for trialling would have to be from outside the single phase limits. Fortunately though there are many systems that are close to the single phase limits. So if the range is extended slightly (10MeV/atom on both limits) it means there are many systems from which to select compositions. From these systems the compositions were selected that had the lowest $\delta$ with a $\Delta H_{mix}$ value within the Zhang et al. limits. These compositions are listed in Table 5.7.

Table 5.7: The compositions for the alloys selected as part of the preliminary experiments of the HOSP HEA alloy trial.

| | Element at.% | | | | | | | | | | | | |
|---|---|---|---|---|---|---|---|---|---|---|---|---|---|
| Alloy | Ti | V | Cr | Mn | Co | Ni | Cu | Zr | Nb | Mo | Hf | Ta | W |
| HOSP-Pre1 | 20 | 10 | | | | | | 10 | 20 | 10 | | 20 | 10 |
| HOSP-Pre2 | 20 | | | 10 | | | | 10 | 20 | 10 | | 20 | 10 |
| HOSP-Pre3 | 10 | 10 | | 20 | | | | | 10 | 20 | | 10 | 20 |
| HOSP-Pre4 | | | 20 | 20 | 20 | 20 | | | | 10 | | | 10 |
| HOSP-Pre5 | | 20 | 10 | | | | | | 20 | 20 | | 10 | 20 |
| HOSP-Pre6 | 10 | 10 | | | | | | | 20 | 20 | | 20 | 20 |

The $\delta$ and $\Delta H_{mix}$ of these systems are plotted in Fig. 5.9.

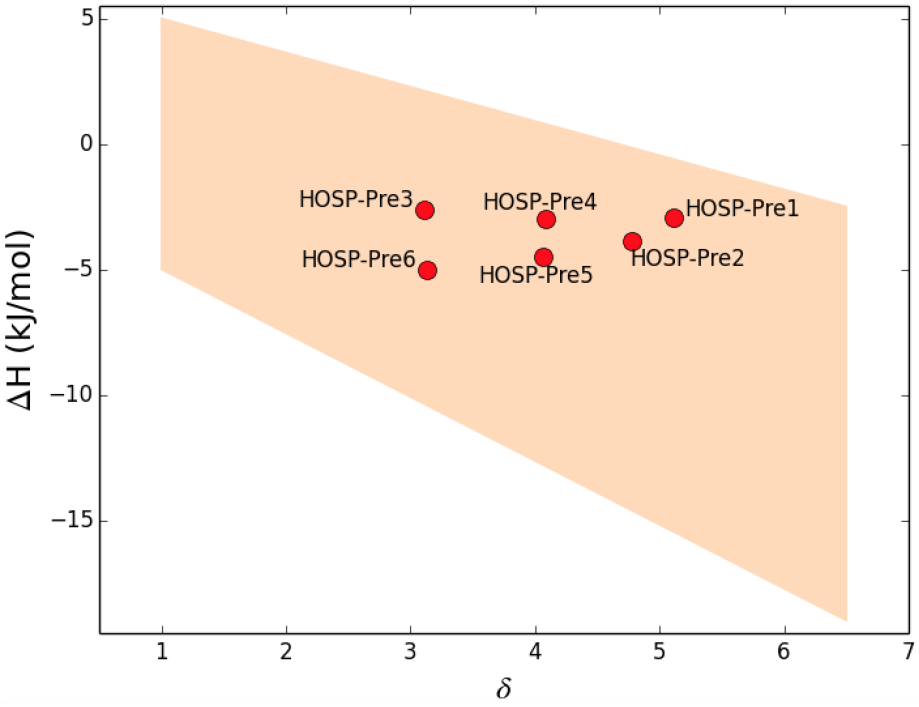


Figure 5.9: The plotted results of the HOSP-Pre range of alloys.

The results of these alloys were difficult to evaluate though. The alloys were

produced in the same Edmund-Buehler MAM1 arc-melter as all the HEAs have previously. There were difficulties with the alloy production for a number of reasons (detailed in the next subsection). There was also difficulty in telling the difference between alloys that were not melted correctly and alloys that would not form a HEA even with ideal melting. This was particularly the case with the alloys that had significant quantities of very high melting elements.

Only one of the compositions (HOSP-Pre4) successfully formed an alloy, with all other attempts either not melting successfully or having macro-segregation. The successful alloy was not single phase, but it did have one phase dominating over the other. There were some noticeable differences in the composition, likely arising from elements being ejected from the melt, elements evaporating away or receiving ejected elements from another melt. The composition, measured by XRF, is shown in Table 5.8 compared to the intended composition.

Table 5.8: The intended composition of HOSP-Pre4 and the resultant composition after production and analysis with XRF.

| | Element at.% | | | | | |
|---|---|---|---|---|---|---|
| Alloy | Cr | Mn | Co | Ni | Mo | W |
| HOSP-Pre4 - Intended | 20 | 20 | 20 | 20 | 10 | 10 |
| HOSP-Pre4 - Measured | 17.3 | 28.5 | 15.6 | 15.6 | 18.2 | 4.4 |

The measured results show the HEA composition limits were very nearly adhered to with only W being slightly below the 5 at.% limit. The composition is significantly different from the intended though. The best explanation for this is that melt received some additional manganese and molybdenum from other melts in the vacuum chamber. The XRD trace of this alloy is shown in Fig. 5.10. The XRD trace was measured using the Bruker D2 Phase as with all XRD measurements in this chapter.

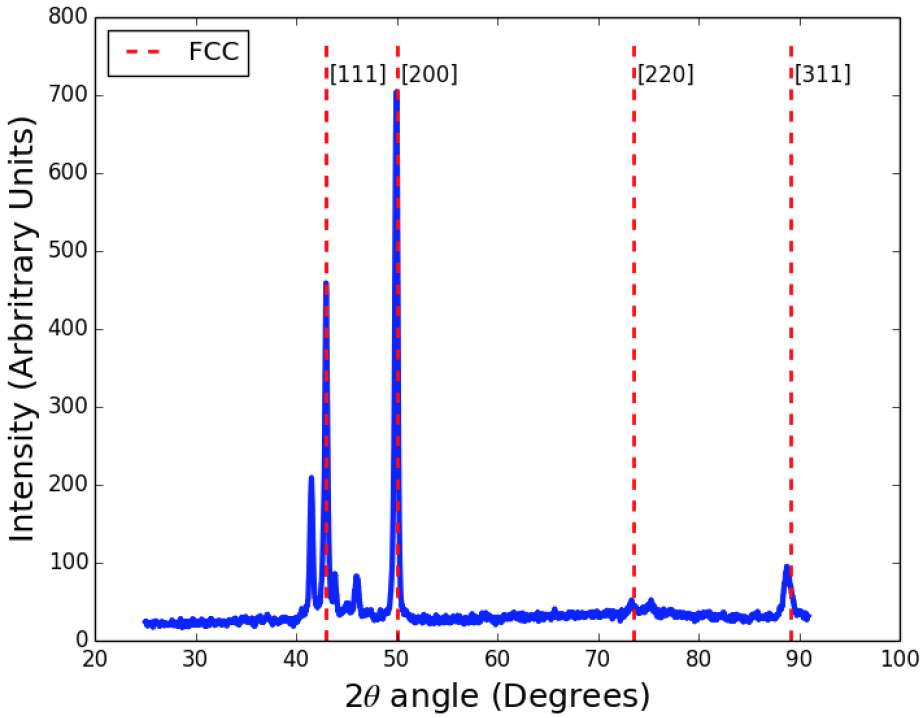


Figure 5.10: The XRD trace for HOSP-Pre4 alloy. The dominant phase is a FCC with a lattice spacing of 3.644$\mathring{A}$. The secondary phase could not be identified.

The XRD results showed that the alloy had one dominant phase but also the presence of a second phase. The largest peaks referred to a FCC with a lattice spacing of 3.644Å. The secondary phase could not be identified. The unknown peaks did not match a FCC or BCC structure, so it is likely a different structure. The two phase nature of the alloy, and the compositions of each phase, were checked and confirmed with SEM and EDX analysis using a Philips XL 30S electron microscope. A micrograph from the analysis is shown in Fig. 5.11.

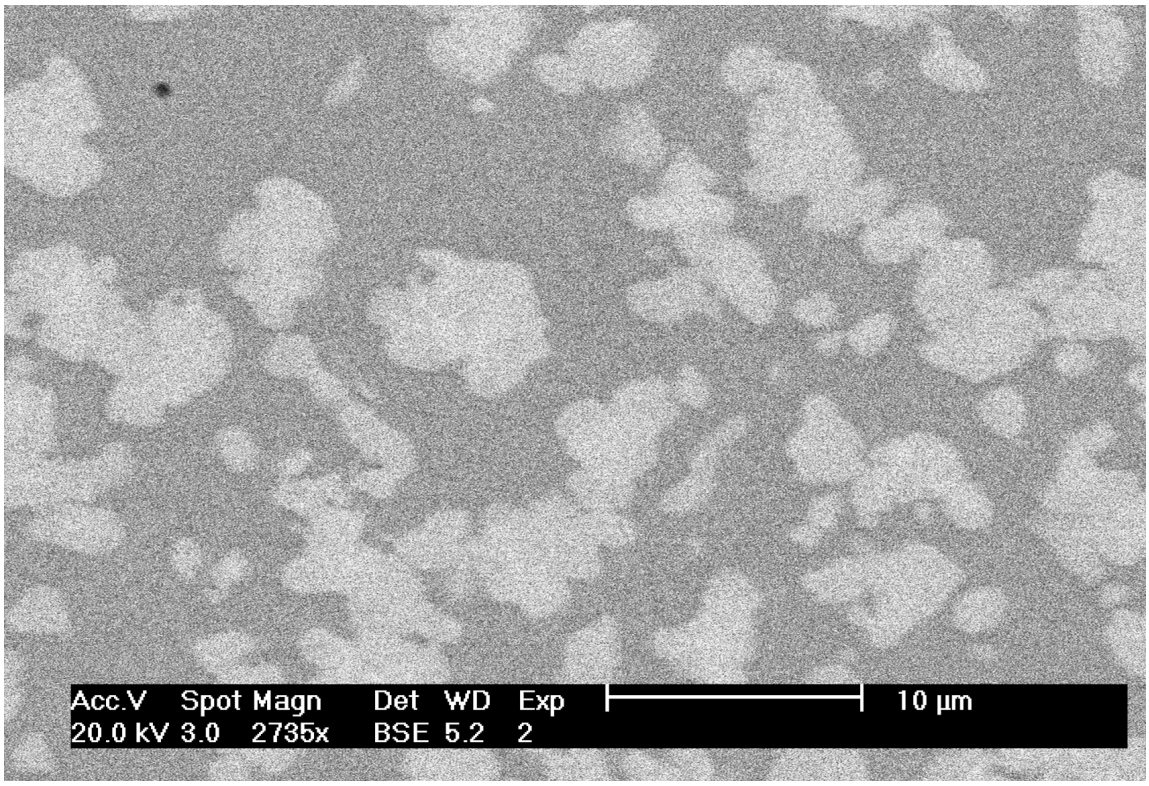


Figure 5.11: A backscattered electron image of HOSP-Pre4 showing that there are two phases present.

The results from this preliminary trial were not successful but did provide enough evidence to suggest that achieving HOSP HEAs using this method is possible. The main problem with this approach related to the production of the alloys rather than any fundamental flaw with the method. The results showed that the likely best way to proceed was to adapt the method slightly by taking a more in-depth approach to element selection and the melting process. Wholesale changes to the the modelling method are unnecessary and can be repeated with only a few minor tweaks. This is the approach adopted in the next section.

### 5.3.3 Further Experimental Work

#### Changes to the Model

This alloy search in terms of method and procedure is essentially the same as the work that generated alloy HOSP-Pre4. The main difference here is that the elements available for selection have been reduced in order to make alloy production easier. Manganese was removed as it was too volatile, especially with the very high melting points of the other elements. Zinc, which had been included in trials previously but had never been used, was also excluded.

Originally the plan following the preliminary work was to also exclude tungsten and perhaps even the other very high melting point elements. While the arc-melter is capable of melting these alloys, achieving good mixing and not overheating the other elements can be a problem during the heating process. However, early modelling results showed the importance of these elements and how much poorer both the single phase and HEA formation properties are if these elements are excluded completely. Instead, these elements were allowed to remain as part of the trial but there was some consideration about how much of the high melting elements should be allowed in each alloy. These considerations are discussed in more detail later as part of the alloy selection process.

One possible route that was looked into but not explored experimentally was to use an induction furnace with a borax cover as a production route. This could be used as an alternative production method to the arc-melter that could melt the volatile elements manganese and zinc. The downside to this method is the lack of power compared to arcmelting. Achieving temperatures hot enough to melt the higher melting elements (any element over 1500°C) would be very difficult.

Also limiting the amounts of high melting point elements is the method by which oxidation is prevented. At higher temperatures the zinc is able to escape the protective borax layer, causing oxidation and dangerous bubbling of the molten borax. There

were only a handful of high order systems to chose from once the high melting point elements had been excluded and the remaining systems had poor modelled properties that were not worth investigating.

### New Alloy Selection

Based on the preliminary results, a larger selection of six and seven element alloys was made. The process of finding these alloys was similar to the preliminary selection but now with no manganese. The consideration for the tungsten and other high melting point elements was also applied in this process. The problem here is that tungsten and the other high melting elements (e.g. molybdenum) feature in the majority of the best modelled results. Excluding these elements would leave very few viable compositions for trialling. However, the high melting point and difficulty in ensuring proper mixing is the one of the main reasons why five out of six of the preliminary compositions had macro-segregation.

The solution was to select compositions with a variety of high element contents. There were three sub-trials within the larger trial of finding HOSP HEAs. One trial excluded tungsten entirely, another optimised alloys for low melting temperature and one had a free choice of the available compositions. In total ten compositions were selected for trialling, shown in Table 5.9.

There were six alloys with six elements and four alloys with seven components. Alloys HOSP-6-1 and HOSP-7-4 were selected as they had no tungsten. Alloys HOSP-6-2 and HOSP-6-3 were selected as they had a low overall melting temperature. Melting temperatures were evaluated by taking a weighted average of the elemental melting temperatures. This approach for melting temperature modelling was simple but quick, essential for the number of alloys that are being modelled. The remaining alloys were selected with no filters but still with manganese removed from the trials. For the alloys with additional filters the $H_f$ limits were expanded to an extra 100 meV/atom to allow for a fuller picture of the available low-melting point systems

Table 5.9: The compositions for the alloys selected as part of the main experiments of the HOSP HEA alloy search.

| | Element at.% | | | | | | | | | | | | |
|---|---|---|---|---|---|---|---|---|---|---|---|---|---|
| Alloy | Ti | V | Cr | Mn | Co | Ni | Cu | Zr | Nb | Mo | Hf | Ta | W |
| HOSP-6-1 | | 30 | 10 | | 10 | | | | 10 | 30 | | 10 | |
| HOSP-6-2 | | 30 | 10 | | 10 | | | | 10 | 30 | | | 10 |
| HOSP-6-3 | | 30 | 10 | | 30 | 10 | | | | 10 | | | 10 |
| HOSP-6-4 | 30 | | | | | | | 10 | 10 | 10 | 10 | | 30 |
| HOSP-6-5 | 10 | | | | | | | 10 | 30 | 10 | | 30 | 10 |
| HOSP-6-6 | | 10 | | | | | | 10 | 30 | 10 | | 20 | 20 |
| HOSP-7-1 | | 10 | 10 | | 10 | | | | 10 | 30 | | 10 | 20 |
| HOSP-7-2 | 10 | 10 | | | | | | 10 | 30 | 10 | | 10 | 20 |
| HOSP-7-3 | 10 | 10 | | | | | | | 30 | 10 | 10 | 15 | 15 |
| HOSP-7-4 | | 30 | 10 | | 15 | | 10 | | 10 | 15 | | 10 | |

These alloys were produced using the same arc-melter as the previous alloys in this chapter. The results were much more successful than the preliminary trials had been. Out of the ten alloys selected seven were successfully melted and alloyed. The alloys were classed as being unsuccessfully melted rather than macro-segregating. Sometimes distinguishing between alloys that segregated and alloys that have not been properly melted can be difficult. In the case of these alloys though there was evidence of elements in the final melt which had not been melted but were hidden in the bulk of the alloy. An example of this is shown in Fig. 5.12.


Figure 5.12: A photo of the unsuccessful melt of HOSP-6-5. Shown on top of the sample is the end of an unmelted tantalum rod, shown by the red arrow. Scale shown is in cm.

Even with the changes to element selection the alloys were still difficult to produce. Extremely high temperatures were required to ensure proper mixing and it was very easy for elements to be ejected from the hearth during the violent melting process. The resultant compositions that were measured, using XRF, often had significant differences from the intended composition set out in Table 5.9. Fortunately, using the narrower composition limits of 10 at.% to 30 at.% meant that most of the alloys had compositions that still abided by the HEA composition limits 5 at.% to 35 at.%. The composition results for the alloys from Table 5.9 are shown in Table 5.10.

Table 5.10: The compositions of the alloys produced as part of the HOSP HEA alloy search. Results were measured using XRF.

| | Element at.% | | | | | | | | | | | |
|---|---|---|---|---|---|---|---|---|---|---|---|---|
| Alloy | Ti | V | Cr | Co | Ni | Cu | Zr | Nb | Mo | Hf | Ta | W |
| HOSP-6-1 | | 11.5 | 9.7 | 10.9 | | | | 12.5 | 36.0 | | 19.4 | |
| HOSP-6-2 | Not available due to macro-segregation | | | | | | | | | | | |
| HOSP-6-3 | | 3.1 | 4.9 | 33.1 | 12.3 | | | | 27.8 | | | 18.9 |
| HOSP-6-4 | 24.8 | | | | | | 12.6 | 12.8 | 15.5 | | 23.4 | 11.0 |
| HOSP-6-5 | Not available due to macro-segregation | | | | | | | | | | | |
| HOSP-6-6 | Not available due to macro-segregation | | | | | | | | | | | |
| HOSP-7-1 | | 4.5 | 7.9 | 9.0 | | | | 10.6 | 49.5 | | 11.9 | 6.5 |
| HOSP-7-2 | 8.4 | 3.5 | | | | | 9.3 | 39.7 | 25.2 | | 5.5 | 8.5 |
| HOSP-7-3 | 7.4 | 6.0 | | | | | | 23.6 | 16.4 | 14.2 | 13.0 | 19.5 |
| HOSP-7-4 | | 11.0 | 9.2 | 14.9 | | 11.7 | | 11.5 | 30.5 | | 11.2 | |

The structures of the alloys were analysed using XRD. The summarised results, along with the other HEA relevant results, are shown in Table 5.11. Further detail about the phases present is shown in the subsequent figures after Table 5.11.

Table 5.11: The summarised results for the properties of the HOSP HEA set of alloys. Where structures are described as complex this is because the XRD results gave spectra which were difficult to index. The results of the complex alloys are discussed in the next section.

| Alloy Name | Melted Succesfully? | No Macro-Segregation? | Within HEA Composition? | Phase Analysis |
|---|---|---|---|---|
| HOSP-6-1 | Yes | Yes | Yes | Multi Phase - Complex |
| HOSP-6-2 | No | | | |
| HOSP-6-3 | Yes | Yes | No | Two Phase - Complex |
| HOSP-6-4 | Yes | Yes | Yes | Single Phase BCC |
| HOSP-6-5 | No | | | |
| HOSP-6-6 | No | | | |
| HOSP-7-1 | Yes | Yes | No | Single Phase - BCC |
| HOSP-7-2 | Yes | Yes | No | Two Phase - BCC & BCC |
| HOSP-7-3 | Yes | Yes | Yes | Single Phase - BCC |
| HOSP-7-4 | Yes | Yes | Yes | Two Phase - BCC & BCC |

### 5.3.4 Structure Analysis

The results of the structure analyses are summarised in Table 5.11. Often the analyses of these alloys were difficult due to the large number of elements and novel structures involved. The increased number of elements mean many different structures may form. Also, if the alloys are successful and HEA structures were formed, then it is very likely that the structure would not be listed in databases. XRD analysis was carried out using the same Bruker D2 Phaser that was referred to earlier and SEM analysis was done with the Philips XL 30S electron microscope, that was also referred to earlier.

The results of most significance are HOSP-6-4 and HOSP-7-3 that are single phase and meet all the requirements of a HEA. The XRD trace of HOSP-6-4 is shown in Fig. 5.13.

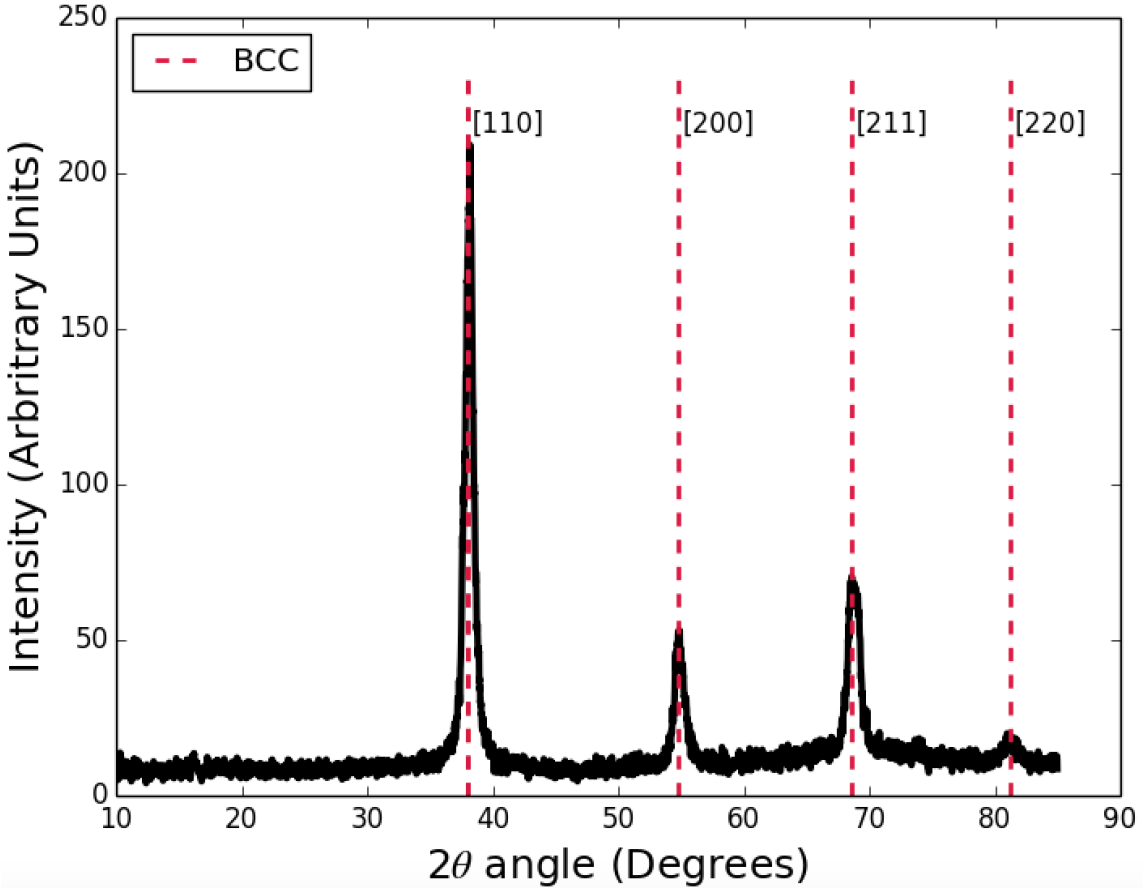


Figure 5.13: The XRD trace for the HOSP-6-4 alloy. The BCC phase marked on has a lattice parameter of 3.35Å.

As well as the XRD analysis there was analysis carried out using SEM and EDX. This additional work on HOSP-6-4 confirmed the single phase nature of the alloy. An image from the SEM analysis is shown in Fig. 5.14.

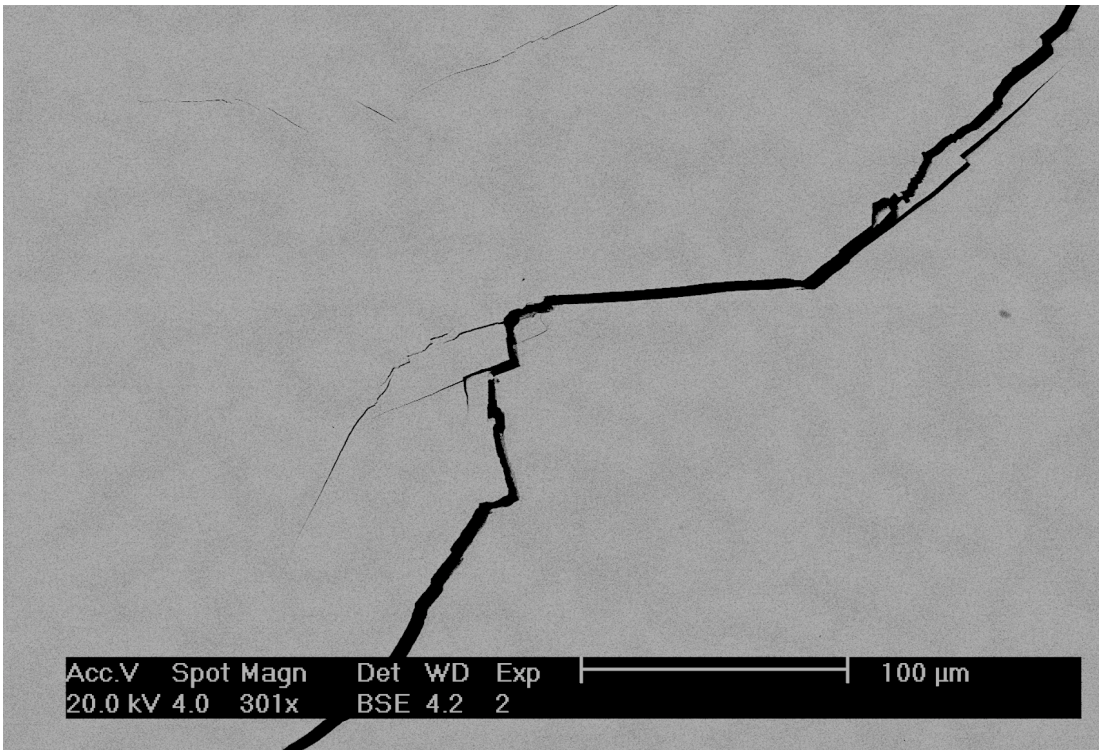


Figure 5.14: A backscattered electron micrograph of the single phase HOSP-6-4. As the surface lacked features this image is purposefully focussed on a crack to show the microscope is in focus.

The other alloy that was single phase and had a composition within the HEA limits was HOSP-7-3. The XRD trace from this alloy is shown in Fig. 5.15.

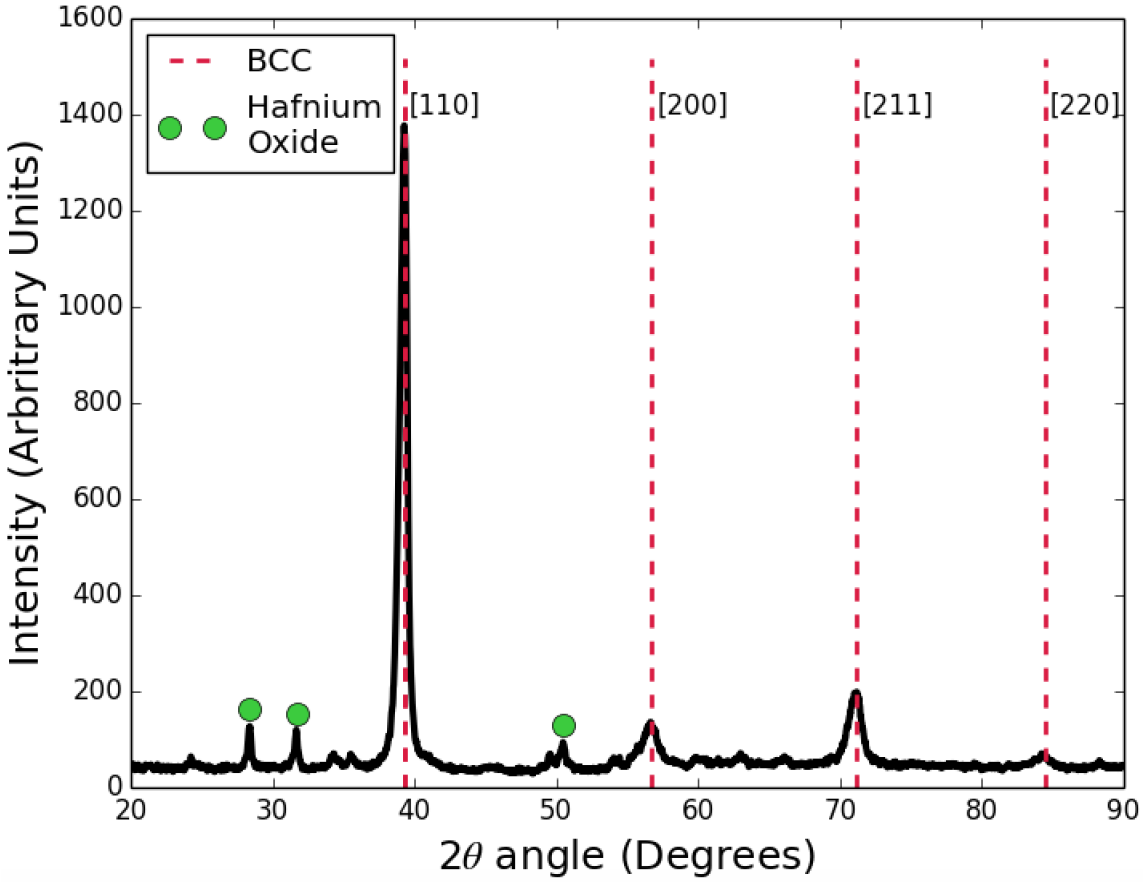


Figure 5.15: The XRD trace for the HOSP-7-3 alloy. The BCC phase marked on has a lattice parameter of 3.245Å. The secondary phase, marked with the green dots, has been identified from the XRD pattern database as hafnium oxide.

The BCC phase in the HOSP-7-3 alloy had a lattice parameter of 3.245Å. The other peaks shown related to hafnium oxide. The presence of hafnium oxide is feasible as the alloy does have hafnium as one of its elements. Also, some of the melts were carried out in less than ideal vacuum conditions. Porosity in the pure elements meant that fully evacuating oxygen out of the melting chamber was extremely difficult. Even using a longer vacuum stage (18 hours rather than 15 minutes), it may have been the case that some of the melts still have had more oxygen present than normal melting conditions.

The alloy was still considered as a likely single phase though as the hafnium oxide

was thought to have a high probability of being on the surface of the alloy and not in the bulk. This could be confirmed by grinding all surfaces of the sample to remove the oxide scale. This process though is difficult as the sample is small, not a perfect button and with a high wear resistance. Instead the single phase status, and the fact that hafnium oxide is on the surface not in the bulk, was confirmed using SEM and EDX analysis. An example micrograph for HOSP-7-3 is shown in Fig. 5.16.

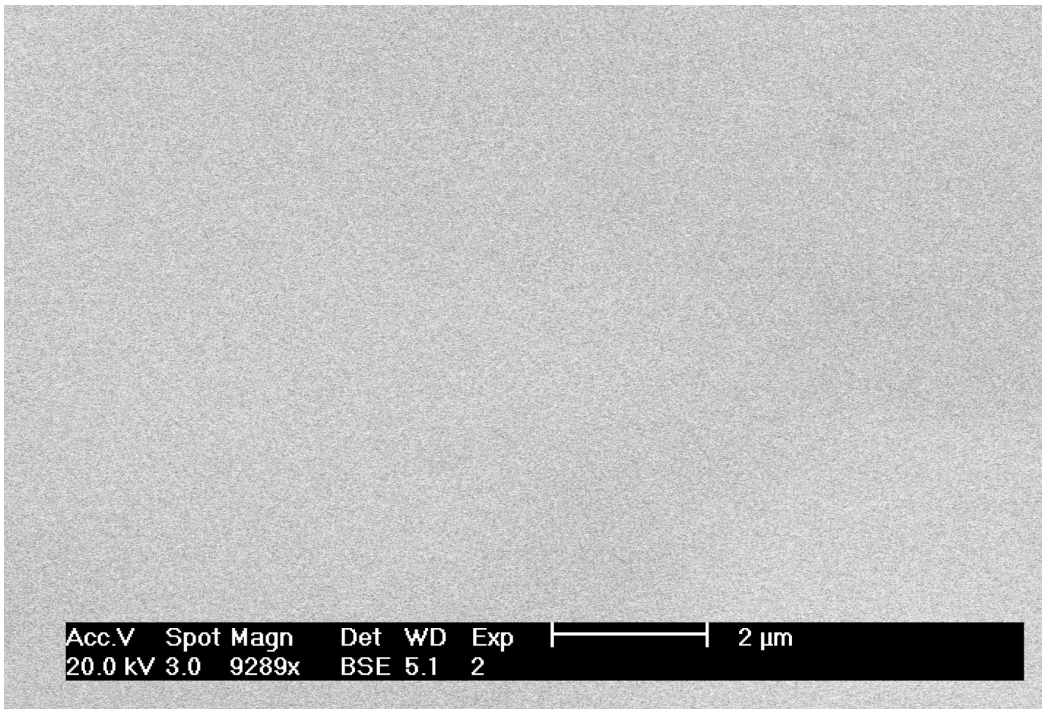


Figure 5.16: A backscattered electron micrograph of HOSP-7-3.

The SEM analysis of the HOSP-7-3 showed only one phase was present. There was no evidence of hafnium oxide, or any other secondary phase, during the SEM analysis. The composition measured by EDX agreed with the XRF measurements also taken.

Of the remaining samples there was one other sample that could be considered single phase. Alloy HOSP-7-1 had a single BCC phase. The composition of the alloy though did not meet the requirements of a HEA, specifically molybdenum that was at 49.5 at.%. The XRD scan of HOSP-7-1 is shown in Fig. 5.17.

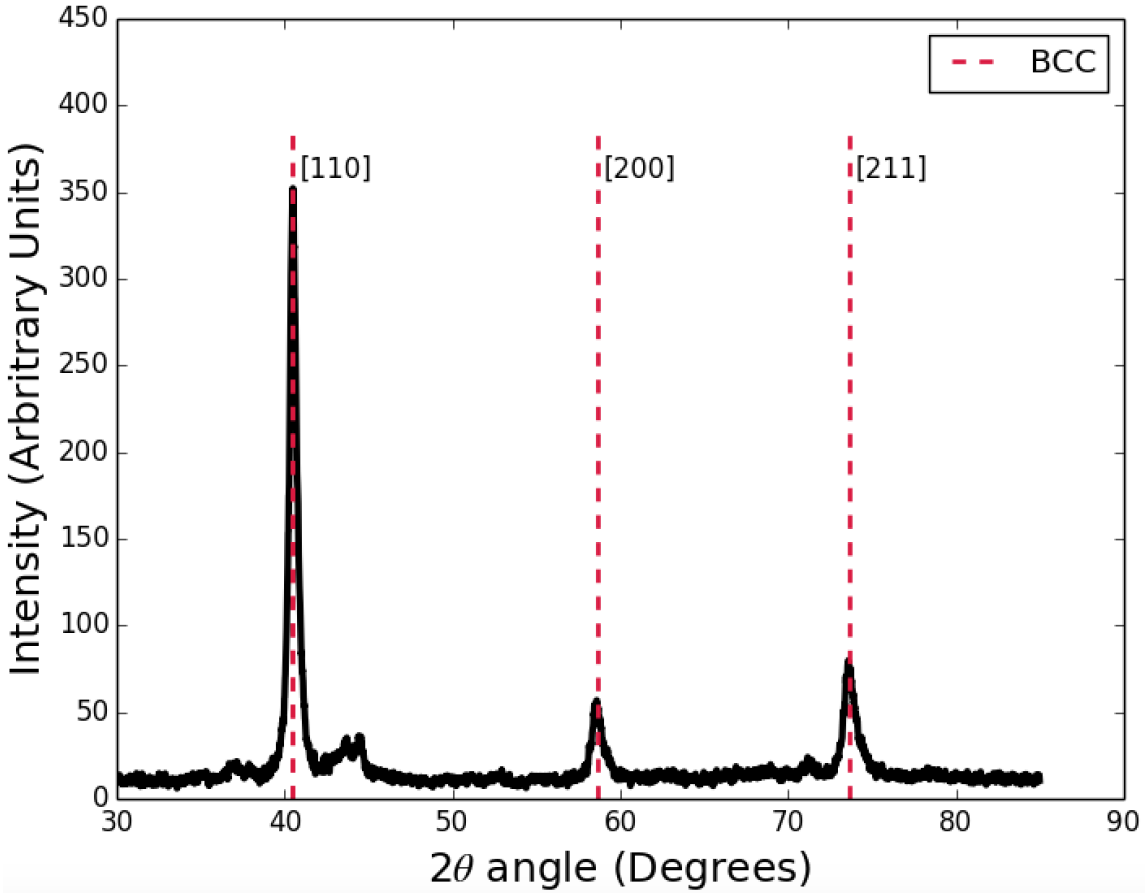


Figure 5.17: The XRD trace for the HOSP-7-1 alloy. The BCC phase marked on has a lattice parameter of 3.15Å.

The XRD scan showed a single phase BCC with a lattice parameter of 3.15Å. There was some additional signal (around 43°). This could have been a small amount of secondary phase or a some amount unmixed element.

None of the remaining alloys were single phase. Of the two phase alloys the complexity of the two phase structures varied significantly. Some of the alloys were combinations of simple structures (e.g. two BCCs) that were easily identified. Other alloys appeared to have many phases present but were actually the result of more complex structures, such as hexagonal. An example two phase structure was found in HOSP-7-2 with two BCC structures forming. The XRD from this graph is shown in Fig. 5.18.

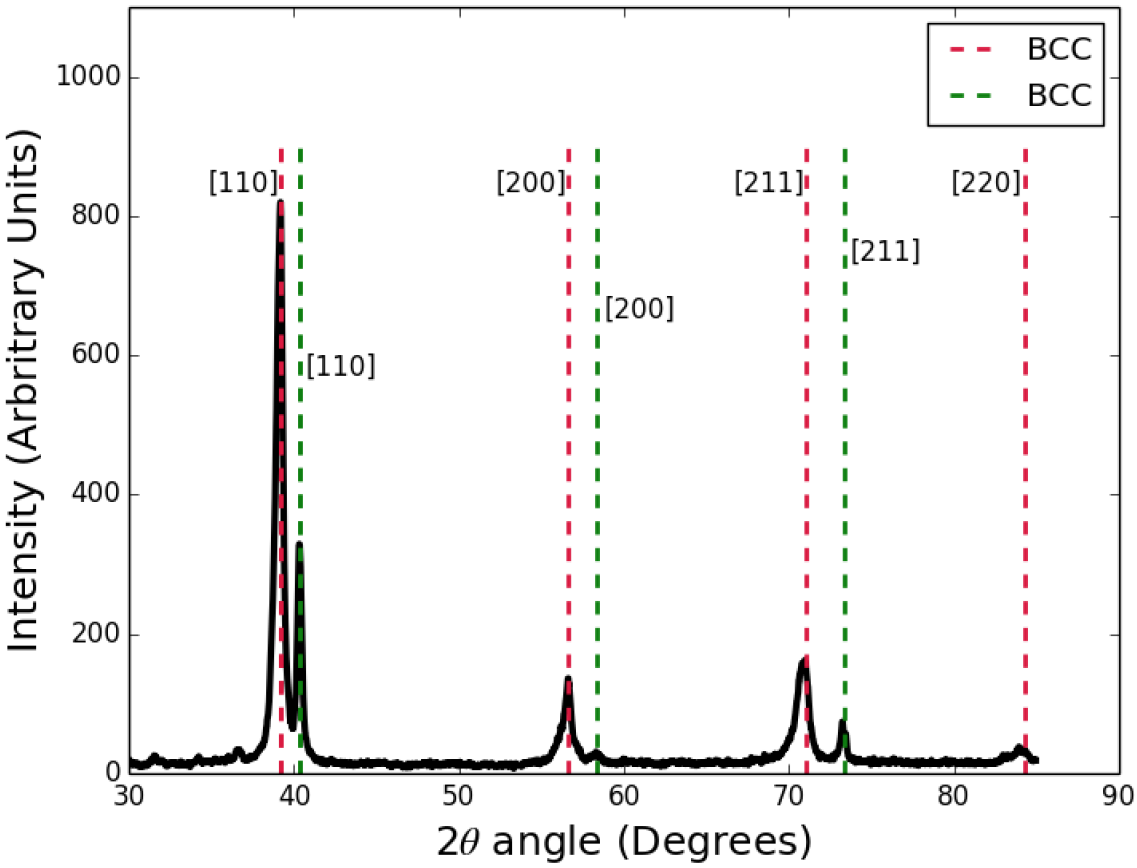


Figure 5.18: The XRD trace for the HOSP-7-2 alloy. There are two BCC phases present. The most prominent BCC phase, marked in red, has a lattice parameter of 3.25Å. The less prominent BCC phase, marked in green, has a lattice parameter of 3.16Å

The presence of two BCC phases and no other phases means that HOSP-7-2 could be classified as a HEA. However, the Nb component is 39.7 at.% and so above the composition limits that are usually required. The secondary phase in HOSP-7-2 was tungsten-based with a small amount of one or more elements included. The lattice parameter measured, 3.16Å, is very similar to the lattice parameter of pure tungsten 3.1652Å[130]. The two phase nature of HOSP-7-2 and the composition of the phases were investigated using the SEM and EDX methods like the other alloys. A micrograph for HOSP-7-2 is shown in Fig. 5.19.

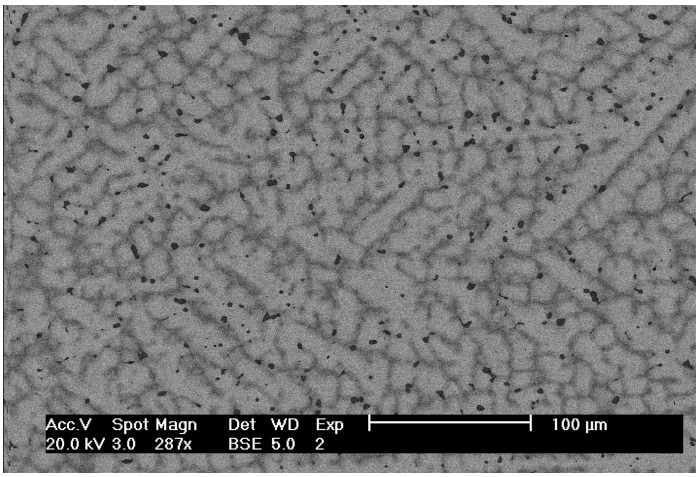


Figure 5.19: A backscattered electron image of HOSP-7-2. The light coloured phase corresponds to the main BCC phase.

The secondary phase contains most of the zirconium in the alloy. The darker boundaries were found to have similar compositions as the very dark spots, suggesting that there are only two phases present. The two phase nature was confirmed using SEM. There is the possibility of three phases in HOSP-7-2 as the SEM does appear to show three different colours.The phases were evenly distributed across the alloy.

Analyses of the other other alloys in Table 5.11 were carried out using the same XRD and SEM techniques as the alloys detailed in this section. The phase results are summarised back in Table 5.11. The compositions indicated as having complex phases were very difficult to identify with confidence. As there are many elements and this is a novel structure, there were numerous possible structures that could have formed and many of the possible structures were not listed in XRD-analysis software. The full details of the phases though were not a priority as this work was focussed on single phase alloys and these alloys were multi-phase.

### 5.3.5 Hardness Measurements

A large part of the interest around HEAs relates to the enhanced properties that can be found in certain HEAs. One property that has been the topic of many publications

is the high hardness values of HEAs [52, 131]. These high values are usually associated with the solid solution strengthening that occurs with the high number of elements that are forced into one or two phases, within a HEA.

The alloys created in this study would appear ideally suited to have high hardness values. There are large numbers of elements that are in a single structure, meaning there should be large amounts of solid solution strengthening. Even the alloys that formed a second phase or are likely to have high hardness values. These alloys have the benefit of secondary phases that will also increase the hardness of the alloys. Finally the selection of the elements also would encourage high hardness. There are no particularly low yield elements, such as Au or Ag, and there are a number of elements that have high hardness values, such as Hf and W.

The measurements were carried out on a Struers Durascan machine with a Vickers indenter. Measurements were taken using HV5 indents that were applied for 15 seconds. There were 15 measurements carried out on each sample. Due to problems with the sample preparation the number of results possible was limited to two. HOSP-6-4 had a hardness value of 442±2. HOSP-7-3 had a hardness value of 483±3.

These are relatively high hardness values for alloys, around the same sort of value as some tool steels [132]. If these HOSP-HEAs are ductile also then they could be particularly interesting for a high-strength applications. Further testing and large samples would be necessary though to confirm the ductility and the other mechanical properties of these alloys.

### 5.3.6 HOSP HEA Conclusion

The modelling and experimental work on HOSP HEAs was successful, with a six element and seven element example found. The biggest problems for this method largely related to production methods rather than any modelling method. Problems with technique meant that element selection had to be limited and a number of the melts that had incorrect compositions.

If this work was to be progressed further a useful place to start would be with elements and alloy production. Using high-cost elements would drastically change the number of systems that can be accessed, including many of the systems that had the best single phase results (see Table. 5.5). Even without a change to the elements available, future work would benefit from the skills and knowledge developed during the melting processes in this work. It should mean that future alloys are melted with a higher success rate and very high melting point alloys will be less of a problem.

## 5.4 Other Variables

### HEA Relevant Variable

In the silver HEA example in Chapter 4.5, the two examples in this chapter and the HEA-type brazing alloys in Chapter 6 the HEA properties were all measured the same way. This was done as $\delta$ and $\Delta H_{mix}$ was thought to offer best compromise between accuracy and simplicity. The two properties, used with the limits set of by Zhang et al., offered an effective discriminator between HEAs and non-HEAs. The properties though were still relatively simple to calculate and could be carried out with a reasonable time scale on the large scales necessary with this method.

A key theme of this chapter is that the modelling method can be changed to fit the needs of different trials. This holds true for the HEA modelling method. While all the examples detailed here do not change, there is the function to so if required. This might be a different method of measuring $\delta$ if it provides better results for certain elements or using some the bulk modulus calculations from Toda-Caraballo and Rivera-Diaz-del-Castillo [89] if that is of particular importance for some reason, for example if a high strength HEA was being designed. There are still limitations though on what can be trialled on a large scale and many of the methods (e.g. ab initio) would still not be practical.

Any alloy property that has can be described or approximated by a relatively

simple set of formulae can potentially be included in this trial. Melting temperature is a prominent example that will be used extensively in Chapter 6. Other examples include the electrical resistivity using Vegard's law [62] and density using a rule of mixtures approximation. Both of these examples have been used implemented in the model developed here, and employed in other research projects.

If a more complex variable modelling formulae was desired then there is an approach for saving reducing the calculation time needed. The approach is to put a filter within the calculations stage in Fig. 5.3. This filter judges the compositions based on their HEA formation properties on the fly. This can be a strict limit or a loose one depending on the precise details of the trial. The complex modelling process will then only be used on the alloys that pass the HEA formation filters. This can significantly reduce the computational time required and means less time is wasted modelling the properties of alloys that will never be selected.

## 5.5 Conclusion

This chapter set out to demonstrate the adaptability of the large-scale modelling method by using the method in two examples. In one example the silver HEA work from chapter 4.5 had filters added based on single phase formation properties of the system, based on the model created by Troparevsky et al. The second example used the same single phase formation rules but with the intention of finding HOSP HEAs from a set of 17 easily accessible elements.

The modelled results of first trial indicated that single phase silver HEAs would be difficult to produce. There were no alloys that had suitable modelled properties and many of the best alloys had already been produced as part of the silver HEA work in Chapter 4.5. Out of all of the silver HEAs that were trialled all the results were either two-phase HEAs or failed to form a HEA at all.

The second trial had more positive results. The modelled results in this trial

had many more systems and compositions that were close to the single phase limits. The most significant problem with this trial was the production of the alloys for testing. High order alloys with very high melting elements proved to be challenging to melt. Many alloys that were melted failed to be mixed properly or had compositions that were noticeably different from the intended composition. Even so, there were successful HOSP HEAs that formed. A six-element HEA and a seven-element HEA were produced, tested and both were found to have single phase structures.

# Chapter 6

# Novel Brazing Alloys using HEA-type Modelling

This chapter is the practical culmination of the work discussed in the previous chapters. Chapter 3 showed that thermodynamic methods were unlikely to find brazing alloys with significantly improved properties. This meant that more novel approaches, such as HEA prediction methods, became a more enticing prospect. Chapter 4 used HEA modelling as part of a large-scale modelling method in order to find silver HEAs. Chapter 5 used the same approach with the code adapted for single-phase modelling. This method is another version of the large-scale method tailored for brazing alloys.

This chapter will start by defining the parameters of the novel brazing alloy search, both in terms of the input parameters and the output properties. Some of these output properties, such as melting temperature, have options for how they are calculated and these are discussed in this chapter.

The trial produces a large amount of results, which are then filtered and optimised to find potential alloys. From this a range of alloys are then trialled and analysed. Some trials were then carried out to investigate more subtle composition changes. These two trials were exploring compositions within a single system and looking at the effect that small amounts of elements had on a HEA-type brazing alloy.

## 6.1 Parameters for the Novel Brazing Alloy Search

The objective of this search is to find a HEA that is suitable for brazing and improved properties. This could either be a lower melting temperature or a lower cost compared to the already existing brazing alloys.

There are a number of parameters to decide upon for this alloy search. The elements, compositions and systems all need to be selected for this particular trial. As with the previous examples of this method the selections need to be made that balance the time taken to complete the trial and the thoroughness of the trial to ensure that no potentially good compositions are missed. Also, as well as the materials properties there needs to be some consideration of the commercial aspects of brazing alloys.

The elements selected for this trial were all found in existing brazing alloys. This was decided upon as it meant that there was already knowledge of how the elements behave in brazing alloys and brazed joints. There is also a commercial benefit in avoiding unusual elements. Convincing customers to switch to a novel alloy is made much harder if the alloy contains elements that have never been used in brazing. While the elements are not novel in this alloy search the compositions and alloy systems are.

There are many elements that feature in brazing alloys. Including all of these elements would make the trial needlessly large with many systems that are of no interest. The intended use of the large-scale modelling was to be able to include high quantities of low cost or low melting point elements without the formation of IMCs. Also, as these trials had to be produced with the equipment available some considerations were allowed for how easily the elements could be melted.

The elements selected were Ag, Cu, Zn, Sn, Mn, Ni, Co, In and Ga. These elements are the main alloying elements for silver brazing alloys, with the addition of some low melting elements. Other precious metals, such as Au and Pd, were excluded as they were high melting and high cost. The melting points of the elements included in the alloy search are shown in Fig. 6.1.

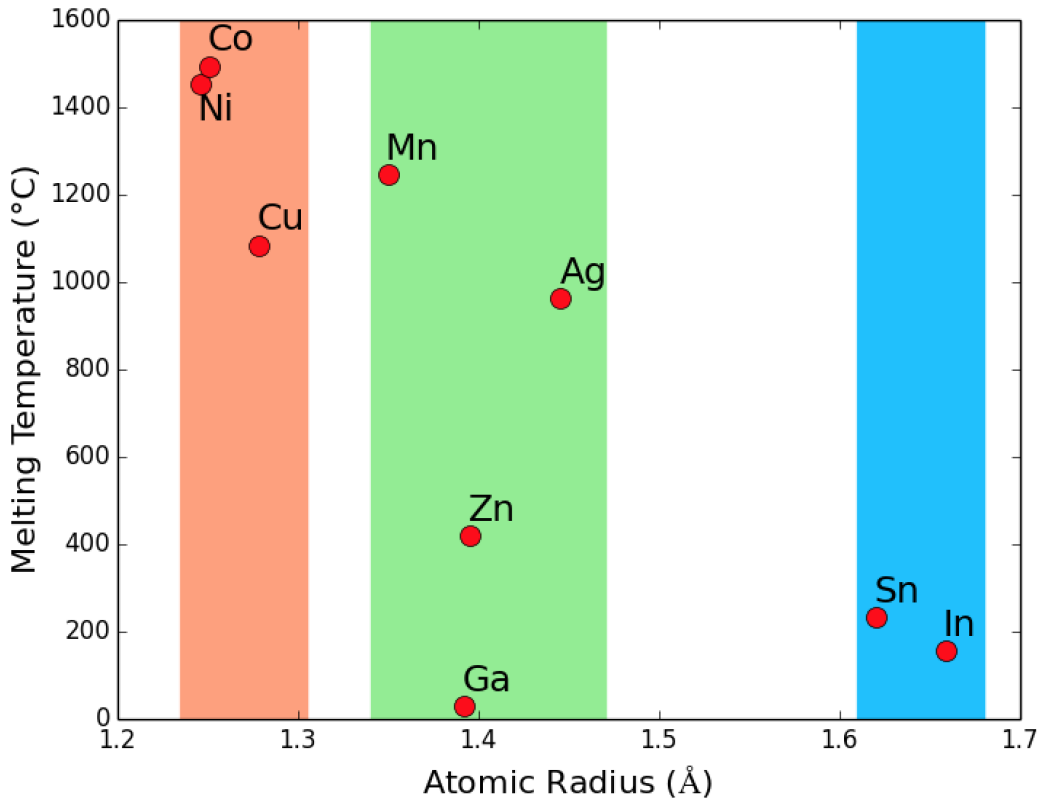


Figure 6.1: The atomic radii and the melting points of the elements in this brazing alloy scan. The atomic radii values are from Guo et al. [81]. The coloured regions refer to groupings of similarly sized atoms.

As well as the brazing-related properties it is relatively important also that these elements have favourable HEA formation properties. However, some of the elements have relatively poor HEA values, with atomic size differences away from the other elements and highly positive Miedema enthalpy values. These elements were allowed to remain in the trial though as alloys may still be able to incorporate those elements in small amounts. For the elements in Fig. 6.1 the enthalpy values for these combinations are shown in Table 6.1.

Table 6.1: The Miedema enthalpy values for the elements involved in this brazing alloy search. All values are in units of kJ/mol. Values are from Takeuchi and Inoue [82] and can be found in the complete table in Appendix A.

| | Miedema Enthalpy Values (kJ/mol) | | | | | | | | |
|---|---|---|---|---|---|---|---|---|---|
| Elements | Ag | Cu | Zn | Sn | Mn | Ni | Co | In | Ga |
| Ag | 0 | 2 | -4 | -3 | 13 | 15 | 19 | -2 | -5 |
| Cu | 2 | 0 | 1 | 7 | 4 | 4 | 6 | 10 | 1 |
| Zn | -4 | 1 | 0 | 1 | -6 | -9 | -5 | 3 | 0 |
| Sn | -3 | 7 | 1 | 0 | -7 | -4 | 0 | 0 | 1 |
| Mn | 13 | 4 | -6 | -7 | 0 | -8 | -5 | 3 | -13 |
| Ni | 15 | 4 | -9 | -4 | -8 | 0 | 0 | 2 | -15 |
| Co | 19 | 6 | -5 | 0 | -5 | 0 | 0 | 7 | -11 |
| In | -2 | 10 | 3 | 0 | 3 | 2 | 7 | 0 | 3 |
| Ga | -5 | 1 | 0 | 1 | -13 | -15 | -11 | 3 | 0 |

Given the relatively small number of alloy systems in this trial there was less need to compromise on the paramaters of the composition search. This allowed for a relatively fine step size and wide limits on the minimum and maximum amounts of each element. The HEA compositional limits usually imposed do not have to be adhered to in this alloy search. This is because it is the beneficial properties of a HEA-type structure that are desired, rather than the technical designation of a HEA. As such the alloy search here will seamlessly look across HEA alloy space and non-HEA alloy space. It is also more correct to call these alloys 'HEA-type alloys' or 'IMC-suppressed alloys', (intending to make use of this aspect of HEA behaviour), rather than HEAs.

As this research is primarily focussed on silver brazing alloys there was some consideration about whether to make silver mandatory in all the systems selected. This

was not the chosen approach though and instead all possible systems were trialled. This was decided on as there was the potential, even if relatively unlikely, to have some non-silver systems that could rival the silver containing systems. If the computational time required had been an issue then silver may have been made mandatory in order to reduce the systems that were analysed, but this was not necessary. For the system sizes the range selected was from four element systems up to six element systems.

As with previous alloy searches the composition step size used was different depending on the order of the system. The details are shown in Table 6.2. As the HEA composition limits are not important here the lower limit used was 4 at.% and the upper limit 70 at.%. It is worth noting though that this large upper limit was selected so that trends could be analysed over large ranges. In practise alloys were not selected with a component above 60 at.% and for most alloys the largest component was below 50 at.%.

Table 6.2: The details of the composition searches that were carried out for each system, based on the order of the system.

| System Order | Number of Systems | Step Size (at.%) | Composition Limits (at.%) | Alloys per System |
|---|---|---|---|---|
| 4 | 126 | 1 | 4 - 70 | 100,675 |
| 5 | 126 | 2 | 4 - 70 | 134,101 |
| 6 | 84 | 4 | 4 - 68 | 42,378 |

It is also worth noting that in this chapter it was necessary to switch between at.% and wt.%. The HEA formation calculations and the other property calculations were done using at.%. However, the cost of elements is calculated by mass and so the wt.% of the alloy is also important.

## 6.2 Properties to be Measured

The parameters used here are again $\delta$ and $\Delta H_{mix}$. In terms of brazing properties the most important two properties to consider are the cost and the melting points. For the remainder of this chapter the melting temperature that is referred to is the liquidus temperature.

The approximate cost can be calculated by multiplying the weight fractions of each element by the costs of each element. However, as the precious metals are so much more costly than the other elements this can be simplified to just comparing the precious metal contents of prospective alloys.

The modelled melting temperatures for these multicomponent alloys can be calculated in a number of different ways. Many of the approaches have been mentioned previously as part of the thermodynamic modelling of brazing alloys or as part of the HEA calculations. In chapter 3 the melting temperature is calculated using CALPHAD as one of the functions within the Thermo-Calc program. The melting temperature has also been approximated by averaging the melting temperatures (as seen in the Yang Parameter [90]) and by using the heat of fusion for each component (as used in the Poletti parameter [91]).

For this trial CALPHAD was thought to be too time consuming and so was not considered. A much faster method was to take a weighted average of melting temperatures. The drawback to this method is that the effect of eutectic ratios was not factored into calculations. For some alloys this has significant effects, with Ag-Cu and Cu-Mn being two examples of higher melting point elements that have deep eutectic compositions. To account for this a portion of code was added that could factor in the effect of eutectics and adjust the predicted temperature.

### 6.2.1 The Eutectic Adjustment

The weighted average melting temperature method has two prominent advantages. It is an extremely quick calculation method that is quick to code and to run. The other advantage is that for all non-eutectic pairs of elements then the estimated temperature is usually quite accurate. Preserving these strengths is important for the eutectic adjustment.

The eutectic adjustment manages to maintain both. The calculation speed is maintained by keeping the code and calculations relatively simple. The accurate measurements of non-eutectic pairs is also maintained, as these binary pairs are left alone. These binary pairs are not recalculated, as the eutectic measurements merely adjust the weighted average measurement, rather than calculating every value from scratch.

A more formal melting temperature method (e.g. CALPHAD) was not adopted for a number of reasons. The most significant reason is the time taken to calculate melting temperatures. Although relatively large trials were carried out using CALPHAD in Chapter 3 these are orders of magnitude smaller in size compared to these HEA trials. Furthermore, the predictions can be inaccurate, especially when dealing with alloys systems that might have data missing.

The eutectic adjustment works by considering each binary pair of elements. For each binary pair the difference between the average melting point and the eutectic values is estimated. This is then scaled according to how much of those two elements are present in the composition. Once this is done for all binary pairs in the alloy then the new melting temperature is recorded.

#### Ag155 Example

To show how this eutectic adjustment calculates temperatures the main alloy from Chapter 3, Ag155, is used as an example. The composition of this alloy is Ag55Cu21Zn22Sn2 wt.%. For these calculations the composition needs to be converted to at.%. The tem-

perature calculated using weighted melting points is 832.6°C and the temperature measured by DTA is 665.7°C, a difference of 166.9°C

The first binary pair of elements to consider are Ag and Cu. There is 42.7 at.% Ag and 27.7 at.% Cu in the alloy. This equates to 60.7 at.% Ag on the Ag-Cu phase diagram. This value is used for estimating the temperature difference between the weighted average temperature and the eutectic temperature for this binary pair of elements. This temperature difference is shown on an annotated Ag-Cu phase diagram in Fig. 6.2.

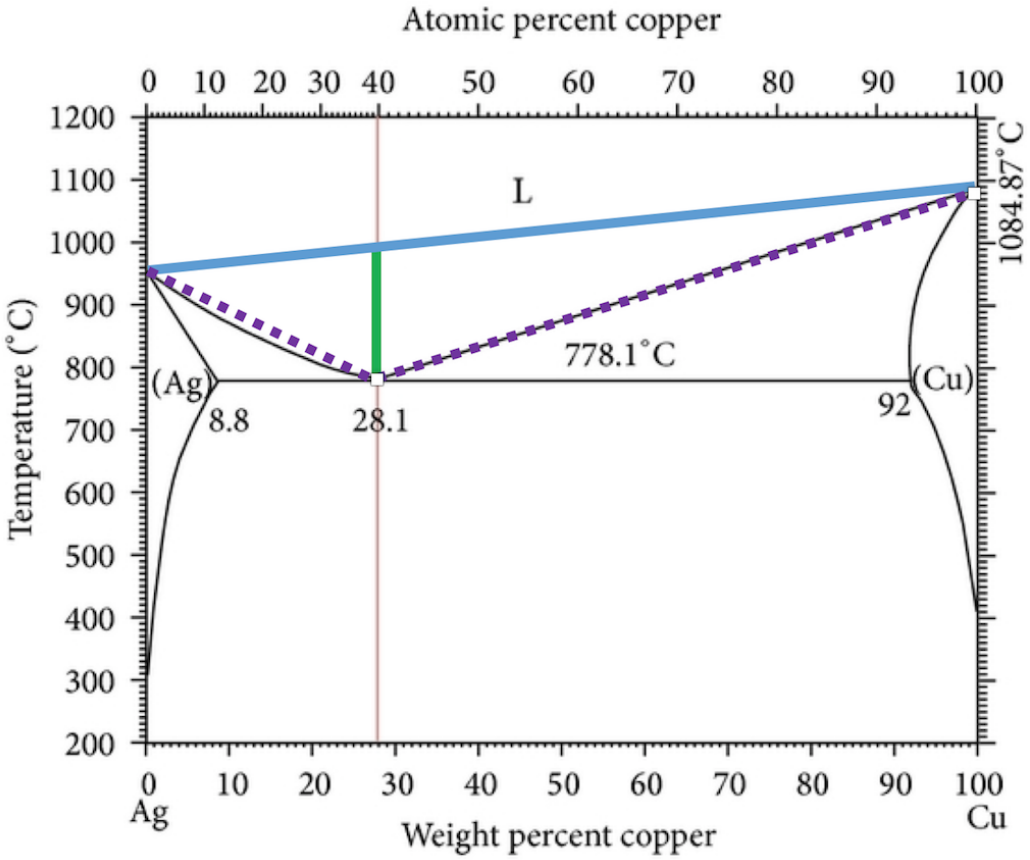


Figure 6.2: An annotated Ag-Cu phase diagram. The ratio of Ag-Cu in this example is at the eutectic. The purple lines show the linear approximation of the liquidus line that is necessary in this method. Original phase diagram from NPL [33]

The phase diagram in Fig.6.2 indicates that for this ratio of Ag and Cu the liquidus

temperature using the weighted average is 1010°C. This is 232°C higher than the value using the eutectic temperature. If the alloy was entirely Ag-Cu, with no other elements, then this would provide the estimated change in temperature due to the eutectic. In this case though, Ag-Cu does not make up the entire alloy and there are other elements present that will reduce the effect of this temperature reduction. In this example there is 42.7 at.% Ag and 27.7 at.% Cu, so the Ag-Cu pair make up 65.4 at.% of the alloy. The temperature reduction is therefore scaled by a factor of 0.654.

While the initial setup of this method stated that all binary pairs are analysed, in practice only the systems that have a eutectic need to be analysed in this method. In this example it means that Zn-Sn needs analysis and that is the only other eutectic that needs to be assessed. Once these have been calculated the adjustments can be made.

The Ag-Cu pair reduces the temperature by 151.7°C. The only other eutectic in this example is the Zn-Sn pair, which reduces the temperature by another 17.1°C. This leaves a eutectic adjusted temperature of 663.8°C. This is a much better estimate of the melting temperature which was measured at 665.7°C. It must be noted that this is a particularly accurate example, larger discrepancies between predictions and results are observed for other compositions. In all the examples that were experimentally verified the eutectic adjustment gave a better estimate than the weighted average method.

### Eutectic Approximations

Enacting the technique described in the Ag155 example requires some approximations to ensure the calculations can be carried out quickly. The biggest approximation is to the phase diagrams that describe the eutectic temperatures. Instead of recreating the phase diagrams using CALPHAD or some other method, the liquidus line across the top of a phase diagram is approximated by two straight lines that meet at the eutectic point.

The two straight lines in the example of Ag-Cu (the purple lines on Fig. 6.2) are a good approximation for the liquidus line. However for some other systems the liquidus line is highly non-linear. Inevitably linear approximations of these lines will lead to some inaccuracy. The benefit to using two straight lines to describe the liquidus though is that it does make it much easier to input data for eutectics. The only inputs required for each eutectic calculation are the eutectic composition and eutectic temperature. All the other necessary data are already saved or can be calculated on the fly.

There are other approximations that are unseen in this adjustment. The kinetics and the mixing of the alloys are all assumed to be random. For example, if a eutectic composition only makes up half the composition then the reduction in temperature is assumed to be halved. This may not be true though, as these atoms may preferentially interact or not interact and so have a larger or smaller temperature reduction.

The eutectic approximation provided a more accurate measurement of the melting temperature for novel alloys. As this approach was informal and not widely tested the weighted melting temperature was still calculated and the values recorded. This was done as an additional check in case the eutectic adjustments were predicting large temperature reductions that seem unfeasible for alloys.

## 6.3 Modelled Results

As with previous trials, some of the alloy systems in this trial have no compositions of interest and can be removed entirely. These systems were excluded on the basis of poor HEA formation or high melting points. There could have been an additional system filter based on cost, however, this was unnecessary as the systems with high precious metal content (e.g. four component systems containing Ag, In and Ga) were already eliminated in the HEA formation filter. Some example systems are shown in Fig. 6.3 with two eliminated systems and one promising system.

In Fig. 6.3 the areas represent the possible values for all the compositions that were analysed in each system. Two of the systems, Ag-Cu-Ni-Co-In (in blue) and Zn-Sn-Ni-Co (in red) are systems that can be eliminated entirely. The Ag-Cu-Zn-Mn is a promising system where a number of compositions have values within the HEA formation region (the peach trapezoid). This promising system will have its compositions analysed individually to find the best compositions.

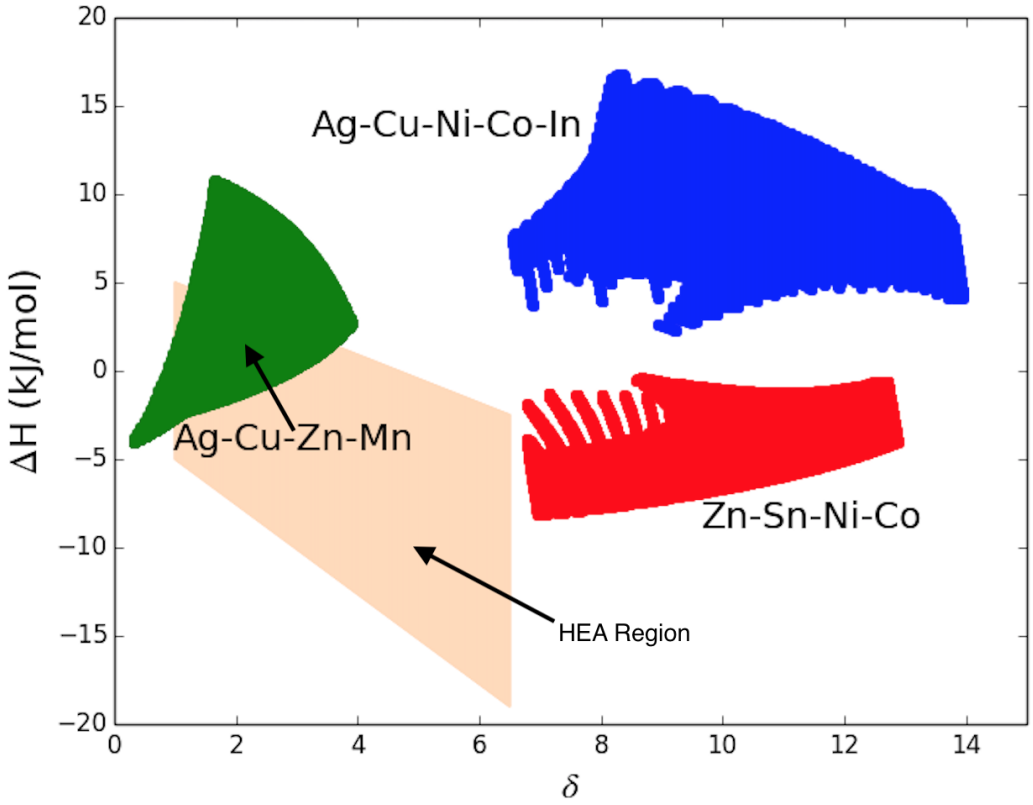


Figure 6.3: The $\delta$ and $\Delta H_{mix}$ values for the three systems from the HEA-type brazing alloy search.

The excluded example systems from Fig. 6.3 (red and blue) were indicative of a trend that occurred in many of the alloy systems that were analysed. Of the systems that had large $\delta$ values most of them had certain combinations of elements occurring. These combinations were found to be problematic regardless of the other elements that were included. Examples from Fig. 6.3 are Co with In and Ni with Sn.

It is apparent from the formula for $\delta$ that having large radii atoms mixed with small radii atoms will lead to large $\delta$ values. In this example this can be seen with the nine elements involved in this trial. Atomic radii for the elements are plotted back in Fig. 6.1. To help explain which element pairs produce large $\delta$ values the plot has been shaded with the elements grouped into small, medium and large atomic radii.

Generally speaking any system that featured both large atomic radii elements and small atomic radii elements had large $\delta$ values. These systems were excluded using the filters on the HEA formation values. There were occasional exceptions to this, usually when the compositions are at the edges of the composition search (e.g. a 46-46-4-4 composition).

As small radii elements cannot be mixed with large radii elements, it means that the the remaining systems fall into two distinct categories. These are the small to medium atomic radii elements (Ni to Ag on Fig. 6.1) and the medium to large atomic radii elements (Mn to In on Fig. 6.1). Of these two categories the large atomic radii had the more limited options. There were only a handful of Sn or In containing alloys with suitable HEA formation values. These were produced and tested in the next subsection.

Gallium is used in brazing alloys, but less frequently than the other elements, and so is handled separately. Gallium has many favourable properties in this trial. The atomic radius is towards the middle of the range, the Miedema enthalpy values are generally favourable and the melting temperature is very low. Consequently gallium features heavily in a number of the best alloys that are predicted. The downside to gallium is the relatively high cost.

While it is not such a high cost as to preclude it from the trial entirely it does mean there are limits on the selection. For any alloy that contained gallium the properties had to be significantly better than the non-gallium alternative in order to justify the high cost of the alloy. No gallium-containing alloy could be found that justified the high cost.

There were many more systems and alloys that had good HEA formation values using the smaller atomic radii atoms. Some of these alloy systems, for example Cu-Mn-Ni-Co, had excellent HEA formation values but also had high melting points across the entire system. These systems could also be excluded entirely. From the lower melts the best results were dominated by systems with Ag-Cu-Zn.

The Ag-Cu-Zn ternary does feature frequently in many existing brazing alloys, including the brazing alloys featured in Chapter 3. The zinc content in these alloys is noticeably different though in this chapter. In these HEA-type alloys the zinc content is significantly higher than in the brazing alloys already in use. Two sets of alloys, a preliminary and a main part, were selected and produced from the available systems.

## 6.4 Experimental Results for Alloy Systems

### 6.4.1 Practical Method

All alloys in this chapter were produced using a small-scale, 2.2kW Ambrell induction melter with a borax cover. The prevalence of zinc in the alloys meant that this method was the only practical method of alloy production. Any method involving a vacuum, exposure to air or a violent heating process would evaporate, oxidise or boil the zinc. The weakness of the induction melter is the lack of power compared to other methods. However, as these alloys are designed to be low melting this was not a problem.

The primary method of composition confirmation was via XRF analysis. This was done with a Panalytical Zetium for all samples in this chapter. For almost all cases the measured compositions were in agreement with the intended composition. When the composition was incorrect the alloy was remade.

Phase analysis was done using a Bruker D2 Phase with Cu k$\alpha$ source. SEM analysis was carried out with a Philips XL 30S electron microscope. The same equipment and methods was used for every sample in this chapter.

### 6.4.2 Preliminary Results

There were a number of systems that had promising results. These alloys were selected from compositions within the HEA formation region, optimised for low temperatures using the eutectic adjustment. As a preliminary search for novel alloys 15 compositions were selected from five different alloy systems. As this was only a preliminary no more than four alloys were selected per system. The compositions selected are shown in Table 6.3. The novel alloys were selected without any consideration about the existing brazing alloys that they might replace or offer an alternative to.

Table 6.3: The compositions of the Brazing HEAs (BHEAs) preliminary set of alloys.

| | Element at.% | | | | | | | | |
|---|---|---|---|---|---|---|---|---|---|
| Alloy | Ag | Cu | Zn | Sn | Mn | Ni | Co | In | Ga |
| BHEA-Pre1 | 40 | 5 | 50 | 5 | | | | | |
| BHEA-Pre2 | 29 | 4 | 58 | 9 | | | | | |
| BHEA-Pre3 | 27 | 4 | 63 | 6 | | | | | |
| BHEA-Pre4 | 37 | 14 | 45 | | 4 | | | | |
| BHEA-Pre5 | 28 | 26 | 42 | | 4 | | | | |
| BHEA-Pre6 | 21 | | 59 | | 14 | 6 | | | |
| BHEA-Pre7 | 15 | | 60 | | 18 | 7 | | | |
| BHEA-Pre8 | 12 | | 59 | | 22 | 7 | | | |
| BHEA-Pre9 | 5 | | 58 | | 22 | 15 | | | |
| BHEA-Pre10 | | 40 | 44 | | 11 | 5 | | | |
| BHEA-Pre11 | | 15 | 50 | | 17 | 18 | | | |
| BHEA-Pre12 | | 12 | 55 | | 28 | 5 | | | |
| BHEA-Pre13 | | 6 | 59 | | 20 | 15 | | | |
| BHEA-Pre14 | | | 60 | 10 | 18 | 12 | | | |
| BHEA-Pre15 | | | 59 | 8 | 21 | 12 | | | |

These alloys were tested in a similar way to the alloys in Chapter 3. The ductility was tested using the rolling procedure. The rolling procedure was a repeat of the ductility test in Chapter 3. The alloys were cold rolled through a roll gap of 6mm followed by rolls with 1mm smaller roll gaps, and a final roll of 0.5mm. The alloys were judged by how and when they broke apart. If the alloy survived all the passes then it was deemed ductile. If the alloy broke on the first pass, with no plastic deformation, then it was deemed brittle. If the alloy broke somewhere in between then the alloy was deemed to be either mostly ductile or mostly brittle, with the distinction being whether the alloy survived the 3mm roll gap. The results are shown in Table 6.4.

Table 6.4: The ductility results for the BHEAs preliminary set of alloys.

| Alloy | Rolls Survived | Roll Test Result |
|---|---|---|
| BHEA-Pre1 | 0 | Brittle |
| BHEA-Pre2 | 0 | Brittle |
| BHEA-Pre3 | 0 | Brittle |
| BHEA-Pre4 | 4 | Mostly Ductile |
| BHEA-Pre5 | 4 | Mostly Ductile |
| BHEA-Pre6 | 0 | Brittle |
| BHEA-Pre7 | 0 | Brittle |
| BHEA-Pre8 | 0 | Brittle |
| BHEA-Pre9 | 0 | Brittle |
| BHEA-Pre10 | 2 | Mostly Brittle |
| BHEA-Pre11 | 0 | Brittle |
| BHEA-Pre12 | 0 | Brittle |
| BHEA-Pre13 | 0 | Brittle |
| BHEA-Pre14 | 0 | Brittle |
| BHEA-Pre15 | 0 | Brittle |

The results for the tin containing alloys were very poor and No tin containing alloys had properties good enough to be selected. The Sn-containing alloys were extremely brittle, often fracturing while handling the alloy before even getting to the rolling machine. The performance of the brazed joints were similarly poor. The joints could either be broken with minimal force or would not form at all. The alloys were also tested by using comparative melting with a torch and brazing an example joint.

The tin alloys were predicted to have very low melting points and the informal brazing testing did confirm this to be the case. The low melting temperature was still an extremely desirable property to have, and so several new tin and indium alloys were trialled. All of these alloys though were uniformly poor with the same problems as the alloys in the preliminary search. Based on these results it was decided to abandon In and Sn and to focus on the Ag-Cu-Zn range of alloys.

As many of these alloys in this preliminary study were brittle and clearly unsuitable for brazing there was no brazability testing carried out on these alloys. In the next section there are more alloys produced and they are more ductile and more likely to form brazing alloys. Brazability testing is carried out on that batch of alloys.

### 6.4.3 Main Results

After the modelling and preliminary results there were now only a few systems remaining from which to select alloys. These systems all contained Ag-Cu-Zn combined with one or more elements from Mn, Ni and Co. A larger trial was selected from these systems and the results were trialled in the same way as before. The compositions are listed in Table 6.5 in at.%. The wt.% of Ag is also shown in Table 6.5. This is useful for gauging the approximate cost of the prospective alloys and which existing brazing alloys have similar silver content.

Table 6.5: The compositions of the Brazing HEAs (BHEAs) main batch of alloys.

| | Element (at.%) | | | | | | Element (wt.%) |
|---|---|---|---|---|---|---|---|
| Alloy | Ag | Cu | Zn | Mn | Ni | Co | Ag |
| BHEA-1 | 37 | 14 | 45 | 4 | | | 49.6 |
| BHEA-2 | 35 | 24 | 37 | 4 | | | 47.6 |
| BHEA-3 | 35 | 14 | 47 | 4 | | | 47.5 |
| BHEA-4 | 34 | 14 | 48 | 4 | | | 46.4 |
| BHEA-5 | 33 | 13 | 49 | 5 | | | 45.5 |
| BHEA-6 | 30 | 14 | 52 | 4 | | | 41.8 |
| BHEA-7 | 28 | 26 | 42 | 4 | | | 39.5 |
| BHEA-8 | 35 | 13 | 48 | | 4 | | 47.3 |
| BHEA-9 | 28 | 17 | 51 | | 4 | | 39.4 |
| BHEA-10 | 28 | 17 | 51 | | | 4 | 39.4 |

Ductility measurements were carried out on these alloys in the same way as the preliminary alloys. The results of the ductility tests were far better and so the brazability tests were also carried out. The brazability test was conducted in the same way as was done previously in Chapter 3. This test was able to filter out obviously poor performing brazing alloys and leave only those that had the potential to be useful. The results of both tests are shown in Table 6.6.

Table 6.6: The ductility and brazability results for Brazing HEAs (BHEAs) main batch of alloys.

| Alloy | Roll Test Result | Brazability |
|---|---|---|
| BHEA-1 | Ductile | Excellent |
| BHEA-2 | Mostly Ductile | Average |
| BHEA-3 | Mostly Brittle | Average |
| BHEA-4 | Mostly Ductile | Good |
| BHEA-5 | Mostly Brittle | Average |
| BHEA-6 | Mostly Brittle | Good |
| BHEA-7 | Mostly Brittle | Average |
| BHEA-8 | Brittle | Average |
| BHEA-9 | Brittle | Poor |
| BHEA-10 | Brittle | Poor |

These results revealed that the alloys containing Ni and Co were too brittle to be used as brazing alloys. It has been mentioned before that brittle brazing alloys can be sold and can be produced via alternative production methods. However, this would require the alloy to have excellent brazing properties to justify the costly production methods and this was not the case for these alloys. The best two alloys from these results was BHEA-1 and BHEA-4, which were selected for further testing.

### DTA Measurements

As with the previous brazing alloy work DTA was used to analyse the alloys that had performed best in the ductility and brazability testing. The best performing alloys was BHEA-1 and the next best performing alloy was BHEA-4, these two were sent for DTA analysis. The silver content of these alloys mean that these alloys are most likely to be in competition with Ag155. The DTA scans of the two alloys are shown

in Appendix C.

The results showed that the melting range of BHEA-1 was 680°C-695°C and the melting range of BHEA-4 was 683°C-695°C. Comparing these melting ranges to similar existing brazing alloys (ISO 17672 Ag 155 and ISO 17672 Ag 145) show that these melting temperatures do not offer an improvement. The result is close though and still worth investigating further. The DTA also confirmed that BHEA-1 is superior to BHEA-4 (shown in the appendix) and so will be the focus of this investigation hence forth.

### 6.4.4 Alloy BHEA-1

Alloy BHEA-1 has a potential use as a rival to ISO 17672 Ag 155 (which has been referred to since Chapter 3 as just Ag155). The silver content of BHEA-1 offers a 5 wt.% reduction compared to Ag155, which would probably mean a noticeable saving in cost to the consumer. However, to justify the commercialisation of the alloy the performance will have to be close to Ag155 and noticeably superior than the lower Ag content alternative (ISO 17672 Ag 145).

The melting point of BHEA-1 is at the boundary for deciding whether to proceed with alloy development. If the melting point was any lower then the alloy would definitely be worth commercialising and if it was any higher then the alloy would clearly show a drop in performance and should be discarded. Of course ultimately the decision about the possibility of commercialising the alloy will not be part of this project.

In terms of ductility and brazing performance the alloy is again on the boundary of the decision process. For ductility and brazing performance the alloy is clearly the best of the alloys produced, but still not quite as good as Ag155.

The alloy does outperform Ag155 in a few ways though. The melting range is narrower than Ag155, so there is less risk of liquation. The brazed joint produced using BHEA-1 is stronger than the joint using Ag155. Although the Ag155 joint can

allow for more plastic deformation before failing.

An interesting aspect of BHEA-1 is that the method in which it achieves the relatively low melting temperature is different from Ag155. In the novel alloy the Ag-Cu ratio is moved away from the eutectic ratio. This increases the melting temperature but means that the HEA properties are improved and this allows for a much higher level of Zn to be included. The higher Zn content then reduces the melting point.

## 6.5 Investigating the Ag-Cu-Zn-Mn System

The best alloy from the broad search across systems was the BHEA-1 alloy from the Ag-Cu-Zn-Mn system. This section of research looked into the changes in performance within this system. This was in order to better understand the trends and transitions of the relevant brazing properties as well as attempting to find some potentially useful alloys.

Selecting alloys with different compositions within this system would be expected to significantly change the melting temperature and the ductility of the alloy, the two main properties of interest for novel brazing alloys. The changes to the melting temperatures of the novel alloys are fairly predictable, even if predicting the absolute melting points can be difficult to do accurately. Increasing the amounts of low melting point elements and moving elements towards eutectic compositions will reduce the melting point of the alloy, with the opposite actions increasing the melting point.

The changes in ductility though are less easy to predict. At some point moving away from the composition of the BHEA-1 alloy will cause different structures to form. However, there may be other changes that occur when altering the composition. The BCC structure of BHEA-1 may remain in some of the new alloys but with a different lattice parameter. It is possible that both the structure and lattice parameter remains the same but some other property causes the ductility of the alloy to change. Finding out the reason why the brittle alloys in this system are brittle may help to direct

future alloy searches.

Ten alloys were selected from the Ag-Cu-Zn-Mn range, nine novel alloys and a repeated melt of BHEA-1. The compositions were selected in order to have values above and below the composition in BHEA-1. The exception to this was manganese, which was already at 4 at.% and so no values below this were considered. The compositions, in both atomic percentage and weight percentage, are shown in Table 6.7.

Table 6.7: The compositions of the Ag-Cu-Zn-Mn (ACZM) batch of alloys.

| | Element (at.%) | | | | Element (wt.%) | | | |
|---|---|---|---|---|---|---|---|---|
| Alloy | Ag | Cu | Zn | Mn | Ag | Cu | Zn | Mn |
| BHEA-1 | 37 | 14 | 45 | 4 | 49.6 | 11.1 | 36.6 | 2.7 |
| ACZM-1 | 32 | 20 | 44 | 4 | 44.1 | 16.3 | 36.8 | 2.8 |
| ACZM-2 | 40 | 12 | 44 | 4 | 52.8 | 9.3 | 35.2 | 2.7 |
| ACZM-3 | 33 | 19 | 44 | 4 | 45.3 | 15.4 | 36.6 | 2.8 |
| ACZM-4 | 44 | 8 | 44 | 4 | 56.8 | 6.1 | 34.5 | 2.6 |
| ACZM-5 | 34 | 28 | 34 | 4 | 46.5 | 22.6 | 28.2 | 2.8 |
| ACZM-6 | 44 | 19 | 33 | 4 | 57.0 | 14.5 | 25.9 | 2.6 |
| ACZM-7 | 31 | 19 | 44 | 6 | 43.1 | 15.6 | 37.1 | 4.2 |
| ACZM-8 | 21 | 19 | 54 | 6 | 30.9 | 16.5 | 48.2 | 4.5 |
| ACZM-9 | 23 | 13 | 60 | 4 | 33.3 | 11.1 | 52.7 | 2.9 |

These alloys were tested in the same way as the other brazing alloys in this chapter. The results were mostly as expected. Alloys that had low levels of silver and high levels of zinc were generally brittle and the alloys that had the opposite were generally ductile. This was not always the case though, and some alloys were surprisingly brittle for the silver content in the alloy. The ductility results are shown in Table 6.8.

Table 6.8: The ductility and brazability results for Brazing HEAs (BHEAs) main batch of alloys.

| Alloy | Roll Test Result | Brazability |
|---|---|---|
| BHEA-1 | Ductile | Excellent |
| ACZM-1 | Mostly brittle | Excellent |
| ACZM-2 | Mostly brittle | Good |
| ACZM-3 | Mostly brittle | Good |
| ACZM-4 | Ductile | Poor |
| ACZM-5 | Mostly ductile | Good |
| ACZM-6 | Ductile | Poor |
| ACZM-7 | Mostly brittle | Excellent |
| ACZM-8 | Brittle | Excellent |
| ACZM-9 | Brittle | Excellent |

In terms of finding a superior brazing alloy, BHEA-1 was already more brittle than Ag155 and so it was decided that no alloy more brittle than BHEA-1 would be suitable. This meant only two of the alloys, ACZM-4 and ACZM-6, were left as potentially suitable alloys. Both of these alloys had high melting points in the brazability and melting tests. The alloys melted significantly above Ag155 and so were removed from consideration, leaving BHEA-1 still as the best alloy found in this trial.

The trends with the changes in composition were generally as expected. Alloys that were high in silver were generally ductile but had poor brazability scores due to high melting points. The alloys that were high in zinc had low melting values but tended to be brittle. The only real compromise selection was the original BHEA-1 that was found in the previous scan.

### 6.5.1 Phase Analysis

Part of this study was not just to find new alloys but to find the mechanisms by which the alloys within this system were ductile or brittle. Alloys were selected that had a variety of ductility performances. The original alloy, alloy BHEA-1, was found to have a single phase BCC structure. The XRD trace did not detect any other structure present. The XRD spectrum is shown in Fig. 6.4.

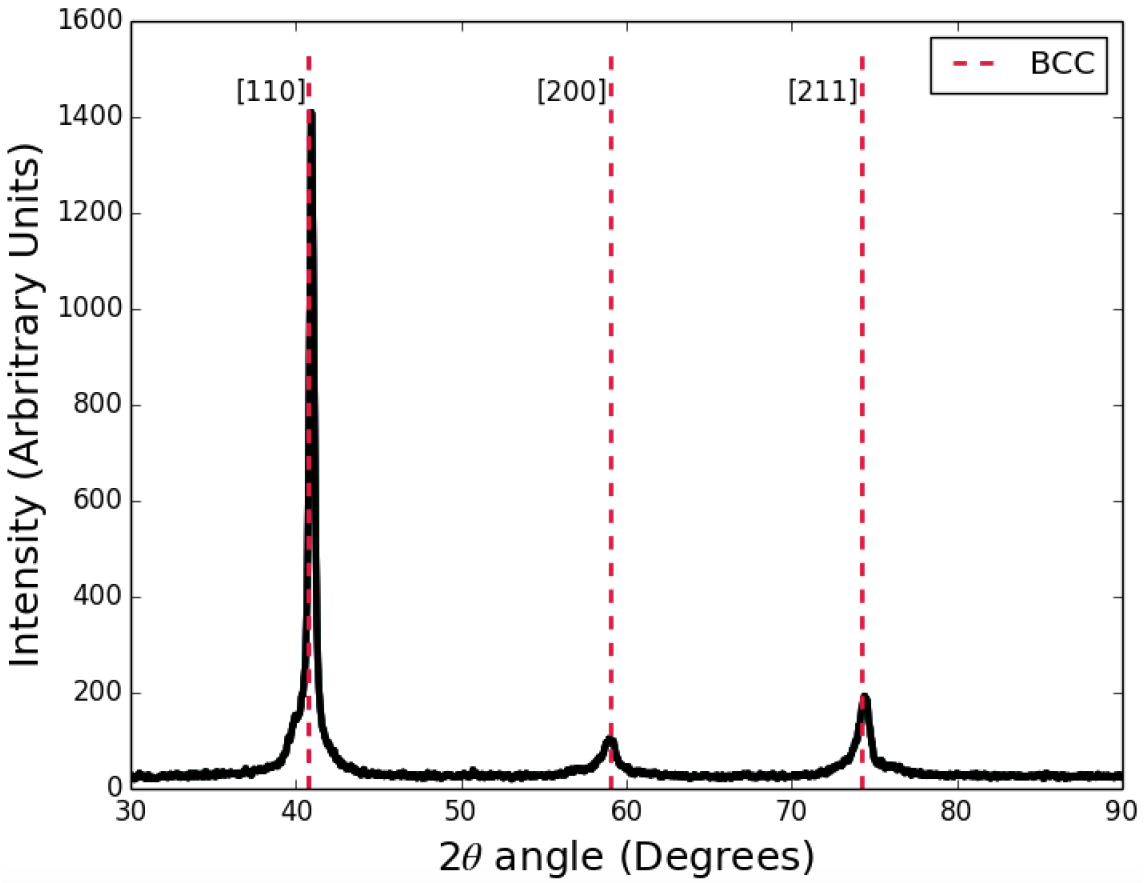


Figure 6.4: The XRD trace for BHEA-1. The single phase BCC peaks have been labelled. This BCC structure has a lattice parameter of 3.13Å.

The single phase nature of alloy BHEA-1 was also checked and confirmed using SEM. A micrograph showing the presence of just one phase is shown in Fig. 6.5.

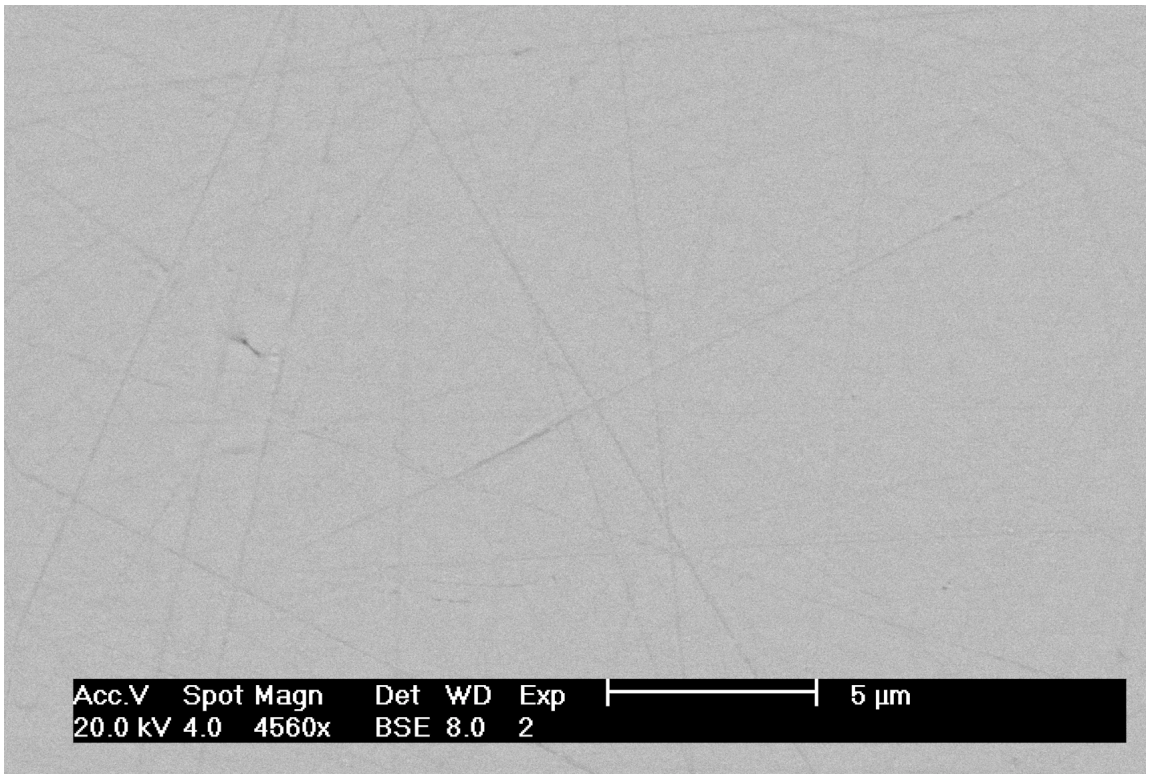


Figure 6.5: A backscattered electron micrograph of BHEA-1. The surface was featureless with no secondary phases detected for any of the settings on the microscope.

Alloy ACZM-9 was selected as an example of an alloy from Table 6.8 that was brittle. The XRD trace from the alloy is shown in Fig. 6.6.

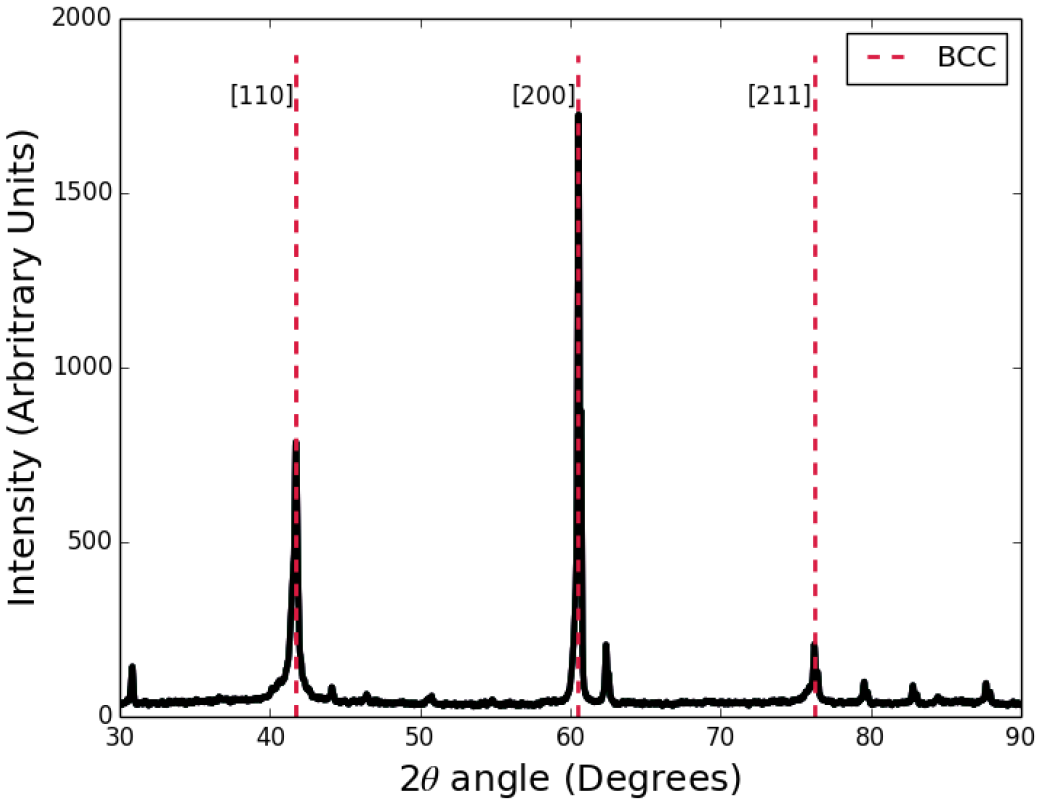


Figure 6.6: The XRD trace for ACZM-9. The most significant phase, with a BCC structure, has been labelled. This BCC structure has a lattice parameter of 3.06Å. There are clearly other phases present that could not be identified definitively.

The ACZM-9 alloy showed the presence of secondary phases through additional peaks compared to the single phase of BHEA-1. A likely second phase is a Zn-Mn IMC. The difficulty in identifying this phase is due to one of the peaks being masked by the [200] peak of the BCC. This does not rule out the existence of a Zn-Mn phase, but it cannot be detected in the SEM either due to size or as it has a similar average atomic mass and appearance as the primary phase. An SEM micrograph for ACZM-9 is shown in Fig. 6.7

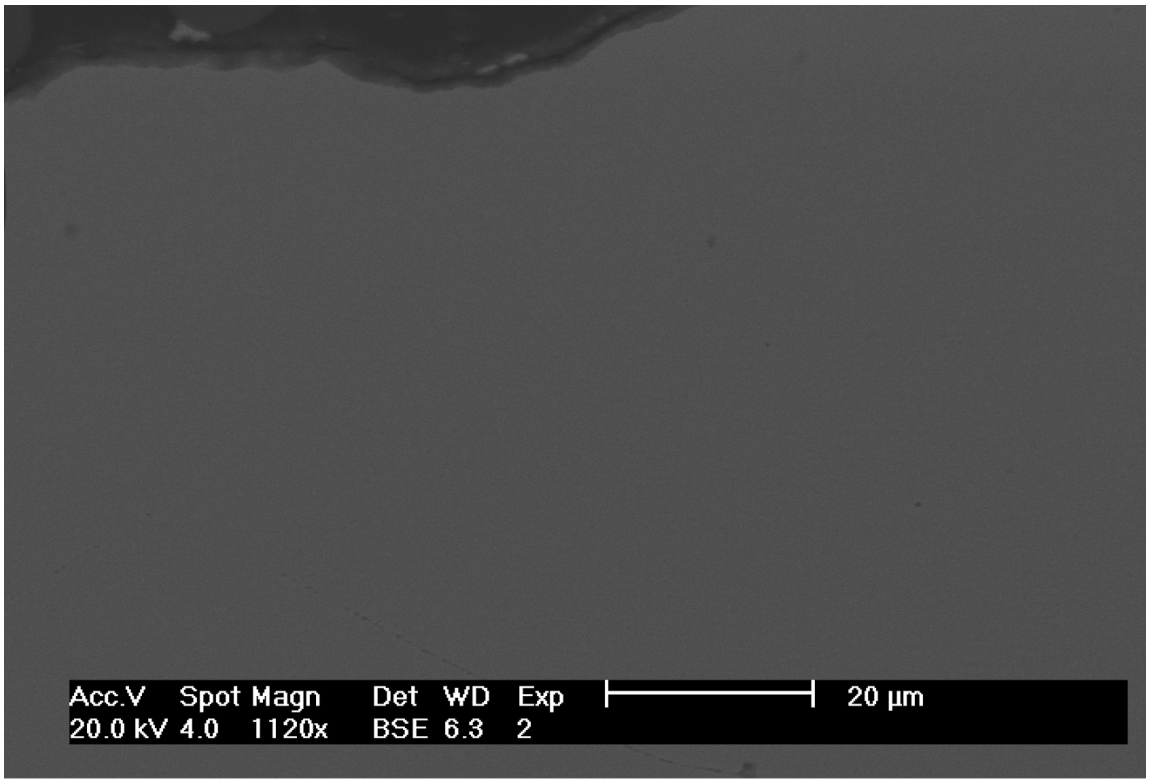


Figure 6.7: A backscattered electron micrograph of ACZM-9. Only phase is present and so to help focus an edge defect has been included at the top.

As an example of an alloy with good ductility ACZM-6 was selected. Although it could not be expressed in Table 6.8 the alloy was actually more ductile than BHEA-1. The XRD trace of ACZM-6 is shown in Fig. 6.8.

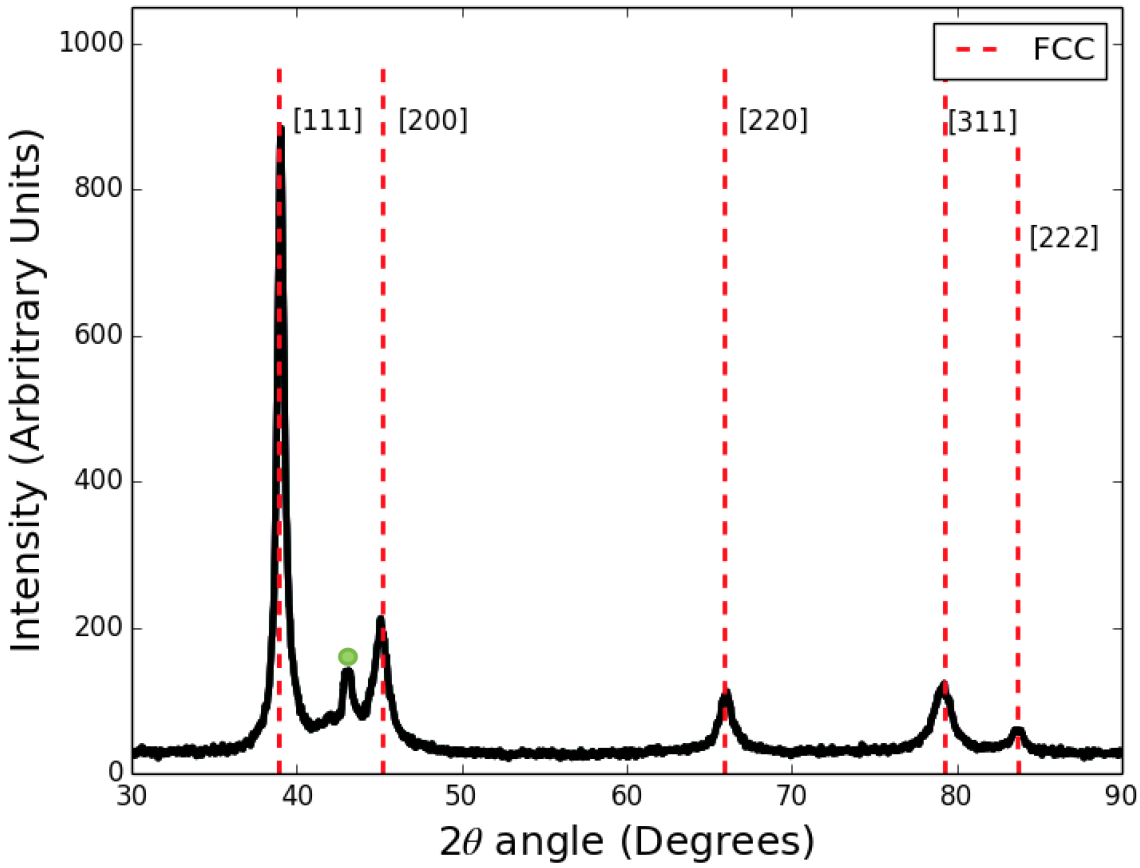


Figure 6.8: The XRD trace of ACZM-6. The structure is primarily a single-phase FCC. The lattice parameter of the FCC structure is 4.01Å. The peak marked with a green dot is likely attributed to pure manganese. A number of other peaks that appear for manganese are masked by the FCC peaks. There is potentially a slight peak around 80° that is part of the [311] peak.

The enhanced ductility of ACZM-6 is likely due to the FCC structure present, compared to the other alloys that are predominantly BCC. The secondary phase present was found to be most likely pure manganese. It was expected that the presence of a secondary manganese phase would embrittle the alloy. However, as the ductility results showed, this was not the case. The effects of an FCC structure meant that the ductility was enhanced. The two phase nature of ACZM-6 was investigated with SEM. A micrograph from the SEM analysis is shown in Fig. 6.9 and shows just the single FCC phase.

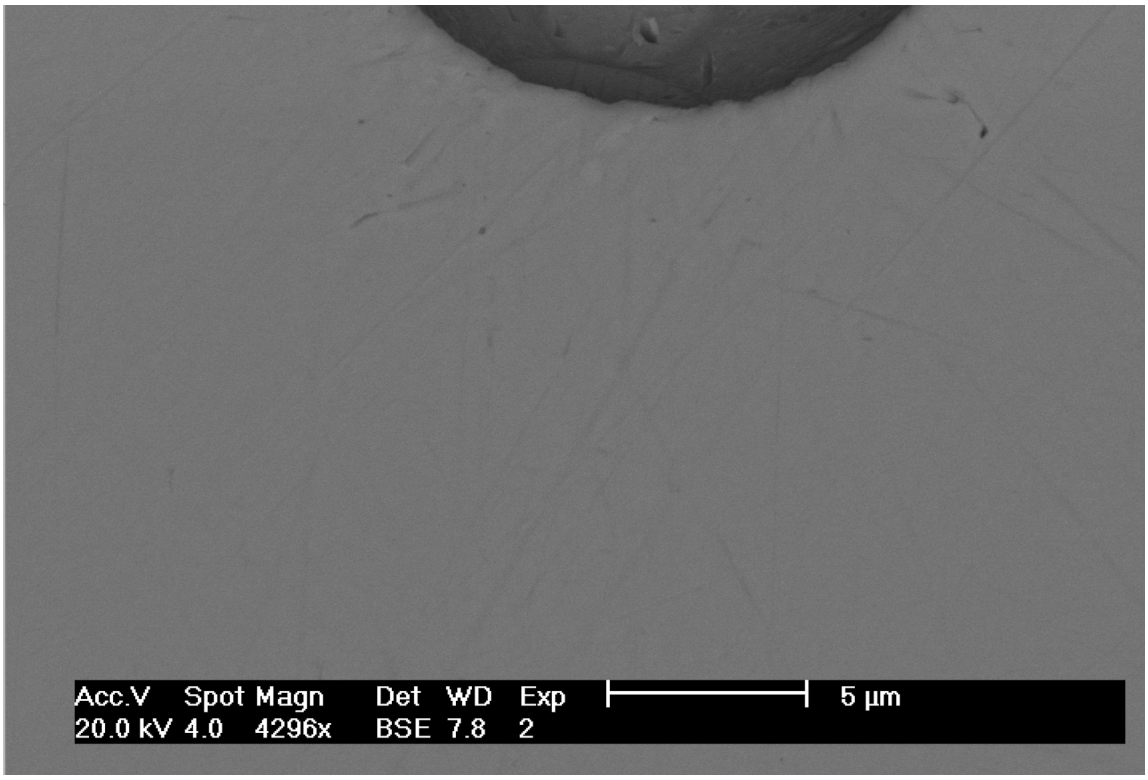


Figure 6.9: The backscattered electron SEM of ACZM-6. As there was no second phase to focus on, or to show contrast with, part of a hole on the surface has been included.

### Conclusions of the Ag-Cu-Zn-Mn System

The investigation of the Ag-Cu-Zn-Mn was brought about due to the success of the alloy BHEA-1. The overall performance of BHEA-1 was judged to be the best of all the alloys trialled across all the systems. The next best alloy, BHEA-4, was also from the Ag-Cu-Zn-Mn alloy system. A number of alloys were selected from this system with the aim of finding an improved an alloy and also investigating the effects of changing elements.

No alloy was found that improved on BHEA-1. The ductility and brazabilty scores of the other ACZM alloys were generally as expected, with improvements to one property only occurring with the detriment of the other. Phase analysis showed that BHEA-1 had a single phase BCC structure. The example brittle alloy, ACZM-9,

was found to have many IMCs present, likely contributing to the brittle performance. The example ductile alloy, ACZM-6, was actually more ductile than BHEA-1. This alloy was found to be primarily be FCC, which is likely the reason why it was the most ductile alloy trialled out of the ACZM range.

## 6.6 Small Element Addition

A common feature of brazing alloys is the addition of a small amount of a low melting element. This is done with the intention of improving the brazing properties, in particular the melting points and the flow properties. The amount of these elemental additions is usually limited to a few percent though, as large amounts of these elements are liable to make the alloys extremely brittle.

The most common small element addition is tin, as it has a low melting point, improves flow and is low cost. The modelled evidence for the improvement to flow was shown earlier as part of surface energy modelling. It was shown, at least in theory and according to the model, that a small amount of an element can have a significant effect on the surface energy.

Tin is the not the only small element addition though. Indium is used in a number of alloys for the same reasons as tin. One drawback to indium though is the high cost as it is a precious metal. Also included in this study is gallium, as a low melting element that might help to reduce the melting temperature.

Investigating the effects of small elements are important for two reasons. It is the final step for optimising the best alloys from the alloy search. The effects of small elements can not be easily modelled and so the only practical solution is to find the best alloys using the large-scale modelling method and then to investigate the effect of adding elements to those alloys.

The other reason small additions are worth investigating is to look into the effect these atoms might have on the HEA structure. The ability of these HEA-type alloys

to incorporate these extra inclusions may not be the same as the conventional brazing alloys. It may be the case that the HEA-type structure is less stable than the conventional alloys and so it is more easily corrupted by low levels of elements like tin and indium. This theory is investigated with a series of alloys that are produced followed by ductility testing and XRD analyses.

### 6.6.1 Ductility Measurements

Melts were planned to have a variety of concentrations with the three elements mentioned; Sn, In and Ga. The base alloy that these elements were added to was BHEA-1 from the Ag-Cu-Zn-Mn system and has been the best overall alloy so far. The concentrations for the small additions were 0.5wt.%, 1wt.% and 2wt.% for each element, with an extra measurement of 3wt.% for Sn. The details of the alloys trialled are shown in Table 6.9.

Table 6.9: The compositions of the small addition to BHEA-1 batch of alloys.

| | Element (wt.%) | | | |
|---|---|---|---|---|
| Alloy | BHEA-1 | Sn | In | Ga |
| 0.5Sn | 99.5 | 0.5 | | |
| 1Sn | 99 | 1 | | |
| 2Sn | 98 | 2 | | |
| 3Sn | 97 | 3 | | |
| 0.5In | 99.5 | | 0.5 | |
| 1In | 99 | | 1 | |
| 2In | 98 | | 2 | |
| 0.5Ga | 99.5 | | | 0.5 |
| 1Ga | 99 | | | 1 |
| 2Ga | 98 | | | 2 |

The ductility measurements were again carried out using the rolling test that has been used on the other brazing alloys in this chapter. The results are shown in Table 6.10. This trial was primarily concerned with the effects on the ductility of the alloy. Brazability tests would have been carried out if the ductility tests had shown any alloys that had a suitable ductility.

Table 6.10: The ductility results for the small addition to BHEA-1 batch of alloys.

| Alloy | Roll Test Result |
|---|---|
| 0.5Sn | Mostly ductile |
| 1Sn | Mostly brittle |
| 2Sn | Brittle |
| 3Sn | Brittle |
| 0.5In | Mostly ductile |
| 1In | Mostly brittle |
| 2In | Brittle |
| 0.5Ga | Mostly brittle |
| 1Ga | Mostly brittle |
| 2Ga | Mostly brittle |

The ductility results for the brazing alloys were generally as expected. The differences in ductility between alloys was not as obvious as it has been in previous trials. This made comparisons between alloys a bit more difficult to judge. Even so, the trends that were expected were definitely present. All the small alloy additions were more brittle than the base alloy. Also, for each element the more that was added the more brittle the alloy became.

### 6.6.2 XRD analysis

There were three competing theories as to why the addition of these elements consistently made the base brazing alloy less ductile. Firstly, the extra elements could be causing the formation of IMCs. Secondly, the additional elements may be changing the lattice parameter of the BHEA-1 structure, causing it to be more strained and brittle. The final option is that the HEA structure is presevered, as is the lattice parameter, but the change in elements may have had an effect that can not be detected via XRD. There could be related to the slip planes, local energies, bulk modulus or one of many other potential reasons that could effect the movement of dislocations in the alloy.

XRD analysis of these alloys was not done in ideal circumstances. The casting of the alloys often produced alloys that were in difficult shapes for XRD analysis. Flat and suitable surfaces could be prepared and measurements could be taken successfully, however, most of the alloys were in a long, thin shape which meant that the alloy could not be rotated during analysis. This could then have an effect on the relative intensities of peaks depending on the orientation of the grains.

#### The Effect of Tin

The XRD trace of the tin containing alloys showed two trends. The alloys containing a small amount of tin showed almost no change in the peak locations. The structures were all single phase with the lattice parameter remaining the same. The XRD traces of BHEA-1 and the low tin alloys (0.5 wt.% and 1 wt.% Sn) are shown in Fig. 6.10.

The results in Fig. 6.10 show that for low levels of tin there is relatively little effect on the structure. The structure labelled on all three traces is a BCC with a lattice parameter of 3.12Å. In all three traces there are no additional phases visible. The higher tin content alloys, (2 wt.% and 3 wt.% Sn), are shown with BHEA-1 in Fig. 6.11.

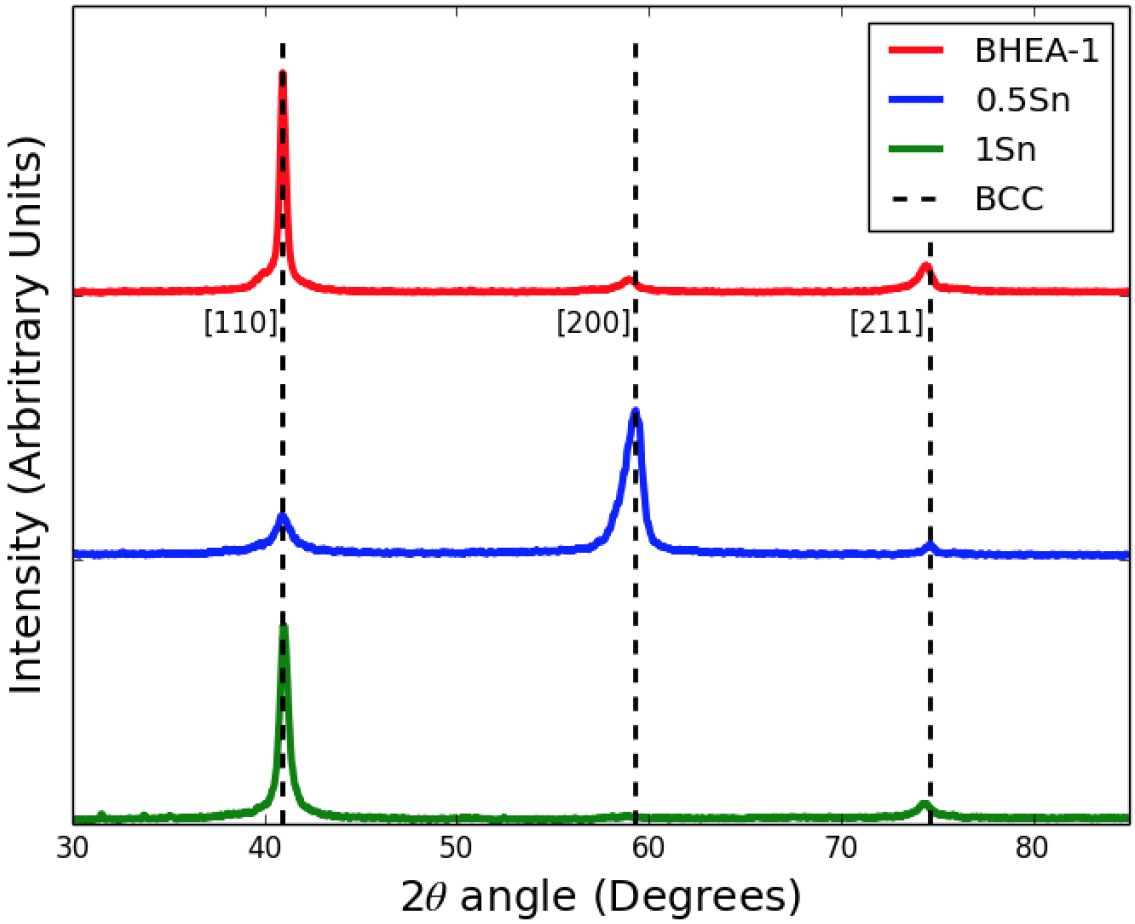


Figure 6.10: The XRD traces of BHEA-1, 0.5Sn and 1Sn. A BCC lattice has a lattice parameter of 3.12Å.

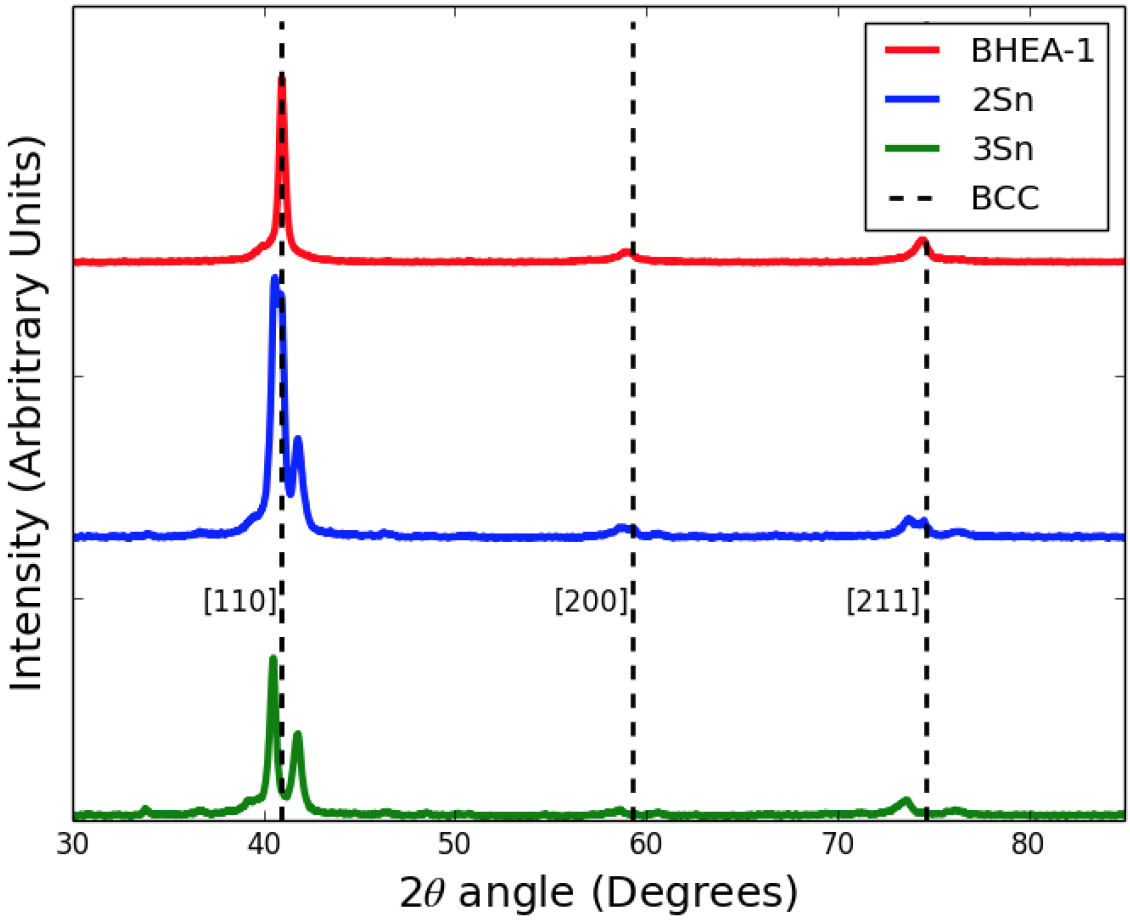


Figure 6.11: The XRD traces of BHEA-1 2Sn and 3Sn. The BCC lattice shown has a lattice parameter of 3.12Å.

The high tin content alloys showed significant changes to the lattice. In Fig. 6.11 the peaks no longer align and there is second phase present. The second phase is likely due to a Zn-Mn IMC, although it is difficult to confirm this without the observation of additional peaks. In order to analyse more closely the changes to the alloys the scans are shown again in Fig. 6.12 but focussed around the peaks at 40°.

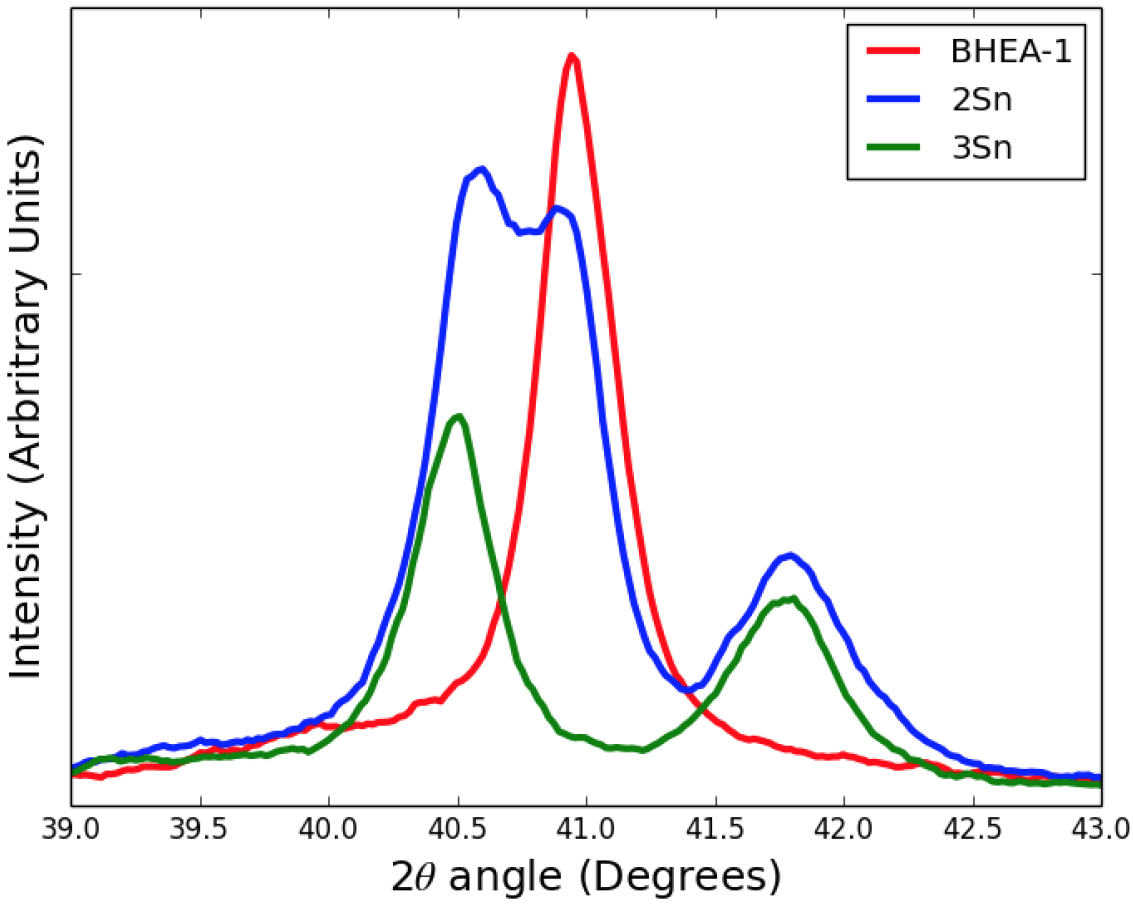


Figure 6.12: The XRD traces of BHEA-1 2Sn and 3Sn. The scan is focussed on the peaks around 40°.

The results in Fig. 6.12 show that the changes with the high levels of tin. The 2Sn alloy shows three phases have formed, with two BCC phases (one with a similar lattice parameter as the BCC phase from BHEA-1) and a Zn-Mn IMC. The two largest peaks represent two similarly sized BCC structures. This pattern of double peaks is found for the [200] peak and the [211] peak at the higher angles that are small but visible in Fig. 6.11.

The 3Sn alloy shows only one BCC phase present but with the same Zn-Mn IMC present as 2Sn. This BCC has a larger lattice parameter than BHEA-1. The two BCC phases in 2Sn are approximately the same as the BCC in BHEA-1 and the BCC in 3Sn. The multiphase nature of alloy 2Sn was verified with SEM. A micrograph for

alloy 2Sn is shown in Fig. 6.13.

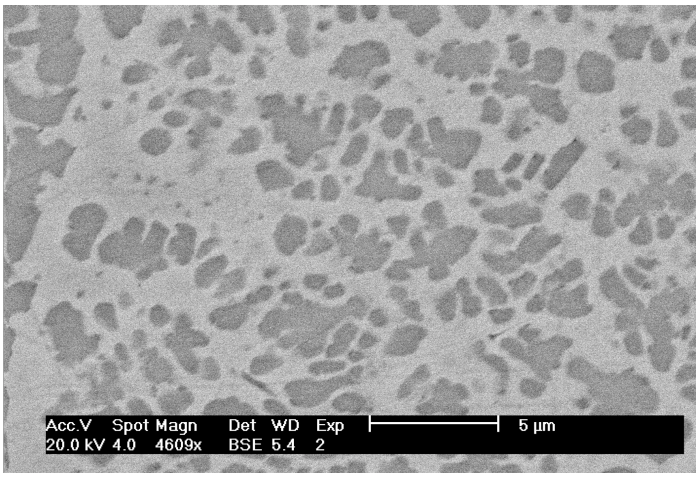


Figure 6.13: The backscattered electron SEM of 2Sn. Two phases are shown, that relate to the BCC phases of 2Sn.

The SEM analysis, with EDX, showed clearly the 2 BCC phases. One of these phases (the darker phase) contained all the tin in the alloy. The other BCC phase, (the lighter phase) contained almost no tin. As with other SEM images in this chapter directly detecting the Zn-Mn phase was difficult due to the similarity in appearance with the BCC phase.

The ductility results of the tin-containing alloys showed that all the alloys were more brittle than the BHEA-1 with no tin. The high tin alloys were likely very brittle due to the formation of an IMC. The low tin alloys were more brittle than BHEA-1 but not as brittle as the high tin alloys. This embrittling for the low tin alloys was likely due to unseen effects on the material properties. The lattice parameter does change slightly, but a more likely reason is that tin has altered some other material property.

### The Effect of Indium

The XRD analysis of the indium alloys showed relatively little change between the alloys. The single phase structure of BHEA-1 remained throughout, with no additional

phases forming. The XRD traces of these alloys can be seen in Fig. 6.14.

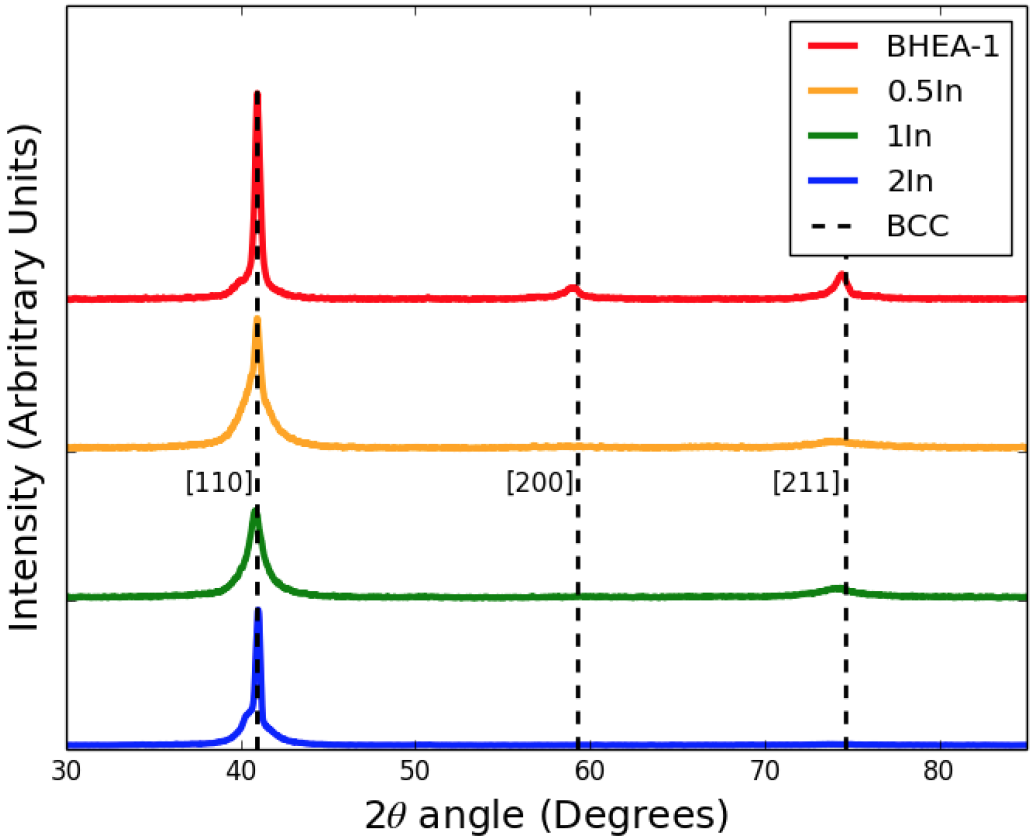


Figure 6.14: The XRD traces of BHEA-1, 0.5In, 1In and 2In. Some of the later peaks ([200] and [211] were low intensity but could be found upon closer inspection.

The results in Fig. 6.14 show that the phase structure remains fairly constant with increasing indium content. No second phase forms in any plot and there are only slight changes in the lattice parameter. Repeat measurements were carried out to confirm that indium was present in the right quantities and this was confirmed.

### The Effect of Gallium

The results of the gallium were similar to the tin XRD traces. The XRD traces of the gallium alloys are shown in Fig. 6.15.

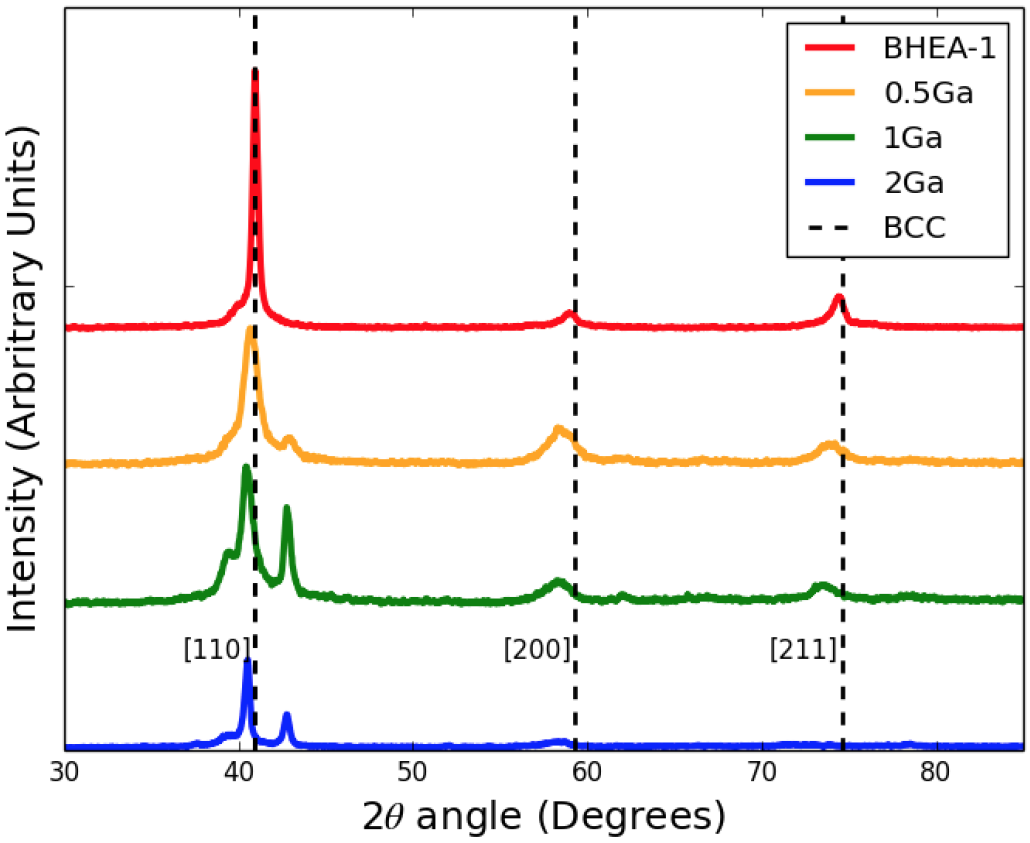


Figure 6.15: The XRD traces of BHEA-1, 0.5Ga, 1Ga and 2Ga. The BCC line is the line from BHEA-1 that is shown in FIg. 6.14. The line shows that the peaks of the gallium alloys have moved off this angle.

The changes in the alloy phases are very similar to the tin changes shown previously. For all the Gallium alloys a secondary phase forms, likely the Zn-Mn IMC. The same trend with the BCC phases is also evident with gallium. The moving peak in Fig. 6.15 shows that increased gallium changes the lattice parameter. The 1Ga alloy shows two BCC phases just like the 2Sn alloy that was analysed previously.

### Small Element Addition Conclusion

The small element additions to BHEA-1 were unsuccessful at improving the alloy. As BHEA-1 was already more brittle than Ag155, no amount of embrittling would be acceptable in any new alloy. All of the small element addition alloys failed due to

this reason.

The trends were generally as expected, with increasing amounts of the additional elements causing the alloy to become even more brittle. The mechanisms by which the alloys became more brittle did vary between alloys. There were examples of changes to the lattice parameter of BHEA-1, the formation of secondary phases and there were some examples where there was no discernible difference between the XRD traces. The alloys that appeared to have the same XRD traces are likely to be brittle due to some changes to way dislocations can move within the alloy, such as the local energies or altering slip behaviour.

## 6.7 Conclusion

This chapter set about using the large-scale modelling method that had been developed and applying it to brazing alloys. The focus was primarily on silver brazing alloys, with a view to achieving brazing alloys with lower melting points or lower silver contents. The intended route to achieving this was by allowing large amounts of low melting point and low cost elements into the alloy, while maintaining a ductile, HEA-type, structure.

A preliminary selection of alloys were made from a number of different alloy systems. The majority of these were found to be extremely brittle and unusable as brazing alloys. The preliminary results showed that the best alloys were based on the Ag-Cu-Zn ternary system with the addition of one or two elements. From the Ag-Cu-Zn alloys that were made the best alloy was BHEA-1 from the Ag-Cu-Zn-Mn alloy system. BHEA-1 offered a 5 wt.% Ag reduction compared to Ag155 but there was a decline in the performance. The Ag-Cu-Zn-Mn alloy system was explored further with the BHEA-1 alloy remaining as the best overall performing alloy.

Lastly, the BHEA-1 alloy had the addition of small amounts of extra elements. The elements (Sn, In and Ga) all embrittled the alloy and so were not suitable as

brazing alloys. The phase analysis of the results showed that there were a variety of reasons for this embrittling. The formation of secondary phases (often IMCs) and changes to the lattice parameter were the most common reason. Ultimately BHEA-1 was the best alloy that was produced using this method and, if any, the alloy most likely to have a commercial application.

# Chapter 7

# Conclusion

The overall aim of this research was to develop new silver brazing alloys with improved properties. Chapter 3 dealt with a conventional, thermodynamic approach to finding new brazing alloys. The approach used CALPHAD modelling to predict the melting temperatures of prospective alloys. The other key property for new brazing alloys was the ductility. This was modelled using the IMC as an equivalent measurement.

Using the modelled results a number of alloys were produced and tested. The new alloys were designed as a replacement for Ag155, one of the most popular brazing alloys in current use. Most of the alloys had at least one flaw that meant they were unsuitable as brazing alloys. The majority of the alloys were brittle and a number were also very high melting point. The best two alloys from the trial had similar properties to Ag155 but only offered very small savings in silver content.

Based on the results of the trial, and other modelled results, it was apparent that this CALPHAD method could not offer significant improvements to brazing alloys. The only alloys that were feasible as brazing alloys were found at compositions close to the alloys they were designed to replace. The limitations of this method meant that an alternative method, in this case a HEA modelling method, was selected as the focus for finding new brazing alloys.

The HEA modelling in this section was based around the parameters $\delta$ and $\Delta H_{mix}$.

There are a number of publications that use this approach and a variety of different limits that are used as the criteria for HEA formation. The limits that were used in this method were the ones set out by Zhang et al. [46].

The next step of the HEA modelling was to apply the rules on a large scale. The idea for this method was to model an extremely wide range of alloys, then to use the computer program to filter out unsuitable compositions and to hone in on the best compositions. The judgement of what alloys are the best is made on the HEA formation and any other parameter that might be desired within a trial.

The first application of this large-scale HEA formation modelling was attempting to create HEAs with a large amount of silver. There are already some published HEAs that contain silver, but they are not common and they tend to contain only a small amount of silver. The result of the alloy search was successful, with 13 silver HEAs produced, analysed and verified as HEA.

The second application looked to advance the work on silver HEAs. All the silver HEAs that were produced previously had two phases, this application looked to find silver HEAs that were single phase. This was done using the single phase modelling technique developed by Troparevsky et al. [80]. However, the modelled results showed that silver HEAs were extremely unlikely with most elements having values that prevented single phase formation.

The single phase modelling was used successfully though in a different application. The next version of the modelling code was not focussed on any particular element but instead attempted to design alloys that had a high number of elements (six or seven) that formed into a single phase. The alloy search for high order single phase HEAs (HOSP-HEAs) was more successful with two HOSP-HEAs produced and experimentally verified. The biggest problem in this work was with the production method. The alloys were high melting, difficult to melt properly and often had unmelted elements in the alloy.

The final application of the large scale modelling method was to use it on silver

brazing alloys. This was done on a wide variety of compositions from a number of different systems. A single alloy, BHEA-1 from the Ag-Cu-Zn-Mn alloy system, was found to be the best overall alloy from the alloy search. This alloy had 5 wt.% less silver and slightly poorer performance than Ag155. The performance though is probably just not good enough to be commercialised.

As part of the HEA-type brazing alloy search approach two extra trials were investigated. A number of alloys were measured all from the same system Ag-Cu-Zn-Mn, but none improved on BHEA-1. The effect of adding small amounts of elements was also analysed. These additions caused the alloys to become more brittle and so were unsuitable as brazing alloys.

Overall this demonstrates that while alternative compositions effective as brazing materials are possible, Ag155 is already a well-optimised brazing alloy of its type.

# Chapter 8

# Future Work

There is a wide variety of future research that could be carried out based on the work that has been conducted so far. Some of this future research is directly related to the work already carried out, with changes to elements or technique allowing for more alloys to be found. Other possible developments include other applications of the large-scale modelling method. There are many unused elements and unexplored alloy applications that could form the basis for a novel alloy search.

Chapter 3, the thermodynamic modelling approach to finding new brazing alloys, focussed on potential improvements to Ag155. Revisiting this alloy search would probably not yield any alloys that were better than the ones already produced. The modelled and experimental results in this chapter all indicated that this method would struggle to find alloys with superior properties. Nevertheless, future work could take a different brazing alloy as a base and attempt to find an improved composition.

Chapter 4, the large-scale modelling approach to finding silver HEAs, was largely successful with a number of alloys meeting the requirements set out. One possible extension from this work was to look at finding a single phase silver HEA, but this has already been explored as part of Chapter 5. While silver was selected as the focus of this chapter, due to its use in brazing alloys, there is no reason that this technique cannot be used for other elements with particular technological interest,

e.g. magnetic materials.

The second part of Chapter 5 was successful as two HOSP-HEAs were found. Extending the model to cover eight or more component alloys may also be possible. The prospects of these alloys would be helped by including the high cost elements that were excluded in the trial. Elements like Ir and Os have very good single phase values and could be a very useful alloying element.

Chapter 6, on HEA-type brazing alloys, already featured a wide array of alloy systems and compositions, with most having poor brazing properties. The wide array of different brazing alloys mean that there will always be a different system or set of elements to use in this method. For example palladium or gold brazing could form the basis of an alloy search. Alternatively there are many niche applications of brazing alloys that could also form the basis of an alloy search.

# Appendix A

# Miedema Enthalpy Table

The Miedema enthalpy table used in Takeuchi et al. had too many elements to be printed in a rectangular table with 73 columns and rows. To save space the repeated measurements are not included, which halves the amount of space required. Next, the triangle is broken up into three sections so that it can be displayed easily in two rectangular tables. The two tables are shown in Fig. A.1 and Fig. B.1.

For a pair of elements, if one element is from the first half of the list and the other element is from the second half then Fig. A.1 is used. If both the elements are from the first half or both the elements are from the second half then Fig. B.1 is used. Fig. B.1 is essentially two tables fitted into one table with a dividing line along the diagonal.

| (a) \ (b) | 1 H | 3 Li | 4 Be | 5 B | 6 C | 7 N | 11 Na | 12 Mg | 13 Al | 14 Si | 15 P | 19 K | 20 Ca | 21 Sc | 22 Ti | 23 V | 24 Cr | 25 Mn | 26 Fe | 27 Co | 28 Ni | 29 Cu | 30 Zn | 31 Ga | 32 Ge | 33 As | 37 Rb | 38 Sr | 39 Y | 40 Zr | 41 Nb | 42 Mo | 43 Tc | 44 Ru | 45 Rh | 46 Pd | (b) \ (a) |
|---|---|---|---|---|---|---|---|---|---|---|---|---|---|---|---|---|---|---|---|---|---|---|---|---|---|---|---|---|---|---|---|---|---|---|---|---|---|
| 46 Pd | -27 | -40 | -8 | -24 | -32 | -62 | -15 | -40 | -46 | -55 | -36.5 | -9 | -63 | -86 | -65 | -35 | -15 | -23 | -4 | -1 | 0 | -14 | -33 | -42 | -43.5 | -36 | -9 | -61 | -84 | -91 | -53 | -15 | -4 | 6 | 2 | Pd | 46 |
| 47 Ag | -10 | -16 | 6 | 5 | -32 | -94 | 0 | -10 | -4 | -20 | -18.5 | 7 | -28 | -28 | -2 | 17 | 27 | 13 | 28 | 19 | 15 | 2 | -4 | -5 | -17.5 | -8 | 7 | -27 | -29 | -20 | 16 | 37 | 24 | 23 | 10 | -7 | Ag 47 |
| 48 Cd | -6 | -13 | 11 | 13 | -27 | -91 | -3 | -6 | 3 | -13 | -11.5 | 1 | -32 | -30 | -8 | 9 | 17 | 2 | 17 | 6 | 2 | 6 | 1 | 1 | -14.5 | -4 | 1 | -33 | -35 | -26 | 11 | 28 | 10 | 9 | -6 | -26 | Cd 48 |
| 49 In | -6 | -12 | 16 | 18 | -27 | -98 | -5 | -4 | 7 | -10 | -10.5 | -4 | -35 | -30 | -5 | 12 | 20 | 3 | 19 | 7 | 2 | 10 | 3 | 3 | -13.5 | -3 | -4 | -37 | -36 | -25 | 15 | 33 | 11 | 10 | -8 | -31 | In 49 |
| 50 Sn | -4 | -18 | 15 | 18 | -23 | -90 | -8 | -9 | 4 | -11 | -7.5 | -7 | -45 | -45 | -21 | -1 | 10 | -7 | 11 | 0 | -4 | 7 | 1 | 1 | -12.5 | -1 | -7 | -46 | -51 | -43 | -1 | 20 | 5 | 4 | -13 | -34 | Sn 50 |
| 51 Sb | -1 | -28 | 18 | 23 | -13 | -74 | -20 | -16 | 2 | -8 | 2.5 | -22 | -62 | -61 | -33 | -8 | 7 | -11 | 10 | 2 | -1 | 7 | -1 | -1 | -10.5 | 3 | -24 | -66 | -68 | -60 | -11 | 17 | 8 | 9 | -8 | -28 | Sb 51 |
| 55 Cs | -16 | 16 | 29 | 29 | -43 | -155 | 3 | 25 | 26 | -3 | -24.5 | 0 | 19 | 70 | 104 | 103 | 97 | 71 | 85 | 58 | 48 | 28 | 15 | 14 | -19.5 | -12 | 0 | 14 | 62 | 101 | 135 | 128 | 69 | 64 | 34 | -9 | Cs 55 |
| 56 Ba | -49 | 0 | -10 | -19 | -90 | -212 | -3 | -4 | -20 | -52 | -85.5 | 6 | 1 | 28 | 57 | 57 | 50 | 29 | 37 | 11 | 0 | -9 | -23 | -30 | -63.5 | -66 | 9 | 0 | 20 | 52 | 81 | 73 | 11 | 6 | -21 | -62 | Ba 56 |
| 57 La | -60 | 6 | -29 | -47 | -116 | -235 | 24 | -7 | -38 | -73 | -112.5 | 46 | 8 | 2 | 20 | 22 | 17 | 3 | 5 | -17 | -27 | -21 | -31 | -41 | -73.5 | -81 | 52 | 14 | 0 | 13 | 36 | 31 | -23 | -28 | -50 | -82 | La 57 |
| 58 Ce | -61 | 7 | -30 | -48 | -116 | -234 | 25 | -7 | -38 | -73 | -112.5 | 47 | 9 | 2 | 18 | 20 | 15 | 1 | 3 | -18 | -28 | -21 | -31 | -41 | -73.5 | -81 | 53 | 15 | 0 | 12 | 34 | 29 | -25 | -30 | -52 | -83 | Ce 58 |
| 59 Pr | -61 | 7 | -31 | -49 | -117 | -233 | 26 | -6 | -38 | -73 | -112.5 | 49 | 10 | 1 | 17 | 18 | 13 | 0 | 1 | -20 | -30 | -22 | -31 | -41 | -72.5 | -81 | 55 | 16 | 0 | 10 | 32 | 26 | -27 | -32 | -53 | -83 | Pr 59 |
| 60 Nd | -61 | 7 | -31 | -49 | -116 | -235 | 26 | -6 | -38 | -73 | -112.5 | 49 | 10 | 2 | 17 | 18 | 13 | 0 | 1 | -20 | -30 | -22 | -31 | -40 | -101.5 | -80 | 55 | 16 | 0 | 10 | 32 | 26 | -27 | -32 | -53 | -83 | Nd 60 |
| 61 Pm | -61 | 8 | -33 | -51 | -118 | -233 | 28 | -6 | -39 | -74 | -114.5 | 51 | 11 | 1 | 15 | 16 | 10 | -2 | -2 | -23 | -32 | -23 | -32 | -41 | -73.5 | -81 | 57 | 18 | 0 | 9 | 30 | 24 | -29 | -34 | -54 | -84 | Pm 61 |
| 62 Sm | -61 | 8 | -32 | -50 | -117 | -202 | 28 | -6 | -38 | -74 | -113.5 | 50 | 11 | 1 | 15 | 17 | 11 | -1 | -1 | -22 | -31 | -22 | -32 | -40 | -72.5 | -80 | 56 | 17 | 0 | 9 | 30 | 24 | -30 | -35 | -54 | -84 | Sm 62 |
| 63 Eu | -45 | -1 | -12 | -19 | -87 | -231 | 0 | -5 | -19 | -49 | -79.5 | 10 | 0 | 21 | 48 | 49 | 43 | 23 | 30 | 7 | -3 | -10 | -21 | -27 | -58.5 | -60 | 13 | 0 | 14 | 42 | 69 | 63 | 6 | 2 | -24 | -61 | Eu 63 |
| 64 Gd | -61 | 8 | -32 | -50 | -117 | -232 | 28 | -6 | -39 | -73 | -113.5 | 50 | 11 | 1 | 15 | 17 | 11 | -1 | -1 | -22 | -31 | -22 | -31 | -40 | -72.5 | -80 | 56 | 17 | 0 | 9 | 30 | 24 | -29 | -34 | -54 | -84 | Gd 64 |
| 65 Tb | -61 | 9 | -33 | -51 | -118 | -232 | 29 | -6 | -39 | -74 | -113.5 | 52 | 12 | 1 | 14 | 15 | 9 | -3 | -3 | -23 | -32 | -23 | -31 | -40 | -72.5 | -80 | 58 | 18 | 0 | 8 | 28 | 22 | -30 | -35 | -55 | -85 | Tb 65 |
| 66 Dy | -61 | 9 | -32 | -51 | -117 | -231 | 29 | -6 | -38 | -74 | -112.5 | 51 | 12 | 1 | 14 | 15 | 9 | -3 | -3 | -23 | -32 | -22 | -31 | -40 | -71.5 | -80 | 58 | 18 | 0 | 8 | 27 | 22 | -30 | -35 | -55 | -84 | Dy 66 |
| 67 Ho | -60 | 8 | -32 | -50 | -116 | -229 | 28 | -6 | -38 | -73 | -111.5 | 51 | 11 | 1 | 14 | 16 | 10 | -2 | -2 | -22 | -31 | -22 | -30 | -39 | -71.5 | -79 | 57 | 18 | 0 | 9 | 28 | 22 | -29 | -34 | -54 | -83 | Ho 67 |
| 68 Er | -61 | 9 | -33 | -52 | -118 | -230 | 30 | -5 | -38 | -74 | -113.5 | 53 | 13 | 0 | 13 | 14 | 8 | -4 | -5 | -24 | -34 | -23 | -31 | -40 | -71.5 | -79 | 59 | 20 | 0 | 7 | 26 | 20 | -32 | -37 | -57 | -85 | Er 68 |
| 69 Tm | -61 | 9 | -33 | -52 | -117 | -229 | 30 | -5 | -38 | -74 | -112.5 | 52 | 13 | 0 | 12 | 13 | 8 | -4 | -5 | -24 | -34 | -23 | -30 | -39 | -71.5 | -79 | 59 | 20 | 0 | 7 | 25 | 19 | -32 | -37 | -56 | -85 | Tm 69 |
| 70 Yb | -45 | -1 | -14 | -22 | -88 | -199 | 2 | -6 | -20 | -51 | -80.5 | 12 | 0 | 16 | 41 | 43 | 37 | 19 | 25 | 2 | -7 | -12 | -21 | -27 | -58.5 | -59 | 16 | 1 | 10 | 36 | 61 | 55 | 1 | -4 | -28 | -62 | Yb 70 |
| 71 Lu | -61 | 10 | -35 | -54 | -119 | -231 | 31 | -5 | -39 | -75 | -114.5 | 55 | 14 | 0 | 11 | 11 | 5 | -6 | -7 | -27 | -36 | -24 | -31 | -40 | -71.5 | -80 | 61 | 21 | 0 | 6 | 23 | 17 | -35 | -40 | -59 | -87 | Lu 71 |
| 72 Hf | -63 | 30 | -37 | -54 | -101 | -173 | 89 | 30 | -19 | -56 | -89.5 | 119 | 60 | 16 | 1 | -1 | -7 | -4 | -15 | -24 | -29 | 2 | -3 | -10 | -37.5 | -45 | 125 | 73 | 27 | 3 | 0 | -5 | -35 | -39 | -45 | -52 | Hf 72 |
| 73 Ta | -46 | 48 | -24 | -54 | -101 | -173 | 89 | 30 | -19 | -56 | -89.5 | 119 | 60 | 16 | 1 | -1 | -7 | -4 | -15 | -24 | -29 | 2 | -3 | -10 | -37.5 | -45 | 125 | 73 | 27 | 3 | 0 | -5 | -35 | -39 | -45 | -52 | Ta 73 |
| 74 W | -24 | 50 | -3 | -31 | -60 | -103 | 97 | 38 | -2 | -31 | -46.5 | 124 | 57 | 9 | -6 | -1 | 1 | 6 | 0 | -1 | -3 | 22 | 15 | 11 | -7.5 | -9 | 129 | 70 | 24 | -9 | -8 | 0 | -7 | -10 | -9 | -6 | W 74 |
| 75 Re | -18 | 29 | 0 | -25 | -42 | -72 | 73 | 21 | -9 | -31 | -32.5 | 95 | 28 | -17 | -25 | -13 | -4 | -1 | 0 | 2 | 2 | 18 | 8 | 3 | -7.5 | -6 | 98 | 39 | -4 | -35 | -26 | -7 | 0 | -1 | 1 | 6 | Re 75 |
| 76 Os | -19 | 11 | -2 | -24 | -35 | -60 | 52 | 5 | -18 | -36 | -29.5 | 70 | 4 | -39 | -41 | -23 | -11 | -9 | -4 | 0 | 1 | 10 | -1 | -7 | -14.5 | -11 | 72 | 13 | -28 | -55 | -76 | -14 | 0 | 0 | 2 | 8 | Os 76 |
| 77 Ir | -20 | -9 | -5 | -26 | -32 | -54 | 28 | -13 | -30 | -43 | -30.5 | 42 | -23 | -62 | -57 | -34 | -18 | -18 | -9 | -3 | -2 | 0 | -13 | -21 | -24.5 | -19 | 44 | -16 | -53 | -53 | -21 | -21 | -2 | -1 | 1 | 6 | Ir 77 |
| 78 Pt | -24 | -33 | -10 | -28 | -30 | -52 | -1 | -35 | -44 | -53 | -34.5 | 9 | -55 | -89 | -74 | -45 | -24 | -28 | -13 | -7 | -5 | -12 | -29 | -38 | -37.5 | -31 | 9 | -50 | -83 | -67 | -28 | -3 | -1 | -2 | 2 | Pt 78 |
| 79 Au | -8 | -37 | 0 | -2 | -20 | -58 | -14 | -32 | -22 | -30 | -13.5 | -9 | -60 | -74 | -47 | -19 | 0 | -11 | 8 | 7 | 7 | -9 | -16 | -19 | -21.5 | -11 | -10 | -59 | -74 | -74 | -32 | 3 | 14 | 15 | 7 | 0 | Au 79 |
| 80 Hg | -3 | -19 | 15 | 19 | -20 | -81 | -11 | -10 | 4 | -10 | -4.5 | -10 | -43 | -37 | -10 | 10 | 21 | 4 | 22 | 12 | 8 | 8 | 1 | 1 | -11.5 | 0 | -11 | -45 | -43 | -31 | 11 | 32 | 18 | 18 | 2 | -18 | Hg 80 |
| 81 Tl | -3 | -15 | 23 | 27 | -19 | -91 | -11 | -3 | 11 | -4 | -1.5 | -13 | -40 | -28 | 2 | 22 | 31 | 11 | 31 | 18 | 13 | 15 | 6 | 6 | -9.5 | 3 | -14 | -44 | -35 | -19 | 26 | 46 | 25 | 24 | 5 | -21 | Tl 81 |
| 82 Pb | -1 | -21 | 25 | 30 | -13 | -82 | -18 | -8 | 10 | -2 | 4.5 | -21 | -52 | -40 | -8 | 15 | 28 | 7 | 29 | 17 | 13 | 15 | 5 | 5 | -7.5 | 6 | -23 | -56 | -48 | -33 | 17 | 42 | 26 | 25 | 6 | -18 | Pb 82 |
| 83 Bi | 0 | -23 | 26 | 31 | -12 | -80 | -20 | -10 | 10 | -2 | 5.5 | -24 | -56 | -46 | -14 | 10 | 24 | 3 | 26 | 14 | 10 | 15 | 4 | 4 | -7.5 | 7 | -26 | -61 | -54 | -40 | 12 | 38 | 23 | 23 | 3 | -21 | Bi 83 |
| 90 Th | -61 | 14 | -37 | -57 | -123 | -237 | 39 | -3 | -40 | -77 | -119.5 | 65 | 19 | 0 | 8 | 9 | 2 | -8 | -11 | -30 | -39 | -24 | -30 | -39 | -72.5 | -82 | 72 | 27 | 1 | 4 | 20 | 13 | -38 | -45 | -63 | -91 | Th 90 |
| 92 U | -53 | 30 | -27 | -54 | -105 | -189 | 65 | 14 | -30 | -66 | -86.5 | 93 | 37 | 3 | 0 | 1 | -3 | -5 | -11 | -23 | -29 | -7 | -15 | -25 | -52.5 | -60 | 99 | 48 | 11 | 3 | 4 | 2 | -31 | -36 | -46 | -59 | U 92 |
| 94 Pu | -54 | 21 | -25 | -50 | -102 | -188 | 49 | 6 | -33 | -66 | -95.5 | 72 | 24 | -1 | 2 | 4 | 2 | -4 | -6 | -19 | -25 | -9 | -20 | -29 | -56.5 | -62 | 77 | 33 | 4 | -3 | 9 | 8 | -26 | -30 | -42 | -58 | Pu 94 |
| (b) \ (a) | 1 H | 3 Li | 4 Be | 5 B | 6 C | 7 N | 11 Na | 12 Mg | 13 Al | 14 Si | 15 P | 19 K | 20 Ca | 21 Sc | 22 Ti | 23 V | 24 Cr | 25 Mn | 26 Fe | 27 Co | 28 Ni | 29 Cu | 30 Zn | 31 Ga | 32 Ge | 33 As | 37 Rb | 38 Sr | 39 Y | 40 Zr | 41 Nb | 42 Mo | 43 Tc | 44 Ru | 45 Rh | 46 Pd | (b) \ (a) |

Figure A.1: The Miedema enthalpy values used for $\Delta H_{mix}$ calculations. Values and tables are from Takeuchi and Inoue [82].

Figure A.2: The Miedema enthalpy values used for $\Delta H_{mix}$ calculations. Values and tables are from Takeuchi and Inoue [82].

# Appendix B

# Troparevsky et al. Single Phase Predictions

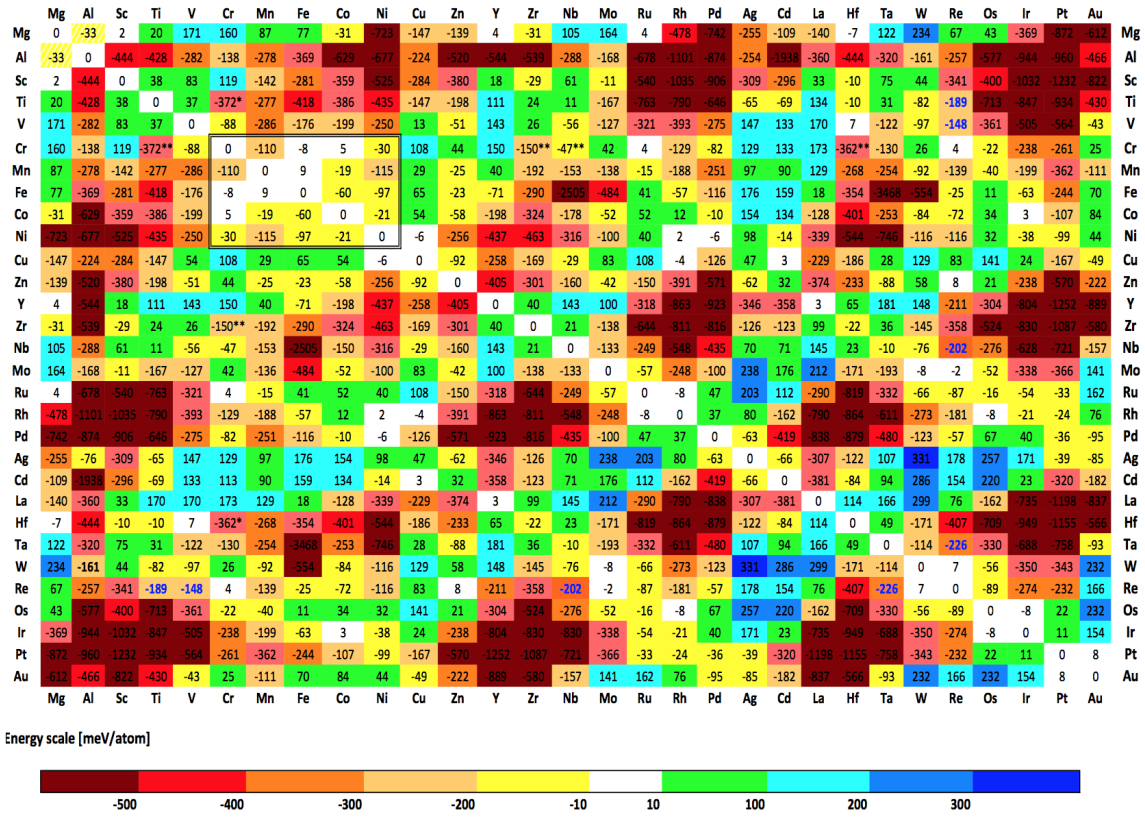


Figure B.1: The full table for the single phase predictions from Troparevsky et al. [80]. This table is found in the supplementary information that is linked to within the report [129].

# Appendix C

# DTA for BHEA-1

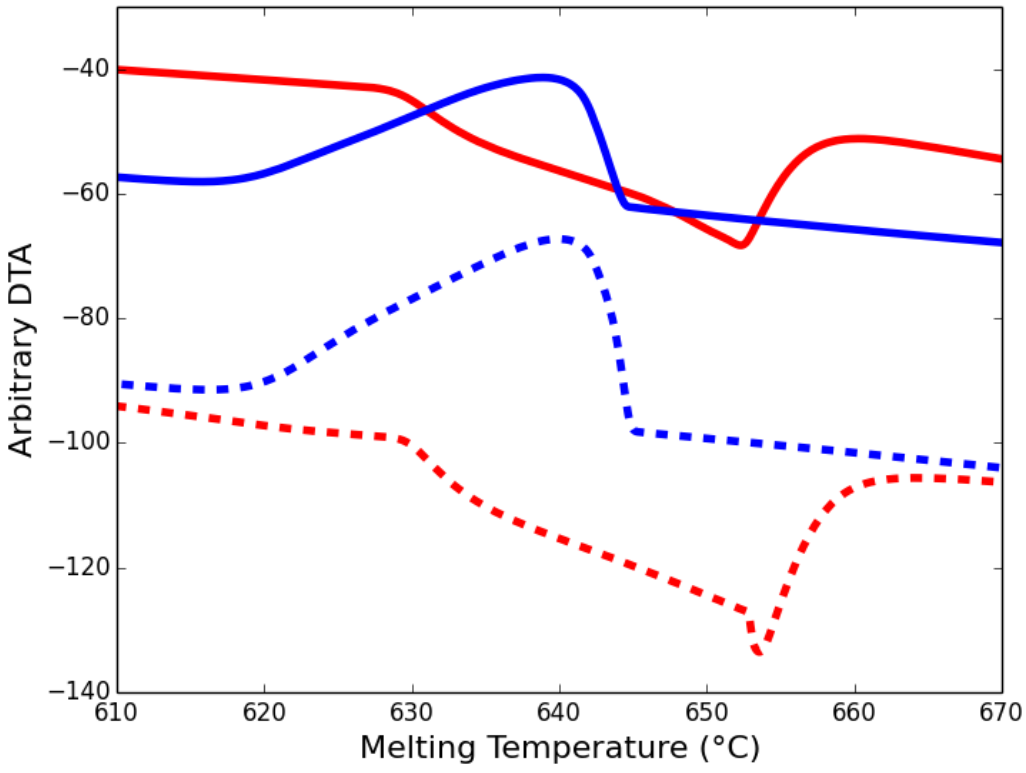


Figure C.1: The DTA results for BHEA1 (the sold lines) and BHEA4 (the dashed lines). The red lines represent the heating and the blue lines the cooling.

# Bibliography


[1] L. Jeffus. *Welding: Principles and Applications*. Cengage Learning, 2016.

[2] J. Nowacki, M. Danielewski, and R. Filipek. Brazed joints evaluation and computer modelling of mass transport in multi-component systems in the au–ni solder-14-5 ph joints. *Journal of Materials Processing Technology*, 157:213 – 220, 2004. Achievements in Mechanical and Materials Engineering Conference.

[3] S. Ghosh, R. Chakraborty, N. Dandapat, K.S. Pal, S. Datta, and D. Basu. Characterization of alumina–alumina/graphite/monel superalloy brazed joints. *Ceramics International*, 38(1):663 – 670, 2012.

[4] C.R. Dodwell. *The Various Arts: De Diversis Artibus*. Medieval texts. Nelson, 1986.

[5] J. Wolters. The origins of gold brazing. *Gold Bulletin*, 10(1):27–28, Mar 1977.

[6] Johnson Matthey. Six steps of successful brazing. *http://www.jm-metaljoining.com/technical-sixsteps*, Last accessed on 17th August 2017.

[7] Lucas Mulhaupt. Proper brazing procedure. *http://www.lucasmilhaupt.com/en-US/brazingfundamentals/properbrazingprocedure/*, August 2017.

[8] Johnson Matthey. Fluxes. *http://www.jm-metaljoining.com/products/brazing-fluxes*, Last accessed on 17th August 2017.

[9] N.H. Tariq, M. Shakil, B.A. Hasan, J.I. Akhter, M.A. Haq, and N.A. Awan. Electron beam brazing of zr62al13ni7cu18 bulk metallic glass with ti metal. *Vacuum*, 101:98 – 101, 2014. Including rapid communications, original articles and a special section: Measurement Characteristics and Use of Quadrupole Mass Spectrometers for Vacuum Applications.

[10] H.P. Hack and ASTM Committee G-1 on Corrosion of Metals. *Galvanic Corrosion*. Number no. 978 in ASTM special technical publication. ASTM, 1988.

[11] William S. de Rosset. Analysis of explosive bonding parameters. *Materials and Manufacturing Processes*, 21(6):634–638, 2006.

[12] M.M. Schwartz. *Brazing, 2nd Edition:*. ASM International, 2003.

[13] P. Roberts. *Industrial Brazing Practice, Second Edition*. CRC Press, 2013.

[14] Johnson Matthey. Brazing filler metals. *http://www.jm-metaljoining.com/products/brazing-products*, Last accessed on 17th August 2017.

[15] Johnson Matthey. Johnson matthey catalogue. *http://www.jm-metaljoining.com/french/pdfs/High%20Temperature%20Brazing%20Alloys.pdf*, Last accessed on 17th August 2017.

[16] TH SCHUBERT, W. LOSER, A. TERESIAK, N. MATTERN, and H.-D BAUER. Preparation and phase transformations of melt-spun al–ge–si brazing foils. *Journal of Materials Science*, 32(8):2181–2189, Apr 1997.

[17] R.K. Roy, A.K. Panda, S.K. Das, Govind, and A. Mitra. Development of a copper-based filler alloy for brazing stainless steels. *Materials Science and Engineering: A*, 523(1):312 – 315, 2009.

[18] R.L. Apps, D.R. Milner, and E.V. Beatson. *Introduction to Welding and Brazing: The Commonwealth and International Library: Welding Division*. Commonwealth and international library. Elsevier Science, 2013.

[19] N. Eustathopoulos, M.G. Nicholas, and B. Drevet. *Wettability at High Temperatures*. Pergamon Materials Series. Elsevier Science, 1999.

[20] K. C. Mills and Y. C. Su. Review of surface tension data for metallic elements and alloys: Part 1 – pure metals. *International Materials Reviews*, 51(6):329–351, 2006.

[21] H. M. Lu and Q. Jiang. Surface tension and its temperature coefficient for liquid metals. *The Journal of Physical Chemistry B*, 109(32):15463–15468, 2005. PMID: 16852961.

[22] George Kaptay. Partial surface tension of components of a solution. *Langmuir*, 31(21):5796–5804, 2015. PMID: 25942049.

[23] K. Landry and N. Eustathopoulos. Dynamics of wetting in reactive metal/ceramic systems: linear spreading. *Acta Materialia*, 44(10):3923 – 3932, 1996.

[24] A. Mortensen, B. Drevet, and N. Eustathopoulos. Kinetics of diffusion-limited spreading of sessile drops in reactive wetting. *Scripta Materialia*, 36(6):645 – 651, 1997.

[25] Nicolas Eustathopoulos. Wetting by liquid metals—application in materials processing: The contribution of the grenoble group. *Metals*, 5(1):350–370, 2015.

[26] P M Roberts. *Brazing*. Engineering design guides ; 10. Oxford University Press for the Design Council, the British Standards Institution, and the Council of Engineering Institutions, London], 1975.

[27] A.M. Aminazad, A.M. Hadian, and F. Ghasimakbari. Investigation on corrosion behaviour of copper brazed joints. *Procedia Materials Science*, 11:672 – 678, 2015. 5th International Biennial Conference on Ultrafine Grained and Nanostructured Materials, UFGNSM15.

[28] Lucas Milhaupt. Brazing filler metals. *http://www.lucasmilhaupt.com/en-US/products/*, Last accessed on 27th September 2017.

[29] D.M. Jacobson and G. Humpston. *Principles of Brazing*. ASM International, 2005.

[30] Rakesh R. Kapoor and Thomas W. Eagar. Oxidation behavior of silver- and copper-based brazing filler metals for silicon nitride/metal joints. *Journal of the American Ceramic Society*, 72(3):448–454, 1989.

[31] J.J. Stephens. *Brazing and Soldering: Proceedings of TheThird International Brazing and Soldering Conference April 24-26, 2006, San Antonio, TX*. ASM International, 2006.

[32] WebElements. *https://www.webelements.com/silver/*, Last accessed on 17th August 2017.

[33] ASM Handbook. Properties and selection: Alloy phase diagrams. *ASM International*, 3, 1991.

[34] E.D. Zysk. *Precious Metals 1981: Proceedings of the Fifth International Precious Metals Institute Conference, Held in Providence, Rhode Island, June 2-5, 1981*. Elsevier Science, 2013.

[35] WebElements. *https://www.webelements.com/copper/*, Last accessed on 17th August 2017.

[36] WebElements. *https://www.webelements.com/periodicity/melting_point/*, Last accessed on 17th August 2017.

[37] T. Saito. *Computational Materials Design*. Springer Series in Materials Science. Springer Berlin Heidelberg, 2013.

[38] J. Sato, T. Omori, K. Oikawa, I. Ohnuma, R. Kainuma, and K. Ishida. Cobalt-base high-temperature alloys. *Science*, 312(5770):90–91, 2006.

[39] R.S. Young. Corrosion resistance of cobalt. *Anti-Corrosion Methods and Materials*, 4(11):396–403, 1957.

[40] M. Kh. Ponezhev, A. B. Sozaeva, and V. A. Sozaev. The polytherms of angles of wetting grade 12kh18n9t steel by indium-sodium melts. *High Temperature*, 46(2):282–283, Apr 2008.

[41] L. Sisamouth, M. Hamdi, and T. Ariga. Investigation of gap filling ability of ag–cu–in brazing filler metals. *Journal of Alloys and Compounds*, 504(2):325 – 329, 2010.

[42] P.M. Roberts. *Introduction to Brazing Technology*. CRC Press, 2016.

[43] A.K. Tyagi and S. Banerjee. *Materials Under Extreme Conditions: Recent Trends and Future Prospects*. Elsevier Science, 2017.

[44] M.C. Gao, J.W. Yeh, P.K. Liaw, and Y. Zhang. *High-Entropy Alloys: Fundamentals and Applications*. Springer International Publishing, 2016.

[45] B.S. Murty, J.W. Yeh, and S. Ranganathan. *High-Entropy Alloys*. Butterworth-Heinemann, 2014.

[46] Y. Zhang, X. Yang, and P. K. Liaw. Alloy design and properties optimization of high-entropy alloys. *JOM*, 64(7):830–838, Jul 2012.

[47] J.M. Zhu, H.M. Fu, H.F. Zhang, A.M. Wang, H. Li, and Z.Q. Hu. Microstructure and compressive properties of multiprincipal component alcocrfenicx alloys. *Journal of Alloys and Compounds*, 509(8):3476 – 3480, 2011.

[48] W.H. Liu, Z.P. Lu, J.Y. He, J.H. Luan, Z.J. Wang, B. Liu, Yong Liu, M.W. Chen, and C.T. Liu. Ductile cocrfenimox high entropy alloys strengthened by hard intermetallic phases. *Acta Materialia*, 116(Supplement C):332 – 342, 2016.

[49] J.-W. Yeh, S.-K. Chen, S.-J. Lin, J.-Y. Gan, T.-S. Chin, T.-T. Shun, C.-H. Tsau, and S.-Y. Chang. Nanostructured high-entropy alloys with multiple principal elements: Novel alloy design concepts and outcomes. *Advanced Engineering Materials*, 6(5):299–303, 2004.

[50] U. Dahlborg, J. Cornide, M. Calvo-Dahlborg, T.C. Hansen, A. Fitch, Z. Leong, S. Chambreland, and R. Goodall. Structure of some cocrfeni and cocrfenipd multicomponent hea alloys by diffraction techniques. *Journal of Alloys and Compounds*, 681(Supplement C):330 – 341, 2016.

[51] F. Rezakhanlou, C. Villani, F. Golse, and S. Olla. *Entropy Methods for the Boltzmann Equation: Lectures from a Special Semester at the Centre Émile Borel, Institut H. Poincaré, Paris, 2001.* Number no. 1916 in Entropy Methods for the Boltzmann Equation: Lectures from a Special Semester at the Centre Émile Borel, Institut H. Poincaré, Paris, 2001. Springer, 2008.

[52] D.B. Miracle and O.N. Senkov. A critical review of high entropy alloys and related concepts. *Acta Materialia*, 122(Supplement C):448 – 511, 2017.

[53] Y.Y. Chen, T. Duval, U.D. Hung, J.W. Yeh, and H.C. Shih. Microstructure and electrochemical properties of high entropy alloys—a comparison with type-304 stainless steel. *Corrosion Science*, 47(9):2257 – 2279, 2005.

[54] G.D. Sathiaraj and P.P. Bhattacharjee. Effect of starting grain size on the evolution of microstructure and texture during thermo-mechanical processing of cocrfemnni high entropy alloy. *Journal of Alloys and Compounds*, 647(Supplement C):82 – 96, 2015.

[55] Duancheng Ma, Blazej Grabowski, Fritz Körmann, Jörg Neugebauer, and Dierk Raabe. Ab initio thermodynamics of the cocrfemnni high entropy alloy: Importance of entropy contributions beyond the configurational one. *Acta Materialia*, 100(Supplement C):90 – 97, 2015.

[56] G. Laplanche, O. Horst, F. Otto, G. Eggeler, and E.P. George. Microstructural evolution of a cocrfemnni high-entropy alloy after swaging and annealing. *Journal of Alloys and Compounds*, 647(Supplement C):548 – 557, 2015.

[57] Chin-You Hsu, Jien-Wei Yeh, Swe-Kai Chen, and Tao-Tsung Shun. Wear resistance and high-temperature compression strength of fcc cuconicral0.5fe alloy with boron addition. *Metallurgical and Materials Transactions A*, 35(5):1465–1469, May 2004.

[58] U.S. Hsu, U.D. Hung, J.W. Yeh, S.K. Chen, Y.S. Huang, and C.C. Yang. Alloying behavior of iron, gold and silver in alcocrcuni-based equimolar high-entropy alloys. *Materials Science and Engineering: A*, 460(Supplement C):403 – 408, 2007.

[59] A. Munitz, M.J. Kaufman, J.P. Chandler, H. Kalaantari, and R. Abbaschian. Melt separation phenomena in conicualcr high entropy alloy containing silver. *Materials Science and Engineering: A*, 560(Supplement C):633 – 642, 2013.

[60] M. A. Laktionova, E. D. Tabchnikova, Z. Tang, and P. K. Liaw. Mechanical properties of the high-entropy alloy ag0.5cocrcufeni at temperatures of 4.2–300k. *Low Temperature Physics*, 39(7):630–632, 2013.

[61] Sungwoo Sohn, Yanhui Liu, Jingbei Liu, Pan Gong, Silke Prades-Rodel, Andreas Blatter, B. Ellen Scanley, Christine C. Broadbridge, and Jan Schroers. Regular article. *Scripta Materialia*, 126(Complete):29–32, 2017.

[62] R.J.D. Tilley. *Understanding Solids: The Science of Materials*. Wiley, 2005.

[63] E. J. Pickering and N. G. Jones. High-entropy alloys: a critical assessment of their founding principles and future prospects. *International Materials Reviews*, 61(3):183–202, 2016.

[64] Khaled M. Youssef, Alexander J. Zaddach, Changning Niu, Douglas L. Irving, and Carl C. Koch. A novel low-density, high-hardness, high-entropy alloy with close-packed single-phase nanocrystalline structures. *Materials Research Letters*, 3(2):95–99, 2015.

[65] Xuzhou Gao, Yiping Lu, Bo Zhang, Ningning Liang, Guanzhong Wu, Gang Sha, Jizi Liu, and Yonghao Zhao. Microstructural origins of high strength and high ductility in an alcocrfeni2.1 eutectic high-entropy alloy. *Acta Materialia*, 141(Supplement C):59 – 66, 2017.

[66] Artur Tamm, Alvo Aabloo, Mattias Klintenberg, Malcolm Stocks, and Alfredo Caro. Atomic-scale properties of ni-based {FCC} ternary, and quaternary alloys. *Acta Materialia*, 99:307 – 312, 2015.

[67] Gokul Muthupandi, Ka Ram Lim, Young-Sang Na, Jieun Park, Dongyun Lee, Hanjong Kim, Seonghun Park, and Yoon Suk Choi. Pile-up and sink-in nanoindentation behaviors in alcocrfeni multi-phase high entropy alloy. *Materials Science and Engineering: A*, 696(Supplement C):146 – 154, 2017.

[68] Juliusz Dabrowa, Witold Kucza, Grzegorz Cieślak, Tadeusz Kulik, Marek Danielewski, and Jien-Wei Yeh. Interdiffusion in the fcc-structured al-co-cr-fe-ni high entropy alloys: Experimental studies and numerical simulations. *Journal of Alloys and Compounds*, 674(Supplement C):455 – 462, 2016.

[69] N. Liu, P.H. Wu, P.J. Zhou, Z. Peng, X.J. Wang, and Y.P. Lu. Rapid solidification and liquid-phase separation of undercooled cocrcufexni high-entropy alloys. *Intermetallics*, 72(Supplement C):44 – 52, 2016.

[70] M. Komarasamy, N. Kumar, Z. Tang, R.S. Mishra, and P.K. Liaw. Effect of microstructure on the deformation mechanism of friction stir-processed al0.1cocrfeni high entropy alloy. *Materials Research Letters*, 3(1):30–34, 2015.

[71] K.-Y. Tsai, M.-H. Tsai, and J.-W. Yeh. Sluggish diffusion in co–cr–fe–mn–ni high-entropy alloys. *Acta Materialia*, 61(13):4887 – 4897, 2013.

[72] Hui-Wen Chang, Ping-Kang Huang, Jien-Wei Yeh, Andrew Davison, Chun-Huei Tsau, and Chih-Chao Yang. Influence of substrate bias, deposition temperature and post-deposition annealing on the structure and properties of multi-principal-component (alcrmositi)n coatings. *Surface and Coatings Technology*, 202(14):3360 – 3366, 2008.

[73] S. Ranganathan. Alloyed pleasures: multimetallic cocktails. *Current Science*, 85:pp. 1404–1406, 2003.

[74] V. Dolique, A.-L. Thomann, P. Brault, Y. Tessier, and P. Gillon. Thermal stability of alcocrcufeni high entropy alloy thin films studied by in-situ xrd analysis. *Surface and Coatings Technology*, 204(12):1989 – 1992, 2010. Proceedings of the European Materials Research Socierty (E-MRS)Spring Meeting 2009.

[75] B. Schuh, F. Mendez-Martin, B. Völker, E.P. George, H. Clemens, R. Pippan, and A. Hohenwarter. Mechanical properties, microstructure and thermal stability of a nanocrystalline cocrfemnni high-entropy alloy after severe plastic deformation. *Acta Materialia*, 96(Supplement C):258 – 268, 2015.

[76] Chun Ng, Sheng Guo, Junhua Luan, Sanqiang Shi, and C.T. Liu. Entropy-driven phase stability and slow diffusion kinetics in an al0.5cocrcufeni high entropy alloy. *Intermetallics*, 31(Supplement C):165 – 172, 2012.

[77] Andrew Cunliffe, John Plummer, Ignacio Figueroa, and Iain Todd. Glass formation in a high entropy alloy system by design. *Intermetallics*, 23(Supplement C):204 – 207, 2012.

[78] S. Mohanty, T.N. Maity, S. Mukhopadhyay, S. Sarkar, N.P. Gurao, S. Bhowmick, and Krishanu Biswas. Powder metallurgical processing of equiatomic alcocrfeni high entropy alloy: Microstructure and mechanical properties. *Materials Science and Engineering: A*, 679(Supplement C):299 – 313, 2017.

[79] B.R. Braeckman and D. Depla. Structure formation and properties of sputter deposited nbx-cocrcufeni high entropy alloy thin films. *Journal of Alloys and Compounds*, 646(Supplement C):810 – 815, 2015.

[80] M. Claudia Troparevsky, James R. Morris, Paul R. C. Kent, Andrew R. Lupini, and G. Malcolm Stocks. Criteria for predicting the formation of single-phase high-entropy alloys. *Phys. Rev. X*, 5:011041, Mar 2015.

[81] Sheng GUO and C.T. LIU. Phase stability in high entropy alloys: Formation of solid-solution phase or amorphous phase. *Progress in Natural Science: Materials International*, 21(6):433 – 446, 2011.

[82] Akira Takeuchi and Akihisa Inoue. Classification of bulk metallic glasses by atomic size difference, heat of mixing and period of constituent elements and its application to characterization of the main alloying element. *MATERIALS TRANSACTIONS*, 46(12):2817–2829, 2005.

[83] U. Mizutani. *Hume-Rothery Rules for Structurally Complex Alloy Phases*. CRC Press, 2016.

[84] Sheng Guo, Qiang Hu, Chun Ng, and C.T. Liu. More than entropy in high-entropy alloys: Forming solid solutions or amorphous phase. *Intermetallics*, 41:96 – 103, 2013.

[85] Y. Zhang, Y.J. Zhou, J.P. Lin, G.L. Chen, and P.K. Liaw. Solid-solution phase formation rules for multi-component alloys. *Advanced Engineering Materials*, 10(6):534–538, 2008.

[86] Zhijun Wang, Weifeng Qiu, Yong Yang, and C.T. Liu. Atomic-size and lattice-distortion effects in newly developed high-entropy alloys with multiple principal elements. *Intermetallics*, 64:63 – 69, 2015.

[87] Y.F. Ye, C.T. Liu, and Y. Yang. A geometric model for intrinsic residual strain and phase stability in high entropy alloys. *Acta Materialia*, 94:152 – 161, 2015.

[88] Tea-Sung Jun and Alexander M. Korsunsky. Evaluation of residual stresses and strains using the eigenstrain reconstruction method. *International Journal of Solids and Structures*, 47(13):1678 – 1686, 2010.

[89] I. Toda-Caraballo and P.E.J. Rivera-Díaz del Castillo. A criterion for the formation of high entropy alloys based on lattice distortion. *Intermetallics*, 71(Supplement C):76 – 87, 2016.

[90] X. Yang and Y. Zhang. Prediction of high-entropy stabilized solid-solution in multi-component alloys. *Materials Chemistry and Physics*, 132(2):233 – 238, 2012.

[91] M.G. Poletti and L. Battezzati. Electronic and thermodynamic criteria for the occurrence of high entropy alloys in metallic systems. *Acta Materialia*, 75:297 – 306, 2014.

[92] Sheng Guo, Chun Ng, Jian Lu, and C. T. Liu. Effect of valence electron concentration on stability of fcc or bcc phase in high entropy alloys. *Journal of Applied Physics*, 109(10):103505, 2011.

[93] Z. Leong, J.S. Wrobel, S.L. Dudarev, R. Goodall, I. Todd, and D. Nguyen-Manh. The effect of electronic structure on the phases present in high entropy alloys. *Scientific Reports*, 7, January 2017.

[94] Isaac Toda-Caraballo and Pedro E.J. Rivera-Díaz del Castillo. Modelling solid solution hardening in high entropy alloys. *Acta Materialia*, 85(Supplement C):14 – 23, 2015.

[95] L.R. Owen, E.J. Pickering, H.Y. Playford, H.J. Stone, M.G. Tucker, and N.G. Jones. An assessment of the lattice strain in the crmnfeconi high-entropy alloy. *Acta Materialia*, 122(Supplement C):11 – 18, 2017.

[96] Fuyang Tian, Lajos Karoly Varga, Nanxian Chen, Jiang Shen, and Levente Vitos. Ab initio design of elastically isotropic tizrnbmovx high-entropy alloys. *Journal of Alloys and Compounds*, 599(Supplement C):19 – 25, 2014.

[97] Suffian N. Khan, J. B. Staunton, and G. M. Stocks. Statistical physics of multicomponent alloys using kkr-cpa. *Phys. Rev. B*, 93:054206, Feb 2016.

[98] O. N. Senkov and D. B. Miracle. A new thermodynamic parameter to predict formation of solid solution or intermetallic phases in high entropy alloys. *Journal of Alloys and Compounds*, 658:603–607, 2 2016.

[99] Y.F. Ye, Q. Wang, J. Lu, C.T. Liu, and Y. Yang. Design of high entropy alloys: A single-parameter thermodynamic rule. *Scripta Materialia*, 104(Supplement C):53 – 55, 2015.

[100] N. Saunders and A.P. Miodownik. *CALPHAD (Calculation of Phase Diagrams): A Comprehensive Guide*. Pergamon Materials Series. Elsevier Science, 1998.

[101] I.R. Management Association. *Materials Science and Engineering: Concepts, Methodologies, Tools, and Applications: Concepts, Methodologies, Tools, and Applications*. IGI Global, 2017.

[102] *CALPHAD: Computer Coupling of Phase Diagrams and Thermochemistry*. Number v. 19. Pergamon Press, 1995.

[103] Höglund L. Shi P.F. Andersson J.O., Helander T. and Sundman B. Thermo-calc and dictra. *Computational tools for materials science. Calphad.*, 26:273–312., 2002.

[104] O.N. Senkov, J.D. Miller, D.B. Miracle, and C. Woodward. Accelerated exploration of multi-principal element alloys for structural applications. *Calphad*, 50(Supplement C):32 – 48, 2015.

[105] D.B. Miracle C. Woodward O.N. Senkov, J.D. Miller. Accelerated exploration of multi-principal element alloys with solid solution phases. *Nat. Commun.*, 6:6529, 2015.

[106] W.D. Callister and D.G. Rethwisch. *Fundamentals of Materials Science and Engineering: An Integrated Approach, 5th Edition*. Wiley, 2016.

[107] D.R. Askeland and P.P. Fulay. *Essentials of Materials Science & Engineering*. Cengage Learning, 2008.

[108] K. Nogi, K. Ogino, A. McLean, and W. A. Miller. The temperature coefficient of the surface tension of pure liquid metals. *Metallurgical Transactions B*, 17(1):163–170, Jan 1986.

[109] Iván Egry and Jürgen Brillo. Surface tension and density of liquid metallic alloys measured by electromagnetic levitation. *Journal of Chemical & Engineering Data*, 54(9):2347–2352, 2009.

[110] WebElements. *https://www.webelements.com/molarvolume/*, Last accessed on 1st January 2018.

[111] Kaptay G and Papp Z. On the concentration dependence of the surface tension of liquid metallic alloys theoretical basis. *Journal of Forensic Research*, 6(5):1 – 3, 2015.

[112] G. Kaptay. A method to calculate equilibrium surface phase transition lines in monotectic systems. *Calphad*, 29(1):56 – 67, 2005.

[113] G. Kaptay and T. BÁrczy. On the asymmetrical dependence of the threshold pressure of infiltration on the wettability of the porous solid by the infiltrating liquid. *Journal of Materials Science*, 40(9):2531–2535, May 2005.

[114] R. Novakovic, E. Ricci, D. Giuranno, and A. Passerone. Surface and transport properties of ag–cu liquid alloys. *Surface Science*, 576(1):175 – 187, 2005.

[115] Przemysław Fima and Natalia Sobczak. Thermophysical properties of ag and ag–cu liquid alloys at 1098k to 1573k. *International Journal of Thermophysics*, 31(6):1165–1174, Jun 2010.

[116] Pavel Sebo, Bernard Gallois, and C. H. P. Lupis. The surface tension of liquid silver-copper alloys. *Metallurgical Transactions B*, 8(3):691–693, Sep 1977.

[117] Joonho Lee, Toshihiro Tanaka, Yuuichi Asano, and Shigeta Hara. Oxygen adsorption behavior on the surface of liquid cu-ag alloys. *MATERIALS TRANSACTIONS*, 45(8):2719–2722, 2004.

[118] Fathi Aqra and Ahmed Ayyad. Theoretical calculations of the surface tension of ag(1x)–cu(x) liquid alloys. *Journal of Alloys and Compounds*, 509(19):5736 – 5739, 2011.

[119] Feng He, Zhijun Wang, Qingfeng Wu, Sizhe Niu, Junjie Li, Jincheng Wang, and C.T. Liu. Solid solution island of the co-cr-fe-ni high entropy alloy system. *Scripta Materialia*, 131(Supplement C):42 – 46, 2017.

[120] Mayur Vaidya, Anil Prasad, Abhinav Parakh, and B.S. Murty. Influence of sequence of elemental addition on phase evolution in nanocrystalline alcocrfeni: Novel approach to alloy synthesis using mechanical alloying. *Materials and Design*, 126(Supplement C):37 – 46, 2017.

[121] S. Varalakshmi, M. Kamaraj, and B.S. Murty. Formation and stability of equiatomic and nonequiatomic nanocrystalline cunicoznalti high-entropy alloys by mechanical alloying. *Metallurgical and Materials Transactions A*, 41(10):2703–2709, Oct 2010.

[122] Anil Kumar Singh and Anandh Subramaniam. On the formation of disordered solid solutions in multi-component alloys. *Journal of Alloys and Compounds*, 587(Supplement C):113 – 119, 2014.

[123] B. Ren, Z.X. Liu, B. Cai, M.X. Wang, and L. Shi. Aging behavior of a cucr2fe2nimn high-entropy alloy. *Materials and Design*, 33(Supplement C):121 – 126, 2012.

[124] Haoyan Diao, Louis J. Santodonato, Zhi Tang, Takeshi Egami, and Peter K. Liaw. Local structures of high-entropy alloys (heas) on atomic scales: An overview. *JOM*, 67(10):2321–2325, Oct 2015.

[125] Jien-Wei Yeh, Shou-Yi Chang, Yu-Der Hong, Swe-Kai Chen, and Su-Jien Lin. Anomalous decrease in x-ray diffraction intensities of cu–ni–al–co–cr–fe–si alloy systems with multi-principal elements. *Materials Chemistry and Physics*, 103(1):41 – 46, 2007.

[126] Y.C. Lin and Y.H. Cho. Elucidating the microstructural and tribological characteristics of nicralcocu and nicralcomo multicomponent alloy clad layers synthesized in situ. *Surface and Coatings Technology*, 203(12):1694 – 1701, 2009.

[127] B. Cantor, I.T.H. Chang, P. Knight, and A.J.B. Vincent. Microstructural development in equiatomic multicomponent alloys. *Materials Science and Engineering: A*, 375(Supplement C):213 – 218, 2004.

[128] Takeshi Nagase, Masanori Suzuki, and Toshihiko Tanaka. Amorphous phase formation in fe–ag-based immiscible alloys. *Journal of Alloys and Compounds*, 619:311 – 318, 2015.

[129] M. Claudia Troparevsky. Supplementary information. *http://link.aps.org/ supplemental/10.1103/PhysRevX.5.011041*.

[130] Periodictable.com. http://periodictable.com/properties/a/latticeconstants.an.html. Last accessed on 29th September 2017.

[131] Khaled M. Youssef, Alexander J. Zaddach, Changning Niu, Douglas L. Irving, and Carl C. Koch. A novel low-density, high-hardness, high-entropy alloy with close-packed single-phase nanocrystalline structures. *Materials Research Letters*, 3(2):95–99, 2015.

[132] E.A. Brandes and G.B. Brook. *Smithells Metals Reference Book*. Elsevier Science, 2013.